UCRL-18347
cy. 2

SEMIANNUAL REPORT
BIOLOGY AND MEDICINE

RECEIVED
RADIATION LABORATORY
JAN 3 1969
LIBRARY AND
DOCUMENTS SECTION

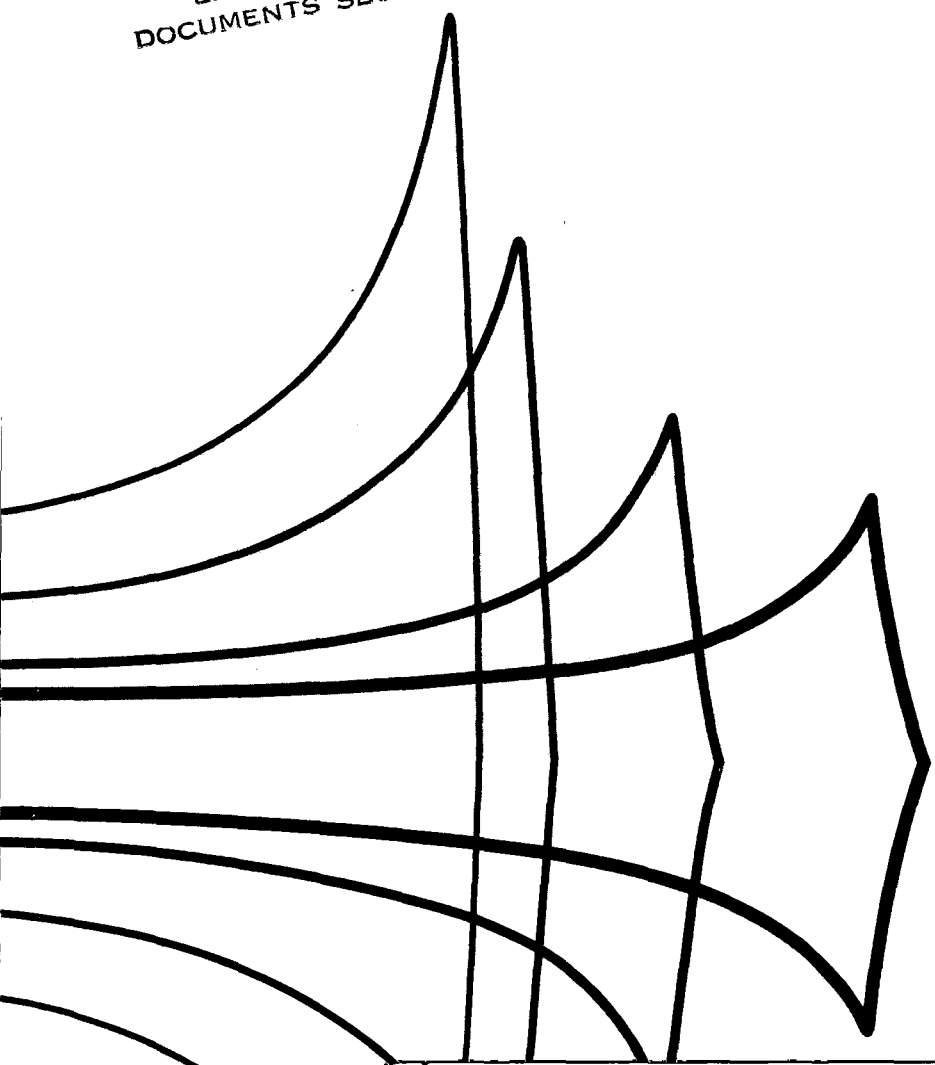

Donner Laboratory
and
Donner Pavilion

Spring 1968

TWO-WEEK LOAN COPY

This is a Library Circulating Copy which may be borrowed for two weeks. For a personal retention copy, call Tech. Info. Division, Ext. 5545

UCRL-18347
cy. 2

LAWRENCE RADIATION LABORATORY · UNIVERSITY OF CALIFORNIA · BERKELEY

DISCLAIMER

This document was prepared as an account of work sponsored by the United States Government. While this document is believed to contain correct information, neither the United States Government nor any agency thereof, nor the Regents of the University of California, nor any of their employees, makes any warranty, express or implied, or assumes any legal responsibility for the accuracy, completeness, or usefulness of any information, apparatus, product, or process disclosed, or represents that its use would not infringe privately owned rights. Reference herein to any specific commercial product, process, or service by its trade name, trademark, manufacturer, or otherwise, does not necessarily constitute or imply its endorsement, recommendation, or favoring by the United States Government or any agency thereof, or the Regents of the University of California. The views and opinions of authors expressed herein do not necessarily state or reflect those of the United States Government or any agency thereof or the Regents of the University of California.

UCRL-18347
UC-48 Biology and Medicine
TID-4500 (52nd Ed.)

Spring 1968

SEMIANNUAL REPORT BIOLOGY AND MEDICINE

John H. Lawrence, M.D., Editor

DONNER LABORATORY AND DONNER PAVILION

LAWRENCE RADIATION LABORATORY UNIVERSITY OF CALIFORNIA
BERKELEY, CALIFORNIA

AEC Contract No. W-7405-eng-48

Foreword

The 19 papers in this Semiannual Report concern progress in several areas of biomedical research. The first report relates to a problem which has concerned us ever since we first used ^{32}P for the successful treatment of polycythemia vera in 1939—i.e., the possible induction of leukemia. Life expectancy is now near normal in those patients so treated, but hematological complications in some patients present a problem. Results of an analysis of 181 patients followed, throughout their course, support the hypothesis that the development of significant splenic myeloid metaplasia and acute leukemia-like states are part of the evolutionary history of polycythemia. Several centers are now treating patients with polycythemia vera with several different chemotherapeutic agents, but enough experience has not yet been gained to learn the incidence of leukemia in patients so treated, or the degree of extension of life.

Two articles concern important applications of the rapid-imaging whole body scanner, an instrument devised and built by Anger in this Laboratory; used with ^{59}Fe it is possible, in addition to visualizing erythropoietic-marrow distribution, to obtain information which may serve as a valuable check on external monitoring during iron kinetic studies and, in certain cases, helps resolve ambiguities that sometimes occur in the interpretation of activity curves derived from such data. In association with ^{18}F the whole body scanner provides a simple, rapid, and accurate method for the radioisotopic survey of the entire skeleton, and the positron/gamma scintillation camera may then be used to examine at high resolution any abnormal or suspicious areas detected on the skeletal survey; this is probably the most efficient means yet developed for detection of metastatic bone disease.

A method for using digital computers to analyze breath-$^{14}CO_2$ data is presented, along with two studies utilizing such computer analysis in conjunction with ^{14}C tissue and blood studies to investigate the effects of glucagon and of hydrocortisone on the kinetics of histidine metabolism. A tissue culture study is reported which showed that thyroxine, for the most part, increases the growth rate of human kidney ("T") cells by shortening the time required for the cell to complete the G_1 period—a finding of particular interest because this same stage (G_1 or pre-DNA synthetic stage) shows the most change when a cancerous cell is compared with its normal counterpart.

The generation of subjective sensations of light flashes in humans by means of external-electrode electrical stimulation is reported, and these preliminary experiments indicate that the development of a head-mounted photodetector system using external electrodes may eventually prove to be an important aid to visually impaired or blind patients.

Further studies concerning space radiation are presented. In one, the radiation-hypoxia problem was investigated by studying the erythropoietic response in dogs given sublethal whole body proton irradiation and subsequently kept in an altitude chamber at a simulated altitude of 18,000 feet. The finding that the combined effect of radiation and hypoxia is not synergistic

but rather that hypoxia appears to favorably modify the damage induced by radiation on the erythropoietic system and to accelerate recovery, has important implications in the evaluation of the radiation-hypoxia problem as related to space travel. In another study, possible radiation effects of primary galactic protons were studied by determining the effect of 47-MeV cyclotron-accelerated protons (which have the same degree of penetration) on the bioelectric activity of frog sciatic nerve.

Applications of scanning electron microscopy continue, and a report concerning the three-dimensional structure of the blood clot is presented; a knowledge of the microarchitecture of clots formed both in vivo and in vitro would be of value in understanding the normal clotting process and in assessing the problem of abnormal thrombus formation. Electron microscopy was used to study the general morphology and the fine structure of oxyntic cells of the metamorphosing tadpole gastric mucosa and showed that membrane transformations play an integral role in the mechanism of HCL secretion. Another report concerns electron microscopy and its use for the analysis of molecular structure; electron diffraction can be used to evaluate the preservation of labile specimens to a structural "resolution" considerably better than that which is possible by conventional electron microscopy. A novel image-scanning mode of the transmission electron microscope is proposed and evaluated with respect to possible improvement of the quality of the images through the use of computer analysis.

Further studies of stem cell kinetics are reported, employing the spleen colony technique and erythropoietin sensitivity test. Two lipoprotein studies are presented, one concerning sex differences in several characteristics of the major component of the S_f° 0-12 low-density lipoprotein class, and the other, the effect of incubation of human serum plasma for 24 hours at 37° C on subsequent centrifugal patterns. In another study, the radiosensitivities of the synthesis of DNA thymine and adenine utilizing monocarbon units from ^{14}C-labeled formate or #3-^{14}C-labeled serine and of the incorporation of tritiated thymidine into DNA thymine were compared, with the finding that the former is more radiosensitive than the latter.

Tissue activation studies were carried out by using the positron scintillation camera to visualize the activation pattern of the alpha particle beam. By making it possible to visualize the end of the beam track in tissue, the tissue activation technique could provide an important on-line alignment tool for patient therapy utilizing the Bragg peak. In another study it was shown that the Bragg peak of a high-energy neon beam was not spread out appreciably by the presence of secondary particles from nuclear reactions in water.

Table of Contents

Leukemia in Polycythemia Vera: Relationship to Splenic Myeloid Metaplasia and Therapeutic Radiation Dose
JOHN H. LAWRENCE, H. SAUL WINCHELL AND WILLIAM G. DONALD, JR. 1

Whole Body Scanning of ^{59}Fe in Evaluation of Body Distribution of Erythropoietic Marrow, Splenic Sequestration of Red Cells and Hepatic Deposition of Iron
PETER RONAI, H. SAUL WINCHELL, HAL O. ANGER AND JOHN H. LAWRENCE 10

Skeletal Survey for Metastatic Tumors of Bone Using ^{18}F and ^{85}Sr with Scintillation Camera and Whole Body Scanner
PETER RONAI, H. SAUL WINCHELL AND HAL O. ANGER 23

Computer Analysis of Breath $^{14}CO_2$ Data
H. SAUL WINCHELL AND KENNETH G. WILEY 36

Increased Histidine Turnover in Rats Following Administration of Glucagon
LOUIS L. SHANE, H. SAUL WINCHELL, NANCY N. FINLEY, BARBARA A. SHIPLEY AND JOHN H. LAWRENCE 42

The Influence of Hydrocortisone upon Histidine Kinetics in the Rat
LOUIS L. SHANE, H. SAUL WINCHELL, BARBARA A. SHIPLEY AND NANCY N. FINLEY 53

Human Cell Control Mechanisms. I. Effects of Thyroxine on Cell Life Cycle Parameters
H. JOHN BURKI 59

Indirect Electrical Stimulation of the Visual Apparatus
THOMAS F. BUDINGER 64

Erythropoietic Response in Dogs Given Sublethal Whole Body Proton Irradiation Followed by Hypoxic Hypoxia
HENRY ACETO, JR., ROBERT W. SPRINGSTEEN, W. GEE AND H. SAUL WINCHELL 71

Changes in the Bioelectric Activity of Sciatic Nerve After Irradiation with Cyclotron-Accelerated Protons
CORNELIUS T. GAFFEY 82

The Microarchitecture of a Whole Blood Clot
THOMAS L. HAYES 96

Studies of Stem Cell Kinetics Utilizing the Spleen Colony Technique and the Erythropoietin Sensitivity Test
JOHN C. SCHOOLEY 99

Parallel Development of Intracellular Membranes and the Acid Secretory Mechanism of Oxyntic Cells of the Metamorphosing Bullfrog Tadpoles
GERTRUDE M. FORTE, JOHN G. FORTE AND LIANGCHAI LIMLOMWONGSE 112

Flotation Rates, Molecular Weights and Hydrated Densities of the Low-Density Lipoproteins
FRANK T. LINDGREN, LIN C. JENSEN, ROBERT D. WILLS AND NORMAN K. FREEMAN 129

Physical-Chemical Changes in Serum Lipoproteins During Incubation of Human Serum
ALEXANDER V. NICHOLS, ELAINE L. COGGIOLA, LIN C. JENSEN AND ELAINE H. YOKOYAMA 140

Relative Effects of Radiation on de Novo DNA Base Synthesis and Thymidine Incorporation into DNA
H. SAUL WINCHELL, SERENE L. VIMOKESANT AND ROSANNE B. RALEY 149

Tissue Activation Studies with Alpha Particle Beams
HOWARD D. MACCABEE, UDIPI MADHVANATH AND MUDUNDI R. RAJU 155

Secondary Particle Contributions to the Bragg Peak of a High-Energy Heavy-Ion Beam
STANLEY B. CURTIS 171

Proposed Experimental Systems for Digital Analysis and Improvement of Fourier Contrast Images in Biological Electron Microscopy
ROBERT M. GLAESER AND GARETH THOMAS 175

Leukemia in Polycythemia Vera: Relationship to Splenic Myeloid Metaplasia and Therapeutic Radiation Dose

John H. Lawrence, H. Saul Winchell and William G. Donald, Jr.

Subsequent to our introduction of $^{32}PO_4$ for the treatment of polycythemia vera in 1936 it has become clear that the use of this agent reduces morbidity and results in significant prolongation of life over that of patients treated without myelosuppressive therapy (1, 2). Although the therapeutic benefits of ^{32}P in polycythemia vera (PV) remain unchallenged, recent reports have suggested that the high incidence of acute leukemia-like states appearing late in the course of this disease is due to prior radiation therapy (3, 4). That radiation may increase the incidence of leukemia has been known for some time (5, 6), and was well appreciated by us when we first began using ^{32}P in human disease more than 30 years ago (7). However, it was our contention that the benefits attendant upon the management of PV patients with ^{32}P justified the possible risk of leukemia induction by such therapy. Nonetheless, in our therapeutic protocols we have avoided administration of excessive amounts of this agent.

Because of current interest in the possible relationship between therapeutic radiation dose and development of acute leukemia-like states in PV, we reviewed our experience and related the occurrence of this complication to the development of splenic myeloid metaplasia (MM) and the radiation dose used in therapy.

Since radiation effects generally show some radiation dose dependency, we correlated radiation dose with presence of acute leukemia (AL) at death in our series of 181 PV patients who had died at the time of initiation of this study. This paper documents a lack of a positive relationship between radiation dose and development of AL, and discusses the implications of this finding.

MATERIALS AND METHODS

In most cases studied, therapy and long-term follow-up were performed at this clinic, often in association with the referring physician. Complete records were kept of all pertinent medical information on procedures performed elsewhere throughout the patient's life. The decision as to whether the patient had a terminal hematologic complication was made on the basis of both the patient's course and the findings at post-mortem examination.

Prior to 1949 the diagnosis of PV had been made on the basis of a sustained elevation of the red cell count in excess of 7 million cells per mm^3. Subsequent to 1949, all patients were diagnosed as having PV on the basis of an increased circulating red cell volume (exceeding

34 ml/kg body weight), a normal arterial oxygen saturation, and exclusion of disorders associated with secondary erythrocytosis. The red cell volume was determined by using ^{32}P phosphate labeling of autologous red cells (8). Tumors associated with secondary erythrocytosis were excluded on the basis of complete medical evaluation (exclusion of renal disease, etc.) during clinic visits, subsequent long-term follow-up of the patient's course, and findings including post-mortem examination. In each case one or more of the following findings were present: an enlarged spleen, persistent thrombocytosis (in excess of 400,000 per mm^3 by direct method), or leukocytosis (WBC in excess of 10,000 per mm^3).

Significant splenomegaly (spleen tip extending more than 3 cm beneath C. M.), leukocytosis, and characteristic changes in RBC, WBC, and platelet morphology were noted prior to death in each case of "significant splenic myeloid metaplasia." The presence of significant splenic MM was confirmed at the time of post-mortem examination on the basis of histologic findings of myelopoiesis with megakaryocytes clearly identifiable in the spleen. In recent years we attempted to distinguish this state from chronic myelogenous leukemia by performance of leukocyte alkaline phosphatase and chromosome studies. In those cases with MM for which the determinations were performed, leukocyte alkaline phosphatase was either normal or elevated and the Philadelphia chromosome was absent. All cases in this category were placed within the "death with significant splenic myeloid metaplasia" group (MM). "Acute myelogenous leukemia with myeloid metaplasia" (ALw/MM) was the term applied to those cases with leukocytosis and preceding significant splenic MM with terminal findings of more than 20% blast cells in the circulating blood. Patients in this category usually had generalized infiltration of tissues by blast cells at post-mortem examination. Generally, in these cases, the peripheral blood contained a spectrum of cells at various levels of differentiation, from the mature granulocyte to the myeloblast.

"Acute myelogenous leukemia without myeloid metaplasia" (AL) was the term applied to those cases without preceding significant splenic MM who suddenly developed depression of the number of normal circulating cellular elements associated with a variable number of myeloblasts in the peripheral blood, without evidence of differentiation of these cells to more mature elements.

In the series reported here of 181 cases with PV followed to death, ^{32}P was the sole radiation modality used in 123 cases. In the remaining cases both X irradiation and ^{32}P were used in therapy. (In all cases venesection was used as supplemental therapy.) In 12 of this latter group accurate measurement of X-radiation dose was not available, and these cases were not used in analysis of radiation dose administered. Millicuries ^{32}P was converted to "equivalent R" exposure by use of the figure suggested by Osgood of 15 R/mCi (9). [This figure is higher than that used previously (1).] When X irradiation was used in therapy the maximum radiation dose received by any myelopoietic area (bone or spleen) was taken as the "equivalent R" exposure for the entire body. Thus, values for radiation exposure in "equivalent R" represent maximum values. The product mCi ^{32}P or "equivalent R" times months at risk was obtained by multiplying mCi or "equivalent R" times the time in months between administration and death for each radiation exposure and summing all such values for each patient.

Values were calculated for the mean and the standard error of the mean for each parameter. The probability that the value obtained for a given parameter in comparisons between groups of patients would be higher or lower by chance alone (P values) was determined by using routine statistical techniques utilizing tables of students' "t" distribution.

RESULTS

Table 1 presents a comparison of the age at onset and the duration of disease between groups of patients with PV treated with ^{32}P and other radiation modalities. Clinically the patients were separated into two major groups comprised of those patients who had, and had not, demonstrated evidence of significant splenic MM. Under each of these major headings the patients were further subdivided into those who were judged to have developed a terminal acute leukemia-like state (AL) and those who did not show evidence of such a development.

In the patients listed on this table 45/181 (25%) developed significant splenic MM and 26/181 (14%) developed an acute myelogenous leukemia-like state. Sixteen cases had both "acute leukemia" (AL) and significant splenic MM (i.e., 16/45 or 36% of all cases with MM developed AL) and 10 cases had only AL but no significant splenic MM (i.e., 10/136 or 7% of all cases without MM developed AL).

Patients who developed significant splenic MM or AL prior to death were found to be younger both at the age of onset and at diagnosis, and to survive longer than patients who developed neither MM nor AL (uncomplicated group) (see Table IV for results of test of significance between groups). Conversely stated, those patients who failed to develop significant splenic MM or AL prior to death were older at the time of onset and diagnosis and failed to live as long after onset of their disease as those patients who did develop these findings.

Among the group of patients who developed significant splenic metaplasia prior to death there was no significant difference, in terms of onset and duration of disease, between those who developed acute leukemia-like states (ALw/MM) and those who died without development of this complication (MM).

Table 2 presents results summarizing the total dose for PV patients treated with ^{32}P as the only source of radiation used in therapy. The dose is given as cumulative mCi ^{32}P and also as the sum of the products mCi ^{32}P administered times months at risk (time in months from ^{32}P administration to death). The largest doses, expressed either as total mCi administered or as the product mCi times months at risk, were received by patients who developed significant splenic myeloid metaplasia but who did not show signs of acute leukemia (MM group). The three other groups (uncomplicated, AL, and ALw/MM) had comparable total doses of ^{32}P expressed as mCi. The patients who died with "acute leukemia" but without significant splenic myeloid metaplasia (AL) survived longer from the start of ^{32}P therapy and correspondingly had a larger value of "dose risk" expressed as mCi-months than did the uncomplicated and ALw/MM groups.

Table 1. Age at onset and duration of disease for various categories of deceased patients with polycythemia vera treated with radiation.*

	Lack of significant splenic MM prior to death		Significant splenic MM prior to death	
	No leukemia (uncomplicated) (N = 126)	Terminal acute leukemia (AL) (N = 10)	No leukemia (MM) (N = 29)	Terminal acute leukemia (ALw/MM) (N = 16)
Age at onset	57.9 ± 1.0	51.5 ± 3.6	50.9 ± 2.1	49.2 ± 2.2
Age at diagnosis	59.7 ± 1.0	53.8 ± 3.2	52.6 ± 1.9	50.6 ± 2.2
Duration to death from onset	11.6 ± 0.5	15.1 ± 3.1	15.1 ± 1.1	13.0 ± 1.3
Duration to death from diagnosis	9.9 ± 0.5	11.7 ± 2.0	13.4 ± 1.1	11.6 ± 1.2

*For each category values for the mean and standard error of the mean are given.

Table 2. Radiation dose for deceased polycythemia vera patients treated with ^{32}P radiation alone.*

	Lack of significant splenic MM prior to death		Significant splenic MM prior to death	
	No leukemia (uncomplicated) (N = 92)	Terminal acute leukemia (AL) (N = 8)	No leukemia (MM) (N = 17)	Terminal acute leukemia (ALw/MM) (N = 6)
Total dose (mCi)	25.4 ± 2.5	29.0 ± 5.0	40.3 ± 4.8	26.4 ± 6.1
Duration to death from start of ^{32}P (years)	7.9 ± 0.5	13.2 ± 1.8	10.4 ± 1.4	7.4 ± 2.0
Total mCi-Months	1942 ± 244	3098 ± 624	3788 ± 717	1726 ± 744

*For each category values for the mean and standard error of the mean are given; mCi-months was determined in each case as the sum of the product of each dose of ^{32}P (mCi) times months from administration to death.

Similar findings are noted when all patients treated with either ^{32}P alone or ^{32}P and X irradiation are considered (Table 3). In this tabulation both groups of patients who developed splenic myeloid metaplasia (MM and ALw/MM) received larger doses than those who failed to develop splenic MM. Within each major category (presence vs. absence of significant splenic MM) there was no significant difference in radiation dose between those developing AL or those not developing it.

Table 4 shows results of test of significance.

Table 3. Radiation dose for deceased polycythemia vera patients treated with ^{32}P and other radiation modalities.*

	Lack of significant splenic MM prior to death		Significant splenic MM prior to death	
	No leukemia (uncomplicated) (N = 114)	Terminal acute leukemia (AL) (N = 10)	No leukemia (MM) (N = 29)	Terminal acute leukemia (ALw/MM) (N = 16)
Total dose (R)	545 ± 73	468 ± 68	1027 ± 235	1386 ± 419
Total R-months	36,882 ± 4,616	39,418 ± 8,761	70,255 ± 16,309	58,987 ± 17,191

*For each category values for the mean and standard error of the mean are given. The values for R-months were determined by assuming each mCi ^{32}P is equivalent to 15 R (Ref. 9).

DISCUSSION

In many patients with PV the condition can be viewed as a progressive process in which the initial increase in the rate of erythropoiesis is followed by progressive reduction in red cell survival, incompletely compensated for by increase in the rate of red cell production (10). During the course of this process the erythropoietic bone marrow extends from its normal central location--in vertebral bodies, pelvis, and proximal femori and humeri--down the shafts of the long bones and into the distal extremities, in association with progressive loss of such erythropoietic marrow from central marrow cavities (11). At variable times during this course, extramedullary erythropoiesis may appear, first in the spleen and then in the liver (2, 10). Comparable changes seem to be occurring in the white cell series. The number of white cells appearing in the circulation generally increases as the disease progresses (10) in association with a variable increase in their degree of "immaturity." During the course of this process, a sudden change in the number or state of differentiation of circulating white blood cells is often described as a "leukemic" transformation. Whether or not such "leukemic" transformations in the course of PV are etiologically identical to clinically similar leukemias occurring without the prior presence of PV remains open to conjecture. Certainly the leukocytosis and splenomegaly occurring in PV patients with MM simulating chronic myelogenous leukemia (CML) appears to differ from that seen in classical CML. In the former the Philadelphia chromosome is generally absent and the leukocyte alkaline phosphatase is not depressed. Will future techniques demonstrate similar differences between the acute leukemia-like syndromes developing in PV and the more classical forms of AL?

In order to analyze the effect of radiation dose on the incidence of AL in PV it is important to define groups comparable with respect to age at onset, diagnosis, duration, and course but differing only in regard to radiation dose and presence or absence of AL. Ideally we would wish to pair patients in terms of comparable myelokinetics, but, unfortunately, the only readily defined "signposts" in the evolution of cell kinetics in PV are the development of significant splenic MM and the development of AL (2). Therefore we have classified our patients

Table 4. Significance of differences between values given in Tables 1, 2, and 3.*

Table #/category		ALw/MM	MM	Uncomplicated
1/Age at onset	AL	0.296	>0.400	0.045
	ALw/MM	-	0.291	<0.005
	MM		-	<0.005
1/Age at diagnosis	AL	0.210	0.375	0.041
	ALw/MM	-	0.251	<0.005
	MM	-	-	<0.005
1/Duration to death from onset	AL	0.271	>0.400	0.138
	ALw/MM	-	0.115	0.163
	MM	-	-	<0.005
1/Duration to death from dx.	AL	0.400	0.233	0.193
	ALw/MM	-	0.144	0.097
	MM	-	-	<0.005
2/Total dose (mCi)	AL	0.382	0.061	0.263
	ALw/MM	-	0.045	<0.400
	MM	-	-	<0.005
2/Duration to death from start of ^{32}P	AL	0.026	0.120	<0.005
	ALw/MM	-	0.120	>0.400
	MM	-	-	0.048
2/Total mCi-Months	AL	0.093	0.241	0.045
	ALw/MM	-	0.031	0.392
	MM	-	-	0.008
3/Total dose (R)	AL	0.022	0.015	0.222
	ALw/MM	-	0.232	0.024
	MM	-	-	0.025
3/Total R-Months	AL	0.166	0.052	0.400
	ALw/MM	-	0.320	0.109
	AL	-	-	0.025

*"P" values from students' "t" test are listed for comparisons between values in groups.

into groups dependent on the presence or absence of significant splenic MM or AL. The findings that patients who die without development of these hematologic complications were older at onset and diagnosis and lived for a shorter time interval than those who did develop MM or AL suggest that development of MM or AL is part of the natural history of PV and that, had these individuals who died without these "complications" survived sufficiently long with their disease, many of them would have developed these complications. Furthermore our results suggest that the usual hematologic progression in this disease involves development of significant splenic MM prior to the appearance of an acute leukemia-like syndrome, as evidenced by the high incidence of significant splenic MM in the patients with AL.

Presently available data indicate that in man the probability for development of leukemia is 1 to 2 per million exposed population per roentgen per year averaged over the time period of 1 to 15 years following radiation exposure (12). The subjects in such previous studies were not considered at risk during the first year following radiation exposure. In the present series

the average exposure dose times the total months at risk subsequent to a given dose of radiation was 44,852 R-months for all groups studied. This is equivalent to 3,738 R-years. Multiplying this radiation exposure by 1 to 2 times 10^{-6} per R per year yields an expected incidence of leukemia from radiation exposure alone in the present series of approximately 0.37% to 0.74%, as opposed to 14% actually observed. One should note that in the present series the patient was considered to be at risk from leukemia immediately after a given radiation exposure, and thus this calculated incidence of radiation-induced leukemia for our patients would be expected to be a high estimate. Since the observed incidence of AL in this series of PV patients treated with radiation was roughly 20 to 40 times that expected in other nonpolycythemic groups within the population exposed to ionizing radiation, one must conclude either that the appearance of acute leukemia-like states in patients with PV is relatively independent of radiation dose or that patients with PV are more highly susceptible to radiation-induced acute leukemia-like states than other members of the population. [Similar findings have been previously reported by Osgood (13).]

If this latter were the case then one would expect that those patients dying with an acute leukemia-like state would have larger values of the product, radiation dose times months at risk, than comparable patients who failed to develop an acute leukemia-like state.* In this series such was not the case. Indeed, the group which received the highest radiation dose was those patients who developed significant splenic myeloid metaplasia prior to death but failed to develop "acute leukemia." These patients also had the longest survival from onset or diagnosis of any of the remaining three groups. It has been known for many years that myeloid metaplasia is a frequent complication of PV (1, 2). It is also noteworthy that in recent years increasing numbers of cases with acute leukemia have been observed among PV patients who did not receive ^{32}P or X-ray therapy but were managed with chemotherapeutic agents.

---

*For a group homogeneous with respect to survival time and susceptibility of AL development from radiation exposure but differing with respect to radiation dose, let: D_i equal the value of "equivalent R" exposure times time at risk defining the ith group; N_i equal the number of subjects in the ith group; P equal the fractional probability of AL development per equivalent R exposure per unit time at risk. Average radiation exposure times time at risk (R) for all patients in the group is equal to

$$\sum_i N_i D_i / \sum_i N_i. \qquad (1)$$

Average radiation exposure times time at risk for patients in groups not developing AL is equal to

$$(\sum_i N_i D_i - P \sum_i N_i D_i^2)/(\sum_i N_i - P \sum_i N_i D_i). \qquad (2)$$

It is clear the first term in the numerator and the first term in the denominator in Eq. 2 are identical to the numerator and denominator, respectively, in Eq. 1. Since D_i has integer values greater than one it is also clear that $\Sigma_i N_i D_i^2 > \Sigma_i N_i D_i$. Thus, Eq. 2 yields values smaller than Eq. 1. Consequently, the average radiation exposure times time at risk for patients failing to develop AL must be lower than the values obtained for the entire group. (Note that this simplified argument applies only when development of AL does not influence survival, as is the case in the present study in comparing patients having MM with those having AL and MM.)

SUMMARY

Since the initial use of $^{32}PO_4$ in our clinic for the treatment of polycythemia vera (PV) in 1936 we have followed to termination 181 cases of PV treated with ^{32}P or with ^{32}P and X ray. Of these, 45/181 (25%) developed significant splenic myeloid metaplasia and 26/181 (14%) developed an acute myelogenous leukemia-like state. Sixteen cases had both "acute leukemia" (AL) and significant splenic myelopoiesis or myeloid metaplasia (MM) (i.e., 16/45 or 36% of all cases with MM developed AL), and 10 cases had only "acute leukemia" but no significant splenic myeloid metaplasia (i.e., 10/136 or 7% of all cases without MM developed AL).

Patients who failed to develop MM or AL or both were older at the time of onset and diagnosis and failed to survive as long as those who did develop MM or AL or both. The survival of patients who developed "acute leukemia" (AL) was not significantly different from that of patients who died with significant myeloid metaplasia (MM) alone.

The largest values of overall radiation exposure (both ^{32}P and X ray) times time at risk were received by patients dying with splenic MM alone.

The overall incidence of AL in this series of patients with polycythemia vera is 20-40 times that expected for a population of "normal human subjects" exposed to similar radiation doses and times at risk.

These data are consistent with the hypotheses: that development of significant splenic myeloid metaplasia (MM) and acute leukemia-like states (AL) are part of the evolutionary history of PV; that MM usually precedes the appearance of AL; that the incidence of AL in our patients treated with ^{32}P is primarily a result of prolonged survival rather than of radiation dose.

REFERENCES

1. Lawrence, J. H.: Polycythemia. Physiology, diagnosis and treatment based on 303 cases (Modern Medical Monograph). New York and London, Grune and Stratton, 1955.
2. Wasserman, L. R.: Polycythemia vera--its course and treatment: relation to myeloid metaplasia and leukemia. Bull. N. Y. Acad. Med. 30: 343 (1954).
3. Modan, B.; and Lilienfeld, A. M.: Polycythemia vera and leukemia--the role of radiation treatment. Medicine 44 [4]: 305 (1965).
4. Perkins, J.; Israels, M. C. G.; and Wilkinson, J. F.: Polycythemia vera: clinical studies on a series of 127 patients managed without radiation therapy. Quart. J. Med. New Series 33 [132]: 499 (1964).
5. Court Brown, W. M.; and Abbott, J. D.: The incidence of leukemia in ankylosing spondylitis treated with X-rays. Lancet 1: 1283 (1955).
6. Folley, J. H.; Borges, W.; and Yamawaki, T.: Incidence of leukemia in survivors of the atomic bomb in Hiroshima and Nagasaki, Japan. Am. J. Med. 13: 311 (1952).
7. Erf, L. A.; and Lawrence, J. H.: Clinical studies with the aid of radio-phosphorus. III. The absorption and distribution of radio-phosphorus in the blood of, its excretion by and its therapeutic effect on patients with polycythemia vera. Ann. Intern. Med. 15: 276 (1941).

8. Berlin, N. I.; Lawrence, J. H.; and Gartland, J.: Blood volume in polycythemia as determined by ^{32}P-labeled red blood cells. Am. J. Med. 9: 747 (1950).
9. Osgood, E. E.: The relative dosage required of total body X ray vs. intravenous ^{32}P for equal effectiveness against leukemic cells of the lymphatic series or granulocytic series in chronic leukemia. J. Nucl. Med. 6: 421 (1965).
10. Pollycove, M.; Winchell, H. S.; and Lawrence, J. H.: Classification and evolution of patterns of erythropoiesis in polycythemia vera as studied by iron kinetics. Blood 28 [6]: 807 (1966).
11. Van Dyke, D.; Lawrence, J. H.; and Anger, H. O.: Whole body marrow distribution studies in polycythemia vera. Battelle-Northwest Symposium on Myeloproliferative Disorders in Animals and Man, 1968 (in press).
12. Cronkite, E. P.; Moloney, W.; and Bond, V. P.: Radiation leukemogenesis. Am. J. Med. 28: 673 (1960).
13. Osgood, E. E.: Contrasting incidence of acute monocytic and granulocytic leukemias in ^{32}P-treated patients with polycythemia vera and chronic lymphocytic leukemia. J. Lab. Clin. Med. 64 [3]: 560 (1964).

Whole Body Scanning of ^{59}Fe in Evaluation of Body Distribution of Erythropoietic Marrow, Splenic Sequestration of Red Cells and Hepatic Deposition of Iron

Peter Ronai, H. Saul Winchell, Hal O. Anger and John H. Lawrence

The technique of iron kinetics analysis was pioneered at the Donner Laboratory by Huff and co-workers (3, 4) and developed into a detailed multicompartmental analysis by Pollycove and Mortimer (5). The technique presently used at this Laboratory involves analysis of plasma disappearance and erythrocyte incorporation of radioiron by repeated blood sampling, and determination of sites of erythropoiesis and iron storage by external monitoring of counting rates over spleen, liver, sacrum, and thigh. This procedure alone does not provide information concerning the body distribution of erythropoietic marrow.

In vivo marrow distribution has been determined by Anger and Van Dyke (2) and by Van Dyke and co-workers (6, 7) using ^{52}Fe and the Anger positron camera. Unfortunately, neither ^{52}Fe nor the positron camera is generally available. In any case, the rapid decay of ^{52}Fe makes the latter technique unsuitable for determination of sites of sequestration of newly formed red cells. Further, the Anger gamma camera, which is now in use in many centers, is unsuitable for imaging the readily available ^{59}Fe, while rectilinear scanning with ^{59}Fe is limited by the time involved in scanning the entire body.

A simple, rapid-imaging whole body scanner has recently been devised and built by Anger in this Laboratory (1). The study reported here demonstrates that, with ^{59}Fe and the whole body scanner, it is possible not only to determine the distribution of erythropoietic marrow but also to evaluate sites of sequestration of newly formed red cells, to detect the deposition of plasma iron in hepatic stores, and in general to check the accuracy of external monitoring data obtained during iron kinetics analysis.

MATERIALS AND METHODS

Patients reported in this study attended the Donner Clinic for initial iron kinetics studies and then returned at intervals for follow-up. Iron kinetics studies were performed according to the technique of Pollycove and Mortimer (5) and Pollycove, Winchell and Lawrence (8). The Anger Mark II whole body scanner (Fig. 1) has been reported elsewhere (1). Eleven-minute whole body scans were performed at 24 hours and 2 weeks after ^{59}Fe injection (Fig. 2).

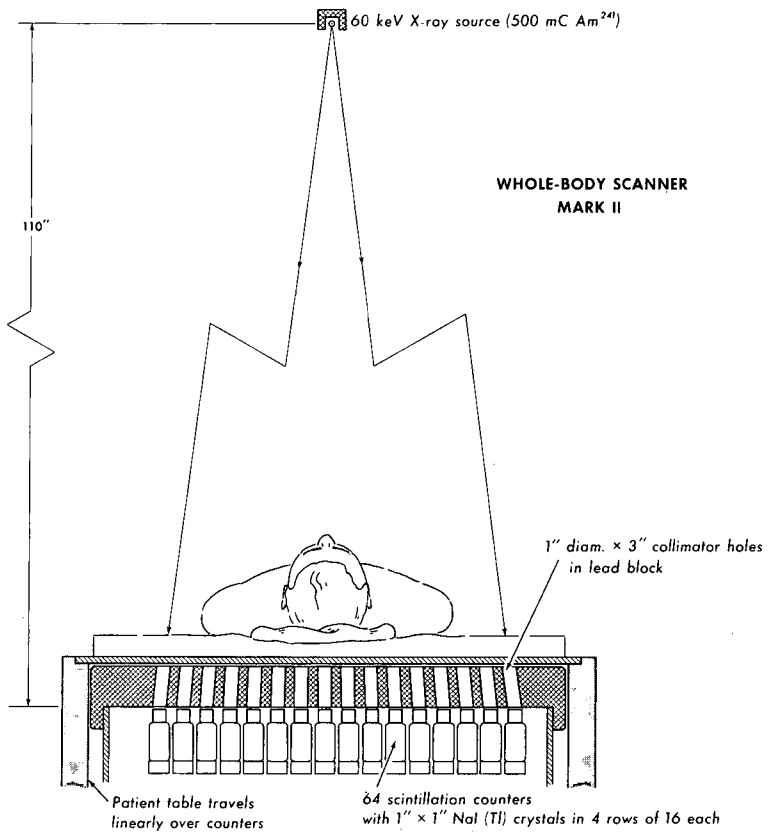

Fig. 1. The Anger whole body scanner Mark II. The patient traverses over a fixed array of 64 scintillation counters each with a 1-inch-diameter by 1-inch-thick sodium iodide crystal. Each counter has a single-channel collimator aimed upward towards an ^{241}Am source located 10 feet above.
MUB-12492

RESULTS

Case 1 (Fig. 3). Peripheral extension of erythropoietic marrow and splenic sequestration of red cells

A 14-year-old white female with a history of cystic fibrosis and resultant chronic pulmonary and hepatic disease was referred for evaluation of progressive anemia. Physical examination revealed advanced pulmonary emphysema and hepatosplenomegaly of approximately 4 cm. Initial hemoglobin was 8.8 grams % with a hematocrit of 29.5%, a slightly subnormal MCHC, and a reticulocyte count of 7.4%. There was mild thrombocytopenia and a white cell count of 6,700. Iron kinetics study showed (Fig. 3a) markedly increased erythropoiesis with initial uptake of radioiron in sacral marrow and subsequent complete release. However, maximum sacral counting rate was subnormal. There was a marked secondary increase in counting rate over the spleen consistent with splenic sequestration of red cells. Whole body scan at 24 hours after radioiron administration (Fig. 3b) showed extension of erythropoietic marrow into distal humeri, distal femora, and proximal and distal tibiae. The low sacral counting rate and the results of the 24-hour scan indicate that major erythropoiesis was occurring in peripheral

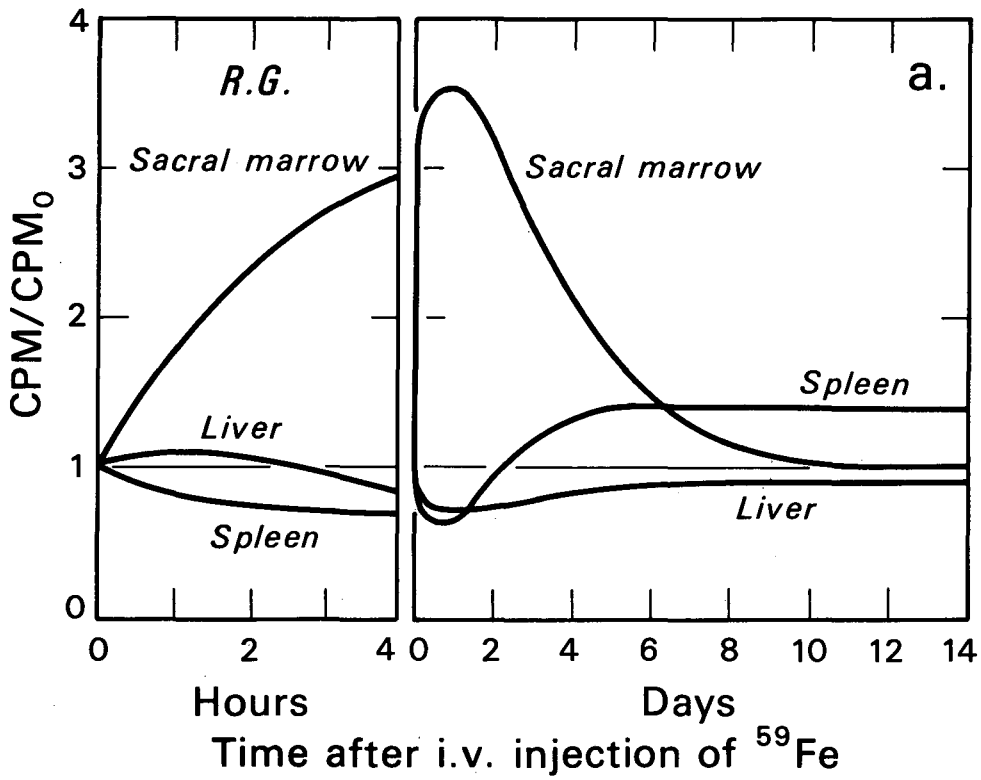

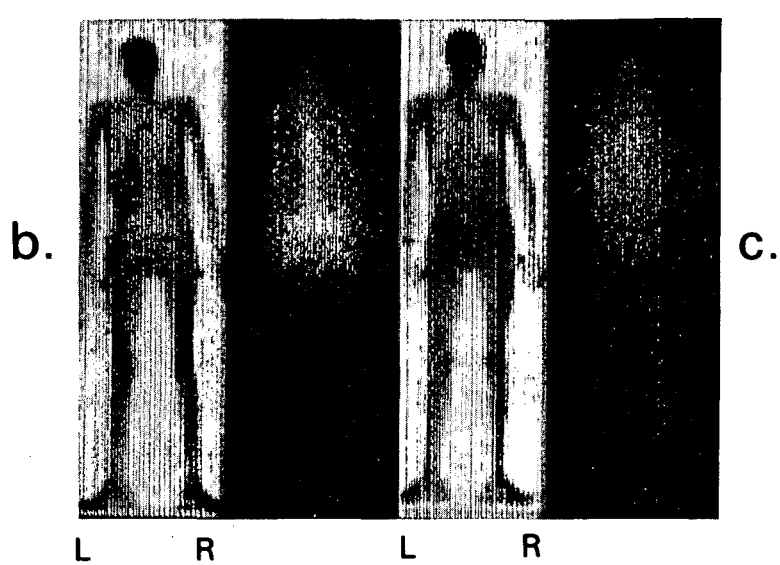

Fig. 2. Whole body scans (posterior views) at 24 hours and 2 weeks after radioiron administration in a patient with endogenous hemochromatosis after depletion of iron stores by phlebotomy. Distribution of radioiron is essentially normal save for minimal splenic red cell sequestration. Figure on the left in both 2a and 2b is ^{241}Am transmission picture to show the body outline. In this and subsequent figures external monitoring curves obtained during iron kinetics analysis are shown above the whole body scans.

XBB683-1405

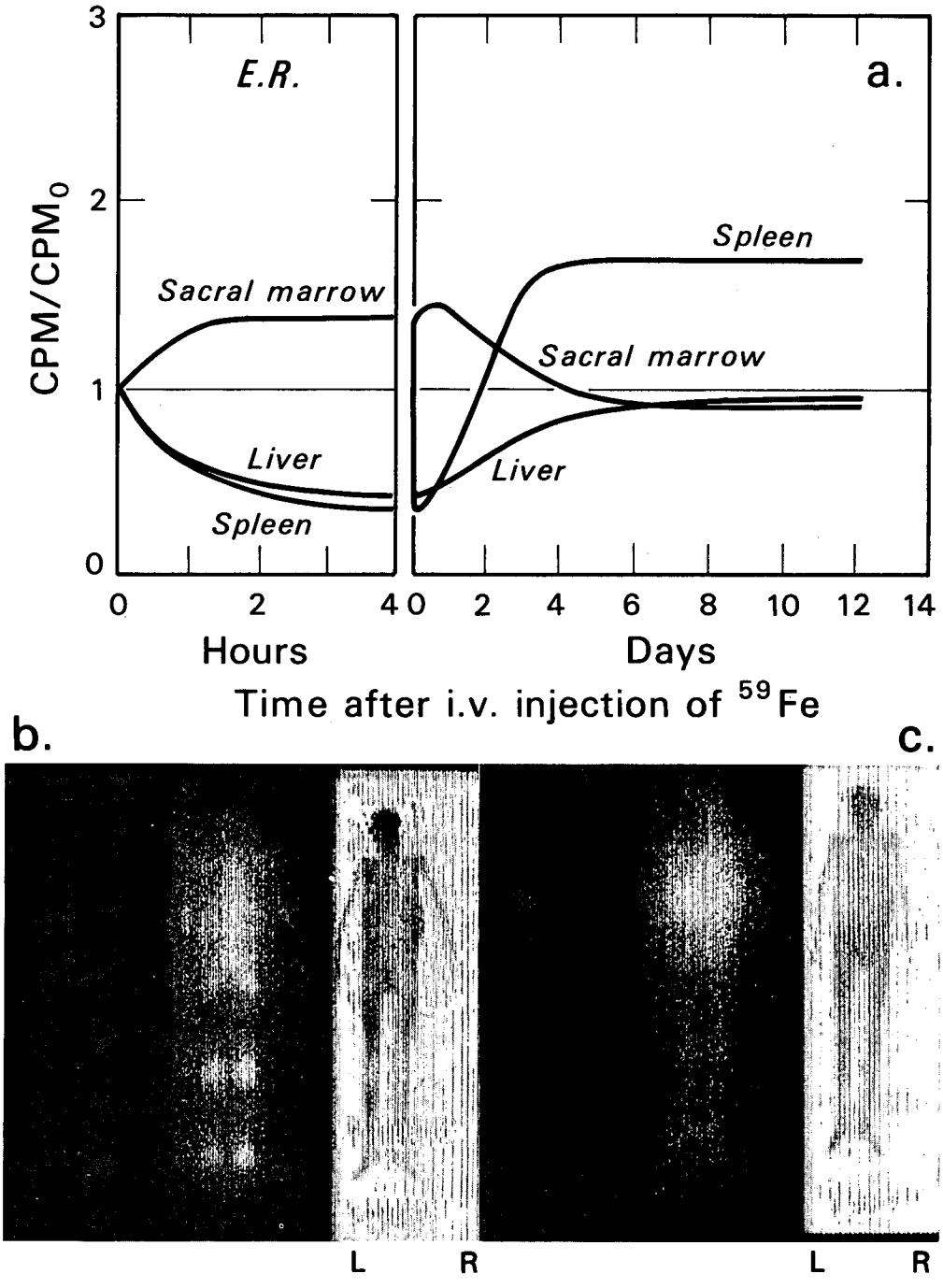

Fig. 3. (Case 1.) Whole body scans (posterior views) to show peripheral extension of erythropoietic marrow and splenic sequestration of red cells in a 14-year-old girl with cystic fibrosis.

In these and subsequent scans the figure on the right in each case represents the ^{241}Am body outline and the remaining figures are varying exposures of the ^{59}Fe emission scan.

XBB683-1406

marrow sites. Whole body scan at 2 weeks after radioiron administration (Fig. 3c) confirmed the marked splenic sequestration of red cells.

Case 2 (Fig. 4). Loss of erythropoietic bone marrow and myeloid metaplasia in spleen with splenic sequestration of red cells

A 56-year-old Swedish man showed increasing fatigue and exertional dyspnea. On physical examination, pallor and gross splenomegaly were discovered. Hemoglobin was 7 grams %, hematocrit 28%, white cell count 11,400, platelets 52,000, reticulocytes 3%. Anisopoikilocytosis and some tear-drop-shaped red cells were noted. There were circulating normoblasts and myelocytes. The reticulocytosis suggested the possibility that splenic sequestration of red cells was in excess of splenic erythropoiesis.

Iron kinetics study showed (Fig. 4a) very little accumulation of radioiron in the sacrum. Primary accumulation of radioiron occurred in the spleen and liver. There was only a modest release of radioiron from the spleen and additional secondary accumulation in the liver.

Whole body scan (Fig. 4b) showed that although erythropoiesis was absent from the pelvis, erythropoiesis in the vertebral bodies was preserved. There was no evidence of marrow development in peripheral sites. Whole body scan (Fig. 4c) also confirmed minimal net release of radioiron from the spleen, indicating that splenic sequestration of red cells almost matched splenic erythropoiesis. Primary hepatic deposition of radioiron and secondary hepatic accumulation as tagged red cells appeared in the circulation were also confirmed.

Case 3 (Fig. 5). Moderate peripheral extension of erythropoietic marrow without central loss associated with both intramedullary hemolysis and mild splenic sequestration of red cells, plus primary storage deposition of iron in liver and spleen

A 69-year-old white male showed anemia of at least 6 years' duration previously characterized as chronic refractory sideroblastic anemia unresponsive to therapy with pyridoxine, parenteral iron (1800 mg), folic acid, folinic acid, and vitamin B12. Marrow aspirate showed sideroblastic erythroid hyperplasia. Liver and spleen were both enlarged 5 cm below the costal margins, hemoglobin was 10.2 grams %, hematocrit 30%, reticulocytes 7%. Red cell indices were normal. External monitoring (Fig. 5a) during iron kinetics study showed initial accumulation of radioiron in the sacrum with subsequent incomplete release, suggesting a degree of intramedullary hemolysis. The characteristic decrease in counting rate over the spleen during the first few days after radioiron administration was not seen. Counting rate over the liver also failed to decrease significantly during the first day. These findings suggested some early iron deposition by increased storage exchange in spleen and liver. In addition a subsequent mild increase in counting rate over the spleen indicated some splenic sequestration of red cells. Whole body scan at 24 hours (Fig. 5b) showed initial deposition of iron in central marrow as well as peripherally in the distal femora and tibiae. There was also early deposition in liver and spleen, confirming the external monitoring data. The 2-week scan (Fig. 5c) showed further iron accumulation in the spleen and incomplete marrow release,

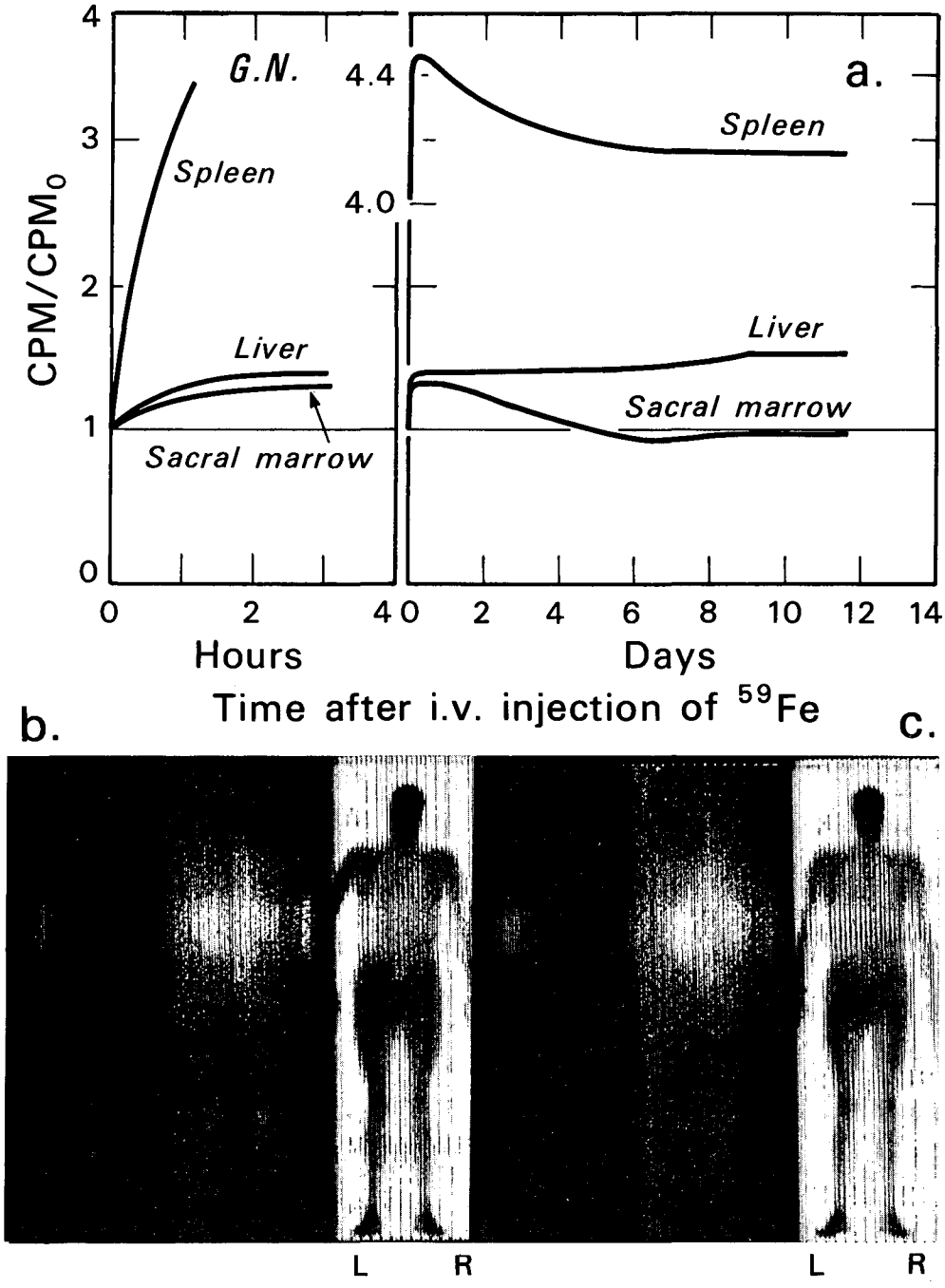

Fig. 4. (Case 2.) Whole body scans (posterior views) to show loss of erythropoietic marrow and myeloid metaplasia in spleen, with splenic sequestration of red cells. The patient was a 56-year-old man with a diagnosis of "myelofibrosis."

XBB683-1404

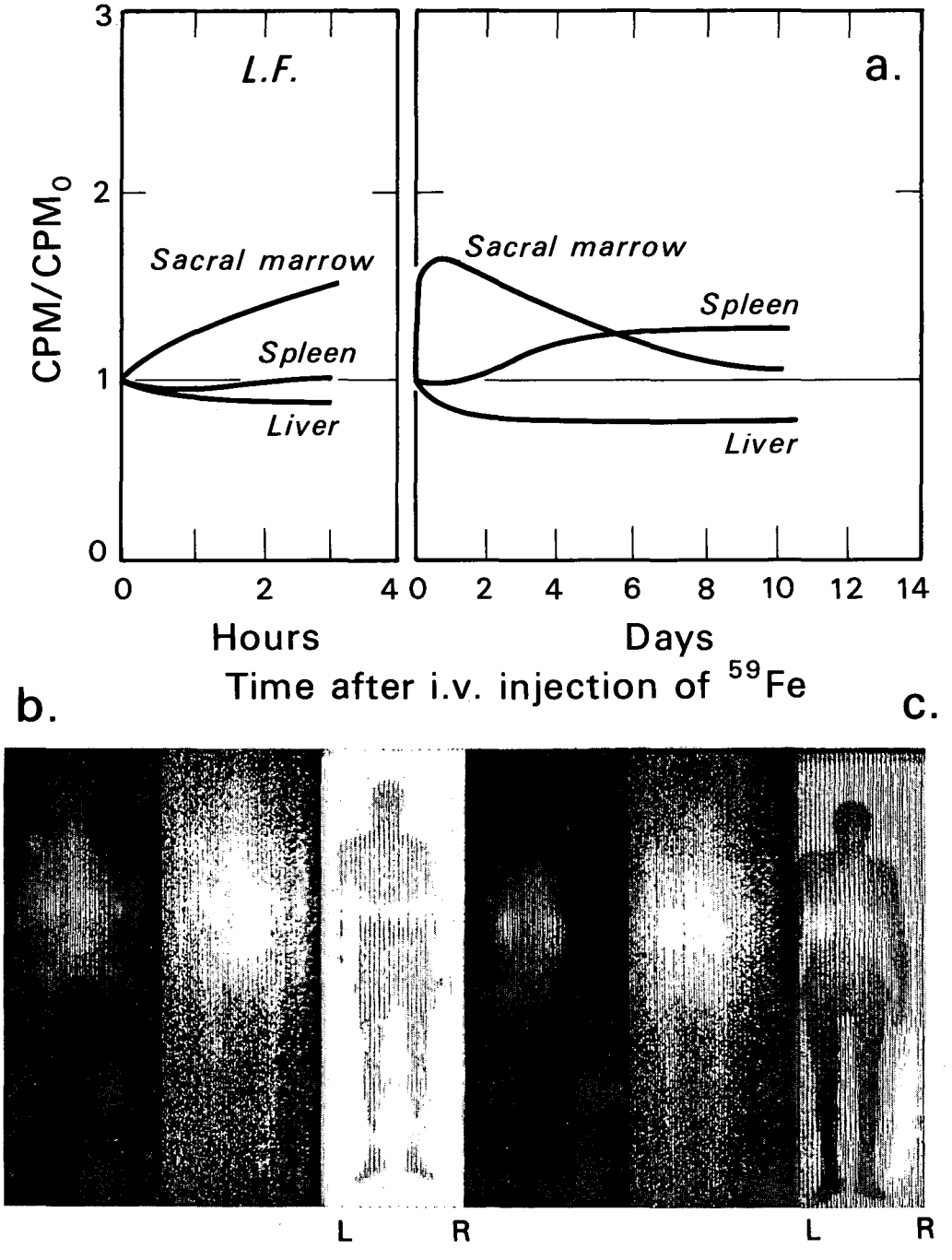

Fig. 5. (Case 3.) Whole body scans (posterior views) to show moderate peripheral extension of erythropoietic marrow without central loss associated with both intramedullary hemolysis and mild splenic sequestration of red cells plus primary storage deposition of iron in liver and spleen. The patient was a 69-year-old man with chronic refractory sideroblastic anemia.

XBB683-1407

confirming the impression of mild splenic sequestration of red cells and of intramedullary hemolysis as suggested by the iron kinetics analysis.

Case 4 (Fig. 6). Fanconi's anemia with normal juvenile distribution of erythropoietic marrow and ambiguous hepatic radioiron deposition

A 9-year-old white female had recent onset of pancytopenia prior to referral to the Donner Clinic. She had two brothers who died in childhood with characteristic Fanconi's anemia, and an additional sibling who died soon after birth with multiple congenital defects. Initial physical examination was unremarkable except for occasional café-au-lait spots and generalized sallow complexion. Hemoglobin was 6.7 grams %, hematocrit 18%, reticulocytes 3.4%. Peripheral blood smear showed macrocytosis and an occasional nucleated red cell. The platelet count was 35,000, and the white cell count 2,500, consisting mainly of mature lymphocytes. Analysis of external counting rate changes during the course of iron kinetics study (Fig. 6a) showed sacral marrow uptake and release of radioiron, and an apparent secondary accumulation of iron in the liver. There was no evidence of secondary iron accumulation in the spleen. This suggested the unusual situation of hepatic sequestration of red cells without concomitant splenic sequestration. Whole body scanning at 24 hours (Fig. 6b) demonstrated primary radioiron accumulation in both central (vertebrae and pelvis) and peripheral (distal femora and proximal tibiae) marrow sites. This is probably within normal limits for a child of this age (7). There was also significant primary accumulation in the liver which had not been detected by external counting rate measurements. There was further accumulation of iron in the liver in the 2-week scan (Fig. 6c). Thus the whole body scans demonstrate initial iron deposition in hepatic stores and a secondary increase in hepatic radioactivity resulting from circulating newly formed labeled red cells within the liver. The spuriously low external count rate over the liver in the early phase of the external monitoring study may have been due to error in zero-time extrapolation of the hepatic count-rate curve or to errors in positioning the hepatic probes.

Case 5 (Fig. 7). Combined intramedullary hemolysis with splenic and hepatic sequestration of red cells

A 21-year-old white male was first seen in this Laboratory in 1959 at the age of 12 years to evaluate a mild anemia present since birth. Iron kinetics study in 1959 showed increased hemoglobin synthesis rate with marked intramedullary hemolysis. Although fetal hemoglobin was elevated, hemoglobin A_2 was within normal limits and the patient's red cell morphology was not characteristic of thalassemia. The patient was scheduled to undergo cholecystectomy for bilirubin stones secondary to his hemolytic process, and the advisability of splenectomy at this operation was considered. An iron kinetics study was therefore performed in August 1967 to evaluate the degree of splenic sequestration of red cells. At that time he had a hemoglobin of 11.5 grams %, a hematocrit of 33%, a reticulocyte count of 4.2%, and normal red cell indices. The iron kinetics study demonstrated a hemoglobin synthesis four to five times normal. There was an initial accumulation of radioiron in the sacrum (Fig. 7a) with incomplete subsequent release as seen with intramedullary hemolysis. There was a mild secondary rise in counting rate over the spleen, indicating some splenic sequestration of red cells. However, the counting rate over the liver approached the zero-time extrapolate counting rate despite a maximum incorporation of radioiron into red cells of only 20%. This suggested hepatic sequestration of

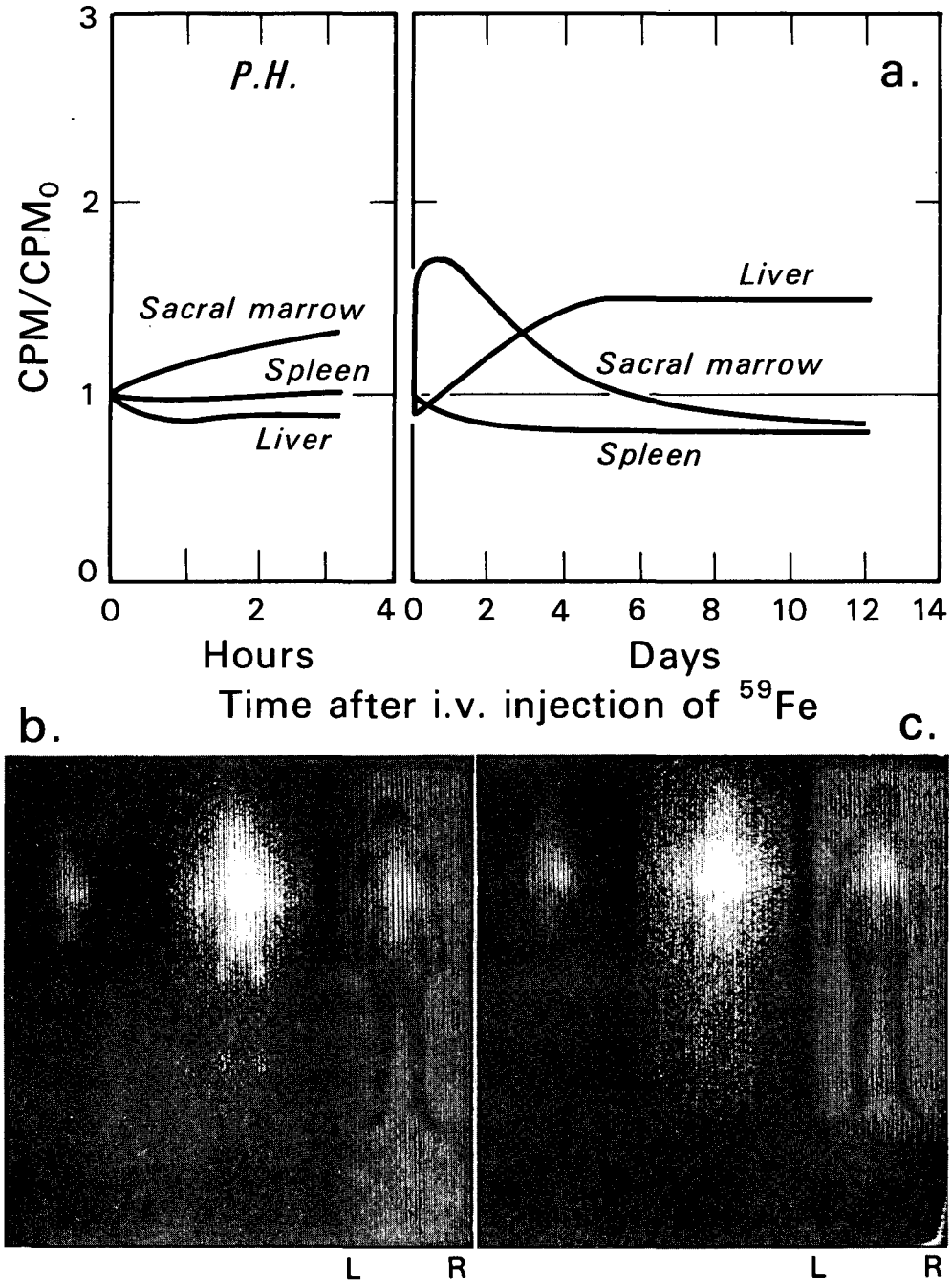

Fig. 6. (Case 4.) Whole body scans (posterior views) to show normal juvenile distribution of erythropoietic marrow and hepatic radioiron deposition in a 9-year-old girl with Fanconi's anemia.

XBB683-1408

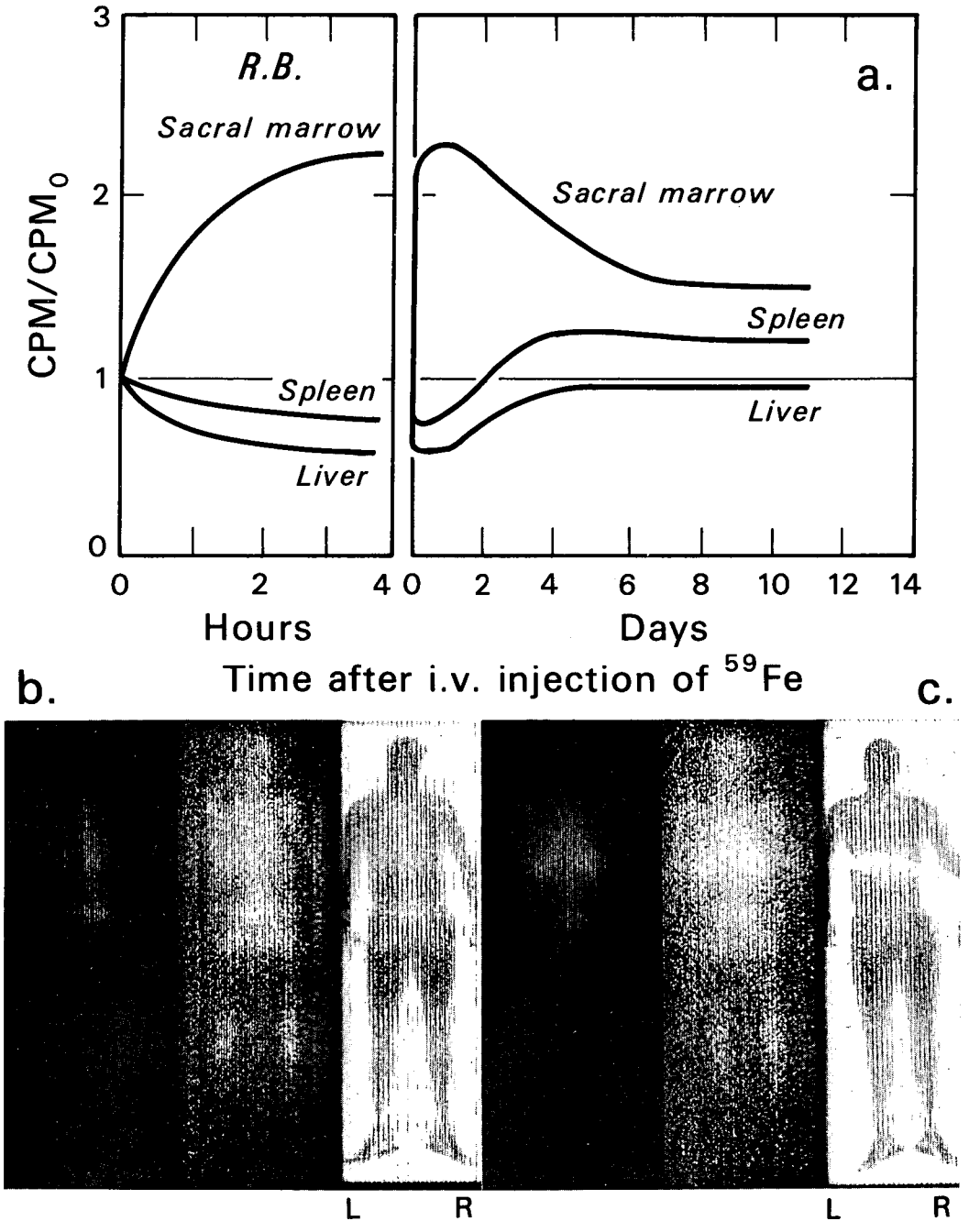

Fig. 7. (Case 5.) Whole body scans (posterior views) to show intramedullary, splenic, and hepatic sequestration of red cells in a 21-year-old man with a congenital hemolytic anemia

XBB683-1409

red cells, although an artifactual rise in liver activity due to intrusion of the vertebral marrow or the enlarged spleen into the field of view of the liver probe needed to be ruled out. A whole body scan (Fig. 7b) 24 hours after radioiron injection showed extension of marrow into the distal femora and proximal tibiae. The 2-week scan (Fig. 7c) demonstrated significant marrow retention of iron and secondary accumulation of iron in both liver and spleen (compare liver activity with that of heart). This confirmed the splenic and hepatic sequestration of red cells as well as intramedullary destruction. Removal of the spleen alone appeared unlikely to produce significant clinical improvement.

DISCUSSION

Erythropoietic sites are characterized by initial accumulation of radioiron with subsequent release, as newly formed labeled cells are introduced into the circulation. This is determined from external counting-rate measurements by characteristic curves (5). Radioiron deposition in hepatic iron stores is characterized by a primary accumulation in the liver with no significant release over the ensuing 2-week period. In rare cases, rapid turnover of hepatic iron stores can result in a pattern of rapid initial uptake associated with rapid release within the first 24 hours. Thus, in general, erythropoietic sites can be identified, by using whole body scan data, as those areas which show initial uptake in the 24-hour scan and subsequent release with absent activity in the 2-week scan. When there is localized sequestration of red cells, the 2-week scan demonstrates this as accumulation of activity over the site of sequestration (spleen and liver in peripheral sequestration, and marrow in intramedullary sequestration).

As previously demonstrated with ^{52}Fe (2, 6, 7), the normal human adult has evidence of erythropoiesis limited to the proximal skeleton (vertebrae, pelvis, proximal femora, and proximal humeri). Abnormal distribution of erythropoietic marrow is demonstrated in Cases 1, 2, 3, and 5.

When there is a loss of central marrow (Case 2), there is diminished activity in the vertebrae and pelvis in the 24-hour scan. In the presence of myeloid metaplasia, there is an initial accumulation of radioiron in the spleen (and occasionally liver) seen in the 24-hour scan followed by a secondary loss of radioactivity from these sites as ^{59}Fe-containing red cells are released into the circulation (Case 2). A delayed accumulation of radioiron in the spleen or liver detected in the 2-week scan indicates splenic or hepatic sequestration of red cells (Cases 1, 2, and 5), and absence of the secondary fall in marrow activity in the 2-week scan suggests intramedullary hemolysis (Cases 3 and 5). Much of this information can be obtained by examining the external monitoring curves. However, external monitoring curves are critically dependent on correct and reproducible positioning of the probes and also on accurate zero-time extrapolation on the plotted graph. Even when the probes are correctly and reproducibly positioned, the vertebral marrow intrudes into the fields of view of both hepatic and splenic probes. When there is splenomegaly the spleen may contribute significantly to the count rate at the hepatic probe. Similarly the liver may contribute significantly to the count rate at the splenic probe. There is therefore always an element of uncertainty in the external monitoring data. This may be compounded by errors in zero-time extrapolation. That these sources of error can sometimes lead to ambiguous data is demonstrated by Case 5, in which the most unusual

situation of hepatic sequestration of red cells without concomitant splenic sequestration was suggested by the external monitoring data. The whole body scan showed that there was significant primary accumulation of radioiron in the liver with some further accumulation at 2 weeks. The secondary accumulation could be accounted for simply by the appearance of labeled red cells in the hepatic intravascular compartment. The correct interpretation of the hepatic changes was therefore storage deposition rather than sequestration of labeled cells. In Case 5, where splenectomy was dependent on the results of the iron kinetics study, there was no room for any such ambiguity. Confirmation of the external monitoring data by the whole body scans was most reassuring in this case.

CONCLUSIONS

1. A simple, rapid imaging whole body scanner used in conjunction with ^{59}Fe has been found valuable in visualizing marrow distribution, determining sites of red cell sequestration, and evaluating hepatic storage iron deposition.

2. During the course of radioiron kinetics studies, whole body scanning serves as a useful check on the external monitoring activity curves, the accuracy of which is dependent on probe positioning and zero-time extrapolation. Such dependence occasionally results in ambiguities which can be resolved with the whole body scan.

ACKNOWLEDGMENTS

This work was supported in part under AEC Contract W-7405-eng-48; Peter Ronai's participation was supported by a Winston Churchill Memorial Fellowship.

We thank Natalia Kusubov, Rosanne Raley, Barbara Shipley and Dianne Honbo for their technical assistance in the performance of this work.

REFERENCES AND NOTE

1. Anger, H. O.: Whole body scanner Mark II. J. Nucl. Med. 7: 331-332 (1966) (abstract).
2. Anger, H. O.; and Van Dyke, D. C.: Human bone marrow distribution shown in vivo by iron-52 and the positron scintillation camera. Science 144: 1587-1589 (1964).
3. Huff, R. L.; Elmlinger, P. J.; Garcia, J. F.; Oda, J. M.; Cockrell, M. C.; and Lawrence, J. H.: Ferrokinetics in normal persons and in patients having various erythropoietic disorders. J. Clin. Invest. 30: 1512 (1951).
4. Huff, R. L.; Hennessy, T. G.; Austin, R. E.; Garcia, J. F.; Roberts, B. M.; and Lawrence, J. H.: Plasma and red cell iron turnover in normal subjects and in patients having various hematopoietic disorders. J. Clin. Invest. 29: 1041 (1950).
5. Pollycove, M.; and Mortimer, R.: The quantitative determination of iron kinetics and hemoglobin synthesis in human subjects. J. Clin. Invest. 40: 753-782 (1964).
6. Van Dyke, D.: Similarity in distribution of skeletal blood flow and erythropoietic marrow. Clin. Orthop. 52: 37-51 (1967).
7. Van Dyke, D.; Shkurkin, C.; Price, D.; Yano, Y.; and Anger, H. O.: Difference in distribution of erythropoietic and reticuloendothelial marrow in hematologic disease. Blood 30: 364-374 (1967).

8. Pollycove, M.; Winchell, H. S.; and Lawrence, J. H.: Classification and evaluation of patterns of erythropoiesis in polycythemia vera as studied by iron kinetics. Blood 28: 807-829 (1966).

Peter Ronai's present address is Division of Nuclear Medicine, Institute of Medical and Veterinary Science, Frome Road, Adelaide, South Australia, 5000.

Skeletal Survey for Metastatic Tumors of Bone Using ^{18}F and ^{85}Sr with Scintillation Camera and Whole Body Scanner

Peter Ronai, H. Saul Winchell and Hal O. Anger

Radioisotope scanning is able to detect metastatic lesions of bone before radiological changes or even clinical symptoms are present (6, 12, 13). In most centers, clinical symptoms and radiological changes are used as the basis of selection of sites for scanning. Clearly, this approach will fail to detect asymptomatic or radiologically negative lesions. The effective detection of bone metastases demands that the distribution of radioisotope in the entire skeleton be scrutinized. This is impractical with conventional rectilinear scanners because of the time involved. The count rate with strontium-85 is low because of dose limitations, and the scanning of even small areas can be a long and, for the patient, painful process. The short-lived radioisotopes ^{87m}Sr and ^{18}F can be given in relatively large doses, but even with the higher count rates provided by these isotopes, rectilinear scanning of the whole skeleton is not practical.

The concept of the radioisotopic skeletal survey was introduced by DeNardo, Horner, Leach, and Bowes (7), who used the profile scanner (11) to detect regions of abnormal activity after the administration of ^{85}Sr and a conventional rectilinear scanner to examine the abnormal areas in detail. Instead of a profile scanner, a rapid imaging whole body scanner has been used in this Laboratory to determine directly the skeletal distribution of ^{18}F and ^{85}Sr. This device allows direct visualization of areas of abnormal isotope uptake in the entire body in an 11-minute scan. Abnormal or suspicious areas on the whole body scan were then examined at high resolution with the positron-gamma scintillation camera.

The purpose of this paper is to show that with these two instruments, a radioisotopic survey of the entire skeleton can be a simple, rapid, and accurate procedure.

MATERIALS AND METHODS

A. RADIOCHEMICALS Each patient was studied with both ^{18}F and ^{85}Sr so that the efficacy of these two isotopes when used with the whole body scanner and scintillation camera could be compared. ^{18}F was prepared according to the method of Thomas, Sondel, and Kerns (15). It was administered carrier-free as sodium fluoride in physiological saline. ^{85}Sr was obtained from Squibb as strontium chloride in physiological saline with a specific activity of 9.15 mCi/mg.

B. INSTRUMENTATION Initial pictures of the distribution of each isotope were taken with the Mark II Whole Body Scanner. This instrument has been described in detail elsewhere

(2). Collimation was achieved with 64 half-inch-aperture straight-bore collimators. For more detailed pictures of abnormal areas the scintillation camera was used, operating in the positron coincidence mode for ^{18}F and in the gamma mode for ^{85}Sr. This instrument has also been described elsewhere (1). For ^{85}Sr a multichannel collimator with maximum design energy of 445 keV was used. This was the highest-energy collimator available but was not really adequate for the 514-keV γ rays of ^{85}Sr.

Patients were referred for the study because of known metastatic tumors of bone. The study was aimed at delineating known lesions and detecting previously unsuspected ones. Patients were given 500 μCi ^{18}F intravenously and the study was commenced 1 hour later. In the interval patients were given three glasses of water and asked to void twice, since urinary excretion accounts for approximately 50% of the injected activity and the bladder receives the highest radiation dose (16). When the ^{18}F study was completed, patients were given 100 μCi ^{85}Sr intravenously and asked to return in 3 days. During the interval the patients took two doses of a mild laxative and were given an enema on the morning of the strontium study.

The scanning procedure was the same for both radioisotopes. Eleven-minute whole body scans were taken. Only posterior views were taken in the early stages of the study until it was realized that anterior lesions were being missed. Thereafter both anterior and posterior 11-minute scans were performed. The patient was then moved to the scintillation camera and photos of pelvis, hips, vertebrae, and skull taken on each patient. Further photos were taken of any suspicious areas noted on the whole body scans. In the case of ^{18}F, photos of the pelvis were taken soon after the patient voided. Exposure times were 2-3 minutes for ^{18}F and 5-10 minutes for ^{85}Sr.

RESULTS

A summary of results in five patients is presented in Table 1.

Case 1

A 53-year-old white female was admitted to Highland hospital with a fracture of the right hip. A radical mastectomy had been performed 16 years previously for adenocarcinoma of the right breast. For 6 months before the present admission the patient experienced pain in the right hip and progressive weight loss. Roentgenogram of the right hip showed a pathological fracture of the right acetabulum, and biopsy of this area confirmed the presence of adenocarcinoma. A skeletal X-ray survey detected no other metastatic lesions and she was given radiation therapy to the right hip.

After the administration of ^{18}F, whole body scan and positron scintiphotos demonstrated the right hip lesion, and, in addition, areas of increased isotope uptake were seen in the region of the acromion process of the left scapula and in the right ankle (Figs. 1 a, e).

After the administration of ^{85}Sr, whole body scan and gamma scintiphotos detected the hip and shoulder lesions only (Figs. 1 c, f).

Table 1. Summary of scanning results

Case 1	X ray	^{18}F	^{85}Sr
R. hip	+	+	+
L. shoulder	+	+	+
R. ankle	-	+	-
Case 2			
L. tibia	-	+	+
L. ulna	-	+	-
R. ulna	-	+	-
Case 3			
spine	+	+	-*
pelvis	+	+	-*
L. femur	+	+	+
R. femur	+	+	+
ribs	+	+	-*
L. humerus	-	+	+
R. humerus	-	+	+
Case 4			
D 8	+	+	-
D 12	+	+	-
L. hip	-	+	+
L. 7th rib	+	+	+
R. 5th rib	-	+	+
L. scapula	-	+	-
R. scapula	-	+	-
Case 5			
D 11	+	+	-
D 12	+	+	+
L 3	+	+	-
L 5	-	+	-
L. femoral head	+	+	-
L. femoral shaft	-	+	-
R. acetabulum	-	+	-
R. femoral shaft	-	+	-

*Whole body scan only.

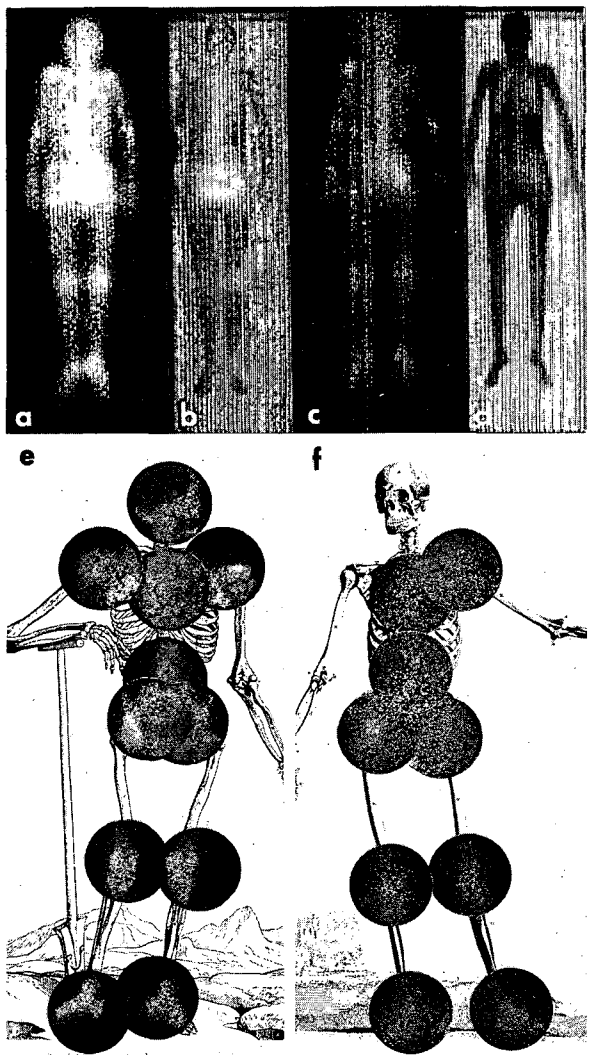

Fig. 1. (a-d) Metastatic breast carcinoma.

Whole body scans of Case 1 after ^{18}F (Fig. 1a) and ^{85}Sr (Fig. 1c). Transmission scans with ^{241}Am taken simultaneously (Figs. 1b, 1d) show the body outline. View is posterior in all cases. Patient's left is to the left of the page.

^{18}F scan: lesions in left shoulder and right hip. Central bright spot in pelvis is bladder. Right ankle shows greater uptake than left. Uptake in vicinity of large joints is greater than normal but symmetrical. Patient had suffered from arthritis for many years.

^{85}Sr scan: shows hip and shoulder lesions but not the increased uptake in the right ankle. Uptake at ends of long bones is normal for ^{85}Sr.

(e) Positron camera scintiphoto study of same patient (Case 1) after ^{18}F anterior view. Patient's left is to the right of the page. Left shoulder lesion is in acromion process. Right hip lesion is in acetabulum. Uptake in right ankle is diffusely distributed over lower tibia and bones of foot. Uptake in knees is greater than normal but is symmetrical.

(f) Gamma camera scintiphoto study of Case 1 after ^{85}Sr. Anterior view. Left shoulder lesion poorly seen. Lesion in right hip is unequivocal.

XBB682-863

Subsequent radiological studies of the left shoulder and right ankle demonstrated replacement of the acromion process of the left scapula by tumor and "degenerative changes" in the right ankle. Biopsy of the left shoulder lesion confirmed the presence of adenocarcinoma.

Case 2

A 54-year-old white male presented in October 1967 with chest pain and hemoptysis. Chest X ray showed carcinoma of the right lung. Skeletal X-ray survey was negative, but pain in the back prompted a ^{85}Sr rectilinear scan of the dorsal spine which gave equivocal results. At the time of the studies in this Laboratory back pain was no longer present.

The ^{18}F study (Figs. 2 a, e) failed to show a lesion in the spine. However, increased isotope uptake was seen in the proximal ends of both ulnae and in the left tibial tuberosity. Only the tibial lesion could be identified in the ^{85}Sr study (Figs. 2 c, f). Biopsy of the left tibial tuberosity showed osteoporosis with no evidence of neoplasm. This patient subsequently had resection of the carcinoma.

Case 3

A 60-year-old negro male was admitted to hospital complaining of frequency, nocturia, dysuria, and multiple aches and pains. On physical examination a small nodule was felt in the prostate and a hard enlarged lymph node in the neck. Biopsy of the lymph node showed adenocarcinoma and a skeletal X-ray survey demonstrated widespread metastatic involvement of the spine, pelvis, femora, and ribs.

^{18}F studies (Figs. 3 a, b, e) confirmed the extensive involvement of the spine, pelvis, femora, and ribs, and in addition detected lesions in the upper ends of both humeri.

In the ^{85}Sr whole body scans (Figs. 3 c, d) count rate was low and abnormal areas could not be identified with certainty. In the ^{85}Sr camera study (Fig. 3 f) lesions were seen in both shoulders and hips. Unfortunately the study had to be discontinued because of withdrawal of patient cooperation.

Case 4

A 55-year-old white female had a left radical mastectomy in 1955 for adenocarcinoma. In 1960 a local recurrence was treated by radiotherapy. In 1961 she developed pain in the right hip and left chest and lost 20 pounds weight. Skeletal X-ray survey detected a pathological fracture of the left 7th rib and metastases in the 8th and 12th dorsal vertebrae. She was given 18,600 rads of α-particle irradiation to the pituitary. An X-ray survey in 1967 showed healing of the rib fracture and little change in the vertebral lesions.

^{18}F studies (Figs. 4 a, b, e, f) showed areas of increased uptake in the 8th and 12th dorsal vertebrae, the left hip, the left 7th rib, the right 5th rib, and both scapulae. In the ^{85}Sr studies (Figs. 4 c, d, g, h) the left hip and rib lesions were seen but not the vertebral or scapular lesions.

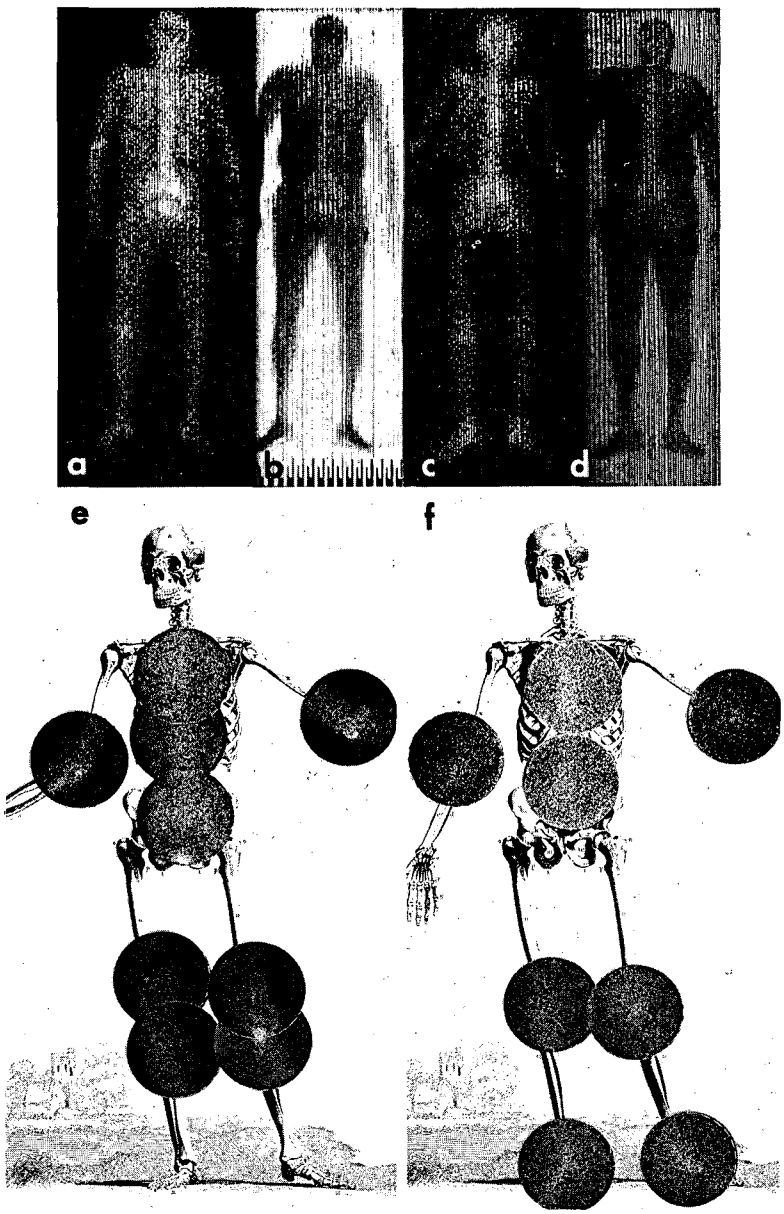

Fig. 2. (a-d) Pulmonary carcinoma.

Whole body scans of Case 2 after ^{18}F (Fig. 2a) and ^{85}Sr (Fig. 2c). Transmission scans taken simultaneously in each case (Figs. 1b, 1d) show the body outline.

View is posterior in all cases so that the patient's left is to the left of the page.

^{18}F scan: increased uptake in left elbow and left knee.

^{85}Sr scan: increased uptake in right elbow and left knee.

(e) ^{18}F camera scintiphotos: increased uptake in both ulnae and in left tibial tuberosity.

(f) ^{85}Sr camera scintiphotos: suggestion of increased uptake in left tibial tuberosity.

XBB682-861

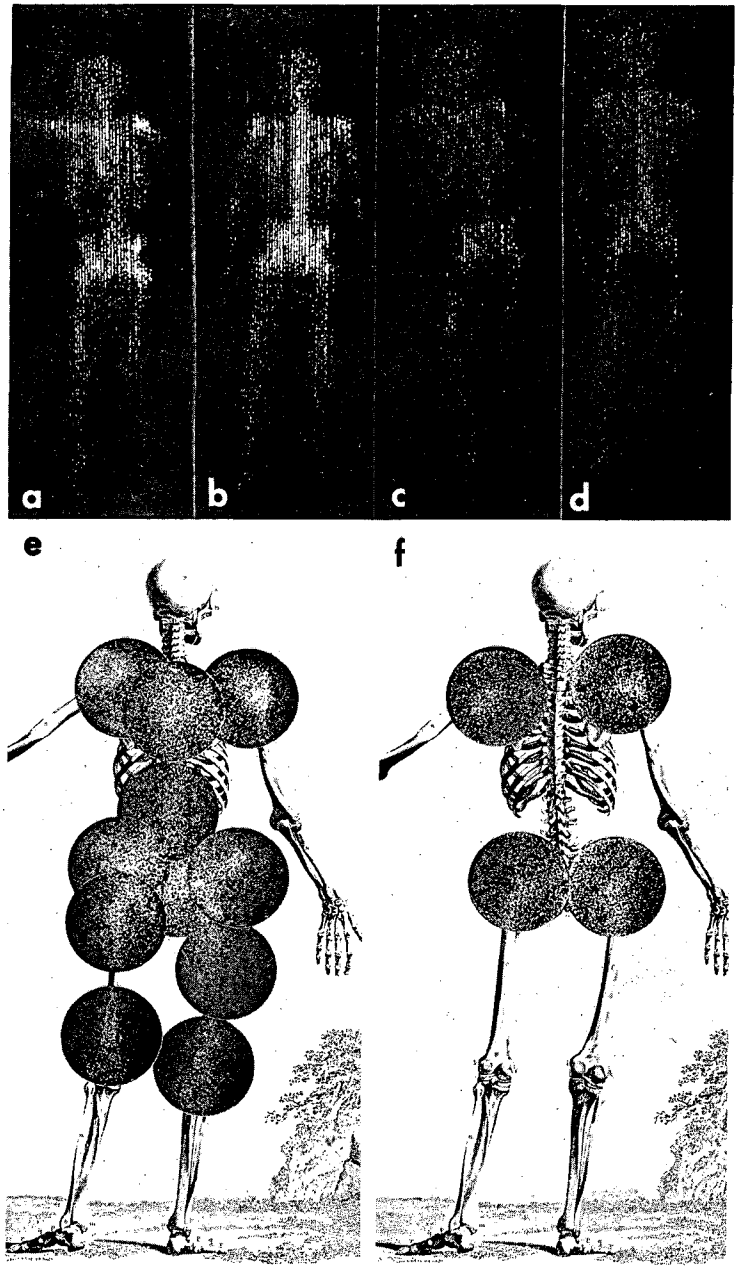

Fig. 3. (a-d) Metastatic prostatic carcinoma.

^{18}F anterior (Fig. 3a) and posterior (Fig. 3b) scans and ^{85}Sr anterior (Fig. 3c) and posterior (Fig. 3d) scans.

^{18}F scans: lesions in femora, pelvis, spine, ribs, and humeri.

^{85}Sr scans: no lesions can be identified with certainty.

(e) ^{18}F camera scintiphotos: widespread metastatic disease of skeleton confirmed. Lesions in femora, pelvis, dorsal spine, and both humeri.

(f) ^{85}Sr camera scintiphotos: study incomplete but lesions seen in both shoulders and both hips.

XBB682-862

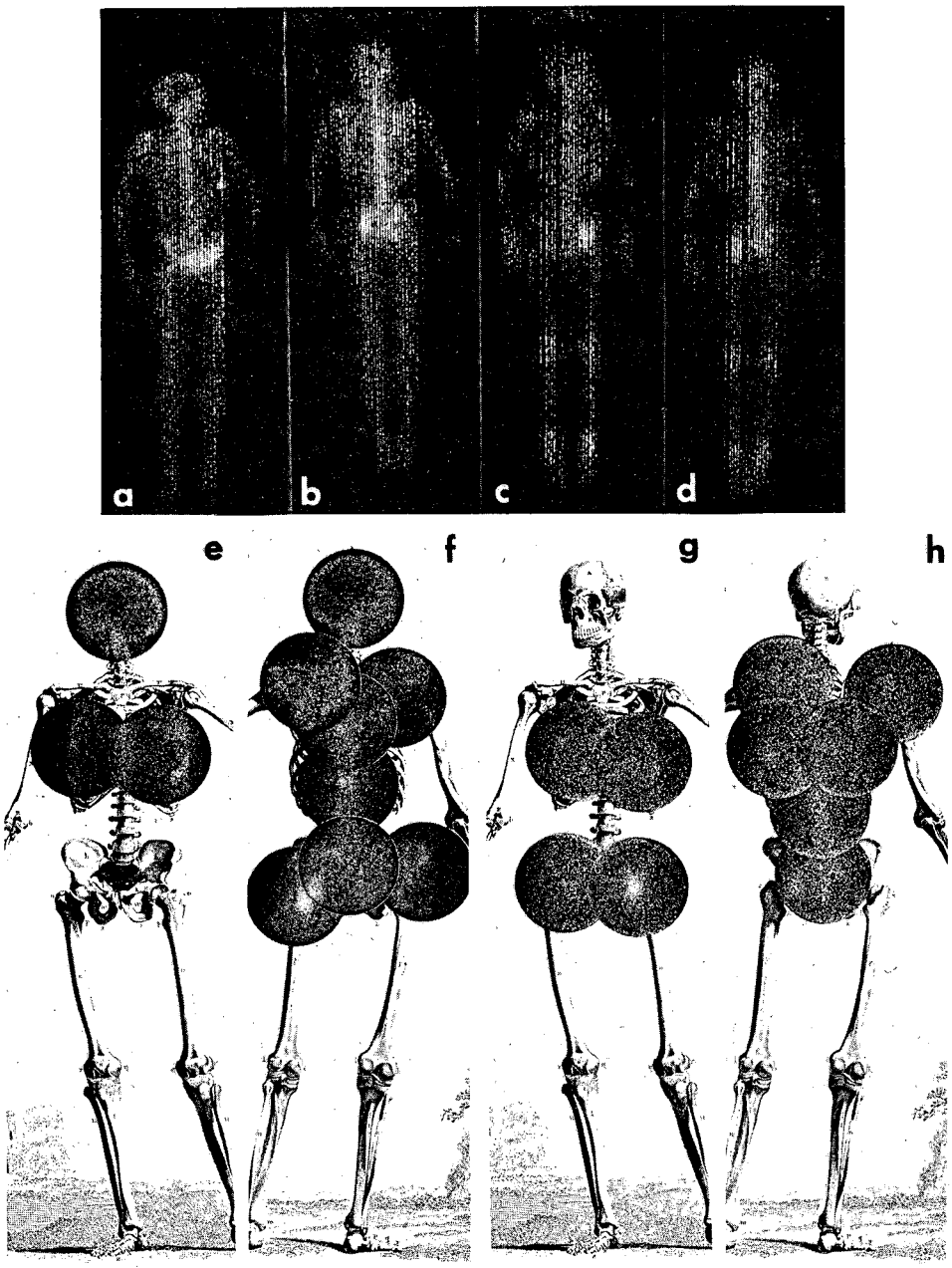

Fig. 4. (a-d) Metastatic breast carcinoma.

^{18}F anterior (Fig. 4a) and posterior (Fig. 4b) scans and ^{85}Sr anterior (Fig. 4c) and posterior (Fig. 4d) scans.

^{18}F scans: lesions in left hip, left chest, right shoulder.

^{85}Sr scans: lesion in left hip only.

(e, f) ^{18}F camera scintiphotos: lesions in left hip, dorsal spine (D8, D12), ribs on both sides of chest, and both shoulders.

(g, h) ^{85}Sr camera scintiphotos: lesions in left hip, ribs on both sides, and right shoulder.

XBB682-865

Case 5

A 46-year-old white female had a radical mastectomy for carcinoma of the left breast in 1963, at which time axillary nodes were found to be involved. In 1965 back pain prompted a skeletal X-ray survey which showed lesions in D11, D12, and L3 vertebrae and in the left femoral head. She was given 17,000 rads of α-particle irradiation to the pituitary, but back pain persisted and she lost weight. At the time of the isotope studies in February 1968 the radiological lesions were unchanged.

In the ^{18}F study (Figs. 5 a, b, e) areas of increased isotope uptake were seen in D11, D12, L3, and L5 vertebrae, in the right acetabulum and upper shaft of the right femur, and in the head and upper shaft of the left femur. The ^{85}Sr study (Figs. 5 c, d, f) showed a lesion only in the dorsal spine.

DISCUSSION

^{85}Sr decays by electron capture with 100% 0.51-MeV γ emission and associated X-ray emission characteristic of ^{85}Rb. Radiation dose to bone has been variously estimated at 1.5 rads/100 μCi (5), 2.3 rads/100 μCi (17), and 4.6 rads/100 μCi (4, 8). ^{18}F decays by 0.65-MeV positron emission with associated 0.51-MeV annihilation γ rays. Radiation dose to bone has been estimated at 0.23 rad/mCi (3) and to bladder at 0.5-1.0 rad/200 μCi (16).

Strontium is a cation and exchanges with calcium ions in the hydroxyapatite crystal, whereas fluoride is an anion and exchanges with hydroxide (10). It has been suggested that strontium uptake reflects osteoblastic activity (6) and fluoride uptake reflects bone blood flow (16). The quantity of an isotope in bone at any time is the net result of deposition rate and resorption rate. The deposition rate depends on vascular perfusion and on the fraction of the isotope cleared by the bone on a given passage of blood though the bone (extraction ratio). The deposition rate is therefore a measure of bone blood flow only when the extraction ratio is the same throughout the skeleton. This latter condition has not been proven for either ^{18}F or ^{85}Sr.

The rapid disappearance of ^{18}F from the blood and the slower disappearance of ^{85}Sr (9) cannot be taken as evidence that ^{18}F uptake measures bone blood flow while ^{85}Sr uptake measures osteoblastic activity. Like chloride, fluoride equilibrates rapidly with the extravascular fluid compartment, and the initial rapid clearance of fluoride from the blood really represents a mixing phase. The slower disappearance of ^{85}Sr from the blood is probably related to binding of strontium to plasma proteins (in much the same way as calcium is bound) and to the more rapid urinary excretion of fluoride. Behavior of the two isotopes at the bone level is in fact remarkably similar. Spencer, Herbert, Rish, and Little (14) found no difference in the concentration of strontium and fluoride in fractured and normal rat fibulae up to 3 hours after injection. French and McCready (9) found identically shaped uptake curves when ^{87m}Sr and ^{18}F were injected simultaneously and uptake into a femoral bone tumor was measured over half an hour.

Possibly the major difference between the distribution of the two isotopes in the skeleton in the present study relates to the fact that scans are taken 1 hour after ^{18}F administration

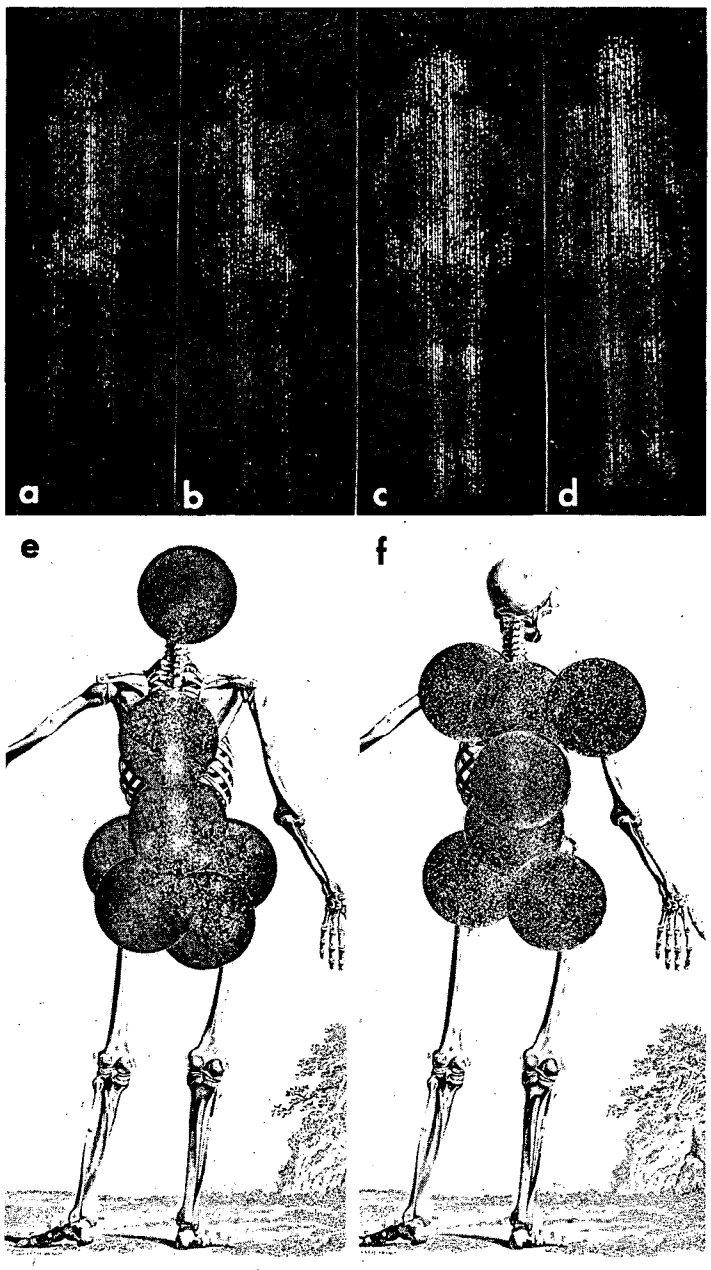

Fig. 5. (a-d) Metastatic breast carcinoma.

^{18}F anterior (Fig. 5a) and posterior (Fig. 5b) scans and ^{85}Sr anterior (Fig. 5c) and posterior (Fig. 5d) scans.

^{18}F scan: lesions in multiple areas of spine, right hip and upper femur, and left upper femur.

^{85}Sr scan: lesion in right hip only. Uptake in other joints normal for ^{85}Sr.

(e) ^{18}F scintiphotos: lesions in D11, D12, L3, L5, right acetabulum, right upper femur, left femoral head, and left upper femur.

(f) ^{85}Sr scintiphotos: lesion in D12 only.

XBB682-864

and 3 days after ^{85}Sr administration. If there were significant feedback of strontium from certain bone lesions into the blood, the distribution of ^{85}Sr could be considerably altered over 3 days. This could explain at least in part why some lesions visualized with ^{18}F are missed with ^{85}Sr and why scanning at 1 hour with ^{87m}Sr is more successful than at 3 days with ^{85}Sr (14).

Admittedly the ^{85}Sr scintiphotos were technically poor because the γ-ray energy of the isotope exceeded the design energy of the collimator. For this isotope, the whole body scanner or a special high energy rectilinear scanner would be the instrument of choice. However, a valid comparison of the two isotopes could be made in the whole body scans because the γ-ray energies were virtually identical and the same collimation method was used for both isotopes. In the whole body scans, fewer lesions were detected with ^{85}Sr than with ^{18}F. At least some of the additional lesions detected by ^{18}F were radiologically confirmed metastatic lesions (see Cases 3, 4, and 5).

This study also confirms the findings of others (6, 12, 13) that radioisotope scanning can detect bone metastases before X-ray changes are found. In Case 1 the left shoulder lesion was detected radiologically only in retrospect. In Case 3 the humeri were radiologically normal but strikingly positive in the ^{18}F scintiphotos. The same applies to the left hip lesion in Case 4 and the lesions in L5 and both femora in Case 5. Since increased ^{18}F uptake is seen in nonmetastatic lesions as well as metastatic lesions (16) it is possible that some of these radiologically negative lesions were nonmetastatic (e.g., the tibial lesion in Case 2). It seems most unlikely, however, that they were all nonmetastatic. In this particular study it was difficult to justify biopsying lesions in patients with known multiple metastases. In any case, fluorine-18 scanning and scintiphotography serve, not to make a definitive pathological diagnosis, but to indicate areas for careful radiological assessment and, if necessary, biopsy.

SUMMARY

Although no attempt has been made in this study to accumulate a series large enough for statistical analysis, it can be concluded that:

1. A rapid radioisotopic skeletal survey is feasible using ^{18}F, the whole body scanner, and the positron scintillation camera.
2. A larger number of bone lesions can be detected with ^{18}F than with either conventional skeletal X-ray surveys or ^{85}Sr radioisotopic skeletal surveys.
3. ^{18}F is taken up by both malignant and nonmalignant lesions of bone and the ^{18}F skeletal survey primarily serves to indicate areas for careful radiological assessment and, if necessary, biopsy.
4. Since ^{85}Sr radioisotopic skeletal surveys have previously demonstrated the practicability of detecting metastatic bone lesions in the absence of radiologic changes, and since the present study strongly suggests the superiority of ^{18}F over ^{85}Sr in this regard, we propose that ^{18}F skeletal survey using a whole body scanner and positron camera is the most efficient means yet developed for detection of metastatic bone disease.

ACKNOWLEDGMENTS

This work was supported in part under AEC Contract W-7405-eng-48; Peter Ronai's participation was supported by a Winston Churchill Memorial Fellowship.

The authors acknowledge the invaluable aid provided by Dr. Fish of the Palo Alto Medical Clinic, Palo Alto, Calif., Dr. Linfoot of the Donner Laboratory, and Dr. Parker and Dr. Tenny of the Highland General Hospital, Oakland, California, in referring and clinically evaluating the patients reported in this study.

REFERENCES AND NOTE

1. Anger, H. O.: Radioisotope cameras, in Instrumentation in Nuclear Medicine, Ed. by Gerald J. Hine, New York, Academic Press, 1967, pp. 485-552.
2. Anger, H. O.: Whole body scanner Mark II. J. Nucl. Med. 7: 331-2 (1966).
3. Blau, M.; Nagler, W.; and Bender, M. S.: Fluorine-18: a new isotope for bone scanning. J. Nucl. Med. 3: 332-334 (1962).
4. Charkes, N. D.; and Sklaroff, D. M.: The radioactive strontium photoscan as a diagnostic aid in primary and metastatic cancer in bone. Radiol. Clin. N. Am. 3: 499-509 (1965).
5. Corey, K. R.; Kenny, P.; Greenberg, E.; and Laughlin, J. S.: Detection of bone metastasis in scanning studies with calcium-47 and strontium-85. J. Nucl. Med. 3: 454-471 (1962).
6. DeNardo, G. L.; and Volpe, J. A.: Detection of bone lesions with the strontium-85 scintiscan. J. Nucl. Med. 7: 219-236 (1966).
7. DeNardo, G. L.; Horner, R. W.; Leach, P. J.; and Bowes, D. J.: Radioisotope skeletal survey, J. Am. Med. Assoc. 200: 111-113 (1967).
8. Fleming, W. H.; McIlraith, J. D.; and King, E. R.: Photoscanning of bone lesions utilizing strontium-85. Radiology 77: 635-636 (1961).
9. French, R. J.; and McCready, V. R.: The use of ^{18}F for bone scanning. Br. J. Radiol. 40: 655-661 (1967).
10. Neuman, W. F.; and Neuman, M. W.: The chemical dynamics of bone mineral. Chicago, University of Chicago Press, 1958, p. 95.
11. Pochin, E. E.; Hilton, G.; Myant, N. B.; and Honour, A. J.: The indications for radioiodine treatment of thyroid carcinoma. Brit. Med. J. 2: 1115-1121 (1952).
12. Rosenthall, L.: The role of strontium-85 in the detection of bone disease. Radiology 84: 75-82 (1965).
13. Sklaroff, D. M.; and Charkes, N. D.: Diagnosis of bone metastases by photoscanning with strontium-85. J. Am. Med. Assoc. 188: 1-4 (1964).
14. Spencer, R.; Herbert, R.; Rish, M. W.; and Little, W. A.: Bone scanning with ^{85}Sr, ^{87m}Sr, and ^{18}F. Physical and radiopharmaceutical considerations and clinical experience in 50 cases. Brit. J. Radiol. 40: 641-654 (1967).
15. Thomas, C. C.; Sondel, J. A.; and Kerns, R. C.: Production of carrier free fluorine-18. Intern. J. Appl. Radiation Isotopes 16: 71-74 (1965).
16. Van Dyke, D.; Anger, H. O.; Yano, Y.; and Bozzini, C.: Bone blood flow shown with ^{18}F and the positron camera. Am. J. Physiol. 209: 65-70 (1965).

17. Vennart, J.; and Minski, M.: Radiation doses from administered radionuclides. Brit. J. Radiol. 35: 372-387 (1962).

Peter Ronai's present address is Division of Nuclear Medicine, Institute of Medical and Veterinary Science, Frome Road, Adelaide, South Australia, 5000.

Computer Analysis of Breath $^{14}CO_2$ Data

H. Saul Winchell and Kenneth G. Wiley

INTRODUCTION

Subsequent to administration of many carbon-14-labeled materials, $^{14}CO_2$ is excreted in the breath. The shape of such breath $^{14}CO_2$ curves, as well as their amplitude, is related in part to the kinetics of the metabolic processes responsible for the eventual oxidation of the carbon atom in the position labeled with carbon-14. To provide an objective method for the analysis of breath $^{14}CO_2$ data, we have devised models and derived the corresponding mathematical functions containing the parameters describing the measured rate of appearance of $^{14}CO_2$ in a form suitable for analysis by digital computers.

MATHEMATICAL ANALYSIS OF $^{14}CO_2$ DATA

The rate at which $^{14}CO_2$ is measured in expired air subsequent to the intravenous administration of ^{14}C-labeled materials (^{14}C-R) is a function of the physical parameters involved in delivery and removal of the material to and from metabolic sites, the kinetics of the metabolism of the material, and the delays inherent in the measuring device between the time $^{14}CO_2$ actually appears in the breath and the recording of this occurrence (see Fig. 1). Analysis of each of these factors is presented separately in the following discussions.

A. DELAYS IN $^{14}CO_2$ MEASUREMENT INHERENT IN THE MEASURING DEVICE When a constant infusion of $^{14}CO_2$ was delivered into the patient helmet, or through the animal holding chamber, of devices used for continuous measurement of $^{14}CO_2$ exhalation in man (1) or rodents (2, 3), the readings of the vibrating-reed electrometer increased according to the function $C(1-e^{-kt})$, where C and k are constants and t is units of time. This suggested that changes introduced in the measurement of $^{14}CO_2$ excretion by delays inherent in the measuring devices could be accounted for by considering the measuring devices as a compartment with a fractional turnover rate of k (time^{-1}) (right side of Fig. 1). If we let F(t) be the rate of expiration of $^{14}CO_2$ by the experimental subject, then N(t), the amount of $^{14}CO_2$ in the measuring apparatus, is given by

$$N(t) = e^{-kt} \int_0^{\tau} e^{kt} F(t)\, dt. \qquad (1)$$

B. ACTUAL METABOLISM OF ^{14}C-LABELED MATERIAL (^{14}C-R) For compartmental analysis of the actual metabolism of ^{14}C-R we can state that, following instantaneous introduction of ^{14}C-R into one of the compartments, the rate of $^{14}CO_2$ production is given by $\Sigma_i A_i e^{-r_i t}$, where A_i and r_i are constants, and t is time after introduction of ^{14}C-R. Since at t = 0 there

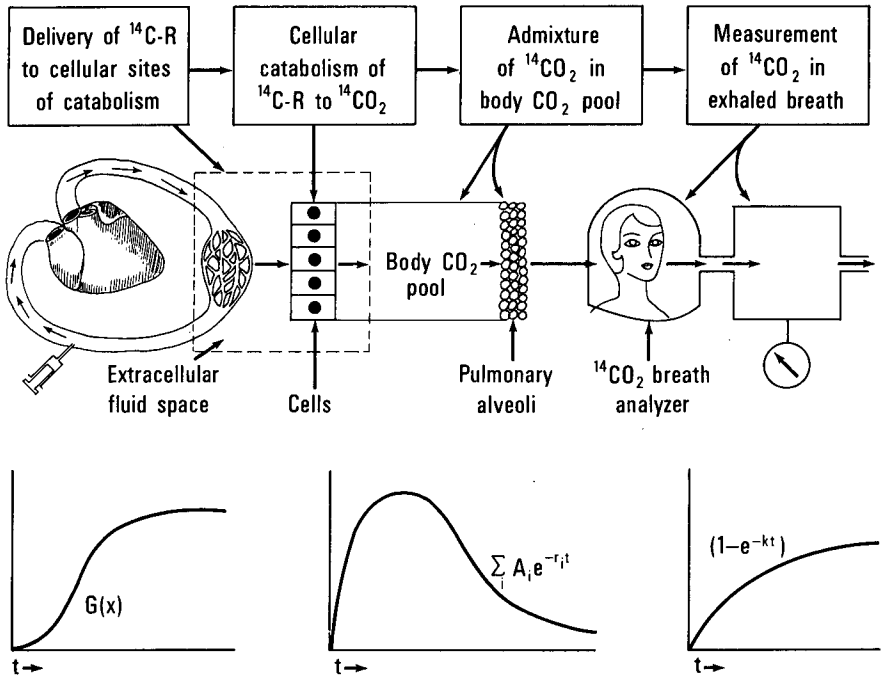

Fig. 1. Schematic representation of physical, biochemical, and technical factors involved in measurement of $^{14}CO_2$ in breath subsequent to IV administration of ^{14}C-labeled material (^{14}C-R). The verbal descriptions of the processes involved are noted in the upper portion of the figure and the corresponding processes are diagrammatically presented in the center of the figure. The estimated forms of the isolated mathematical functions describing each component of the model are shown in the lower portion of the figure. For a discussion of the specific mathematical forms consult text of paper.
DBL676-1680

is no production of $^{14}CO_2$, $\Sigma_i A_i = 0$. There are thus 2i -1 parameters in this function, and the maximum number of rate constants which can be defined in any compartmental model generating this function is likewise 2i -1 (4).

At present it appears that most, if not all, of the $^{14}CO_2$ produced from metabolism of ^{14}C-R must traverse the "CO_2 pool" prior to exhalation in the breath. If we consider only that component of the CO_2 pool in which $^{14}CO_2$ entering from metabolism of ^{14}C-R is subsequently expired into the breath according to a single time-independent rate constant, we can identify the CO_2 pool thus defined as the final pool through which $^{14}CO_2$ enters and exits unidirectionally. Definition of the nature of and interconnections between the remaining pools in the system requires a priori knowledge of the metabolic system being studied independent of the data obtained from observation of $^{14}CO_2$ exhalation. An exception is when only two compartments must be assumed in order to fit the data and one of these compartments can be identified with the CO_2 pool. In this case the remaining compartment may feed only into the CO_2 pool or into

other compartments with sufficiently slow rates of feedback to preclude obtaining evidence of their existence during the time of the study.

C. ANALYSIS OF PHYSICAL PARAMETERS INVOLVED IN DELIVERY AND REMOVAL OF THE ^{14}C-MATERIAL TO AND FROM METABOLIC SITES Subsequent to the rapid intravenous administration of ^{14}C-R there is a definite delay before the radioisotope is "homogeneously" mixed in the initial metabolic pool involved in its metabolism. The tracer material must traverse the intravascular space until the capillaries are reached, it must then traverse the capillary endothelium and mix in the extravascular-extracellular fluid space. It must subsequently cross the cell membrane and enter the intracellular site associated with its subsequent metabolism. Such processes are not instantaneous, and some function must be introduced to account for their occurrence.

Let G(x) be the fractional rate of introduction of ^{14}C-R into the primary metabolic pool, x time units after the administration of ^{14}C-R. If we consider the actual metabolism of ^{14}C-R to be adequately described by a compartmental system we can write the following form for F(t), the rate of appearance of $^{14}CO_2$ in the breath (5):

$$F(t) = \int_{\tau = 0}^{\tau = t} (\sum_i A_i e^{-r_i \tau})\, G(t - \tau) d\tau \,. \qquad (2)$$

G(x) primarily influences the early portion of the $^{14}CO_2$ breath curve. The physiologic functions determining its form are complex and it is difficult to derive its form from first principles. We have thus utilized arbitrary, but convenient, forms for G(x) in the present analysis. In Fig. 2 results are presented for three forms of G(x). In this example actual data describing the measured rate of appearance of $^{14}CO_2$ in the measuring apparatus following a single intravenous administration of histidine-imidazole-2-^{14}C was fitted to Eq. 1 by using the two-compartmental solution of Eq. 2 (i = 2) [presented in the upper portion of this figure as F(t)] and utilizing a variable metric minimization program in a CDC 6600 computer (6). Three forms of G(x) are presented. G(x) = delta function is comparable to assuming a single unique delay time, μ, as characteristic of the delay between IV injection of ^{14}C-R and its final equilibrium in the primary metabolic pool. $G(x) = (1 - e^{-ax})$ is comparable to assuming that the delay between administration of ^{14}C-R and its final equilibrium in the primary metabolic pool is characterized by the introduction of an initial mixing "compartment." $G(x) = e^{ax}/(e^{a\mu} + e^{ax})$ is comparable to assuming that delays during administration of ^{14}C-R and its final equilibrium in the primary metabolic pool are characterized by a Verhulst-Pearl growth curve (7). This latter is similar to the assumption that the probability of delivery of ^{14}C-R from its site of injection to the primary metabolic pool is a Gaussian function with mean transit time μ, and $\phi = 1.7/a$ (8). Although this last form of G(x) gives the best fit of the fitting function to the data, the exact determination of a and μ requires that very exact data be available during the first 5 minutes of the study. In practice when the total μCi dose of ^{14}C-R is minimized the $^{14}CO_2$ data during the first 5 minutes of a study are poorly defined, and it is convenient to use the simplest form of G(x) = delta function.

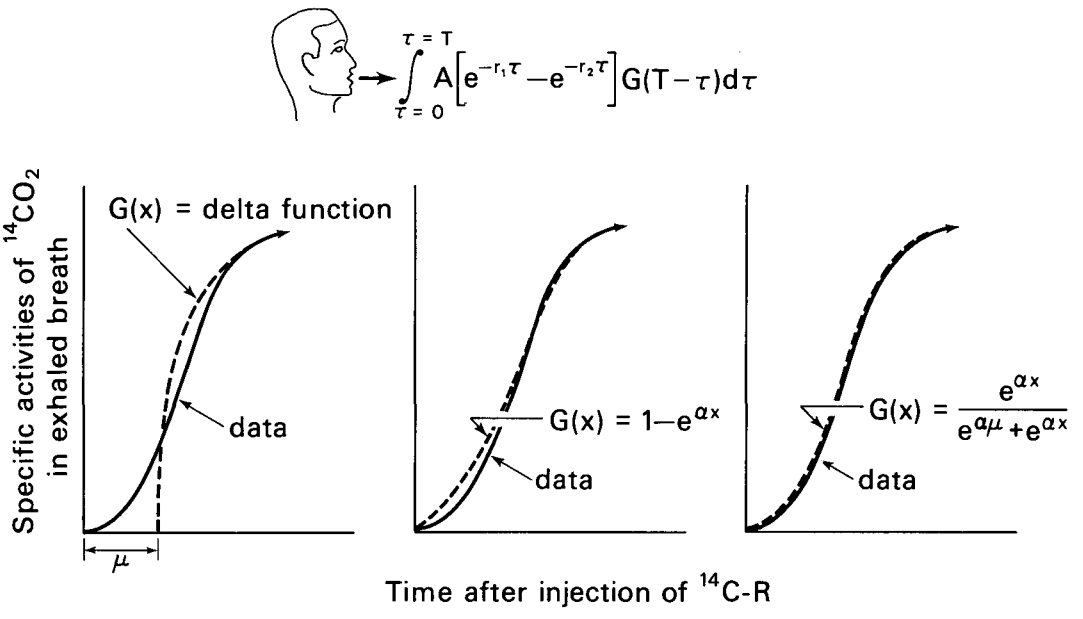

Fig. 2. Three solutions for G(x), the function corresponding to digression of observed data from ideal compartmental behavior. Solid lines represent actual data values obtained in a study of $^{14}CO_2$ expiration in the breath of a human subject given histidine-imidazole-2-^{14}C. After the first 5 minutes the metabolism of the material during the 2-3 hours following its IV administration is described well by a two-compartment system. The broken lines represent the least-squares best fit to the early portion of the curves for forms of F(t) generated by using the form of G(x) shown for each curve.
DBL676-1681

D. ESTIMATION OF NUMBER OF COMPARTMENTS IN METABOLIC SYSTEM To estimate the number of compartments or pools in any metabolic model which may be defined by the data the following empirical approach may be tried. In the final form of Eq. 1 let i take on integer values from unity to "n," generating n solutions for the equation. Determine the least-squares best fit for each solution and record the value of chi squared (χ^2). As the value of i increases the χ^2 becomes smaller, but a value of i is reached beyond which the rate of change of χ^2 is minimal. The value of i corresponding to the solution of Eq. 1 which first results in a "minimum" value of χ^2 is equal to the maximum number of exponential terms--and therefore compartments in the model--that may be defined by the data.

E. DETERMINATION OF MINIMUM DURATION OF DATA COLLECTION TO DEFINE PARAMETERS OF MODEL For any given model it is necessary to know the minimum duration of data collection to define the parameters of the model. An example of how this may be estimated is given in the following discussion of Fig. 3.

In this example $^{14}CO_2$ excretion in the breath was measured for 240 minutes following the IV administration of histidine-imidazole-2-^{14}C, and the data were offered to the computer for the time interval $0 \leq \tau \leq t$ (where t varied from 60 to 240 minutes). The computer was programmed to determine the least-squares best fit of the data to a fitting function derived from a two-compartmental model incorporating a delay time μ [G(x) = delta function]. {The actual

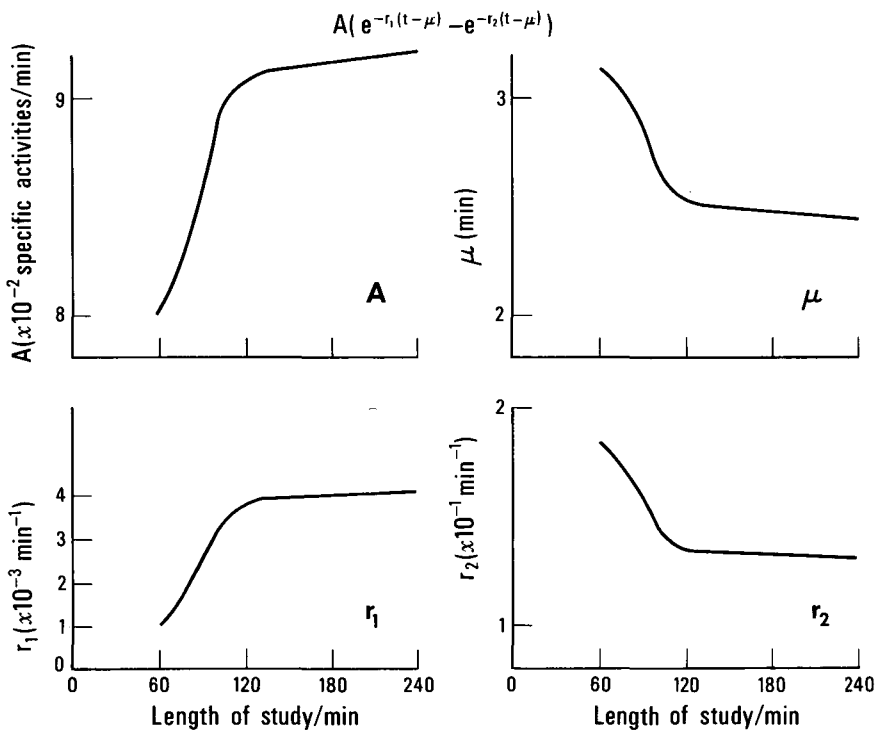

Fig. 3. Duration of data collection required to define parameters of a given model describing $^{14}CO_2$ production from histidine-imidazole-2-^{14}C (see text of paper for explanation). The values for the fitting parameters A, μ, r_1, and r_2, calculated by the computer for data limited to the interval $0 \leq \tau \leq T$, are plotted on the ordinates and the corresponding values of T are plotted on the abscissa.

DBL676-1683

fitting function was the solution of Eq. 1, using $F(t) = A[e^{-r_1(t-\mu)} - e^{-r_2(t-\mu)}]\}$. It should be noted that variable values of A, μ, r_1, and r_2 are obtained for studies of different duration within the range of 60 to 120 minutes of study. However, for studies longer than 120 minutes little difference between these fitting parameters is noted. One can thus state that for the quality of data and the model in question, data must be collected for at least 120 minutes after the injection of ^{14}C-R in order to define the fitting parameters. Similar maneuvers must be performed for each model and set of data to determine the minimal duration of the study required to define the fitting parameters (an alternative approach is to utilize "real-time programming").

SUMMARY

Previous experience with graphical analysis of breath $^{14}CO_2$ curves suggested that the late portion of the curve was well fitted by a series of exponential terms ($\Sigma_i A_i e^{-r_i t}$). In this paper one of these terms is identified with the turnover rate of $^{14}CO_2$ in the measuring device employed, whereas the remaining terms are identified with compartments involved in the

metabolism of ^{14}C-labeled material being studied. To correct for digression of the observed data from idealized compartmental behavior a function G(x) is defined. Examples are presented for G(x) = (delta function), $\Sigma_j A_j e^{-Y_j x}$, and $e^{kx}/(C + e^{kx})$. A method is presented for objectively evaluating the minimum length of time data must be collected to define the fitting parameters of a given model and for estimating the maximum number of compartments that can be defined by a set of $^{14}CO_2$ data.

REFERENCES

1. Fish, M. B.; Pollycove, M.; and Feichtmeier, T. V.: Differentiation between Vitamin B_{12}-deficient and folic acid deficient megaloblastic anemias with ^{14}C-histidine. Blood 21: 447-461 (1963).
2. Tolbert, B. M.; Kirk, M.; and Barker, E. M.: Continuous $^{14}CO_2$ excretion studies in experimental animals. Am. J. Physiol. 185: 263-273 (1956).
3. Domingues, F. J.; Gildner, K. J.; Baldwin, R. R.; and Lowry, J. R.: An instrument and technique for the continuous measurement of respiratory CO_2 patterns in metabolic tracer studies. Intern. J. Appl. Radiation Isotopes 7: 77-86 (1959).
4. Sharney, L.; Wasserman, L. R.; Gevirtz, N. R.; Schwartz, L.; and Tendler, D.: Multiple-pool analysis in tracer studies of metabolic kinetics. J. Mt. Sinai Hosp. 32 [3] (May-June 1965).
5. Branson, H.: The integral equation representation of reactions in compartment systems. Ann. N. Y. Acad. Sci. 108 [art 1]: 4-14 (May 1963).
6. Davidon, W. C.: Variable metric minimization. Argonne National Laboratory Report ANL-5990, Rev. 1959.
7. Pearl, R.: Introduction to medical biometry and statistics, Ed. 3. Philadelphia, Pa., Saunders, 1940.
8. Landaw, S. A.: Studies of RBC lifespan distribution using endogenous ^{14}CO production. Donner Laboratory Semiannual Report, UCRL-17481, Spring 1967, p. 43.

Increased Histidine Turnover in Rats Following Administration of Glucagon

Louis L. Shane, H. Saul Winchell, Nancy N. Finley, Barbara A. Shipley and John H. Lawrence

INTRODUCTION

Past studies of glucagon action have been concerned with stimulation of glucose production via glycogenolysis (1, 2) and gluconeogenesis (2-5). The majority of such previous experiments used isolated perfused tissues in which variable glucagon depletion presented an uncontrolled variable.

In this paper we present a method for evaluating kinetics of the metabolism of a particular amino acid and its control by glucagon in the intact nonfasting animal. Subsequent to the rapid intravenous administration into rats of an amino acid labeled with ^{14}C at a carbon atom site having a known unique metabolic fate in its catabolism to CO_2, the rate of $^{14}CO_2$ appearance in the breath was measured. The rate of $^{14}CO_2$ appearance was analyzed by using a digital computer by least-squares best fit of the data to mathematical functions derived from compartmental theory. The effects of glucagon on the intercompartmental exchange rates related to metabolism of the amino acid and calculated from such analyses were determined by application of the above method to data obtained in rats both prior and subsequent to administration of glucagon. These results were correlated with determinations of plasma histidine levels and serial ^{14}C-protein specific activity values in similarly treated rats.

MATERIALS AND METHODS

$^{14}CO_2$ PRODUCTION STUDIES Male buffalo rats (Simonson Laboratory, Gilroy, California) weighing 280-300 grams, selected for this study, were allowed free access to food and water until the beginning of the experiment.

Two experimental groups were established. The control group consisted of six rats which had no prior treatment. The group receiving glucagon was comprised of seven animals which were prepared with 39 μg of crystalline glucagon* dissolved in 1 ml of dilute HCl (pH: 2.5-3.0) and injected subcutaneously 0.5 hour prior to the administration of ^{14}C-labeled histidine. The dosage of 39 μg glucagon was chosen on the basis of preliminary experiments which indicated that this amount of hormone was the minimal amount required for maximal increase in $^{14}CO_2$ production. Each animal was anesthetized with diethyl ether, and 5 μCi of L-histidine-2-imidazole-^{14}C (specific activity 267 μCi/mg, Nuclear Chicago Corp., Des Plaines, Ill.) was

*Kindly provided by Dr. William W. Bromer of the Lilly Research Laboratories.

administered intravenously through a tail vein to those animals used in the $^{14}CO_2$ breath studies. The rat was placed in a sealed metabolic cage through which room air was passed at a constant rate of 0.40 liter/minute. The gas flow was then directed through a $^{14}CO_2$ ionization chamber and a CO_2 infrared analyzer (Fig. 1). Similar apparatus has been described previously (6, 7). Rats used in the ^{14}C-tissue specific activity studies were handled in an identical fashion save that they received 10 μCi of DL-histidine-2-^{14}C (specific activity 10-25 μCi/mg, New England Nuclear Corp., Boston, Mass.).

DATA ANALYSIS In preliminary experiments using the apparatus described in Fig. 1 it was determined that readings on the vibrating-reed electrometer increased according to the function $c(1-e^{-kt})$ (where $k = 0.24\ min^{-1}$) when a constant infusion of $^{14}CO_2$ was introduced into the animal holding chamber. This suggested that changes introduced in the measurement of $^{14}CO_2$ excretion of the experimental animals by delays inherent in the measuring apparatus could be accounted for by considering the measuring apparatus as a compartment with a turnover rate of $k = 0.24\ min^{-1}$ (see Fig. 2). If we let F(t) be the rate of expiration of $^{14}CO_2$ by the experimental animal, then N(t), the amount of $^{14}CO_2$ in the measuring apparatus, is given by

$$N(t) = e^{-kt} \int_0^t e^{kt} F(t)\, dt. \qquad (1)$$

If we wish to analyze the rate of $^{14}CO_2$ excretion [F(t)] by the experimental animal by utilizing compartmental analysis, we can identify F(t) as equal to $\Sigma_i A_i e^{-r_i t}$, where i is equal to the number of compartments or pools in the system. Unfortunately, intravenous administration of the tracer material to the experimental animal is not instantaneous, and there is a variable time delay between such injection and placement of the animal in the experimental apparatus. These factors plus the fact that mixture of labeled histidine in the "histidine pools" and mixture of labeled bicarbonate in the bicarbonate pool are not instantaneous processes necessitate introduction of some function that accounts for digression of the observed data from idealized compartmental behavior. The simplest form of this "delay function" is to assume a single "delay time" which would compensate for the above noted experimental deficiencies. Thus, F(t) becomes equal to $\Sigma_i A_i e^{-r_i(t-\mu)}$, where μ = the "delay time" just discussed and A_i and r_i are constants. Obvious additional limitations of this function are that at $t = \mu$, $F(t) = 0$ (and thus $\Sigma_i A_i = 0$) and that for all values of $t < \mu$, $F(t) = 0$.

In the experiments reported here the values of the rate of $^{14}CO_2$ production were analyzed only during the time period for which two exponential terms could be defined for F(t), in general 40-60 min, and thus $A\,[e^{-r_1(t-\mu)} - e^{-r_2(t-\mu)}]$* was used as the function describing the

*In this representation
t is time after initiation of the study.
r represents the slope of an exponential term used to fit the experimental data in a nonfeedback system (or, as in this case, a feedback so slow as to have insignificant effect on $^{14}CO_2$ production during the duration of the study). The r values can be identified with the fractional turnover rate of the compartments in the system. In these studies the r_1 slopes can be identified with the turnover rate of the HCO_3^- pool, and the r_2 slope with the turnover rate of the histidine pool. A represents the zero intercept of the second exponential term. It is related to amplitude and characterizes the total fraction of administered ^{14}C-labeled material appearing in the breath.

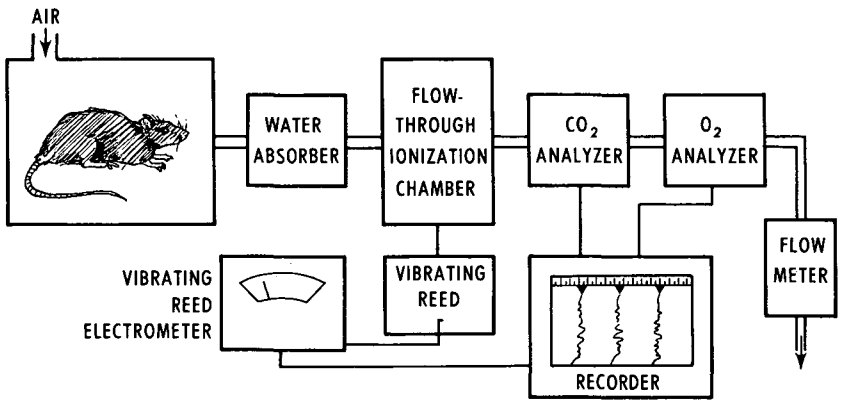

Fig. 1. Diagrammatic representation of the apparatus used in the experiments described. Room air at ambient temperature is passed through the chamber containing the experimental animal (0.4 liter/min flow rate through the rat-holding chamber). The expired air is then serially passed through a water absorber (Indicator Drierite), a flow-through ionization chamber (vol. 0.377 liter), an infrared CO_2 analyzer, a paramagnetic O_2 analyzer, and a wet flow-meter. XBL674-1331

rate of excretion of $^{14}CO_2$ by the rat, and the following solution of N(t) was used to fit the observed values of $^{14}CO_2$ in the measuring device:

$$N(t) = K_1 e^{-r_1 t} - K_2 e^{-r_2 t} - K_3 e^{-0.24t}, \tag{2}$$

where

$$K_1 = \frac{Ae^{r_1\mu}}{k-r_1}, \quad K_2 = \frac{Ae^{r_2\mu}}{k-r_2}, \quad K_3 = \frac{Ae^{k\mu}}{k-r_1} - \frac{Ae^{k\mu}}{k-r_2} .$$

Since the rate of $^{14}CO_2$ excretion depends on the rate of CO_2 excretion, the $^{14}CO_2$ excretion data were "corrected" for such variations in CO_2 excretion rate by division of the $^{14}CO_2$ excreted per minute, expressed as a fraction of the ^{14}C administered, by the simultaneous CO_2 excretion during the same time interval divided by the average rate of CO_2 excretion during the time of the study. Mathematically stated the data fitted to Eq. 2 were of the form

$$N(t) = \frac{^{14}CO_{2(t)}}{CO_{2(t)}} \times \overline{CO}_2, \tag{3}$$

where $^{14}CO_{2(t)}$ = fraction of the ^{14}C administered as histidine-imidazole-2-^{14}C present in the measuring apparatus at time t,

$CO_{2(t)}$ = total CO_2 in the measuring apparatus at time t,

$\overline{CO}_2$ = average amount of CO_2 in the measuring apparatus during the time of the experiment.

Data in the form given in Eq. 3 were fitted to Eq. 2 by determining best-fit values of A, r_1, r_2, and μ, utilizing a variable metric minimization program in a CDC 6600 computer (8).

Since ^{14}C atoms oxidized to $^{14}CO_2$ must traverse the H_2CO_3-HCO_3^- pool prior to exhalation in the breath as $^{14}CO_2$, one can readily identify one of the compartments in this system as the H_2CO_3-HCO_3^- pool. In actual experiments in which a constant infusion of $H\,^{14}CO_3^-$ was given for 1 hour to reach mixing equilibrium with the H_2CO_3-HCO_3^- pool, and the subsequent rate of appearance of $^{14}CO_2$ in the breath was studied, the rate of turnover of the H_2CO_3-HCO_3^- pool thus measured was equivalent to that calculated in this paper using the above noted equations and identifications. The remaining compartment we may call the "histidine-imidazole-2C" pool without performing any further biochemical identifications. The only possible modes of exit from this latter compartment are to the H_2CO_3-HCO_3^- pool and to other compartments that are turning over sufficiently slowly to preclude obtaining evidence of "feedback" of label to the "histidine-imidazole-2C" pool during the time of study. One would expect that a large component of such slowly turning over pools receiving label from the "histidine-imidazole-2C" pool would be histidine-containing proteins. The identification of the rate constants defining the movement of label through the compartments of the model presented in Fig. 2 with the data-fitting parameters (A, r_1, r_2) is trivial, and is given in the lower portion of Fig. 2.

TISSUE AND BLOOD STUDIES Two groups of rats, controls and glucagon-treated, were selected and prepared in the same fashion as those included in the breath studies. In this part of the experiment animals injected with DL-histidine-2-^{14}C were sacrificed under ether anesthesia by exsanguination. This was achieved by bleeding through an incision in the jugular vein with concomitant infusion through the abdominal aorta of 250 ml saline under high pressure. Prior studies using this technique have demonstrated that less than 1% of the original hepatic blood volume remains in the liver (9). Animals were sacrificed over a period ranging from 7 minutes to 24 hours. In determining values for each point in time during the course of study seven animals were sacrificed.

Immediately following death the liver and diaphragm were removed and frozen. The entire liver was homogenized with cold water in a Waring Blender. The final volume was measured and recorded. One ml of the homogenate was precipitated with 1 ml 20% cold trichloroacetic acid (TCA), the whole was centrifuged, and the supernatant was discarded. The precipitate was resuspended in 2 ml 10% cold TCA, and heated to 90°C for 15 minutes. It was then cooled, centrifuged, and the supernatant again discarded. The precipitate was washed with 2 ml of an ethanol-ether mixture (50%, V:V). The suspension was centrifuged, the supernatant discarded, and the precipitate washed with 2 ml ether. Again, following centrifugation the supernatant was discarded. The precipitate was dissolved in 1.5 ml 0.4 N NaOH and then diluted to a volume of 2 ml with 0.4 N NaOH.

The diaphragms were frozen in liquid nitrogen and pulverized. The whole diaphragm was precipitated with 1.5 ml 20% cold TCA and the extraction was continued as for liver.

Biuret determinations of protein were performed as has been described previously (10). Standard curves were established by using serial dilutions of bovine albumin aqueous solution (B grade) obtained from Cal Biochem (Box 54282, Los Angeles, Calif.). One hundred λ of the purified protein was used for biuret determination.

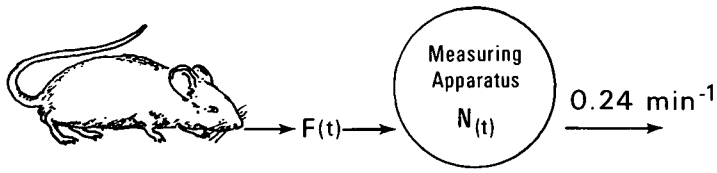

For $F(t) = A(e^{-r_1(t-\mu)} - e^{-r_2(t-\mu)})$

The following two-compartment model can be defined:

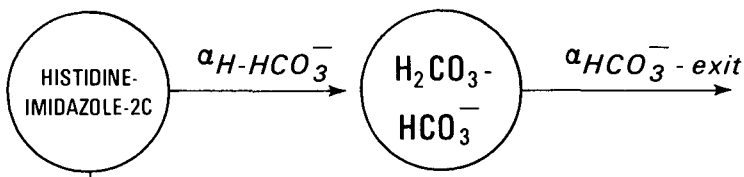

$\alpha_{HCO_3^-\text{-exit}} = r_1$ $\qquad$ $\alpha_{H\text{-}HCO_3^-} = \dfrac{A(r_2 - r_1)}{r_1}$

$\alpha_{H\text{-exit}} + \alpha_{H\text{-}HCO_3^-} = r_2$ $\qquad$ $\alpha_{H\text{-exit}} = r_2 - \alpha_{H\text{-}HCO_3^-}$

Fig. 2. Diagrammatic representation of the model used for analysis of effects of $^{14}CO_2$ measuring equipment on the measured rate of $^{14}CO_2$ appearance (shown above) and the model used for analysis of metabolism of histidine-imidazole-2C (shown below). See text for mathematical analysis of model. DBL670-1825

For determination of ^{14}C activity 100 λ of protein extracted in the above manner was added to 0.5 ml NCS (Nuclear Chicago) solubilizer solution to which was then added 15 ml scintillation solution, and was counted in a Nuclear Chicago Mark I Liquid Scintillation Counter.

The concentration of L-histidine in the plasma was determined on samples from control animals and in animals 0.5 hour after administration of glucagon. Such determinations were kindly performed by Dr. M. Fish at the San Francisco General Hospital, by use of High Voltage paper electrophoretic separation and spectrophotometric analysis of the methanol-eluted cadmium ninhydrin chromagen, utilizing instrumentation and techniques similar to those described by Dreyer and Bynum (11).

RESULTS

BREATH ANALYSIS A summary of the values obtained from application of Eq. 2 to the data describing the rate at which exhaled $^{14}CO_2$ from control and glucagon-treated animals appeared in the breath-analysis device is shown in Table 1. The means and standard deviations for each of the fitting parameters (A, r_1, and r_2) are presented for each group of animals studied. The parameters A and r_1 are not significantly different in control or glucagon-treated animals. However, in glucagon-treated animals the value of r_2 is approximately four times

Table 1. Means and standard deviations for values of the parameters of Eq. 2 (A, r_1, and r_2) describing the rate of expiration of $^{14}CO_2$ in control and glucagon-treated rats subsequent to the IV administration of L-histidine-2R-^{14}C. The computer-derived values listed were obtained from six control and seven glucagon-treated animals.

	Control	Glucagon
A	$(3.154 \pm 0.634) \times 10^{-3}$	$(2.710 \pm 0.883) \times 10^{-3}$
r_1	$(2.538 \pm 0.889) \times 10^{-2}$	$(2.579 \pm 0.753) \times 10^{-2}$
r_2	0.1681 ± 0.0335	0.6919 ± 0.2052

control values ($p < 0.05$). The difference between representative curves obtained in glucagon-treated and control rats is graphically demonstrated in Fig. 3.

Application of the relationships previously derived between the values obtained for A, r_1, and r_2 and the rate constants in the compartmental model shown in Fig. 2 yielded the values for intercompartmental rate constants shown in Table 2. It can be seen from Table 2 that the turnover rate of the "$H_2CO_3^-$ pool" is unchanged by the administration of glucagon. However, glucagon administration is associated with a significant increase in both the fraction of the "histidine-imidazole-2C pool" entering oxidative pathways leading to production of CO_2 from this carbon site and the fraction of this labeled pool entering relatively "fixed" metabolic pools (e.g., such as labeled histidine incorporated into proteins).

TISSUE AND BLOOD STUDIES Tables 3 and 4 present time sequence changes in protein ^{14}C specific activity in rat liver and diaphragm, respectively, following IV administration of DL-histidine-2-^{14}C. The level of ^{14}C specific activity noted at 2-4 hours in both these tissues is generally comparable for both the glucagon-treated and control animals. However, the glucagon-treated animals generally reach maximum protein ^{14}C specific activity levels more rapidly than the control animals.

Table 5 presents values of plasma histidine concentration in three control animals and in three animals given glucagon 0.5 hour prior to blood sampling. These data demonstrated little if any change in plasma histidine concentration following administration of glucagon.

DISCUSSION

Metabolism of the imidazole-2C site of L-histidine may be thought of as proceeding in two general directions. The oxidation of this site proceeds by a unique metabolic pathway involving formation of formiminoglutamic acid with transfer of the carbon atom in question to tetrahydrofolic acid, from which point it is oxidized to CO_2 (12). No other known metabolic pathway for histidine results in oxidation of the imidazole-2C site to CO_2. In these nonoxidative pathways incorporation of histidine into protein is most likely the largest single component (Fig. 4).

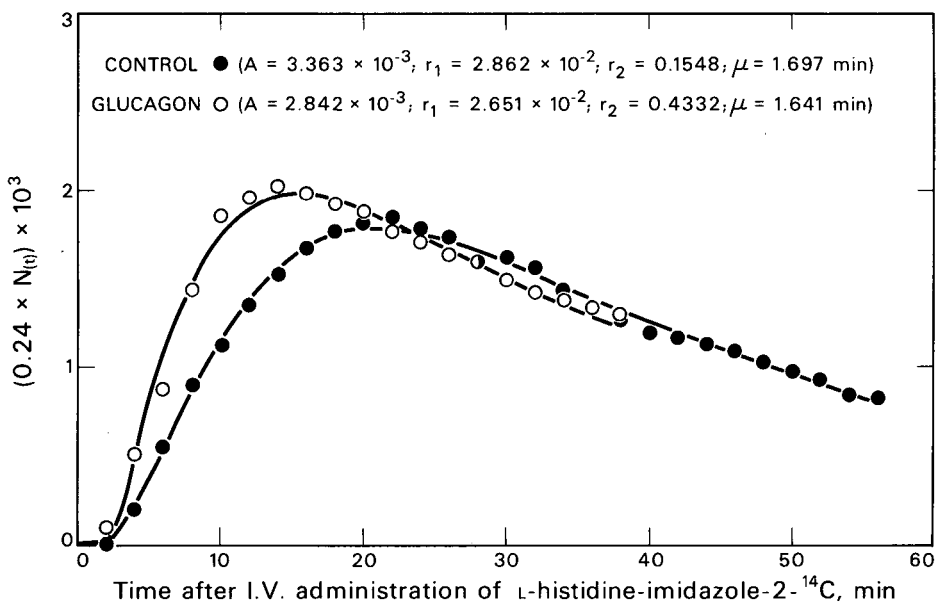

Fig. 3. Representative curves demonstrating computer-generated curves (solid lines) for least-squares best fit to data obtained in a control rat (solid circles) and in a glucagon-treated rat (open circles). The turnover rate of $^{14}CO_2$ in the measuring device expressed as fraction of the injected ^{14}C excreted per minute is plotted on the ordinate, and time after IV administration of labeled histidine is plotted on the abscissa. In the upper portion of the figure the actual calculated values for the parameters A, r_1, r_2, and μ defining the computer-generated curves are presented for the two animals.
DBL686-4766

In the work reported here the analysis of appearance of $^{14}CO_2$ in the breath subsequent to the intravenous administration of L-histidine-imidazole-2-^{14}C demonstrates increased turnover of the "histidine-imidazole-2C" pool subsequent to the administration of glucagon. This conclusion is further supported by study of the incorporation of ^{14}C from histidine into liver and muscle protein, which suggests more rapid attainment of maximum specific activity levels in glucagon-treated than in control animals. This does not, however, establish that net turnover of this pool results from administration of glucagon, since net turnover rate of any pool is the product of pool size and fractional turnover rate. If glucagon resulted in a fourfold or greater decrease in the "histidine-imidazole-2C" pool size, then a fourfold increase in fractional turnover rate would merely result in constant net turnover of the histidine pool. That the "histidine-imidazole-2C" pool size is not diminished fourfold, or more, subsequent to the administration of glucagon is suggested by the finding in these experiments that plasma histidine levels were not markedly altered subsequent to the administration of glucagon.

Similar findings were reported by Shoemaker and Van Itallie (13) in experiments in which they noted that portal vein plasma amino nitrogen levels remained unchanged for at least 30 minutes following the administration of glucagon. This time period corresponds to the time period in the experiments reported here between the administration of glucagon and the admin-

Table 2. Means and standard deviations for values of the calculated rate constants describing movement of tracers between compartments of model presented in Fig. 2. The values listed were obtained from six control and seven glucagon-treated animals. [These values were obtained from fitting parameters (A, r_1, r_2) listed in Table 1.] $^{\alpha}HCO_3^-$ - e = fractional turnover rate of HCO_3^- pool (min^{-1}), $^{\alpha}H\text{-}HCO_3^-$ = fractional turnover rate of the "histidine-imidazole-2C" pool entering HCO_3^- pool (min^{-1}), $^{\alpha}H$-e = fractional turnover rate of the "histidine-imidazole-2C" pool entering slowly-turning-over pools other than HCO_3^- pool (min^{-1}).

	Control	Glucagon
$^{\alpha}HCO$-e	$(2.538 \pm 0.889) \times 10^{-2}$	$(2.579 \pm 0.753) \times 10^{-2}$
$^{\alpha}H\text{-}HCO_3^-$	$(1.716 \pm 0.413) \times 10^{-2}$	$(7.512 \pm 3.935) \times 10^{-2}$
$^{\alpha}H$-e	0.1509 ± 0.0303	0.6167 ± 0.1677

Table 3. Mean values of specific activity in rat liver (dpm/μCi injected/g of tissue) and standard deviations for control and glucagon-treated animals at various time periods following IV injection of DL-histidine-2-^{14}C. The values at each time represent data from seven rats.

Time of sacrifice	Controls	Glucagon-treated
7 min	22.29 ± 7.47	27.38 ± 6.44
15 min	40.25 ± 5.78	49.57 ± 13.33
30 min	47.63 ± 12.19	65.55 ± 5.77
1 hour	74.78 ± 11.74	65.10 ± 10.43
2 hours	80.29 ± 11.74	72.57 ± 9.15
4 hours	64.30 ± 6.07	68.06 ± 6.51

istration of labeled histidine. In that study at times greater than 30 minutes following the administration of glucagon, alpha amino nitrogen levels rose. Glucagon has been found to decrease blood amino nitrogen, but these are relatively long-term experiments (4, 14).

We may conclude that the most consistent interpretation of our data and those reported in the literature is that glucagon results in a marked increase in both the net turnover rate and the fractional turnover rate of histidine. Our observations of increased L-histidine catabolism

Table 4. Mean values of specific activity in rat diaphragm (dpm/μCi injected/g of tissue) and standard deviations for control and glucagon-treated animals at various time periods following IV injection of DL-histidine-2-^{14}C. The values at each time represent data from seven rats.

Time of sacrifice	Controls	Glucagon-treated
7 min	94.30 ± 11.8	113.9 ± 15.9
15 min	128.29 ± 28.9	241.8 ± 129.5
30 min	219.61 ± 69.2	303.0 ± 70.4
1 hour	300.04 ± 71.0	333.6 ± 65.9
2 hours	492.50 ± 34.0	606.0 ± 157.6
4 hours	888.49 ± 283.0	639.2 ± 73.5

Table 5. L-histidine concentration in plasma obtained from three control and three glucagon-treated rats expressed both as micromoles per μM/liter and mg/100 ml plasma.

Control		Glucagon-treated	
μM/liter	mg/100 ml	μM/liter	mg/100 ml
23	0.357	30	0.465
38	0.590	25	0.388
33	0.512	26	0.404
av.	0.486	av.	0.419

correlate well with the experimental conclusions of other investigators (4, 15-18). These in vitro studies indicate that glucagon stimulates the conversion of amino acids to carbohydrate and increases urinary nitrogen excretion.

The finding that glucagon increases the rate of protein synthesis in vivo may be an indirect function of the hormone mediated by its stimulation of insulin secretion (19-24). The rate-limiting step may be one of amino acid transport (25, 26) or stimulation of protein synthesis independent of amino acid transport (27).

SUMMARY

These experiments are intended to establish the effect of glucagon on the in vivo kinetics of histidine metabolism in the rat. L-histidine-2-imidazole-^{14}C was administered to each of a group of control animals and a group of animals pretreated with glucagon 1/2 hour prior to

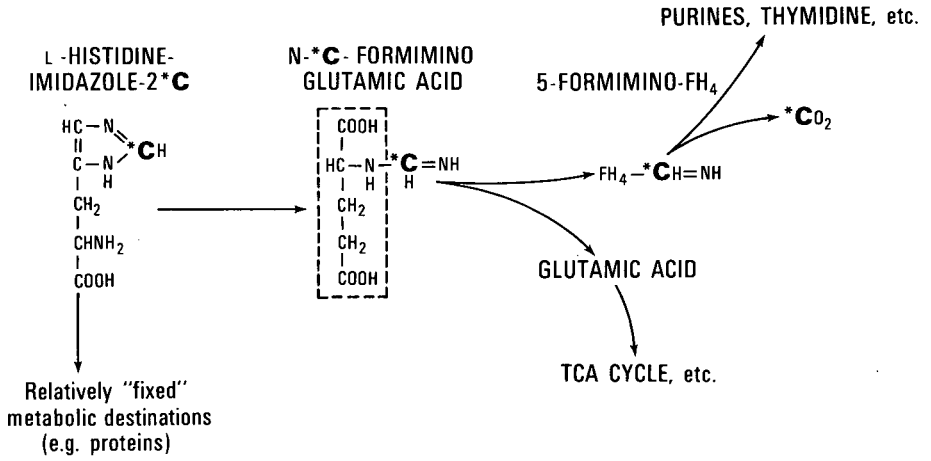

Fig. 4. Representation of the pathway through which histidine may be metabolized. The imidazole-2C site proceeds uniquely through tetrahydrofolic acid to the single carbon pool when histidine is catabolized. Incorporation into protein is the major nonoxidative pathway.

DBL686-4777

injection of histidine. The rate of metabolism of this material to $^{14}CO_2$ during the first hour of each study was fitted to a two-exponential function $F(t) = A(e^{-r_1 t} - e^{-r_2 t})$. Although the fitting parameters A and r_1 were very nearly the same for the control and glucagon-treated animals ($A \approx 3 \times 10^{-3}$, $r_1 \approx 2.5 \times 10^{-2}$), the values for r_2 were very different in the two groups. For the controls $r_2 = 0.1681 \pm 0.0335$ and for the glucagon-treated animals $r_2 = 0.6919 \pm 0.2052$. Application of a two-compartment nonfeedback model to the curve-fitting function led to an estimation of a fourfold increase in the fractional turnover of the histidine compartment into both anabolic and catabolic processes attendant on the administration of glucagon. The relative patterns of incorporation of ^{14}C from labeled histidine into liver and diaphragm protein are consistent with this conclusion. That net turnover of histidine is also increased by glucagon is suggested by the findings of comparable plasma histidine concentration in control and glucagon-treated animals.

REFERENCES AND NOTE

1. Sokal, J. E.; Sarcione, E. J.; and Henderson, A. M.: Endocrinology 74: 930 (1964).
2. Shoemaker, W. C.; and Van Itallie, T. B.: Endocrinology 66: 260 (1960).
3. Miller, L. L.: Recent Progr. Horm. Res. 17: 539 (1961).
4. Izzo, J. L.; and Glasser, S. R.: Endocrinology 68: 189 (1961).
5. Exton, J. H.; Jefferson, L. S.; Butcher, R. W.; and Park, C. R.: Am. J. Med. 40: 709 (1966).
6. Tolbert, B. M.; Kirk, Martha; and Barker, E. M.: Am. J. Physiol. 185: 263-273 (1956).
7. Domingues, F. J.; Gildner, K. J.; Baldwin, R. R.; and Lowry, J. R.: Intern. J. Appl. Radiation Isotopes 7: 77-86 (1959).
8. Davidon, W. C.: Argonne National Laboratory Report ANL-5990, Rev. 1959.

9. Donald Van Dyke (Donner Laboratory, University of California, Berkeley), personal communication.
10. Weichselbaum, T. E.: Am. J. Clin. Pathol., Tech. Sect. 10: 40-49 (March 1946).
11. Dreyer, W. J.; and Bynum, E.: Methods in Enzymology, Vol. 11, Ed. W. Hirs, New York, Academic Press, (1967).
12. Fish, M. B.; Pollycove, M.; and Feichtmeir, T. V.: Blood 21: 447-461 (1963).
13. Shoemaker, W. C.; and Van Itallie, T. B.: Endocrinology 66: 260 (1960).
14. Helmer, O. M.; Kirtley, W. R.; and Ridolfo, A. S.: J. Lab. Clin. Med. 50: 824 (1957).
15. Garcia, A.; Williamson, J. R.; and Cahill, G. F., Jr.: Diabetes 15: 188 (1966).
16. Kalant, N.: Proc. Soc. Exptl. Biol. Med. 86: 617 (1954).
17. Sokal, J. E.: Endocrinology 78: 538 (1966).
18. Sokal, J. E.: Am. J. Med. 41: 331 (1966).
19. Samols, E.; Marri, G.; and Marks, V.: Diabetes 15: 855 (1966).
20. Crockford, P. M.; Porte, D., Jr.; Wood, F. C., Jr.; and Williams, R. H.: Metabolism 15: 114 (1966).
21. Ryan, W. G.; Nibbe, A. F.; and Schwartz, T. B.: Lancet 1: 1255 (June 10, 1967).
22. Samols, E.; Marri, G.; and Marks, V.: Lancet 2: 415 (Aug. 28, 1965).
23. Simpson, R. G.; Benedetti, A.; Grodsky, G. M.; Karam, J. K.; and Forsham, P. H.: Metabolism 15: 1046 (1966).
24. Karam, J. H.; Grasso, S. G.; Wegienka, L. C.; Grodsky, G. M.; and Forsham, P. H.: Diabetes 15: 571 (1966).
25. Manchester, K. L.: Excerpta Medica Foundation (1965).
26. Buse, M. G.; and Buse, J.: Diabetes 16: 753 (1967).
27. Wool, I. G.; Rampersad, O. R.; and Moyer, A. N.: Am. J. Med. 40: 716 (1966).

This investigation was supported in part by a Public Health Service Fellowship #2-F3-CA-29, 6020-02 from the National Cancer Institute and in part under A.E.C. Contract No. W-7405-eng-48.

The Influence of Hydrocortisone upon Histidine Kinetics in the Rat

Louis L. Shane, H. Saul Winchell, Barbara A. Shipley and Nancy N. Finley

INTRODUCTION

Corticosteroids cause loss of body weight, depletion of tissue protein, and excretion of increased amounts of nitrogen in the urine (1-3). Although administration of corticosteroids to an animal is accompanied by loss of nitrogen and by tissue breakdown, the liver of these animals maintains or even augments its weight and protein content (4, 5). The kinetic mechanisms by which these hormones participate in the regulation of these processes is not clearly established. The experiments reported here have been performed with the intention of elucidating the role of hydrocortisone in the kinetics of histidine metabolism with respect to pathways leading to CO_2 production and pathways leading to incorporation into protein.

MATERIALS AND METHODS

The methods for $^{14}CO_2$ breath analysis and for tissues and blood studies have been presented in the preceding paper in this semiannual report.

All rats used for this study were allowed free access to food and water. Control animals were given no treatment prior to the administration of ^{14}C-labeled histidine. Steroid-treated animals were given 5 mg of hydrocortisone subcutaneously twice daily for 6 days prior to the IV injection of the ^{14}C-labeled histidine. L-histidine-2-imidazole-^{14}C (Nuclear Chicago Corp., Des Plaines, Ill., S. A.: 267 μCi/mg) was used for the breath analysis studies. In the studies of histidine incorporation into liver and diaphragm protein, DL-histidine-2-^{14}C (New England Nuclear Corp., Boston, Mass., S. A.: 10-25 μCi/mg) was used, and hydrocortisone administration was continued until the animal was sacrificed. At least seven rats were sacrificed after each time interval in determining ^{14}C-protein specific activity values.

Test of significance between groups of values obtained was performed by using Student's "t" test tables (p values).

RESULTS

A summary of the values describing the rate of metabolism to $^{14}CO_2$ of L-histidine-2-imidazole-^{14}C in control and steroid-treated animals is shown in Table 1. The control group comprised six animals and the steroid-treated group seven. The means and standard deviations of the fitting parameters (A, r_1, and r_2) are presented for each group of animals studied. Although there is no statistical difference between the values obtained for control and steroid-

Table 1. Parameters describing the metabolism of L-histidine-imidazole-2-^{14}C to $^{14}CO_2$ in rats.

	Control (6 rats)	Hydrocortisone (7 rats)
A	$(3.154 \pm 0.634) \times 10^{-3}$	$(4.261 \pm 1.749) \times 10^{-3}$
r_1	$(2.538 \pm 0.886) \times 10^{-2}$	$(2.875 \pm 1.137) \times 10^{-2}$
r_2	0.1681 ± 0.0335	0.3385 ± 0.2744

treated animals, the mean values for r_2 (identified with fractional turnover rate of the "histidine-imidazole-2C pool") is greater in the steroid-treated group.

Table 2 presents values of plasma histidine concentration in three control animals and in three animals given hydrocortisone for 6 days prior to blood sampling. These demonstrate an average decrease in plasma histidine concentration of approximately 35% following the administration of the steroid.

Tables 3 and 4 present sequential changes in protein ^{14}C specific activity of rat liver and diaphragm respectively following IV administration of DL-histidine-2-^{14}C. Mean values and standard deviations for each group of rats (at least seven animals for each point) are presented, as are the p values derived from Student's "t" test of significance between control and steroid-treated groups. The rate of ^{14}C incorporation into diaphragm and liver protein is greater in steroid-treated than in control animals. Roughly estimated turnover time of ^{14}C in "liver protein precursor" of control animals was approximately 60 minutes. In the steroid-treated group the turnover time was approximately 17 min. The turnover time of ^{14}C in diaphragm "protein precursor" of control animals was roughly estimated as 1.7 hours, and in the steroid-treated group was approximately 1 hour. The maximum level of ^{14}C specific activity reached in liver protein of steroid-treated animals is greater than in the controls. In contradistinction, hydrocortisone diminishes the maximum level of ^{14}C specific activity attained by diaphragm protein. Figures 1 and 2 present these results graphically.

DISCUSSION

In these studies hydrocortisone had no significant effect upon the pattern of $^{14}CO_2$ production from L-histidine-imidazole-2-^{14}C. The observation of a diminished plasma histidine concentration may be a reflection of the total body histidine pool, and suggests that the net pool turnover may be decreased. It has been reported that adrenocortical extracts and cortisone increase the concentration of amino acids in plasma (6-9). In one study, the concentrations of 8 of the 14 amino acids assayed in the plasma were little affected by adrenalectomy or hydrocortisone administration (9). Only six amino acids were significantly different, but these were so changed that the total amino acid differences were quite prominent. Histidine was not measured. In another study, which presented plasma histidine levels, the incremental increase in plasma histidine following adrenal stimulation was lowest of all the amino acids assayed and the change was least significant (8).

Table 2. L-Histidine concentration in rat plasma in control and hydrocortisone-treated rats.

Control		Hydrocortisone-treated	
μM/liter	mg/100 ml	μM/liter	mg/100 ml
23	0.357	19	0.295
38	0.590	18	0.280
33	0.512	24	0.372
av.	0.486	av.	0.315

Table 3. ^{14}C specific activity of liver protein following IV injection of DL-histidine-2-^{14}C in the rat.

Time following injection	^{14}C specific activity $\frac{(dpm/mg\ protein)}{\mu Ci\ injected}$		
	Controls	Steroids	p value
7 min	22.295 ± 7.471	20.340 ± 4.305	<0.40
15 min	40.250 ± 5.784	48.228 ± 9.401	<0.10
30 min	47.629 ± 12.189	89.342 ± 6.127	<0.005
1 hr	74.783 ± 11.030	96.593 ± 14.944	<0.025
2 hr	80.290 ± 11.735	102.760 ± 8.156	<0.005
4 hr	64.300 ± 6.066	75.508 ± 18.104	<0.01
24 hr	58.033 ± 5.623	69.740 ± 6.953	<0.1
48 hr	52.294 ± 4.943	61.941 ± 6.732	<0.01

Accumulation of ^{14}C into liver and diaphragm protein proceeds at a more rapid rate following hydrocortisone administration than for control animals. This indicates that for these particular tissues the "protein precursor pool" derived from DL-histidine-2-^{14}C is turning over at a more rapid rate after glucocorticoids. Data of Wool demonstrate a similar cortisone-induced increase in the rate of incorporation of ^{14}C into diaphragm protein from L-histidine-imidazole-2-^{14}C (10). In these studies the time at which protein ^{14}C activity in control diaphragm tissue reaches its maximum value is between 120 and 180 min, while the maximum incorporation of ^{14}C into protein in steroid-treated tissue is 30 min. In both our study and that of Wool the maximum ^{14}C specific activity levels attained in diaphragm protein of steroid-treated animals were less than for the controls.

In the liver both the rate of incorporation into protein from the "protein precursor pool" and the maximum level of ^{14}C-protein specific activity reached in hydrocortisone-treated animals were greater than attained by control animals. In addition it is apparent that the admin-

Table 4. ^{14}C specific activity of diaphragm protein following IV injection of DL-histidine-2-^{14}C in the rat.

Time following injection	^{14}C specific activity $\frac{(dpm/mg\ protein)}{\mu Ci\ injected}$		
	Controls	Steroids	p value
7 min	2.196 ± 0.281	3.497 ± 1.888	<0.025
15 min	3.291 ± 0.622	5.825 ± 1.203	<0.005
30 min	5.317 ± 1.885	9.766 ± 2.189	<0.005
1 hr	7.806 ± 1.369	10.330 ± 1.809	<0.025
2 hr	13.073 ± 1.815	14.098 ± 0.852	<0.20
4 hr	18.578 ± 2.340	15.141 ± 1.296	<0.10
24 hr	18.729 ± 1.692	17.273 ± 1.572	<0.005
48 hr	19.393 ± 3.350	15.299 ± 1.574	<0.01

istration of hydrocortisone was accompanied by a relatively greater incorporation of ^{14}C from histidine into liver protein than into diaphragm protein. (Ratio of maximum ^{14}C-protein specific activity attained by liver to that in diaphragm was approximately 4:1 in control rats and approximately 6:1 in hydrocortisone-treated rats).

SUMMARY

L-histidine-2-imidazole-^{14}C was administered to each of a group of control animals and a group of animals pretreated with hydrocortisone for 6 days prior to injection of histidine. The rate of metabolism to CO_2 during the first hour of each study was fitted to a two-exponential function $F(t) = A(e^{-r_1 t} - e^{-r_2 t})$. There was no significant difference in the fitting parameters A, r_1, and r_2 for the two groups. The calculated fractional turnover of the histidine compartment following the administration of hydrocortisone was consequently unchanged in the direction of either anabolic or catabolic processes. However, the plasma histidine concentration in hydrocortisone-treated animals was diminished by approximately 35%, suggesting that the net turnover of the histidine pool may be decreased following such treatment.

In the diaphragm, the rate of ^{14}C incorporation into protein from DL-histidine-2-^{14}C was greater in steroid-treated animals, but the maximum levels reached were less than in the controls. In the liver both the rate of ^{14}C incorporation and the maximum ^{14}C incorporation into protein from DL-histidine-2-^{14}C in hydrocortisone-treated animals were greater than in the controls. These findings indicated that the turnover rate of the histidine-containing "protein precursor pool" in both the diaphragm and liver was increased following steroid administration. In addition the administration of hydrocortisone resulted in a relatively greater incorporation of ^{14}C from histidine into liver protein than into diaphragm protein.

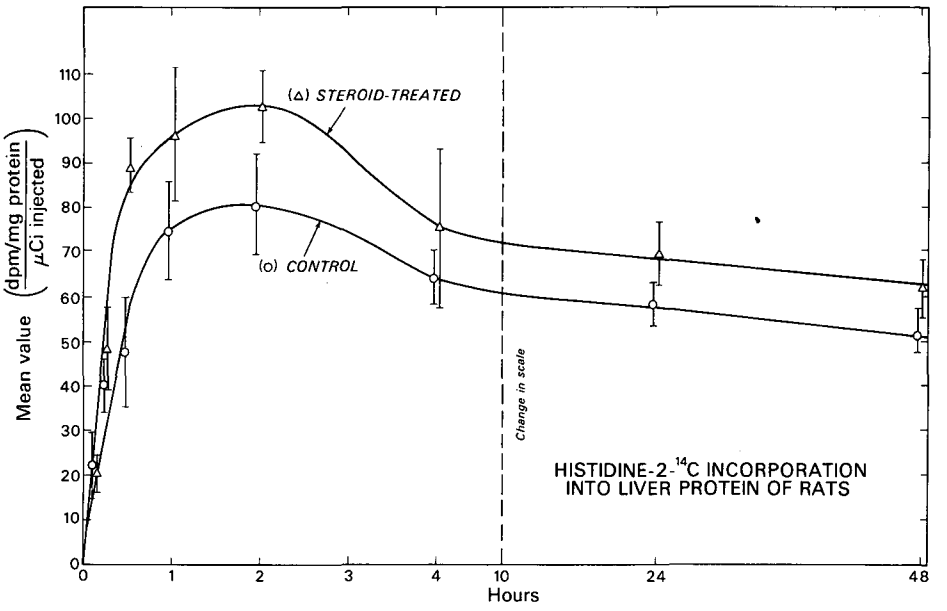

Fig. 1. Changes with time in ^{14}C-specific activity in rat liver protein following IV administration of DL-histidine-2-^{14}C. The ordinate represents disintegrations per min per mg liver protein per μCi injected, and the abscissa represents time in hours after injection of radioisotope. Individual points correspond to those presented in Table 3. Brackets about each point represent 1 standard deviation of the plotted mean value.

DBL686-4775

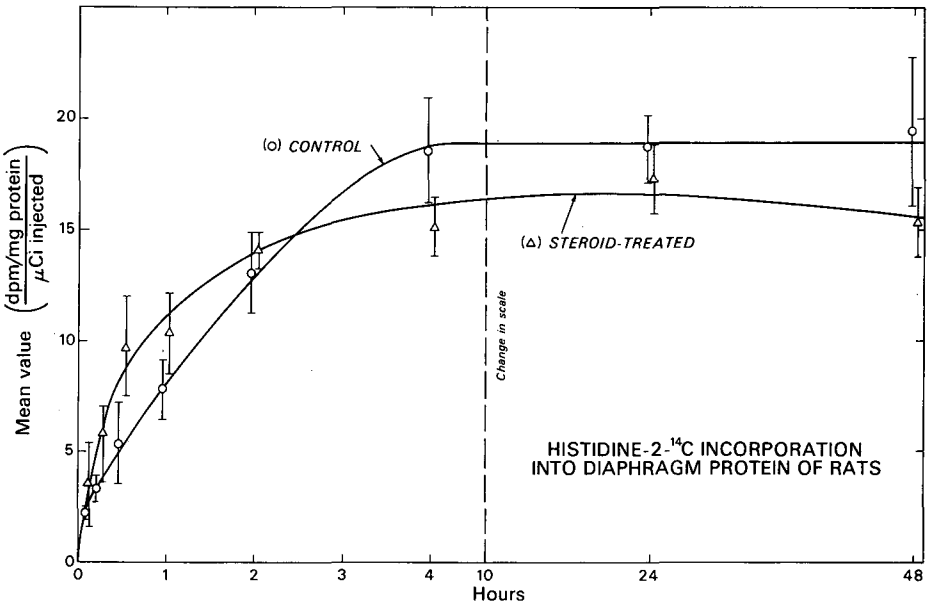

Fig. 2. Changes with time in ^{14}C-specific activity in rat diaphragm protein following IV administration of DL-histidine-2-^{14}C. The ordinate represents disintegrations per min per mg diaphragm protein per μCi injected, and the abscissa represents time in hours after injection of radioisotope. Individual points correspond to those presented in Table 4. Brackets about each point represent 1 standard deviation of the plotted mean value.

DBL686-4776

REFERENCES AND NOTE

1. Long, C. N. H.; and Lukens, F. D. W.: J. Exptl. Med. 63: 465 (1936).
2. Long, C. N. H.; Katzin, B.; and Fry, E. C.: Endocrinology 26: 309 (1940).
3. Ingle, D. J.: in "Steroid Hormones," Ed. E. S. Gordon, Madison, University of Wisconsin Press, 1950, p. 150.
4. Clark, I.: J. Biol. Chem. 200: 69 (1953).
5. Silber, R. H.; and Porter, C. C.: Endocrinology 52: 518 (1953).
6. Bondy, P. K.: Endocrinology 45: 605 (1949).
7. Friedberg, F.; and Greenberg, D. M.: J. Biol. Chem. 168: 405 (1947).
8. Lotspeich, W. D.: J. Biol. Chem. 185: 22 (1950).
9. Kaplan, S. A., and Shimizu, C. S.: Endocrinology 72: 267 (1963).
10. Wool, I. G.: Am. J. Physiol. 199: 715 (1960).

This investigation was supported in part by a Public Health Service Fellowship #2-F3-CA-29, 602-02 from the National Cancer Institute and in part under A.E.C. Contract No. W-7405-eng-48.

Human Cell Control Mechanisms.

I. Effects of Thyroxine on Cell Life Cycle Parameters

H. John Burki

INTRODUCTION

Recent studies by Siegel and Tobias (1, 2) have shown clearly that thyroxine changes the growth rate of human kidney cells ("T" cells) in culture. The presence of this hormone facilitates the plating efficiency of the cells in culture and stimulates increased uptake of tritiated uridine into the cellular RNA (1, 2). These growth rate changes and other effects are dependent upon the concentration of the hormone in the media; moreover, the stimulation effects are chemically specific (1, 2). Thus, the system of these "T" cells when treated with thyroxine provides a quantitative system in which to study some aspects of the control of human cell growth in vitro.

Since it was known that the growth rate of "T" cells was increased by thyroxine, it was decided to determine which aspects of the cell life cycle were changed by administration of this hormone.

MATERIALS AND METHODS

A heteroploid cell line of human kidney origin (3) obtained from Dr. Bootsma, which had been frozen and stored in liquid nitrogen for the last four years (4), has been maintained in monolayer cultures on plastic tissue culture dishes in our Laboratory for the last 6 months. These "T" cells were used for this study. The growth media consisted of 0.5% lactalbumen hydrolysate, and 5% newborn calf serum in Hanks salt solution supplemented with 100 I. U. penicillin and 0.10 mg streptomycin per ml. This media was supplemented in certain cases with ℓ-thyroxine in the manner described by Siegel and Tobias (1, 2). Colcemid (0.25 μg/ml) [CIBA] and H^3TdR (New England Nuclear) were also used in some experiments. The growth rate of the cells was measured by determining the colony multiplicity or by determining the cells per ml (using an electronic cell counter) of a cell suspension prepared by trypsinizing the cells by use of 0.1% standard trypsin.

Radioautographs were prepared in the following way: Approximately 3×10^4 cells were placed in glass tissue culture dishes which contained seven small glass coverslips. The cells were grown for 5.5 days and then were labeled with tritiated methyl thymidine in the manner described below. At specific times the cover slip cultures were removed from the incubation mixture, added to 50% saline solution for 5 min, fixed for 10 min in Carnoy's fixative, rinsed in 70% alcohol, air dried, and mounted on slides by use of Permount diluted with toluene. The

slides were dipped in NTB-2 nuclear track emulsion in a dark room, placed in light tight boxes containing a drying agent, and stored until development at 4°F. The slides were developed in dektol for 5 min, fixed with Kodak acid fixer for 10 min, and washed for 1 hour in cool water. The slides were then air dried and stained with Giemsa. For determination of the percent labeled cells at least 300 cells were scored.

The mitotic index was determined by recording the number of cells having mitotic figures per 1000 cells scored.

RESULTS

When control cells are incubated with tritiated methyl thymidine (10 μCi/ml or 13.7 Ci/mM) and with colcemid (0.25 μg/ml) the results given in Figs. 1 and 2 were obtained. The percent of cells having silver grains as a function of the time of sampling is given. The intercept of the straight line drawn is 24%. This indicates that the percentage of the cells engaged in DNA synthesis at any time in this asynchronous population is 24%.

In the absence of colcemid the curve would reach almost 100% labeled cells. However, in this experiment a plateau is reached, indicating that 15% of the cells blocked by colcemid are unlabeled. This means that most of these cells were in the G_2 period at the time of labeling. In these control conditions the mitotic index was found to be 4% and the population doubling time was 27 hours.

When all the conditions in the control cells are maintained, except that ℓ-thyroxine in optimum amounts is used to grow the cells for radioautography, the results in Fig. 2 are found. From this figure it may be seen that the quantity of "S" stage cells has increased to 31%. However, the approximate number of cells in the G_2 period in this case is slightly less than in the controls. Measurement of the mitotic index in hormone-treated populations indicated that 2.3% were in mitosis. The population doubling time was reduced to 20 hours when hormone was applied.

DISCUSSION

The relationships between the various life cycle parameters have been developed mathematically by Stanners and Till (5) and a simple graphical method of solution of these equations has been described by Okada (6). By use of this graphical method the complete life-cycle characteristics of human cells in culture with and without hormone treatment may be compared. The comparative values are given in Table 1.

It is clear from this table that the greatest temporal change in the cell life cycle is in the G_1 period, which is reduced from 15.4 to 10.3 hours. The inference which one might make therefore is that the cellular control of the rate of growth of "T" cells by thyroxine is expressed in the G_1 stage. This is of great interest, since this pre-DNA synthetic stage is the one showing greatest difference when a cancerous cell is compared with its normal counterpart (7). The G_1 period is also affected by less specific factors such as temperature (8) and media serum content (9). It is interesting to note that hydrocortisone appears to affect mammalian cells in

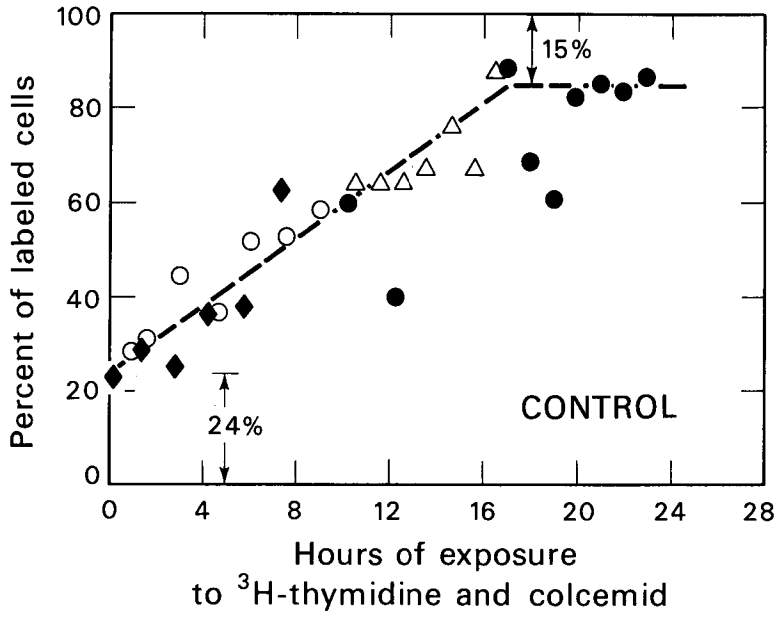

Fig. 1. Radioautographic data. Results of three replicate experiments. Control. DBL688-5373

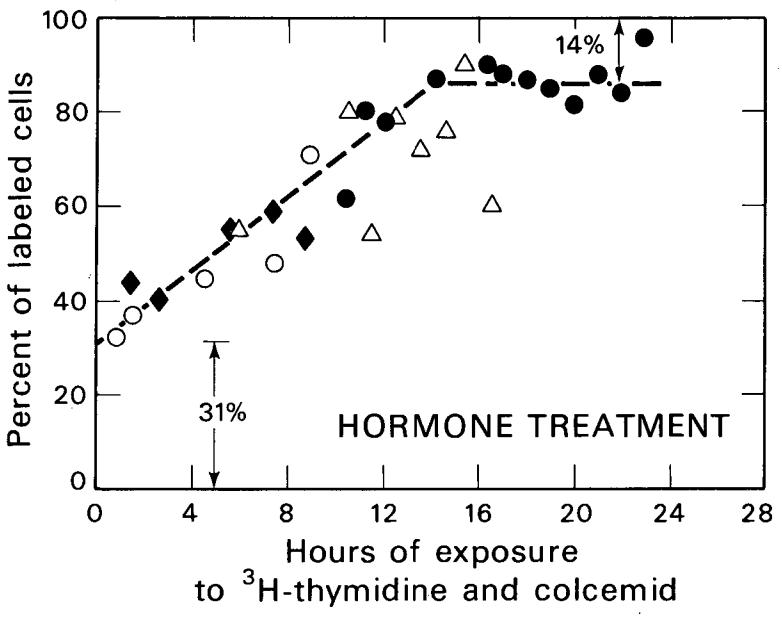

Fig. 2. Radioautographic data. Results of three replicate experiments. Hormone treatment. DBL688-5374

Table 1. Life-cycle characteristics.

		Control	Hormone
Measured	T_d	27.0 hr	20.0 hr
	M/N	4.1%	2.3%
	S/N	24%	31%
	G_2/N	15%	14%
Calculated	G_1/N	57%	53%
	t_m =	1.0 hr	0.7 hr
	t_s =	6.6 hr	6.4 hr
	t_{g_1} =	15.4 hr	10.3 hr
	t_{g_2} =	4.0 hr	2.5 hr

Key:

T_d = population doubling time

M/N = mitotic index

S/N = percent of cells in the DNA synthetic phase

G_1/N = percent of cells in the G_1 phase

G_2/N = percent of cells in the G_2 phase

t_m = average time for a cell to complete mitosis

t_s = average time for a cell to complete DNA replication

t_{g_1} = average time for a cell to complete the G_1 stage

t_{g_2} = average time for the cell to complete the G_2 stage.

the G_1 stage also (10). It is clear from the results that the "S" period is not changed by thyroxine, and hence the rate of DNA synthesis probably is similar in both cases. These preliminary results appear to show that the G_2 stage may also be shortened. However, a more accurate method of estimating this stage is in progress, and additional data are necessary before this point can be demonstrated. The results also seem to indicate that the mitotic time may be

slightly shorter in hormone-treated cells, although a change this small is difficult to demonstrate by using only the data presented above.

Thus, one may conclude that thyroxine, which controls the rate of growth of human cells in culture, does so for the most part by shortening the time that the cell needs to complete the G_1 period.

SUMMARY

Asynchronous exponentially growing human cells in culture were grown with and without the growth-stimulating hormone ℓ-thyroxine. The life-cycle characteristics of these cells in both cases were determined. It was found that the stage of the life cycle shortened considerably with hormone treatment was the G_1 stage. Therefore, the control exercised by thyroxine may be chiefly to facilitate the passage by a human cell through those reactions occurring in the G_1 stage.

ACKNOWLEDGMENTS

The author thanks Dr. C. A. Tobias for enabling him to come to the Donner Laboratory to study the "T" cell-thyroxine system. The technical support of Mrs. K. Boerke as well as special assistance of Mrs. W. Jackson is greatly appreciated.

REFERENCES

1. Siegel, E.; and Tobias, C. A.: Actions of thyroid hormones on cultured human cells. Nature 212: 1318 (1966).
2. Siegel, E.; and Tobias, C. A.: Subcellular interactions in cultured cells. Science 153: 763 (1966).
3. van der Veen, J.; Bots, L.; and Mes, A.: Establishment of two human cell strains from kidney and reticulosarcoma of lung. Arch. Virusforsch. 8: 230 (1958).
4. Bootsma, D.: private communication, 1968.
5. Stanners, C. P.; and Till, J. E.: DNA synthesis in individual L strain mouse cells. Biochem. Biophys. Acta 37: 406 (1960).
6. Okada, S.: A simple graphic method of computing the parameters of the life cycle of cultured mammalian cells in the exponential growth phase. J. Cell. Biol. 34 [3]: 915 (1967).
7. Reiskin, A. B.; and Mendelsohn, M. L.: Comparison of the cell cycle in induced carcinomas and their normal counterpart. Cancer Res. 24: 1131 (1964).
8. Watanabe, I.; and Okada, S.: Effects of temperature on the growth rate of cultured mammalian cells (L5178Y). J. Cell Biol. 32: 309 (1967).
9. Hahn, George; and Bagshaw, M. A.: Serum concentration: Effects on cycle and X-ray sensitivity of mammalian cells. Science 151: 459 (1966).
10. Kollmorgen, G. M.; and Griffin, M. J.: The radiosensitivity of HeLa cells grown in media containing hydrocortisone (Abstract). Radiation Research Society Meeting, April 1968.

Indirect Electrical Stimulation of the Visual Apparatus

Thomas F. Budinger

INTRODUCTION

Visual impressions can be produced in blind patients by electrical or electromagnetic stimulation of the visual apparatus without the use of internal electrodes. Many environmental sensors and aids for the blind are available which use tactile or auditory pathways as the mode of information input to the brain (1); however, electrical stimulation of the visual apparatus, although a procedure of some antiquity, has not been incorporated in research toward extending human perceptive abilities until recently. This report presents a survey of the progress in the field of indirect electrical stimulation of the visual cortex with some simple experiments which show that light flashes can be induced in blind patients by external-electrode electrical stimulation.

BACKGROUND

Some of the earliest experiments with electricity on the human body and the first cautious suggestion that the use of electrical stimulation might relieve blindness were made by Benjamin Franklin in 1751 (2). A few years later LeRoy reported the induction of flashes in a blind patient by using a Leyden jar discharge (3). The electrophysiology associated with electrical stimulation of the visual apparatus was studied by Volta, who experienced a flashlike sensation of light (known as Purkinje patterns or more commonly as phosphenes) when a small potential difference was induced between his eyelids and some other part of his body (4). During the nineteenth century the phenomenon of pressure (deformation phosphenes) (5) or electrically induced flashes was investigated by Brennen, DuBois-Reymond, Finkelstein, Helmholtz, Müller, Purkinje, Ritter, and others (6). The phenomenon of flash sensation was also elicited by using induction coils not touching the head by d'Arsonval (7) in 1896 and later independently by Thompson (8). Since these discoveries a few careful investigations of electrical (9) and magnetic (10) stimulation of man's visual apparatus have been made. The flash sensation phenomenon has been generally accepted as the result of retinal stimulation by a current emanating radially from the electrode through the eye globe (11). The conclusion that electrically induced phosphenes are mediated solely by the retina should be qualified. Russian workers demonstrated in the 1930's that phosphenes can be electrically induced in patients after enucleation but before optic nerve degeneration (12). However, only with an intact retina do the thresholds of electrical sensitivity remain normal, and only with a well preserved, attached retina are the normal adaptive changes in electrical sensitivity present (13). Fortunately, even if the retina were necessary for the induction of phosphenes, most blind patients have intact retinas and might benefit from a device which along with normal head scanning proprioception produces a pattern of light suggestive of the shape of objects in the environment. Atrophy of the retina of

an eye with severe visual defect might be circumvented by periodic electrical stimulation.

The direct approach to stimulation of the visual cortex by implanted electrodes was suggested by the pioneering work of Penfield (14) and implemented in an attempt to build a visual prosthesis by Button and Putnam in 1961 (15). This approach had some success, as has electrode implantation in the eighth cranial nerve for auditory stimulation (16). Brindley and Lewin (17) have recently (1968) confirmed and extended these results by producing phosphenes using radio-receivers connected to electrodes in direct contact with the visual cortex.

Other than Barnard's suggestions in 1947 (18), little has been reported regarding the practical use of electrical stimulation of the visual apparatus, and there has been little active research until recent years. In 1964 Barraquer (19) discussed the phenomenon of phosphene production by inducing alternating current in the head, and suggested that a transistorized photodetector device might be used as an aid for the blind. Such a system has been developed independently by us and, prior to our efforts, by a group at the University of Mexico sparked by Dr. Armando del Campo. These recent investigations have raised the question of whether the sensation of light produced in either blind or normal subjects is entirely phosphenes or might be mediated by a pathway from the supra- or infraorbital branches of the trigeminal nerve to the visual tract, perhaps via the reticular formation (20). The fact that visual impressions can be produced in blind patients as reported by the University of Mexico studies, and our studies in children with retrolental fibroplasia, prompts us to report some facts and ideas which might lead to the practical implementation of electrical and particularly electromagnetic stimulation of the visual cortex.

METHODOLOGY

The sensation of a light flash is elicited by application of 2 to 4 volts potential difference across the head using a 1-cm metal disk electrode on a ciliary arch or the forehead and a similar electrode placed on the back of the neck (Fig. 1). Electrolyte paste or sodium chloride solution is used to establish less than 10,000 ohms resistance. A sensation of "flash" is generated on making or breaking the circuit (rise time should be less than 100 msec). A flicker phenomenon can be generated by pulse trains or ac stimulation (fusion cannot be obtained at 60 Hz--normal upper limit for photic stimulation fusion); chronaxie is about 1 msec (21). The intensity of the flash is a function of current (usually about 0.3 mA), rise time, repetition rate, past stimulation experience, concomitant auditory noise, and even time of day, as the sensitivity of the eye to electrical stimulation has a circadian rhythm (22). Rise-time dependency might be more an electrode counter-EMF phenomenon than a characteristic of phosphene generation, as may be optimum repetition rate. Theoretically waveform should be important, particularly in color production, as early experiments demonstrated that different colors could be elicited depending on whether the anode or the cathode was nearer the eye being stimulated. The spatial identification of the flash is a function of the location of electrode application on the forehead or face; e.g., an electrode applied over the right temporal area gives an impression of a flash, usually a bluish-white crescent, a few meters above and to the right of the subject and an electrode placed on the forehead midline will give a sensation of a flash in

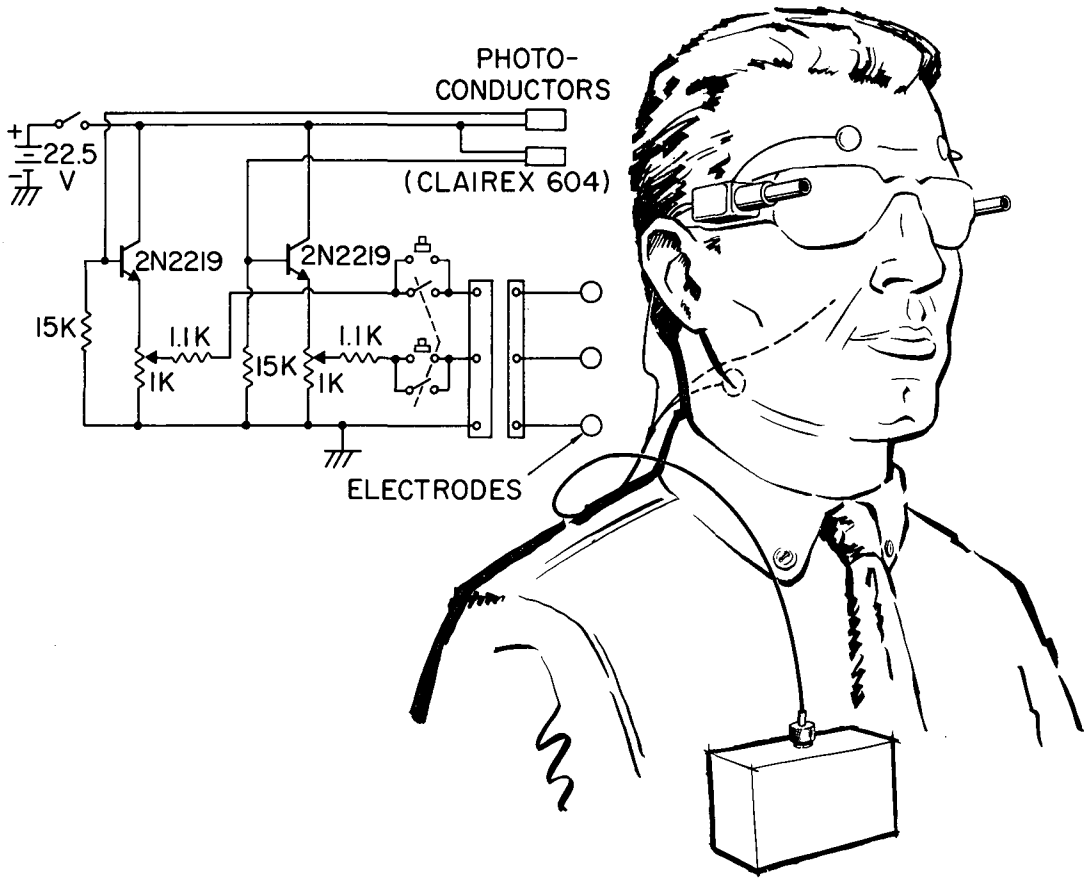

Fig. 1. Schematic diagram and electrode placement locations for induction of flash sensations (phosphenes). Output is about 6 V for bright objects.

DBL689-5446

both eyes located centrally a few meters ahead of the subject. Experiments with multiple electrode systems using intensity and delay combinations have not been conducted.

A simple device weighing 1 kilogram was made (Fig. 1), using two photodetectors mounted on ordinary glasses frames, and two independent amplifying systems, one connected to each photodetector, with a common electrode to the neck. The system shown in schematic fashion (Fig. 1) was designed to deliver 0 to 10 volts depending upon the luminosity of the light at which the sensor is "looking." The device has been used in the pulse mode wherein the experimental subject interrogates the environment either on the left, right, or center by manually depressing buttons and a flash is detected when the luminosity "seen" by the photodetectors changes. Electrode polarization and skin resistance problems are still troublesome. An automatic pulsing circuit with rise time (Fig. 2) or current intensity dependent upon light luminosity "seen" by the photodetectors would probably be a better environment sensor. The use of an electromagnet induction coil and appropriate circuit might enable one to achieve similar results without the cumbersome electrodes.

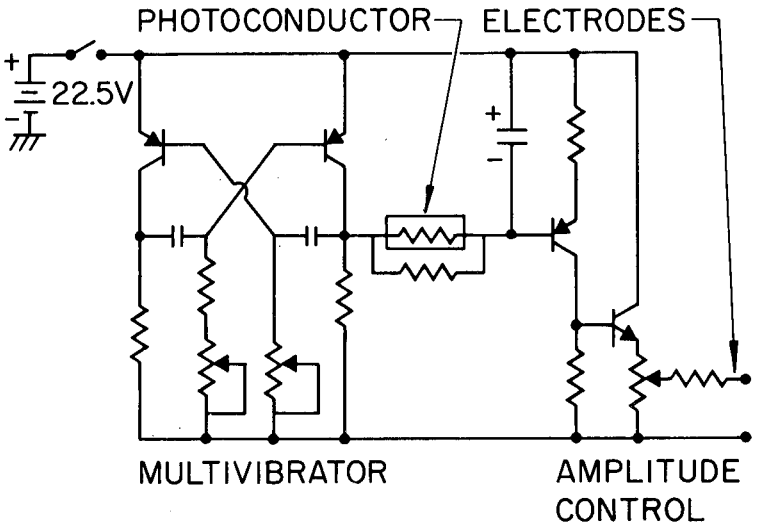

Fig. 2. Schematic diagram for a circuit which gives visual flicker sensation with subjective intensity controlled by external light luminosity "seen" by photodetectors.

DBL689-5447

RESULTS

Experiments are being conducted using the simple device of Fig. 1 with the purpose of ascertaining whether phosphene generation is a practical means of transferring information about the environment to the visually impaired. As shown in Table 1, the experimental subjects have been children with retrolental fibroplasia or retinal blastoma. The results indicate that a device as simple as that illustrated by Fig. 1 would allow some visually impaired children to navigate in areas where the light-dark contrast is great. Children having no memory of light as a sensation characterize the impulse as something new, describing it as a "bong" or "tap." Voltage threshold for pain is only slightly higher than the electrical phosphene threshold. Therefore, the responses of subjects with poor or no light memory are hard to interpret. Further, some aphasia or other difficulty communicating with the subjects made it impossible to quantitate the results. Experiments with enucleated patients have been inconclusive, but promising. A trigeminal to visual cortex pathway might have an anatomic basis, but production of phosphenes via this route seems physically untenable.

Two children with severe visual impairment were able to navigate better than usual using natural light following use of the device. This suggests that electrical stimulation of the defective retina might effect a lowering of the threshold to natural photic stimulation; however, navigation enhancement is often the case after a training session with other prosthetic devices.

DISCUSSION

Extension of these experiments to blind adults with and without intact retinas is indicated.

Our experiments and similar investigations by the University of Mexico team indicate a visual prosthesis using phosphene production has promise for some blind patients. The hypothesis that color is a function of waveform and the relationships between flash intensity, voltage, and rise time (dv/dt) need further investigation. If these questions are resolved, pattern

Table 1. Results of tests with device shown in Fig. 1.

Patient	Age (yrs.)	Sex	Disease	State	Results
J. T.	16	M	Retinal blastoma	Enucleation	Distinguished "like a tap" from high voltage pain "sting".
D. T.	14	M	Retinal blastoma	Enucleation	Distinguished "impulse" from high voltage "sting".
J. M.	16	M	Retrolental fibroplasia	Slight light perception	Distinguished phosphene from high voltage "sting" as "volts man volts". Unequivocal.
R. M.	12	F	Retrolental fibroplasia	No vision since 6 years old	Distinguished "shock" from "sting". Equivocal.
F. B.	14	M	Retrolental fibroplasia	Light perception only	Very positive results with patterns of light fingers and shadows. Saw "sparks" and "shocks".
H. M.	13	F	Retrolental fibroplasia	O. D. light perception, O. S. blind	Saw light circles and lines O. D. > O. S.
A. R.	14	M	Retrolental fibroplasia	Blind (aphasic)	"Stinging" only.
W. R.	14	M	Retrolental fibroplasia	Blind (aphasic)	Reported "motion". Equivocal results.
J. M.	14	F	Retrolental fibroplasia	Blind	Distinguished "bong" or "tap" from high voltage "sting".
C. C.	16	F	Probably hysterical blindness	Subjective blindness	No results to above pain threshold impulses.
15 normal adults		M, F	Normal	Blindfolded	Blue-white or yellow crescents and spots.

development might be implemented by an array of photodetectors connected to a multielectrode system on the forehead or eyeball (18). Results of our studies and the phosphene pattern studies using normal adults (23) suggest that subjective abstract light patterns can be controlled by waveform, repetition rate, electrode placement, and current. Thus, the information capacity of the phosphene mode might be much greater than is apparent on cursory examination.

The development of a system using photodetectors or even infrared sensing devices, sonar, or Gunn Effect radar is dependent on improvement in the electrode coupling. One of the most promising approaches is an electromagnetic coupling system between the environmental sensor and the brain. Using magnetic field fluctuations of about 1000 oersteds with coils about 2 mm from the head, one can induce the flash sensation either through the phosphene-retinal pathway or some other mechanism not yet delineated. Caution should be exercised in experimenting

with static fields over 80 oersteds, as a depression of cellular respiration has been reported (24). We are now conducting experiments with saline-sponge electrodes.

A device based on the concepts discussed here might provide a practical means of transferring information about the environment to the visual cortex without interfering with other sensory modalities.

It remains to be seen whether the practical embodiment of electrical or electromagnetic stimulation of the visual apparatus can provide a more useful prosthesis than tactile and auditory feedback devices now being investigated. At present the cane remains the superior aid for the blind.

SUMMARY

Subjective sensations of light flashes can be generated in humans by means of 0.3 mA current across the head (rise time of about 100 msec). The flash sensation (phosphenes) can be induced by exciting the retina, the optic nerve, or the brain cortex, and has some promise as an aid to the visually impaired patient. Preliminary experiments with normal but blindfolded subjects and children with partial visual impairment or complete enucleation show that fuller development of a head-mounted photodetector system using external electrodes has promise as a visual aid for many blind patients.

ACKNOWLEDGMENTS

Electrical engineering contributions to this study were provided by Dr. T. Huen. The cooperation of the California School for the Blind is appreciated. Some comments from Dr. H. B. Barlow, Dr. L. L. Clark, Dr. L. Harmon, and Dr. R. J. Howerton, who read the manuscript, were incorporated in the final draft. Reservations about the supposition that induced phosphenes can transfer sufficient information to materially aid the blind are shared by the author.

REFERENCES

1. For review of sensory aids see: Zahl, P. A.: Blindness, New York, Hafner Publ. Co., 1962, p. 760; Bennett, E.; Degan, J.; and Spiegel, J.: Human Factors in Technology, New York, McGraw-Hill, 1963, p. 293; Shrager, P. G.; and Süsskind, C.: Advan. Electron. Electron Physics 20: 261 (1964); Clark, L. L. (ed.): Proceedings of Rotterdam Mobility Conference, American Foundation for the Blind, 1965, p. 293; Bliss, J. C.; and Crane, H. D., Experiments in Tactile Perception. Final report for contracts NASA 2-1679 and AF33(615)-1099, Stanford Research Institute, 1965, p. 197; Bach-y-Rita, P.: Acta Neurol. Scandinav. 43: 417 (1967).
2. Franklin, Benjamin: Philos. Trans. Royal Soc. (London) 47: 202 (1751-2).
3. LeRoy, M.: Acad. Roy. Sciences (Paris), Memoires Math. Phys. 60: 87-95 (1755).
4. Volta, A.: Collezione dell' Opere 2 (2); see in particular p. 124 (1796).
5. Brindley, G. S.: J. Physiol. (Proc. Physiol. Soc.) 188: 24 (1967).
6. Reviews of early work can be found in: Finkelstein, L.: Archiv. Psychiatrie 26: 867 (1894); Müller, G. E.: Z. Psychol. Physiol. Sinnesorg. 14: 329 (1897).

7. d'Arsonval, M. C. R.: Soc. Biol. (Paris) 48: 450 (1896).
8. Thompson, S. P.: Proc. Roy. Soc. (London) Ser. B 82: 396 (1910).
9. Bouman, H. D.: Arch. neerl. Physiol. 20: 430 (1935); Barlow, H. B.; Kohn, H. I.; and Walsh, E. G.: Am. J. Physiol. 148: 376 (1947); Bogoslowskiĭ, A. I.; and Segal, J.: J. Physiol. (Paris) 39: 101 (1947); Motokawa, K.; and Iwama, K.: Tohoku J. Exptl. Med. 53: 201 (1950); Brindley, G. S.: J. Physiol. 164: 157 (1962); ibid. 171: 514 (1964).
10. Beer, B.: Wiener klinische Wochenschrift 15: 108 (1902); Dunlap, L.: Science 33: 68 (1911); Magnusson, C. E.; and Stevens, H. C.: Am. J. Physiol. 29: 124 (1911); Barlow, H. B.; Kohn, H. I.; and Walsh, E. G.: Am. J. Physiol. 148: 372 (1947); Valentinuzzi, M.: Am. J. Med. Electron. 1: 112 (1962); Becker, R. O.: Med. Electron. Biol. Eng. 1: 293 (1963).
11. Brindley, G. S.: J. Physiol. 127: 189 (1955).
12. Bogoslowskiĭ, A. I.: v. Graefe's Arch. Ophthal. 133: 195 (1934); Volokhov, A. A.; Gersuni, G. V.; Zagorul'ko, L. T.; and Lebedinskiĭ, A. V.: Fiziologich. zh. 19: (1935); Vishnevskii, N. A.: Vesti. oftalm. 15: 36 (1939); Akimochkina, V. A.: Problemy fiziolog. optiki 1: 125 (1941).
13. Bogoslovskii, A. I.; and Ivanova, E. M.: Problemy fiziolog. optiki 1: 129 (1941).
14. Penfield, W.; and Rasmussen, T.: Cerebral Cortex of Man, New York, Macmillan Co., 1950, p. 140.
15. Button, J.; and Putnam, T.: J. Iowa Med. Soc. 52: 17 (1962); Shaw, J. D.: Method and means for aiding the blind, U. S. Patent No. 2, 721, 316; also see Radio-Electron. Mag. 27: 170 (1956); Shipley, T.: in Technology and Blindness, Vol. II, edited by L. L. Clark, New York, American Foundation for the Blind, 1963, p. 247; Marg. E.; and Dierssen, G.: Confinia Neurol. 26: 57 (1965).
16. Simmons, F. B.; Epley, J. M.; Lummis, R. C.; Guttman, N.; Frishkopf, L. S.; Harmon, L. D.; and Zwicker, E.: Science 148: 104 (1965).
17. Brindley, G. S.; and Lewin, W. S.: J. Physiol. 196: 479 (1968).
18. Barnard, R. D.: Ohio J. Sci. 47: 132 (1947).
19. Barraquer, Tomas: Arch. Soc. Am. Oftal. Optom. 5: 61 (1964).
20. Hernández-Peón, Raúl: in Sensory Communication, edited by W. A. Rosenblith, Boston, MIT Press, 1961, p. 497.
21. Gersuni, G. W.; Lebedinskii, A. W.; Volochov, A. A.; and Zagorul'ko, L. T.: Fiziol. zh. 19: 1123 (1935).
22. Bogoslovskii, A. I.: Byull. Eksperim. Biol. i Med. 3: 140 (1937).
23. Pereira, M. R.; Nutini, L. G.; Fardon, J. C.; and Cook, E. S.: Soc. Exptl. Biol. Med. Proc. 1124: 573 (1967).
24. Knoll, M.; and Kugler, J.: Nature (London) 184: 1823 (1959); Höfer, O.: Electromedizin 8: 72 (1963); Knoll, M.; Höfer, O.; Lawder, S. D.; and Lawder, U. M.: Electromedizin 7: 235 (1962); Kellogg, R.; Knoll, M.; and Kugler, J.: Nature (London) 208: 1129 (1965).

Erythropoietic Response in Dogs Given Sublethal Whole Body Proton Irradiation Followed by Hypoxic Hypoxia

Henry Aceto, Jr., Robert W. Springsteen, W. Gee and H. Saul Winchell

Serial iron kinetics studies and radiophosphorus determinations of total red cell volume were performed in three groups of beagle dogs exposed to hypoxia (pO_2 = 72 mm Hg), sublethal whole body proton irradiation (200 rads MTD), and a combination of these two stresses, respectively. Hypoxia alone resulted in an increase, within one day, in plasma iron turnover rate (PITR), an increase in fractional incorporation of radioiron in red cells and a corresponding elevation in total red cell volume. Sublethal whole body proton irradiation alone resulted in diminution within one day in PITR, and a corresponding marked depression of fractional incorporation of radioiron in red cells. Dogs receiving a combination of whole body proton irradiation followed by hypoxic hypoxia demonstrated an initial increase in PITR for the first 7 days approximating the response seen with hypoxia alone. At 14 days the PITR and the fractional radioiron incorporation into red cells rapidly decreased, approaching, but not reaching, that seen in the dogs receiving radiation alone. Thereafter, the increase in the PITR in these dogs was greater than that seen following radiation alone and by 29 days again approximated that seen in dogs subjected to hypoxia alone. At all times total red cell volume in dogs subjected to combined whole body radiation and hypoxia was maintained at a level intermediate between that seen in dogs subjected to whole body radiation or hypoxia alone.

We conclude that following sublethal whole body proton irradiation, cells responsible for synthesis of hemoglobin are capable of normal or increased rates of hemoglobin synthesis in response to hypoxic stimulation despite severe radiation damage. Red cells produced under such hypoxic stress following whole body irradiation are not extremely short lived and are functionally significant as evidenced by normally shaped red cell iron-59 incorporation curves and red cell volumes which are greater than that noted in dogs receiving radiation alone. Those cells present in the bone marrow at the time of irradiation which were "responsible" for hemoglobin synthesis during the ensuing 7 days are little affected by 200 rads (MTD) of whole body proton irradiation, with regard to their capability of synthesizing hemoglobin in response to hypoxia. Additionally, while those cells present in the bone marrow at the time of irradiation which are "responsible" for hemoglobin synthesis beyond 7 days following irradiation are more affected by 200 rads of whole body proton irradiation than those cells "responsible" for hemoglobin synthesis during the initial 7 days, even these cells are capable of being stimulated by hypoxic hypoxia.

INTRODUCTION

Diminution in plasma iron turnover rate (PITR) and calculated hemoglobin synthesis rate is a well documented quantitative change in erythropoiesis noted following whole body irradiation (1). The finding of elevated plasma erythropoietin levels following whole body irradiation (2) suggests that irradiated erythropoietic cells are incapable of greater hemoglobin synthesis than that observed in the non-stimulated postirradiation state. Indeed, Newsom and Kimeldorf (3) have attributed their observed increased mortality of animals maintained at altitude following radiation exposure to an inadequate erythropoietic response during exposure to hypoxia. The present studies demonstrate that irradiated (200 rads) erythropoietic cells are capable of normal or increased rates of hemoglobin synthesis when subsequently stimulated by hypoxic hypoxia. The results of these findings are discussed both in regard to relative radiosensitivities of erythropoietic cells of different ages as well as in regard to erythropoiesis in astronauts subjected to combined radiation and hypoxic stress.

MATERIALS AND METHODS

Female beagle dogs, approximately 2 years of age, were obtained from the Radiobiology Laboratory, University of California, Davis. These animals are essentially worm free and are immunized for distemper and hepatitis. They were transferred to individual cages upon arrival and after a 3 week holding period, were subjected to a 4 week baseline study. In order to circumvent the complications of red cell measurements introduced by splenic activity in the dog, all of the animals were splenectomized two weeks prior to commencing the baseline work. The 12 animals represented 3 separate experiments each consisting of a group of 4 animals. Upon completion of the baseline study, each group of four animals was divided as follows:

(1) IRRADIATED CONTROL These animals received a sublethal whole body exposure of 200 rads (MTD) delivered by the degraded 730 MeV proton beam whose residual mean energy is 265 MeV. The animals were anesthetized with sodium pentobarbitol, 30 mg/kg, given intravenously immediately prior to irradiation. They were placed in a specially constructed styrofoam holder, positioned with their long axis normal to the beam, and rotated to ensure omnilateral irradiation. Dosimetric measurements utilizing Teflon-encapsulated thermoluminescent lithium fluoride (LiF) dosimeters positioned in a frozen dog cadaver indicate a uniform dose distribution to within 10% over the entire body. The radiation was delivered at a rate of 26 rads/min. Upon completion of the irradiation, the animals were returned to the animal room.

(2) IRRADIATED-HYPOXIC The irradiating procedure for these animals was identical to that of the irradiated-control animals. The animals were immediately transferred to the high altitude chamber within 30 to 60 minutes following irradiation and maintained at a simulated altitude of 18,000 ft (pO_2 = 72 mm Hg) for a period of 57 days. The altitude exposure was interrupted each day for a period of less than an hour for animal maintenance.

At periodic intervals this daily period of recompression was extended to 3 or 4 hours in order that radioisotopic hematological assays could be performed. The total time spent at

altitude amounted to approximately 94% of the 57-day period. Decompression and recompression rates were 2,000 ft/min.

(3) HYPOXIC-CONTROL These animals were anesthetized and sham-irradiated following the procedures for the irradiated animals. They were then immediately transferred to the chamber and maintained at a simulated altitude of 18,000 ft for a period of 57 days. The temperature and relative humidity in the chamber were maintained at 25°C and 50% RH, respectively. The gaseous environment of the chamber was continuously monitored for O_2 and CO_2 levels with a Beckman analyzer and its associated recorder. The periods of decompression and recompression were the same as those for the irradiated-hypoxic animals.

(4) CONTROL These animals were anesthetized and sham-irradiated following the procedures for the irradiated animals and then returned to the animal room.

The following assays were performed on each animal:

1. Red Blood Cell Volume (RBCV). The RBCV was determined by the radiophosphorus tagged cell method of Berlin et al. (4).
2. Serum Iron. The concentration of iron in plasma was determined by the modification of Peters and co-workers of the Ramsey method (5).
3. Plasma Volume. The plasma volume was determined by the ^{59}Fe dilution technique of Apt and co-workers (6).
4. Red Cell Radioiron Uptake. With some modification, the methods described by Huff et al. were employed for these experiments (7).
5. Plasma Iron Clearance Rate (PCR). The measurement of clearance rate of radioiron from the plasma has been described by Huff et al. (8).

Plasma iron turnover rate (PITR) was calculated as the product of plasma volume, net plasma iron concentration, and plasma iron clearance rate.

Effective hemoglobin synthesis was calculated as the product of plasma iron turnover rate, maximal radioiron incorporation in circulating red cells, and the ratio of molecular weight of hemoglobin to four times the molecular weight of iron.

Datum points for these parameters represent the average of values obtained from three separate experiments each of which is within about 10 or 15% of the mean value.

RESULTS

Figure 1 graphically presents serial changes in plasma iron turnover rates (PITR) expressed as a fraction of baseline values obtained in each individual animal at various time intervals following whole body exposure to proton radiation (200 rads MTD) and/or hypoxia (pO_2 = 72 mm Hg). Within one day following exposure to hypoxia alone, PITR increased significantly and remained elevated for the duration of the hypoxic exposure (57 days). Thereafter it immediately fell to below baseline levels.

Within one day following exposure to 200 rads whole body proton radiation the PITR diminished and continued to fall until the 14th day. There is a definite increase in the PITR by the 21st day and it approaches baseline levels by the 28th day. Thereafter, there is an "overshoot" to above normal levels and it again approaches baseline levels by the 80th day.

Within one day following combined exposure to whole body radiation plus hypoxia there was an increase in PITR which continued through the 7th day at a level roughly equivalent to that seen with hypoxia alone. At 14 days the PITR rapidly diminished to a level somewhat greater than that seen with whole body radiation alone. Thereafter the PITR again increased at a greater rate than that seen following radiation alone and by 29 days approximated that seen in dogs subjected to hypoxia. Subsequent to discontinuance of hypoxia at 57 days the diminution in PITR in animals receiving combined radiation followed by hypoxia is comparable to that seen with hypoxia alone.

The pattern of radioiron incorporation into circulating red cells was obtained in animals subsequent to radioiron administration at 1, 7, and 14 days following radiation and/or hypoxia. In each case the radioiron incorporation in the circulating red cells increased rapidly, achieving maximum levels 2 to 3 days following intravenous administration of ^{59}Fe and remained at the maximum levels for the ensuing 3 to 4 days of measurement. In no case was an early decrease in the radioiron content of circulating red cells observed, thus precluding the presence of an early (within 3 to 4 days) destruction of newly formed red cells.

Figure 2 presents red cell ^{59}Fe incorporation curves obtained on animals administered ^{59}Fe 7 days subsequent to exposure to whole body proton irradiation and/or hypoxia. It can be seen that 7 days subsequent to whole body proton irradiation and/or hypoxia the pattern of radioiron incorporation into circulating red cells is essentially identical for the control animals and those subjected to hypoxia alone or total body irradiation followed by hypoxia. There is a marked diminution in the ^{59}Fe radioiron incorporation into circulating red cells in those animals given whole body proton irradiation alone.

Figure 3 is a plot of the incorporation of the radioiron in the circulating red cells as measured on the 6th day following administration of radioiron as a function of days after irradiation and/or hypoxia on which the radioiron was administered. This time (6th day) is taken as "maximum incorporation of ^{59}Fe in red cells" and is expressed as percent of radioactivity injected. The "maximum radioiron incorporation" into red cells in animals exposed to hypoxia alone or whole body proton irradiation followed by hypoxia was close to normal values 1 and 7 days following exposure to irradiation and/or hypoxia. However, on the 14th day, dogs exposed to hypoxia alone achieved a greater than normal "maximum incorporation of radioiron" in circulating red cells (99%) while those treated with whole body proton irradiation followed by hypoxia had a marked diminution in "maximum radiation" incorporation into red cells approaching that seen in animals given whole body radiation alone. Dogs given whole body radiation alone had an immediated diminution in "maximum radioiron incorporation" into circulating red cells (10%), which increased linearly to approximately 35% by day 14.

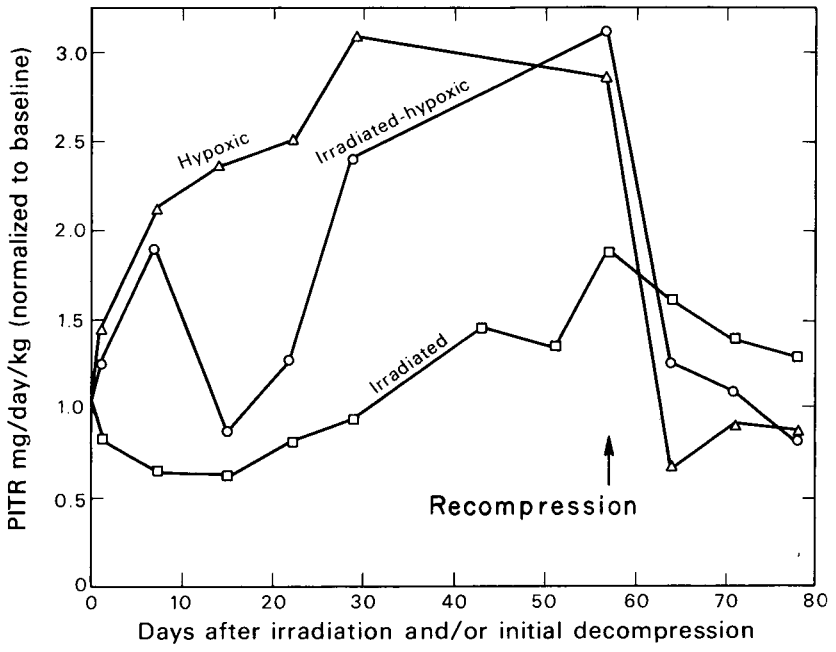

Fig. 1. Serial changes in plasma iron turnover rates (PITR) at various time intervals following whole body exposure to proton radiation (200 rads MTD) and/or hypoxia (pO_2 = 72 mm Hg).

DBL687-4792

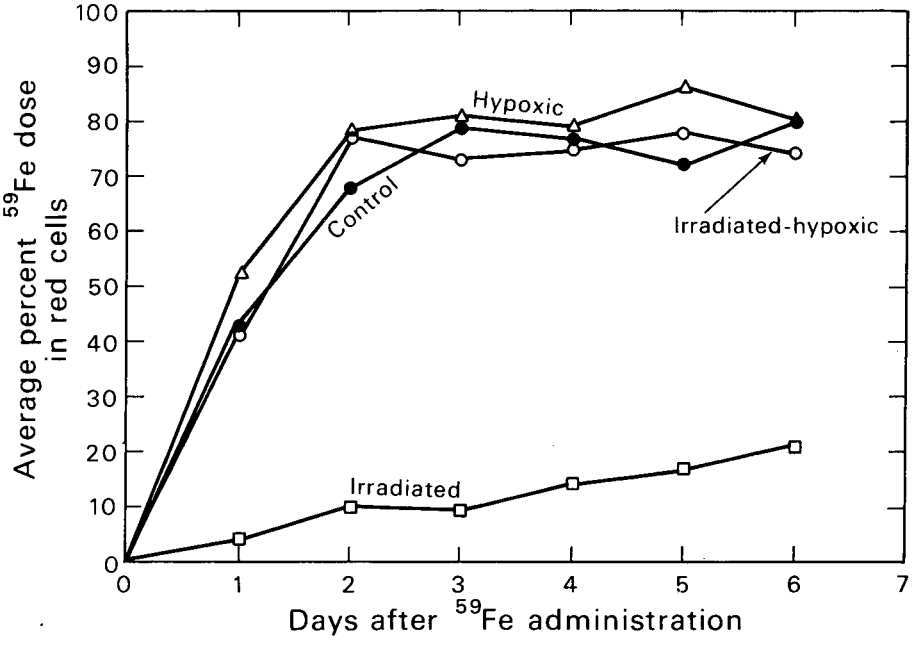

Fig. 2. Red cell ^{59}Fe incorporation curves obtained on animals 7 days subsequent to exposure to whole body proton irradiation and/or hypoxia.

DBL687-4795

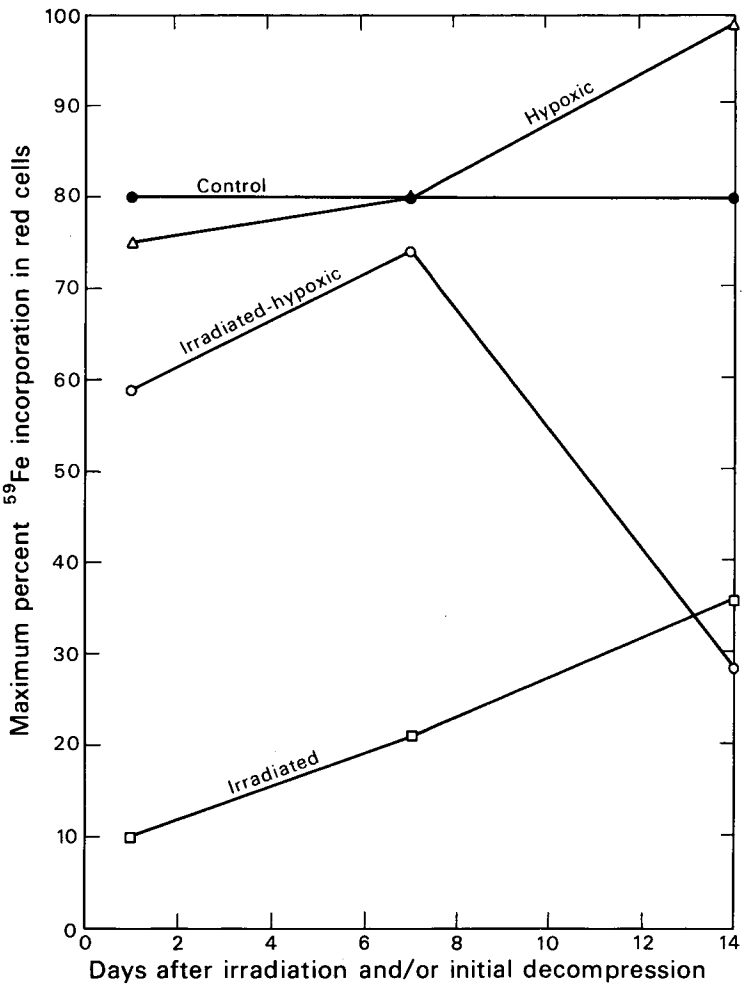

Fig. 3. Plot of the incorporation of radioiron in the circulating red cells as measured on the 6th day following administration of radioiron as a function of days after irradiation and/or hypoxia on which the radioiron was administered. This time (6th day) is taken as "maximum incorporation of ^{59}Fe in red cells" and is expressed as percent of radioactivity injected.

DBL687-4794

Figure 4 presents results of the calculated effective hemoglobin synthesis rates by using the method of Huff et al. (9). An estimate of effective hemoglobin synthesis in this case was obtained by multiplying the "maximal fractional incorporation of radioiron" into circulating red cells by the plasma iron turnover rate and the known relationship between grams hemoglobin synthesized and milligrams iron incorporated into hemoglobin. The data are expressed as a ratio of the calculated effective hemoglobin synthesis rate at various times following irradiation and/or hypoxia to that obtained during the pretreatment observation period. It can be noted that the calculated effective hemoglobin synthesis rate in animals subjected to hypoxia alone increases in essentially a linear fashion from day 1 to day 14. The calculated effective hemoglobin synthesis rate in animals given radiation alone was markedly depressed at 1 day subsequent to such radiation and over the ensuing 2 weeks there was only modest increase in the effective hemoglobin synthesis rate. In animals exposed to sublethal whole body proton radiation followed by hypoxia, the effective hemoglobin synthesis rate was not diminished on the first day following radiation and by the 7th day there was actually significantly increased effective hemoglobin synthesis, approaching that seen in animals subjected to hypoxia alone. At the

14th day there was a rapid diminution in effective hemoglobin synthesis rate to a level approaching that seen in animals treated by radiation alone.

Figure 5 presents the results of serial red cell volume determinations on 3 groups of dogs at various time intervals following whole body proton irradiation and/or hypoxia expressed in milliliters/kilogram body weight and normalized to baseline values. In animals exposed to hypoxic hypoxia alone there was a progressive increase in red cell volume, reaching maximum levels at about the 52nd day. On the 57th day hypoxia was discontinued and there was a brisk drop in the circulating red cell volume. Although the rate at which the red cell volume decreased following the discontinuance of the hypoxia suggests that these cells were being removed from the circulation at a rate faster than that which would be anticipated from normal red cell senescence, the data are too meager to reach any conclusions on this particular point. Animals exposed to whole body proton irradiation alone had a progressive fall in their total red cell volume until approximately the 24th day following irradiation. Since the rate of this fall also appeared to be somewhat steeper than that anticipated from normal red cell senescence, the possibility of blood loss must be entertained in these irradiated animals. Subsequent to 24 days there was a slow increase in the red cell volume in irradiated dogs approaching the pre-irradiation levels by the 72nd day. Animals exposed to whole body proton irradiation followed immediately by hypoxic hypoxia maintained red cell volumes intermediate between that seen in animals treated with hypoxia or whole body irradiation alone.

DISCUSSION

In the present experiment, within 24 hours after exposure to hypoxic hypoxia, a significant increase in plasma iron turnover rate and calculated effective hemoglobin synthesis was noted in dogs. Similar results were previously noted in a human subject (10). Since hemoglobin synthesis occurs largely in the later stages of normoblast development, this early and significant increase in hemoglobin synthesis following hypoxia is most probably due to stimulation of cells well along in their commitment to the formation of red cells rather than to stimulation of an uncommitted or stem cell pool to enter the erythroid cell line.

Previous estimates of the turnover rate of erythroid precursors within the bone marrow are generally less than 5 to 7 days (11). The finding that hypoxic hypoxia following sublethal total body radiation results in an increase in hemoglobin synthesis during the first 7-day period following the application of these stresses suggests that most of the recongizable erythroid precursors in the bone marrow at the time of radiation participated in this erythropoietic response. If this indeed is the case, one must conclude that the majority of cells committed to, or recognizable as, erythroid precursors at the time of radiation were insufficiently damaged by 200 rads to preclude their responding to hypoxic hypoxia with increased synthesis of hemoglobin. Indeed, the response to this hypoxic hypoxia was very close to the response noted in unirradiated animals.

Although it is generally accepted that irradiated erythropoietic cells are incapable of normal or increased proliferation, the contrary results of the present paper actually might be anticipated from theoretical considerations. The viability and functional integrity of the red

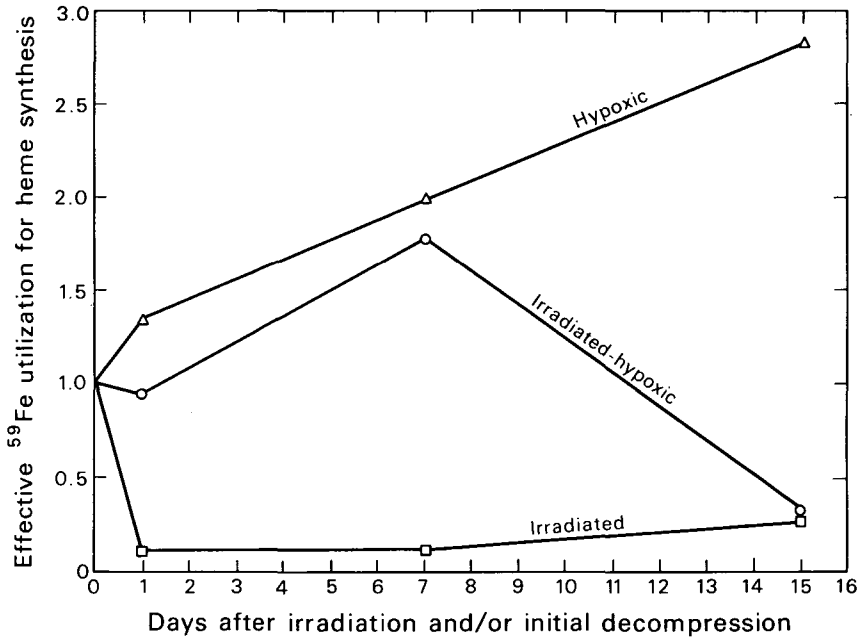

Fig. 4. Results of the calculated effective hemoglobin synthesis rates, using the method of Huff et al. (9). The data are expressed as a ratio of the calculated effective hemoglobin synthesis rate at various times following irradiation and/or hypoxia to that obtained during the pretreatment observation period.

DBL687-4793

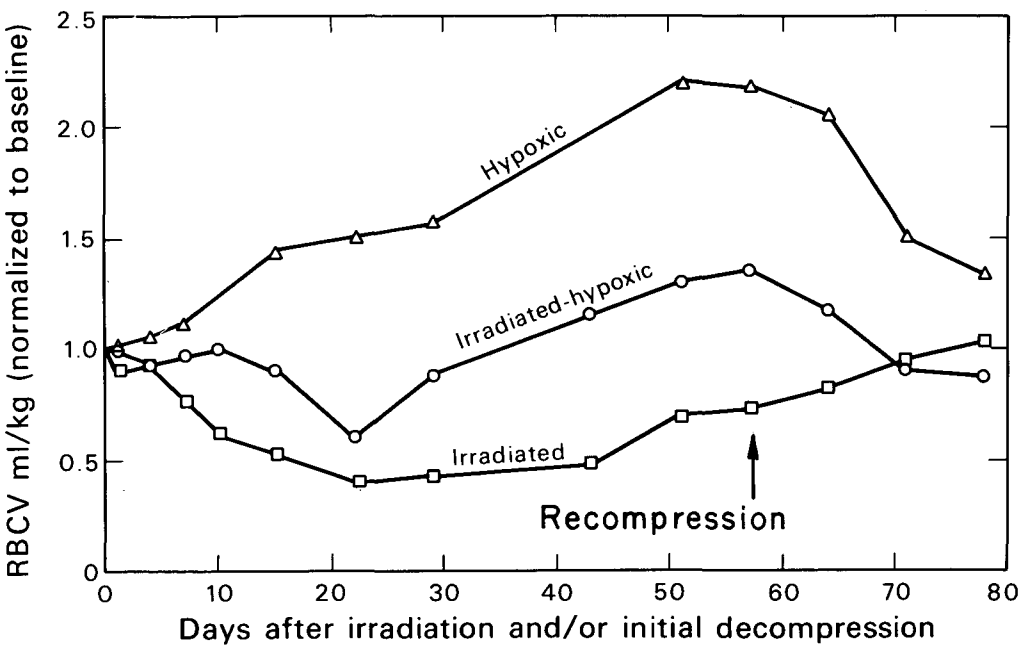

Fig. 5. Results of serial red cell volume determinations on 3 groups of dogs exposed to whole body proton irradiation and/or hypoxia expressed in milliliters/kilogram body weight and normalized to baseline values as a function of days after initial exposure to whole body proton irradiation and/or hypoxia.

DBL687-4791

cells merely requires a prior ability to synthesize a single heme protein, hemoglobin, the structural proteins of the red cell membrane, and possibly stroma, and sufficient enzymes involved in anaerobic glycolysis to produce a source of reducing materials (e.g., TPNH) and a source of energy (e.g., ATP). The production of these constituents accounts for only a small fraction of the total information contained within the DNA of any progenitor cell. Thus a cell, once commited to the red cell line, should be able to endure a great deal of damage to DNA coding for nonessential processes within the cell. As long as a red cell precursor is able to maintain its own integrity, undergo division, synthesize hemoglobin and structural and enzymatic protein, it should be able to give rise to functional red cells. If this indeed is the case, it would explain the present observations.

The finding in the present paper that hemoglobin synthesis diminishes markedly 7 days following irradiation in animals exposed to hypoxia subsequent to whole body radiation is consistent with the suggestion that uncommitted stem cells are significantly more radiosensitive than those committed to the erythroid series. According to this view the initially increased hemoglobin synthesis during the first 7 days post irradiation is occurring in relatively radioresistant cells already committed to the erythroid line. Subsequent to the "exhaustion" of a pool of these cells at the end of a 7-day period, there is a net diminution in hemoglobin synthesis due to radiation damage to the stem cell pool, thus preventing replenishment of the red cell precursor cell series. The finding that hemoglobin synthesis in the animals given hypoxia shortly after whole body radiation is greater than that seen in animals given radiation alone even after the 14th postirradiation day further suggests that even "stem cells" are able to be stimulated to proliferate following radiation by hypoxic hypoxia and thus that they are not being maximally stimulated following radiation in the absence of hypoxic hypoxia.

These results have important implications with respect to space travel since combined stress studies relating the interactive processes induced by the multiple physical and environmental factors of space flight represent perhaps one of the more exigent aspects of space-related research. Bender reported a synergistic effect during the Gemini-3 manned space flight between radiation and "some spaceflight parameter" for the production of human chromosome aberrations in whole blood samples (12). Biomedical data obtained during the Gemini series indicate an "adaptive" red cell volume loss of at least 20% during missions of several days duration (13). The full significance of these observations should be evaluated in terms of those space factors which might serve to further compromise the functional integrity of the erythropoietic system. The radiation-hypoxia problem is an important aspect of such an evaluation. The present results indicate that the combined effect of radiation and hypoxia is not synergistic. Indeed, hypoxia appears to favorably modify the damage induced by radiation on the erythropoietic system and to accelerate recovery. At the same time, the normal homeostatic response to hypoxia appears to be significantly altered by radiation.

The observations in this paper also have implications with regard to possible mechanisms by which recovery rates can be improved following whole body radiation. If indeed following whole body radiation the cells throughout the body are capable of greater proliferation and repair than that spontaneously seen after irradiation, a search is indicated for possible methods

of stimulating such proliferative processes. Unfortunately hypoxic hypoxia, while stimulating erythropoiesis in the irradiated animal, represents an additional undesirable stress. If, however, other means of stimulating cell proliferation and repair could be developed it might be possible to improve postirradiation survival by the use of these agents. Such agents would be particularly useful for astronauts who might unwittingly be exposed to lethal levels of radiation in locations far removed from adequate medical care.

In an additional set of experiments not discussed in the present communication, similar results were obtained in non-splenectomized dogs similarly exposed to whole body proton irradiation and/or hypoxic hypoxia. Thus the results demonstrated in the present communication cannot be ascribed to any effects induced by the absence of the spleen in the animals in the present study.

ACKNOWLEDGMENTS

We are greatly indebted to Dr. D. McKelvie of the Radiobiology Laboratory, School of Veterinary Medicine, University of California, Davis, for providing the beagle dogs used in this work, and to Dr. John Lyman, Mr. Jerry Howard, and Mr. David Love for their assistance during the irradiations.

This research was jointly supported by the U. S. Atomic Energy Commission and by Biotechnology and Human Resources, Office of Advanced Research and Technology, National Aeronautics and Space Administration.

REFERENCES AND NOTE

1. Loeffler, R. K.: Radioiron tracer studies for the evaluation of radiation damage. Am. J. Roentgenol. Radium Therapy Nucl. Med. 77: 836-846 (1957).
2. Gutnisky, A.; Nohr, M. L.; and Van Dyke, D.: Stimulation of erythropoietin production by whole-body irradiation (spleen shielded). J. Nucl. Med. 5: 595-605 (1964).
3. Newsom, B. D.; and Kimeldorf, D. J.: Tolerance of irradiated animals to prolonged hypoxia. Am. J. Physiol. 199: 445-448 (1960).
4. Berlin, N. I.; Lawrence, J. H.; and Gartland, Jean: The blood volume in polycythomin as determined by P^{32} labeled red blood cells. Am. J. Med. 9: 747-775 (1950).
5. Peters, T.; Giovanniello, T. J.; Apt, L.; and Ross, J. F.: A simple improved method for the determination of serum iron. J. Lab. Clin. Med. 48: 274, 281 (1956).
6. Apt, L.; Pollycove, M.; and Ross, J. F.: Idiopathic pulmonary hemosiderosis. A study of the anemia and iron distribution using radioiron and radio-chromium. J. Clin. Invest. 36: 1190 (1957).
7. Hennessy, T.; and Huff, R.: Depression of tracer iron uptake curve in rat erythrocytes following total body X-irradiation. Proc. Soc. Exp. Biol. Med. 73: 436 (1950).
8. Huff, R. L.; Hennessy, T. G.; Austin, R. E.; Garcia, J. F.; Roberts, B. M.; and Lawrence, H. H.: Plasma and red cell iron turnover in normal subjects and in patients having various hematopoietic disorders. J. Clin. Invest. 29: 1041-1052 (1950).
9. Elmlinger, P. J.; Huff, R. L.; Tobias, C. A.; and Lawrence, J. H.: Iron turnover abnormalities in patients having anemia: serial blood and *in vivo* tissue studies with ^{59}Fe.

Acta Haematol. 9: 93-96 (1953).

10. Siri, W. A.; Van Dyke, D. C.; Winchell, H. S.; Pollycove, M.; Parker, H. G.; and Cleveland, A. S.: Early erythropoietin, blood and physiological responses to severe hypoxia in man. J. Appl. Physiol. 21: 1 (1966).
11. Alpen, E.; and Cranmore, D.: Observations on the regulation of erythropoiesis and on cellular dynamics by ^{59}Fe autoradiography; in The Kinetics of Cellular Proliferation, edited by F. Stohlman, Jr., New York and London, Grune and Stratton, 1959, pp. 290-300.
12. Bender, M. A.; Gooch, P. C.; and Kondo, S.: The Gemini-3 space flight radiation interaction experiment. Radiation Res. 31: 91-111 (1967).
13. Bioastronautics Report, Vol. V, No. 9, May 16, 1966.

W. Gee is associated with the Radiobiology Laboratory, School of Veterinary Medicine, University of California, Davis, California.

Changes in the Bioelectric Activity of Sciatic Nerve After Irradiation with Cyclotron-Accelerated Protons

Cornelius T. Gaffey

Electrophysiologic techniques were used to analyze the effects of exposing isolated frog sciatic nerve (Rana pipiens) to cyclotron-accelerated protons (charged hydrogen nuclei, $^{1}_{1}H$). Nerves exposed to 17,500 rads of 47.5 MeV protons suffered a complete suppression of neural activity 65 hours after the termination of radiation. Nerves administered 500,000 rads of protons had an immediate and permanent failure in excitability. Between these two proton doses the postirradiation time for full blockage of conduction was found to be an inverse function of dose. Nerves administered doses between 10,000 and 17,500 rads exhibited a partial loss of their action potential. The dose of protons that did not alter the action potential magnitude of irradiated nerves, even many hours after exposure, was 10,000 rads. This level of irradiation was considered the tolerance dose. Nerves irradiated with less than the tolerance dose demonstrated bioelectric changes indicative of radiation damage other than an attenuation of the action potential. For example, 6000 rads of protons caused an increase in the relative refractory period, latent period, duration of the action potential, peak time, and conduction velocity. The stimulus strength to generate a maximal action potential exhibited no significant alteration, but the submaximal stimulus strength to produce an action potential one-half the maximal action potential decreased after about 1000 rads of proton irradiation, as evidenced by an increase in size of the action potential.

X irradiation of the sciatic nerve with 200-kV X rays produced a prompt inhibition of neural transmission after 300,000 R. This dose of X rays was used to evaluate the RBE (relative biologic effectiveness) of various types of ionizing radiation that possessed different LET (linear energy transfer). For prompt loss of neural activity as a consequence of irradiation, the RBE decreased as the LET values increased. The neurobiologic response of peripheral nerve was treated as a function of LET and its correlation to RBE.

INTRODUCTION

The purpose of this research was to obtain information about changes in the bioelectric properties of frog sciatic nerve as a result of being exposed to cyclotron-accelerated, charged hydrogen nuclei (protons). Since it is known that ionizing radiation injures nervous tissue only after protracted periods (1-3), it was considered strategic to relate action potential survival time to the proton delivered dose.

In studying interactions between radiation and neural function an analysis is frequently complicated, because it is rare that only the nervous system is exposed to radiation. In these experiments irradiation was confined to isolated sciatic nerve, thus restricting the number of variables.

Electrophysiologic techniques permitted the excitable state of nerves to be assessed as frequently as required before and after irradiation. Although the major index of irradiation damage was the ultimate loss of neural activity and the postirradiation time required for this loss, other neural properties were examined to determine their relative radiosensitivity to cyclotron-accelerated proton particles.

Primary galactic radiation is composed of 85% hydrogen nuclei (protons), 14% helium nuclei (alpha particles) and 1% of heavier nuclei (4). The flux of the trapped protons of the inner Van Allen belt rises sharply at 1.5 Earth radii (3185 km) with an integral flux of approximately 10,000 protons per cm^2 sec of 40 MeV minimum energy, and extends to 1 BeV (5). In work to be described here, 47.5 MeV protons were obtained from a terrestrial source, the 88-inch sector-focused (isochronous) cyclotron at Berkeley's Lawrence Radiation Laboratory. Fichtel (6) stated that the flux nuclei of the 11/12/60 solar flare would penetrate 2 g/cm^2 of aluminum. Cyclotron-generated 47.5 MeV protons will be shown to have the same degree of penetration. Hence, the proton particles used in these experiments are of similar nature to some of the primary galactic protons encountered in a space environment. Since there is no report in the literature dealing with the effects of high-energy protons on the bioelectric effects of nerve, we offer the present report.

METHODS

SECTOR-FOCUSED CYCLOTRON In 1962 the 88-inch sector-focused cyclotron at the Lawrence Radiation Laboratory at Berkeley produced its first external beam (7). Our electrophysiologic experiments were initiated to determine the bioelectric sensitivity of sciatic nerve to proton particles. High-energy particles were conducted in a 4-inch-diameter vacuum pipe from the 88-inch cyclotron to a shielded biophysical research cave (8). A quadrupole magnet in the cave focused the cyclotron's beam. A 1-inch circular beam was produced by inserting a particle-absorbing collimator in the beam-path in front of the nerve to be irradiated.

The delivered proton dose was measured by placing a transmission ionization chamber directly in the beam path at a very short distance before the target nerve. As the particle beam passed through the ionization chamber, a charge was collected by the chamber. This integrated charge has been shown to be related to the average dose delivered to a sample (9). Dose-rate measurements obtained with ionization chambers agree well with time-averaged dose-rate measurements determined by using a Faraday cup (8). The beam profile, depth-dose distribution, and homogeneity of 50 MeV protons was rested by scanning the field with silicon diodes (10, 11).

The 88-inch continuous-wave cyclotron could accelerate protons to energies from 6 to 50 MeV/nucleon by adjusting the particle revolution frequency from 5.3 to 16 megahertz (MHz).

By tuning the rf system to about 15 MHz, the cyclotron generated protons with an average energy of 47.5 MeV/nucleon. The external beam power in this operating state was 2.85 kilowatts (47.5 MeV $\times$ 60 μA = 2850 watts). In Table 1 is summarized the performance specifications of the 88-inch cyclotron. The range and stopping power or linear energy transfer were interpolated from Barkas and Berger (12).

BIOLOGICAL PROCEDURE Frogs (Rana pipiens), weighing about 35 grams, were used in these studies. Each frog was sacrificed by decapitation followed by spinal cord destruction. The left and right sciatic nerve was carefully removed, tied at its terminals, and placed in frog Ringer's solution (13). After soaking for 15 to 30 minutes at 22°C (± 1°C), each nerve was placed on Ag-AgCl electrodes in a plastic chamber through which a 96% air/4% carbon dioxide mixture circulated. The gas mixture passed through three water-filled, gas-washing cylinders prior to entry into the nerve chamber.

One pair of Ag-AgCl electrodes in the moist chamber served as a cathode-anode which sent to the central end of the nerve, monophasic rectangular pulses 0.1 msec in duration. The voltage output from a stimulator (Grass, Model S-4 and isolation unit) was adjusted to produce a maximum action potential by the nerve. The action potential was detected by another pair of Ag-AgCl electrodes in contact with the peripheral end of the sciatic nerve. The leads from these electrodes ran to a push-pull ac preamplifier (Grass, Model P-5) which delivered its signal into an oscilloscope (Tektronix, Model 532) with a high-gain differential input amplifier (Tektronix, Type 53/54D). The time sweep of the oscilloscope was 1 msec/cm. Action potentials from nerves were photographed as oscillograms by using a polaroid oscilloscope camera (Fairchild, Model F-286).

WHOLE NERVE PROTON IRRADIATION Nerves were transferred to sample holders for irradiation. Each holder consisted of a hollow plastic disc (2 inches in external diameter $\times$ 1/2 inch) that featured a removable 0.5-mil Mylar window. A nerve was wound in a spiral on the inside surface of the Mylar window, the window was replaced, and the holder sealed. A reservoir of Ringer's solution inside the holder's vault maintained a high relative humidity. The plane of the holder's window was positioned perpendicular to the cyclotron's beam, thus producing whole nerve irradiation. Since the depth of penetration of 47.5 MeV protons in water was over 2 cm, it is certain that the accelerated protons passed through the sciatic nerve. When irradiation was terminated, the nerve was removed from the sample holder, washed in Ringer's solution, and monitored for electrophysiologic activity. Prior to irradiation the action potential from every nerve was photographed. The irradiated and nonirradiated nerves were maintained in Ringer's solution between tests for excitability.

WHOLE NERVE X IRRADIATION Small plastic chambers containing one isolated sciatic nerve per chamber in oxygenated Ringer's solution (96% air, 4% CO_2) were placed 1-1/2 inches from the head of a Philips therapeutic deep X-ray unit. Irradiation was carried out as follows: 200 kV, 15 ma; inherent filtration 0.5 mm Al; added filtration 3 to 4 mm of Ringer's solution; and 0.9 mm plastic of the window of the chamber. Under these circumstances the dose rate was 868 ± 4 R/min as measured with a Victoreen ionization chamber.

Table 1. Operating characteristics of the 88-inch sector-focused cyclotron.

Energy of particles	
Protons ($^{1}_{1}H$)	6 to 50 MeV/nucleon
Deuterons ($^{2}_{1}H$)	10 to 60 MeV/nucleon
Alpha particles ($^{4}_{2}He$)	10 to 120 MeV/nucleon
Beam intensity, maximum current	100 μA
Number of revolutions during acceleration	100 to 600
Distance traveled in accelerator	0.2 to 1.5 miles
Velocity (v/c) ratio, maximum	0.34
Range of 47.5-MeV protons in air	2.31 g/cm^2
Range of 47.5-MeV protons in water	2.00 g/cm^2
Stopping power of 47.5-MeV protons in air	11.488 MeV-cm^2/g or 1.1488 keV/μ
Linear energy transfer of 47.5-MeV protons in water	13.139 MeV-cm^2/g or 1.3139 keV/μ

RESULTS

PROTON IRRADIATION Two sciatic nerves were isolated from each frog. One nerve was exposed to a dose of 47.4-MeV protons, and the other nerve served as a nonirradiated control. A dose-rate of about 50,000 rads/min was used; this relatively high dose-rate made the exposure time in the cyclotron's beam a negligible physiologic factor. The irradiated and nonirradiated nerves were electrically stimulated to generate maximal action potentials at the rate of 30/min. At appropriate postirradiation intervals the nerves were monitored for electrophysiologic changes in stimulus strength, latency period, conduction velocity, and relative refractory period. Concomitantly, oscillograms were made of the nerve's action potentials.

In Fig. 1 are the oscillograms of the action potentials of the left and right sciatic nerve of a frog. Initial action potentials were recorded from both nerves, and then one nerve of the pair was subjected to 250,000 rads of cyclotron-accelerated proton particles. The irradiated nerve had changes in its action potential complex immediately after irradiation: the magnitude of the action potential was reduced; the relative refractory period, the latency period, and the duration of the action potential were increased. Other physiologic tests demonstrated a decrease in the conduction velocity of the neural impulse, by using a dual-trace preamplifier (Tektronix, Type CA). Irradiation did not produce an alteration in the stimulus strength to evoke a maximal action potential. However, the submaximal stimulus strength, defined as the current to produce an action potential one-half the magnitude of a maximal action potential, was found to decrease. This reduction in the submaximal stimulus strength, as measured by an increase in size of the action potential, was found when the sciatic nerve was exposed to only 1000 rads of cyclotron-accelerated protons.

Action potentials which were taken every 2 hours after exposure to 47.5-MeV protons are presented in Fig. 1. This series of oscillograms represents the time course for the suppression of neural activity as a consequence of irradiation, and gives a precise determination of

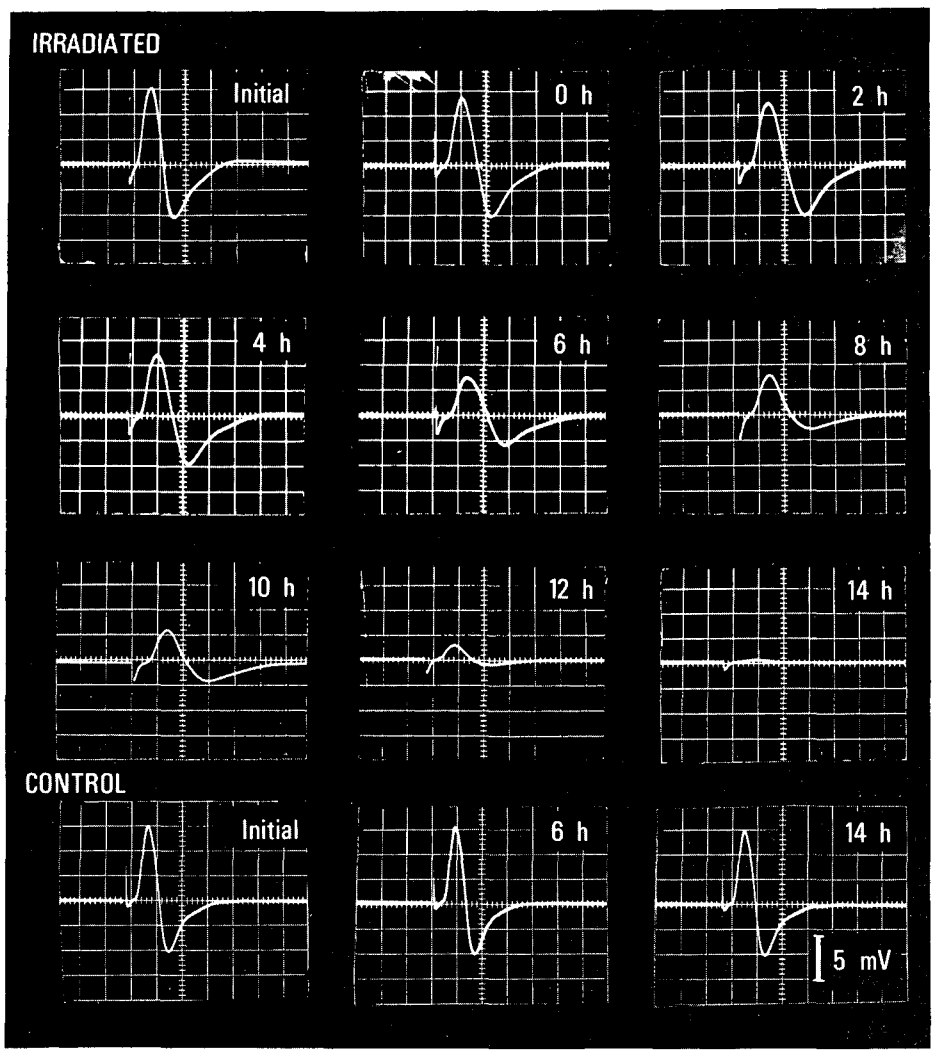

Fig. 1. Oscillograms illustrating action potentials generated by isolated sciatic nerves from a frog. One nerve of a pair was exposed to 250,000 rads of 47.5-MeV protons. A change in the shape of the irradiated nerve's action potential was evidenced immediately after exposure (0 h). Ultimately, a full block of conduction occurred at 14 hours postirradiation. The action potentials from the nonirradiated nerve are presented as the bottom three oscillograms in this composition. One unit on the ordinate was equivalent to 2.5 mV, and one unit on the abscissa was equivalent to 1 msec.

DBL683-4605

the time for a complete suppression of impulse conduction. As a result of receiving 250,000 rads of high-energy protons, the irradiated nerve suffered a total inhibition of excitability in 14 hours. The action potential of the nonirradiated, control nerve remained essentially unchanged during this 14-hour period, as is demonstrated in Fig. 1.

In Fig. 2 the magnitudes of the action potentials, as illustrated in Fig. 1, are plotted on the ordinate as the percent of the initial action potential amplitude. On the abscissa of Fig. 2 are the corresponding postirradiation times given in the composition of oscillograms of Fig. 1. The attenuation of the action potential from a 250,000 rad proton exposure is non-linear. However, the non-linear decline does not prevent an accurate determination of the survival time of excitation. As the complete cessation of bioelectric activity is approached, the frequency of recording action potentials is adjusted to follow the loss of neural activity. In this instance 250,000 rads of protons blocked impulse transmission in 14 hours.

The procedure illustrated in Figs. 1 and 2 of exposing a nerve to a proton dose, and thereafter monitoring action potentials of the irradiated and control nerve, was repeated for various doses of 47.5-MeV protons. A summary is presented in Fig. 3 of many experiments in the form of a semilogarithmic plot of proton dose versus the time for the loss of neural activity. Only dose levels of high-energy protons capable of totally inhibiting neural action potentials are contained in Fig. 3. The partial loss of a neural impulse, as a consequence of irradiation, will be treated elsewhere. It was found that 500,000 rads of protons induced an immediate loss of neural transmission, whereas a 17,500 rad dose caused a permanent failure in excitability only after 65 hours. The data in Fig. 3 indicate that the time for loss of neural activity is a logarithmic function of the delivered protons between 17,500 and 500,000 rads. At doses less than 17,500 rads the time for the loss of neural transmission was of some function other than logarithmic; i. e., the action potential survival was greater than would be expected by Fig. 3. Therefore, it must be stated that the dose-response curve in Fig. 3 cannot be extrapolated below 17,500 rads of protons, because the survival of excitability deviated progressively from the Fig. 3 relationship, and approached 10,000 rads as an asymptotic limit at 96 hours after irradiation. Doses less than 10,000 rads alter the nerve's action potential complex, but do not attenuate the irradiated nerve's action potential during the analysis period permitted by the control nerve. For this reason 10,000 rads of 47.5-MeV protons is referred to as a tolerance dose in this paper.

In experiments in which a nerve was exposed to less than 10,000 rads of 47.5-MeV protons, it was possible to distinguish the irradiated nerve from the nonirradiated nerve by using electrophysiologic criteria. For example, in Fig. 4 a nerve was subjected to 6000 rads of 47.5-MeV protons. Although the initial and 72 hour postirradiation action potential amplitude remained unchanged (14 mV), the duration of the action potential increased from initially 12 to 23 msec, the peak-time shifted from an initial 14 to 19 msec, and the latent period increased from 0.4 to 0.6 msec. These effects required 60 to 72 hours to appear in the 6000 rad exposed nerve. During the same 72-hour time interval the nonirradiated nerve's properties remained unaffected (the sciatic nerve's action potential duration was 12 msec, the peak time was 14 msec, the latent period was 0.4 msec, and the action potential amplitude was 16 mV). With

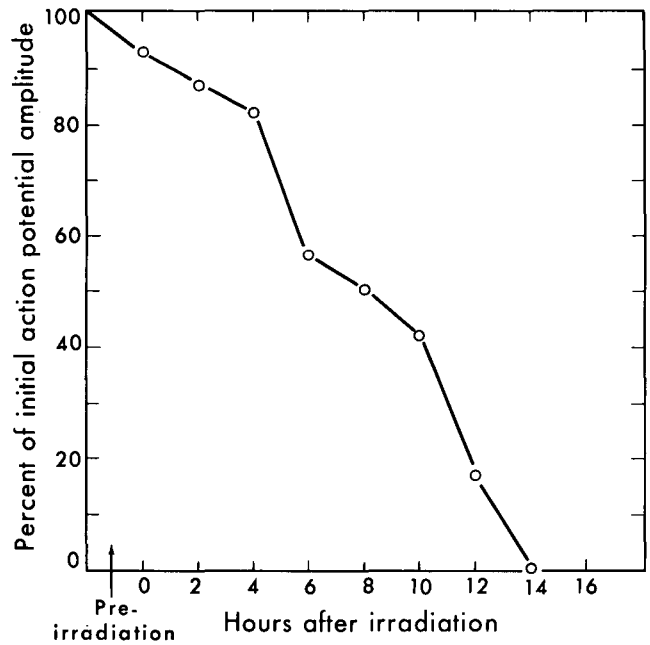

Fig. 2. The percent of the initial action potential amplitude plotted against the postirradiation time for a sciatic nerve which received 250,000 rads of 47.5-MeV protons. The action potential disappeared at 14 hours after exposure to proton particles. The oscillograms in Fig. 1 served as a basis for this figure.

MUB-9563

proton doses greater than 10,000 rads, there was no incident of recovery to the initial nonirradiated state. The changes observed with doses less than 10,000 rads (alterations in the duration, latent period, refractory period, and conduction velocity) did not manifest signs of recovery. The changes that did occur were indicative of injury and were progressive in nature.

It is clear that the magnitude of a nerve's action potential is only one index of the influence of proton irradiation. The earliest sign of an effect in nerves treated with 47.5-MeV protons was a change in the relative refractory period. The following parameters are listed with the most sensitive criteria of radiation damage first: relative refractory period, latent period, duration of the action potential, conduction velocity, and amplitude of the action potential. The threshold strength for a maximal action potential remained unaffected except near the loss of viability of excitation. In distinction to this, the submaximal stimulus required to produce an action potential half the size of the maximal action potential demonstrated a change in value even before the change in the relative refractory period.

In this study there was no evidence of an augmented or increased action potential as a consequence of radiation when the stimulus strength applied was that required for a maximal action potential. The electrophysiologic alterations induced by 47.5-MeV protons were inhibitory in time and irreversible in nature.

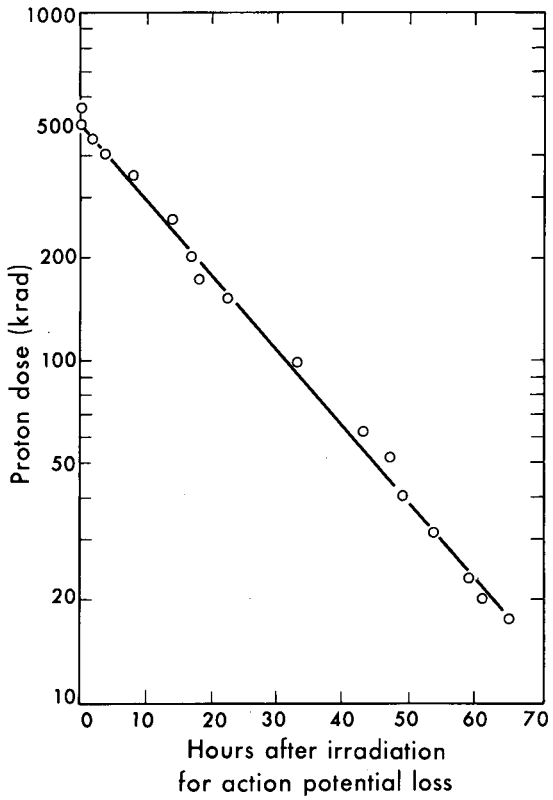

Fig. 3. A plot which demonstrates that the time after irradiation for the complete loss of the action potential of an irradiated nerve is an inverse function of the logarithm of the dose, provided the dose is in excess of 17,500 rads of 47.5-MeV protons. From 100,000 to 500,000 rads, each point is the mean of at least two experiments; each point below 100,000 rads is the average of at least three experiments. For a description of the electrophysiologic effects of 47.5-MeV protons for exposures less than 17,500 rads, see the text of this paper.

MUB-9564

X IRRADIATION X irradiation of the sciatic nerve of the frog with 200-kV X rays produced a prompt loss of neural activity at 300,000 R. A detailed report of this work is forthcoming (14).

Both sciatic nerves were excised from about 85 frogs in order to perform this study.

DISCUSSION

In this work the action potential magnitude of the frog's sciatic nerve was used as the main index of irradiation damage. Electrophysiologic techniques permitted the influence of radiation to be assayed both as a function of dose and the postirradiation interval. It is unfortunate that in research employing the bioelectric approach, it is common to be concerned only with the dose-effect relationship, and to ignore or neglect the time factor involved in the expression of the radiobiologic damage. In this report the time-dose-effect interdependency was studied, and is summarized in Fig. 3. This plot illustrates that the postirradiation time required for the total loss of neural excitability is an inverse function of the proton dose, provided the dose is greater than 17,500 rads.

An immediate block of neural activity was produced by 500,000 rads of 47.5-MeV protons, using isolated sciatic nerve from the frog. Bachofer (15) found 540,000 R of 280-kV X rays were needed to fully inhibit conductivity in the ventral, caudal nerve of the rat, and that 300,000 R was required to destroy the action potential produced by the giant medial and lateral

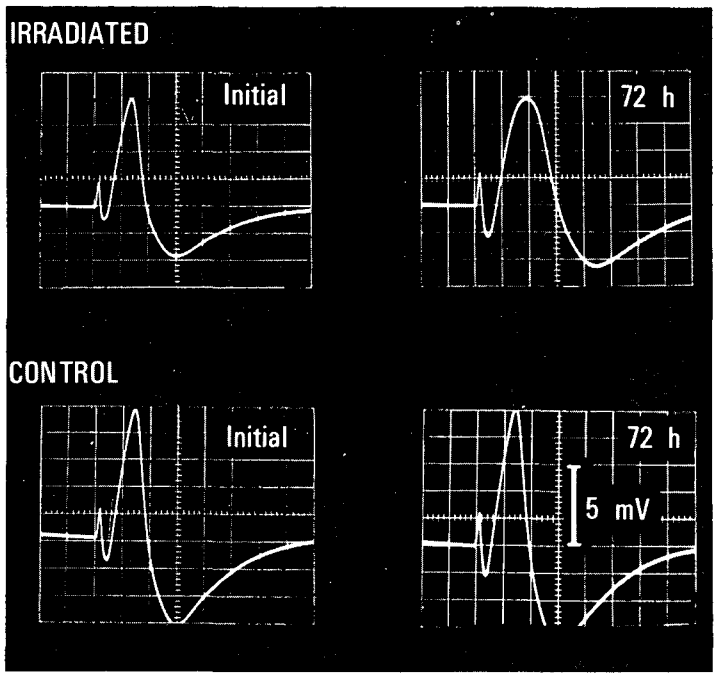

Fig. 4. Oscillograms of the action potentials produced by both sciatic nerves from a frog. Initially, action potentials were recorded and then one nerve (top, left oscillogram) was subjected to 6000 rads of 47.5-MeV protons. The other nerve (bottom oscillograms) functioned as the nonirradiated control. At 72 hours postirradiation the irradiated nerve had an increased latent period, duration, and peak time. One unit on the abscissa was equivalent to 1 msec.

DBL683-4604

fibers in the earthworm (16). Gerstner (17) reported that 300,000 R of 260-kV X ray blocked all transmission in frog sciatic nerve within 1 hour following irradiation, and that gamma fibers were slightly more radiosensitive than beta and alpha fibers. Gaffey (18) demonstrated that 910-MeV alpha particles and 455-MeV deuterons caused an immediated suppression of propagation at 300,000 and 330,000 rads respectively. Although there is variation in the exact dose of radiation to induce a prompt and complete loss of excitation, the evidence seems firm that peripheral nerve requires at least 300,000 rads of hard ionizing radiation to rapidly abolish impulse transmission. Only Bergström et al. (19) maintain that 10,000 rep of 5.3-MeV alpha particles from ^{210}Po causes a complete suppression of the action potential from skin nerve of frogs within a few minutes after irradiation, and that 5,000 rep produces the same inhibition of excitation at 30 minutes postirradiation. One wonders, are Bergström et al. (19) finding a contradiction to the other findings, or can these relatively low dose effects be explained on some other basis? We suggest that the latter is the case, and offer the following consideration in support of this view.

RBE (relative biological effectiveness) expresses the efficiency of different types of radiation in eliciting the same biologic response. Standard RBE values are usually based on the

most detrimental radiobiologic effects. By definition (20), biologic responses are standardized to the effects produced by 200-kV X rays. Radiations that have the same effect for equal doses are said to have an RBE of unity. Radiation with different biologic responses per dose are said to have a RBE greater (or less) than unity.

Table 2 gives RBE values for the rapid loss of neural activity from isolated peripheral nerve as a consequence of exposure to ionizing radiation. The neural blocking dose of 200-kV X rays, used as the standard of comparison, was found to be approximately 300,000 R for sciatic nerve from frog (Rana pipiens). This data soon will be reported (14). The only paper dealing with the influence of 200-kV X rays on the bioelectric properties of peripheral nerve is that of Jansen and Warren (21), but in their endeavor the conduction-blockage dose was not detailed.

The RBE of radiation depends on many factors (22). There are reports (22-24) which suggest a relationship between RBE and LET (linear energy transfer). LET can be regarded as an index of the distribution of ionizing events in the tracks caused by a dose of radiation. There is a current need to determine if biologic effects can be made more meaningful as a function of LET. In Table 3, LET values (keV/μ) are presented for some of the species of radiation listed in Table 2. A comparison between Table 2 (RBE) and Table 3 (LET) illustrates the phenomenon that RBE decreases as LET increases. Ultimately, it would be expected that as LET increased beyond some rather high value, a physical situation would be reached in which energy would be wasted (25). It certainly appears from Table 3 that, for neural death in the cases of 5.3 MeV alpha particles, 200-kV X rays, 910-MeV alpha particles, and 47.5-MeV protons, LET and RBE are definitely inversely related, as demonstrated by the LET ratio, i.e., 3 keV/μ for 200-kV X rays divided by the LET value for some other type of radiation. Future testing of this apparent RBE/LET correlation probably will consider more subtle biologic and physical factors. In any event, the RBE/LET relationship is presently the most logical explanation for the low dose effects of 5.3-MeV alpha particles on nerve reported by Bergström et al. (19).

By tolerance dose is meant the dose below which there is no attenuation of the action potential as a consequence of radiation. This is the sense of tolerance dose as used in this paper. It is concluded from the present research that 10,000 rads of 47.5-MeV protons represents the tolerance dose for the sciatic nerve of the frog within a postirradiation observation interval of 100 hours. For the most part, 10,000 rads is the tolerance dose referred to in the literature. Oishi (26), when monitoring the evoked cerebral response elicited by radial nerve electric stimulation, found no change with 10,000 rads of ^{60}Co (gamma rays). Jansen and Warren (21) stated that 10,000 R of X ray produced no demonstrable histologic or electrophysiologic changes in the sciatic nerve of the rat. Rosen and Dawson (27), using a frog muscle-nerve preparation, found no alterations in the properties of this system 30 minutes after exposure to 10,000 R. Schmitz and Shaefer (28) irradiated the sciatic nerve of frog and found no effect on the action potential at 10,000 R. Sato et al. (29) stated that 13,000 R of X rays did not adversely effect the soma membrane firing potential of isolated ganglia cells. Griffith and Pendergrass (30) found that 165,000 R did not alter or destroy the activity of sympathic ganglia of rats. If

Table 2. Relative biological effectiveness based on the radiation dose necessary to promptly suppress neural activity.

Type of radiation	RBE	Reference
Alpha particles, 5.3 MeV	0.03	19
X rays, 200 kV	1.00	14
Alpha particles, 910 MeV	1.00	18
Protons, 47.5 MeV	1.66	Present report
X rays, 280 kV	1.80	15

Table 3. Linear energy transfer values calculated from the tables of Barkas and Berger (12) and based on the track-segment method (32, 33).

	LET (keV/μ)	LET ratio
Alpha particles, 5.3 MeV	90*	0.03
X rays, 200 kV	3	1.00
Alpha particles, 910 MeV	1.6	1.81
Protons, 47.5 MeV	1.32	2.27

*LET value calculated for the experimental design of Bergström et al. (19) for the physical condition of no inherent filtration. The presence of interposing absorbers in ^{210}Po radiobiologic studies would produce a higher LET (32, 33).

10,000 rads is accepted as the tolerance dose for peripheral nerve, the work of Bergström et al. (19) again becomes a problem since 10,000 rep in their experiments represents the neural-activity killing dose rather than the tolerance dose. The same arguments offered previously with regard to RBE/LET relations apply here to account for this unreal discrepancy.

A tolerance dose, restricted to acute experiments dealing only with the magnitude of an irradiated nerve's action potential, does not imply that lower doses produce no effect. Just the opposite is true. Using other biologic criteria, effects of 47.5-MeV protons have been found below 10,000 rads. For example, in Fig. 4 of this text, 6000 rads of high-energy protons caused a change in shape of the action potential (92% increase in the duration of the neutral impulse), a 36% increase in the peak time of the action potential, and a 50% increase in the latent period and relative refractory period. Although the stimulus strength to produce a maximal action potential remained unchanged after irradiation, the stimulus strength for an action potential half the magnitude of the maximal action potential decreased after 1000 rads of 47.5-MeV protons, as

measured by an increase in size of the neural impulse to the same stimulus strength. Threshold changes in excitability are probably due to slight depolarization of the individual fibers (31).

With doses of irradiation greater than the tolerance dose there has been no instance of recovery of electrophysiologic properties from exposure to 47.5-MeV protons. However, Seymour and Dawson (31) have looked at the phenomenon of recovery at one-hundredth the tolerance dose ($1/100 \times 10{,}000$ R = 100 R), and report that subthreshold stimuli strengths altered by X rays are restored to the initial nonirradiated value during the postirradiation interval. This observation has been used (31) to confute the proposition that peripheral nerve is the most radioresistant part of the nervous system since this radiosensitive phenomenon proceeds down to zero dose.

CONCLUSIONS

It was demonstrated that 500,000 rads of 47.5-MeV protons induced an immediate and total loss of neural conductivity in the sciatic nerve of the frog, whereas 17,500 rads caused a permanent failure in excitability after 65 hours. The postirradiation time for full blockage of neural activity was found to be an inverse function of the proton dose, provided the nerve was exposed to at least 17,500 rads of 47.5 MeV protons. The dose of protons that did not alter the magnitude of the irradiated nerve's action potential, even many hours after irradiation, was 10,000 rads. This level of radiation was considered a tolerance dose. At doses less than the tolerance dose, the irradiated nerve suffered from radiation damage by exhibiting an increase in the relative refractory period, latent period, duration of the action potential, and conduction velocity. These changes occurred while the magnitude of the action potential of the exposed nerve remained unaltered. The submaximal stimulus strength decreased after about 1000 rads of irradiation.

X irradiation of the sciatic nerve with 200-kV X rays produced a prompt depression of excitation at 300,000 R. The LET (linear energy transfer) values in keV/μ are listed in parentheses for the following types of radiation: 47.5-MeV protons (1.32), 910-MeV alpha particles (1.6), 200-kV X rays (3), 5.3-MeV alpha particles (90). The RBE (relative biological effectiveness) of the types of radiation mentioned decreased as the LET values increased.

ACKNOWLEDGMENTS

It is a pleasure to thank Dr. G. P. Welch for his assistance in irradiating isolated, sciatic nerve at the Lawrence Radiation Laboratory's 88-inch cyclotron.

This work was done in part under the auspices of the U. S. Atomic Energy Commission and the National Aeronautics and Space Administration.

REFERENCES

1. Henshaw, P. S.: Whole-body irradiation syndrome; in Radiation Biology and Medicine, edited by W. D. Claus, Reading, Addison-Wesley, 1958, pp. 317-390.
2. Lebedinskiy, A. V.; and Nakhil'nitskaya, Z. N.: Effects of Ionization Radiation on the Nervous System, New York, Elsevier Publishing Co., 1963, pp. 38-61.

3. Van Cleave, C. D.: Irradiation and the Nervous System, New York, Rowman and Littlefield, 1963, pp. 91-112.
4. Langham, W. (ed.): Radiobiological Factors in Manned Space Flight, Washington, National Academy of Sciences, 1967.
5. Schaefer, H.: Local dose from proton and alpha particle enders behind complex shield systems; in Second Symposium on Protection Against Radiation in Space, edited by A. Reitz, Jr., Washington, D. C., Scientific and Technical Information Division, National Aeronautics and Space Administration, 1965.
6. Fichtel, C. E.: Composition of solar cosmic rays; in Proceedings of the Symposium on the Protection Against Radiation Hazards in Space, Washington, D. C., Division of Technical Information, U. S. Atomic Energy Commission, 1962, pp. 33-43.
7. Kelly, E. L.: General description and operating characteristics of the Berkeley 88-inch cyclotron. Lawrence Radiation Laboratory Report UCRL-10081 (1962).
8. Fulton, R. L.; Glasgow, L. R.; and Yanni, N. W.: Modifications to the 88-inch and 184-inch cyclotron: biological research facilities. Lawrence Radiation Laboratory Report UCRL-11128 (1963).
9. Birge, A. C.; Anger, H. O.; and Tobias, C. A.: Heavy charged-particle beams; in Radiation Dosimetry, edited by C. J. Hine and G. L. Brownell, New York, Academic Press, 1956, pp. 623-665.
10. Raju, M. R.: The use of miniature silicon diode as a radiation dosimeter. Phys. Med. Biol. 11: 371-376 (1966).
11. Conzett, H. E.; Robinson, L. B.; and Burger, R. N.: Semi-conductor probe for investigating accelerator beam pulses. Nucl. Instr. Methods 31: 109-111 (1964).
12. Barkas, W. H.; and Berger, M. J.: Tables of energy losses and ranges of heavy charged particles, Washington, D. C., Scientific and Technical Information Division, National Aeronautics and Space Administration, 1964.
13. Mitchell, P. H.: A Textbook of General Physiology, 4th ed., New York, McGraw-Hill, 1948, p. 322.
14. Gaffey, C. T.: Postirradiation effects of various doses of 200 kV X ray on the electrophysiologic properties of sciatic nerve (frog). To be submitted for publication (1968).
15. Bachofer, C. S.: Enhancement of activity of nerves by x-rays. Science 125: 1140-1141 (1957).
16. Bachofer, C. S., and Gautereaux, M. E.: X-ray effects on single nerve fibers. J. Gen. Physiol. 42: 723-735 (1959).
17. Gerstner, H. B.: Effect of high-intensity x-radiation on the A-group fibers of the frog's sciatic nerve. Amer. J. Physiol. 184: 333-337 (1956).
18. Gaffey, C. T.: Bioelectric effects of high energy irradiation on nerve; in Response of the Nervous System to Ionizing Radiation, edited by T. J. Haley and R. S. Snider, New York, Academic Press, 1962, pp. 227-296.
19. Bergström, R. M.; Blafield, R. F.; and Brenner, M. W.: The effect of alpha particles from a ring-shaped Po^{210} source on the action potential of single fibres of the frog. Ann. Acad. Sci. Fennicae, Series A, Medica 82: 1-10 (1961).
20. National Committee on Radiation Protection and Measurements; Permissible Dose from External Sources of Ionizing Radiation. NCRP-NBS Handbook No. 59, Washington, D. C.,

National Bureau of Standards, U. S. Department of Commerce, 1954.

21. Janzen, A. M.; and Warren, S.: Effects of roentgen rays on the peripheral nerve of the rat. Radiology 38: 333-337 (1942).
22. Brustad, T.: Heavy ions and some aspects of their use in molecular and cellular radiobiology; in Advances in Biological and Medical Physics, Vol. VIII, edited by C. A. Tobias, J. H. Lawrence, and T. L. Hayes, New York, Academic Press, 1962, pp. 161-224.
23. Snyder, W. S.: Some data on the relationship between RBE and LET; in Proceedings of the Symposium on the Protection Against Radiation Hazards in Space, Washington, D. C., Division of Technical Information, U. S. Atomic Energy Commission, 1962, pp. 402-408.
24. Sondhaus, C. A.: Biological effects of high-energy protons; in Proceedings of the Symposium on the Protection Against Radiation Hazards in Space, Washington, D. C., Division of Technical Information, U. S. Atomic Energy Commission, 1962, pp. 309-343.
25. Brustad, T.: Molecular and cellular effects of fast charged particles. Radiation Res. 15: 139-157 (1961).
26. Oishi, Y.: Modulated cerebellar evoked potentials after exposure of the cerebellum to ^{60}Co. Kobe J. Med. Sci. 12: 27-40 (1966).
27. Rosen, D.; and Dawson, K. B.: Search for immediate effects of x-radiation on frog nerve-muscle preparation. Radiation Res. 12: 357-370 (1960).
28. Schmitz, W.; and Schaefer, H.: Über den einfluss der roentgenstruhlen auf den nervenaktionsstrom. Strahlentherapie 46: 564-567 (1933).
29. Sato, M.; Austin, G.; and Yai, H.: Radiation and whole light effects on molluscan nerve cells *in vitro*. Radiation Res. 31: 452-466 (1967).
30. Griffith, J. Q.; and Pendergrass, E. P.: A study of the effect of irradiation upon the lumbar sympathetic ganglia in rats. Radiology 23: 463-465 (1934).
31. Seymour, R.; and Dawson, K. B.: Variation in the response and threshold to electrical excitation on x-irradiated isolated frog nerve with dose and dose-rate. Int. J. Rad. Biol. 12: 1-11 (1967).
32. Zirkle, R. E.; and Tobias, C. A.: Effects of ploidy and linear energy transfer on the radiobiological survival curves. Arch. Biochem. Biophys. 47: 282-306 (1953).
33. Barendsen, G. W.; Walter, H. M. D.; Fowler, J. F.; and Bewley, D. K.: Effects of different ionizing radiations on human cells in tissue culture. III. Experiments with cyclotron-accelerated alpha particles and deuterons. Radiation Res. 18: 106-119 (1963).

The Microarchitecture of a Whole Blood Clot

Thomas L. Hayes

INTRODUCTION

The mechanism of formation of the whole blood clot is of considerable interest as a basic biological process and as an important factor in several disease states. The biochemistry of clot formation has been studied extensively and the results of such investigations have been very useful at both the research and clinical level. The physical structure of the clot has also been investigated by using light microscopy and standard electron microscopy, but certain aspects of the structure, for example how the red blood cells are incorporated into the matrix of fibrin, cannot be seen with the resolution available with light microscopy and are very difficult to reconstruct with the two-dimensional ultra-thin section techniques of standard transmission electron microscopy. The scanning electron microscope can help to bridge the gap between the light microscope and the transmission electron microscope and provides a three-dimensional image at magnifications up to 20,000 times by utilizing relatively simple preparation techniques (1). It is hoped that scanning electron microscope studies of the clot microarchitecture can add to our understanding of the blood clotting mechanism.

METHODS

Whole blood from a normal individual was allowed to clot in a moist environment aluminum chamber for 12 hr at room temperature. Blocks were cut approximately 5 mm on a side and placed in neutral buffered formaldehyde fixative (4% formaldehyde, 1.8% sodium acetate, pH 6.8-7.0). Fixation was allowed to proceed at room temperature and a sample was removed after 2 hr fixation and the remainder of the material removed from the fixative after 48 hr. The fixed clot was cut into 2-mm blocks and air dried on a standard light microscope slide. In order to prevent image distortions due to electrical charging of the specimen during observation in the scanning electron microscope, a thin conducting layer of Pt-Pd alloy was deposited by evaporation on the surface of the specimen at normal incidence. The material was examined while on the standard glass slide by using a Japan Electron Optics Laboratory Co. Model JSM scanning electron microscope.

RESULTS AND DISCUSSION

The structure of a clot fixed in formaldehyde for 48 hr is shown in Fig. 1. Red blood cells can be seen enmeshed in bands of fibrin and a thin layer of material covers the surface of the cells nearly completely. With a shorter fixation time of 2 hr the fibrin has not condensed to such a marked degree and the cells are buried in the matrix (Fig. 2). In both cases the red blood cells have retained their bi-concave shape to a large extent, but the clot fixed for only

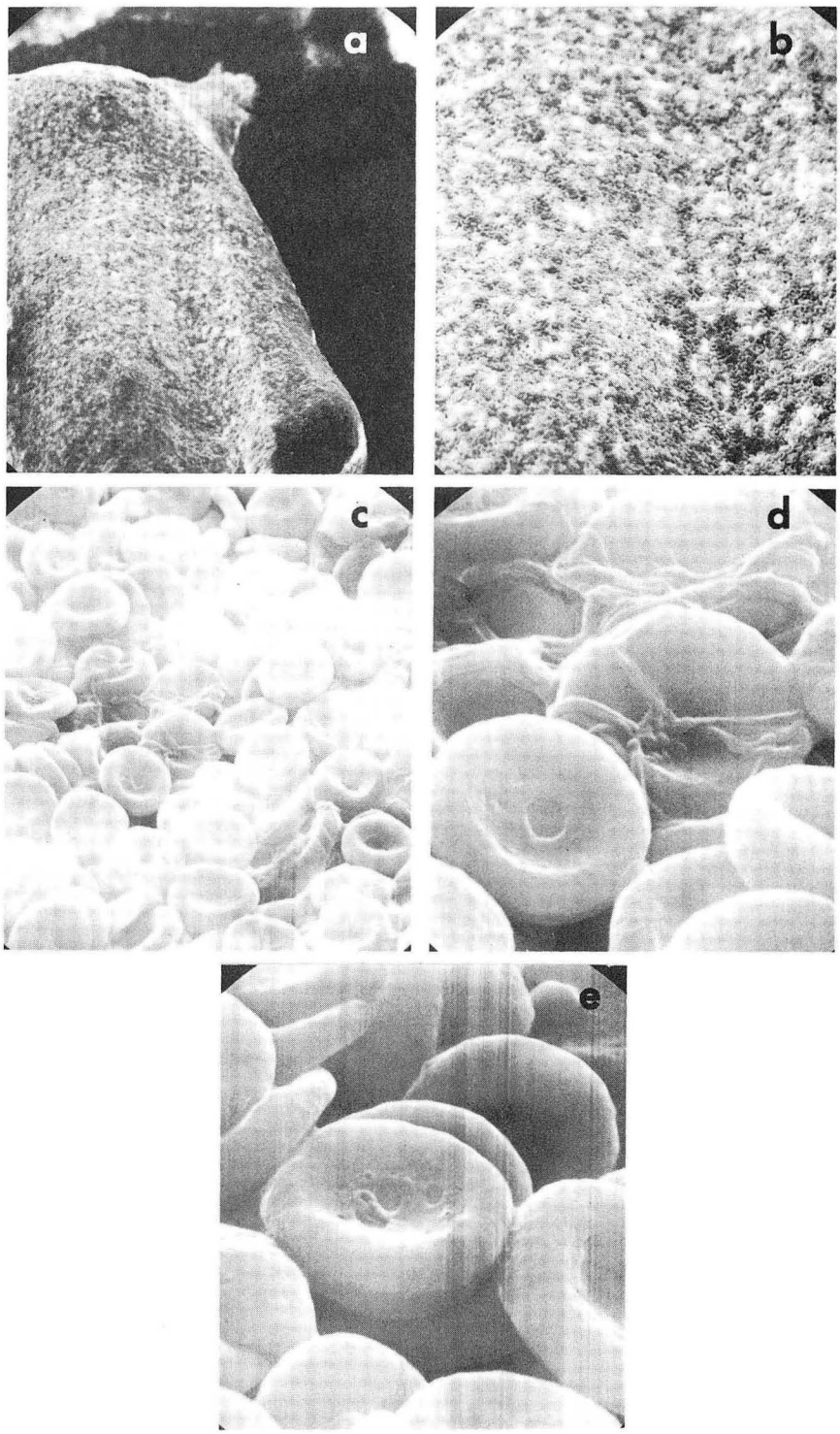

Fig. 1. Whole blood clot. Formalin fixed for 48 hr.
a. × 65, b. × 200, c. × 2000, d. × 6500, e. × 6500

XBB689-5600

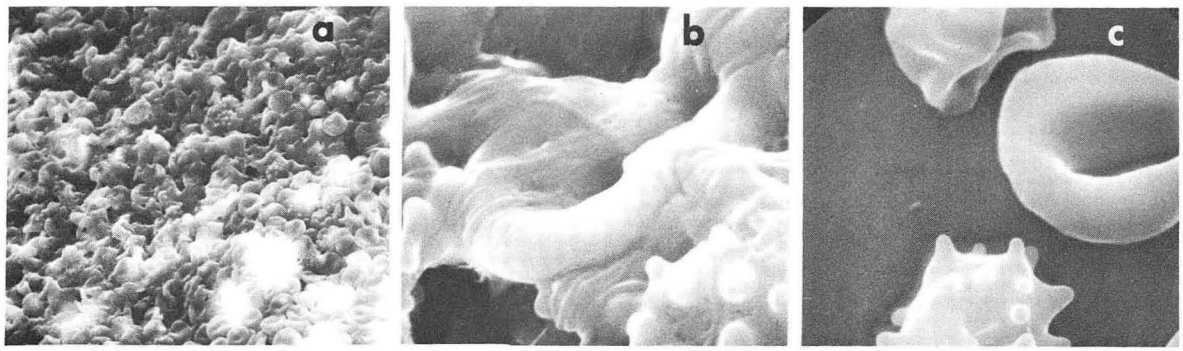

Fig. 2. Whole blood clot. Formalin fixed for 2 hr. Several crenated cells are shown.
a. × 600
b. × 6000
c. Cells outside of the clot and free of the fibrin matrix. Again, crenation is shown. × 6000

XBB689-5601

2 hr shows a greater number of crenated cells, possibly because of the effect of air drying incompletely fixed cells.

The density of cells in the clot can be used as an index of the degree and efficiency of clot retraction, and studies of the cell density at various times following clot formation may help us to quantitate the spatial distribution of cells as a function of retraction.

A knowledge of the micro-architecture of clots formed both in vivo and in vitro would be of value in describing the normal clotting process and in assessing the problem of abnormal thrombus formation.

REFERENCE

1. Hayes, T. L.; and Pease, R. F. W.: in Advances in Biological and Medical Physics, Vol. 12, edited by J. H. Lawrence and J. W. Gofman, New York, Academic Press, 1968.

Studies of Stem Cell Kinetics Utilizing the Spleen Colony Technique and the Erythropoietin Sensitivity Test

John C. Schooley

It appears reasonable to assume that the spleen-colony technique and the erythropoietin-sensitivity test measure the behavior of some primitive precursor or precursors of the hematopoietic system. A comparison of the rate of recovery of colony-forming units (CFU) and erythropoietin sensitivity after mild irradiation, the failure of erythropoietin injections to alter the growth of transplanted CFU in the spleen of polycythemic hosts, and a comparison of CFU content of the spleen and bone marrow and erythropoietin sensitivity in animals maintained polycythemic by transfusion for long periods of time, suggest that erythropoietin does not act directly upon the CFU, but upon some compartment of erythropoietin-sensitive cells ultimately derived from the CFU. Experiments utilizing hypoxia, cold, various hormones, the mitotic poison, vinblastine, and actinomycin D will also be presented to further characterize the CFU and the interrelationships between CFU and the proposed intermediate population or populations of cells sensitive to differentiative agents such as erythropoietin.

The blood-forming tissues consist of a series of pools of maturing and dividing cells which give rise to the non-dividing mature cells of the blood. In the steady state the loss of mature cells from the blood is balanced by the production of new cells which are ultimately derived from a self-sustaining pool or pools of undifferentiated precursor cells or "stem cells," at present morphologically unidentifiable. One of the central problems of hematology, and the subject of much controversy, is the question of the developmental potentialities of the hematopoietic "stem cell."

Radioisotope techniques, autoradiography in particular, have provided much insight into the kinetics of the morphologically recognizable maturing and dividing hematopoietic cells; their life-spans, transit times through the hematopoietic tissue, etc. are known with some precision in several animal species. Autoradiography is of limited value in studying "stem cell" kinetics, since the morphological identity of "stem cells" is only conjectural at present. Studies of "stem cell" kinetics must therefore utilize methods which measure some aspect of the behavior of the "stem cell" population.

The spleen-colony technique and the erythropoietin-sensitivity test are two available experimental procedures which purport to measure the behavior of the "stem cell" population. They depend upon various assumptions concerning the nature and function of "stem cells," and it cannot be assumed that they necessarily measure properties of an identical population of

cells. To avoid ambiguity, therefore, results in this paper will be presented in terms of the particular behavior measured without using the term "stem cell."

The responsiveness of the polycythemic mouse to a standard amount of erythropoietin, injected at various times after mild irradiation, was used by Gurney, Lajtha, and Oliver (1962) to measure "the functional integrity of the stem cell compartment," and to test their models of hematopoiesis (Lajtha et al., 1962; Lajtha, 1966). Within a few days after transfusion-induced polycythemia, erythropoietic activity in the hematopoietic tissue of the mouse is virtually absent. A wave of erythropoietic activity is re-established in such mice by the injection of erythropoietin. The magnitude of this response is generally quantitated by the intravenous injection of ^{59}Fe about 56 hours after the erythropoietin injection and determination of the percentage of ^{59}Fe in the peripheral blood volume 72 hours after the ^{59}Fe injections. About 5 days are required for the entire test.

Gurney (1963) has emphasized that there are several serious limitations to meaningful measurement which should be considered in any interpretation of experimental data obtained by using the erythropoietin-sensitivity test. The most serious is that the challenge to the receptive cells cannot be made instantaneous because of the biological life of the injected erythropoietin. Large doses of erythropoietin may stimulate receptive cells during the entire assay; even rather small doses may stimulate receptive cells for a considerable time if injected subcutaneously or intraperitoneally, because of the time required for absorption of the hormone from the injection site. Using antierythropoietin to limit the time of availability of the injected erythropoietin in the assay animal, we (Schooley, 1965) have demonstrated the responsiveness of hematopoietic tissue to erythropoietin changes following the initial exposure of the tissue to the hormone. Thus it appears likely that when this test is used to measure the recovery of erythropoietin-sensitive cells after mild irradiation, conditions within the cell compartment sensitive to erythropoietin are continuously changing, both as a result of recovery from the irradiation and as a result of the first exposure of the test animal to erythropoietin. To minimize some of these problems only 0.5 to 1.0 I. R. P. (international reference preparation) or erythropoietin was used in the present experiments, and the erythropoietin was administered intravenously.

The spleen-colony technique is based on the finding of Till and McCulloch (1961) that the intravenous injection of suitable numbers of hematopoietic cells into heavily irradiated hosts leads to the formation of nodules which are macroscopically visible on the spleen about 8 to 11 days after transplantation. A linear relationship exists between the number of hematopoietic cells injected and the number of nodules observed on the host spleen. Considerable evidence favors the view that the majority of cells in each nodule are derived from a single precursor and each nodule can be considered a colony (Becker et al., 1963; Welshons, 1964; Fowler et al., 1967; Wu et al., 1967; and Chen and Schooley, 1968). The cells which form colonies are termed "colony-forming units" (CFU).

Many colonies contain large numbers of mature cells characteristic of the erythroid, granulocytic (eosinophilic and neutrophilic), and megakaryocytic series, but in other colonies

mature cells characteristic of only one cell line predominate. Colonies containing predominately nucleated erythroid cells are most frequently observed (Jurášková et al., 1964). Conspicuous accumulations of characteristic lymphoid cells or macrophages are not observed in spleen colonies, but recent experiments suggest that these cells also are descended from CFU, or CFU and these cells have a common progenitor (Wu et al., 1968; Virolainen and Defendi, 1968).

It can be demonstrated by retransplantation into heavily irradiated recipients that individual spleen colonies contain CFU, as well as cells characteristic of the erythroid, granulocytic, and megakaryocytic cells. Siminovitch et al. (1963) have demonstrated that the distribution of CFU among individual colonies is heterogeneous, with many colonies containing only a few CFU and a few colonies containing many. These findings form the basis of a stochastic model of hematopoiesis (Till et al., 1964). CFU obtained from some colonies containing predominately erythroid cells, can, upon retransplantation, give rise to colonies containing granulocytic, megakaryocytic, and erythroid cells (Lewis and Trobaugh, 1964). Fowler et al (1967) were unable to demonstrate a strong correlation between the predominant mature hematopoietic cells in an individual colony and their CFU content, but a tendency was observed for colonies having a high proportion of granulocytes to have a high proportion of CFU.

It is important to emphasize that not all of the potential CFU in a transplant actually settle down in the spleen and give rise to colonies. The fraction, f, of the injected CFU which actually settle in the spleen can easily be measured by injecting a suitable inoculum of bone marrow containing a known number of CFU into an irradiated host. Two hours after transplantation a single cell suspension of the spleen is made and the total number of CFU in the spleen is determined by retransplantation of a suitable dilution of the spleen suspension into another group of irradiated hosts. Siminovitch et al. (1963) have obtained an f value of 0.17, whereas Schooley (1966) obtained a value of 0.24. Recently, we have found that the f value is the same when 90 or 45 or 10 or 2 million bone marrow cells are transplanted. The f value can be varied by experimental procedures. For example, the f value was increased to 0.39 when the hosts had been injected daily for 7 days with 0.25 cc of normal rabbit serum prior to irradiation and transplantation, and the f value was decreased to 0.10 when determined in hosts irradiated 2 days before injection. These changes in the f value are probably related to splenic size at the time of the measurement. The f value for one tibia or one femur is on the order of 0.01-0.02. It can be calculated from these data that about as many CFU settle in the total marrow space as in the entire spleen. The fate of the remaining CFU is unknown.

It has been demonstrated both *in vivo* (Bruce et al, 1966) and *in vitro* (Becker et al., 1965; Bruce and Meeker, 1965) that very few CFU in the adult mouse are at any one time undergoing DNA synthesis, but in the hematopoietic tissue of the fetal liver or in regenerating hematopoietic tissue large numbers of the CFU are synthesizing DNA.

It is tempting to assume that the colony-forming cell is the "stem cell"; certainly the cell satisfies the essential criteria of a stem cell: it is capable of extensive proliferation, it is capable of self-renewal, and it is capable of giving rise to differentiated cells. It seems

likely that the CFU is the most primitive precursor of the hematopoietic system whose behavior can be measured. Our basic hypothesis, which forms the basis for most of the experiments to be presented here, is that the colony-forming cell is the most primitive measurable precursor of erythroid, granulocytic, and megakaryocytic cells. Agents such as erythropoietin which regulate the differentiation of the CFU into each of these cell lines do not act directly on the CFU, but rather upon some population or populations of cells derived from the CFU which are still not recognizable hematopoietic cells. It is assumed that in the case of erythroid cells it is primarily the behavior of this intermediate population of cells which is measured by the erythropoietin-sensitivity test. For convenience, this population will be termed the "erythropoietin-sensitive cell" (ESC).

Bruce and McCulloch (1964) found that prolonged hypoxia markedly decreased the CFU content of the spleen but had little if any effect on the CFU content of the bone marrow. They concluded, in spite of the decreased CFU content of the spleen, that some progeny of the CFU, rather than the CFU itself, was sensitive to the differentiative action of erythropoietin. However, these conclusions could be criticized because elevated erythropoietin levels occur in hypoxic mice only during the first 3 or 4 days of exposure and the animals were not necessarily maximally stimulated erythropoietically during the entire experiment. Using transfusion-induced polycythemic mice as hosts, we (Schooley, 1966) reinvestigated the erythropoietin sensitivity of CFU. We found, in agreement with other workers (Liron and Feldman, 1965; Curry and Trentin, 1967; Curry et al., 1967) that the development of colonies containing erythroid cells was completely suppressed in polycythemic hosts. Indeed, the total number of colonies which could be counted on the spleen was markedly less than that found when the same inoculum of bone marrow was transplanted into normal hosts or polycythemic hosts given erythropoietin. More significant, however, was the observation that the growth of CFU in the spleens of polycythemic hosts was unaffected by the presence or absence of erythropoietin. We previously stated that about 24% of the CFU in a transplant settle in the spleen within 2 hours after transplantation. It can be demonstrated by retransplantation that the CFU content of the spleen does not increase until the 3rd or 4th day when it begins to increase exponentially with a doubling time of about 1 day. This doubling time is unaffected by the presence or absence of erythropoietin. Till et al. (1967) also concluded that CFU proliferation was independent of erythropoietic activity. These experiments strongly support the concept that erythropoietin does not act directly upon the CFU.

It can be determined from the CFU growth curve that by the 4th day after transplantation only about 250 CFU are present in the spleen. These CFU double daily so that by the 6th day after transplantation 1000 CFU are found in the spleen. During this same 2-day period about 25×10^6 nucleated erythroid cells were produced in the same spleens in the erythropoietin-injected host. What cells were the immediate precursors of the nucleated erythroid cells? We concluded previously (Schooley, 1966) that these cells were produced by the action of erythropoietin on large numbers of erythropoietin-sensitive cells either initially present in the transplanted bone marrow and/or derived from the proliferation of CFU during the first 4 days after transplantation.

Table 1. Effect of ESF on the development of spleen colonies.*

	Colonies/10^5 BMC
Normal hosts	23.3 ± 1.7
Polycythemic hosts	
No ESF injected	11.4 ± 1.0
ESF injected, days 1, 2, 3	11.3 ± 1.3
ESF injected, days 4, 5, 6	13.9 ± 1.9
ESF injected, days 7, 8, 9	26.8 ± 2.7
ESF injected, days 1, 2, 3 and 7, 8, 9	26.8 ± 1.2
ESF injected, days 1-9	25.8 ± 1.4

*All mice irradiated 1200 R ^{60}Co and transplanted with 6×10^4 BMC. 15 C_3H mice/group. 1 I. R. P. of ESF given at each injection.

The results presented in Table 1 indicate that erythropoietin-sensitive cells must be produced in host mice in the absence of erythropoietic stimulation. Groups of irradiated transfusion-induced polycythemic mice and an irradiated group of normal mice were transplanted with 4×10^4 bone marrow cells. Erythropoietin was injected into the polycythemic groups of mice as indicated. The total number of macroscopic colonies observed on the spleen 10 days after transplantation was the same in the normal hosts and in the polycythemic hosts which received erythropoietin injections during the entire test period or only on days 7, 8, and 9 after transplantation. The number of colonies in polycythemic hosts receiving no erythropoietin or erythropoietin on only the first 3 or second 3 days after transplantation was considerably less than the previous groups. Mice receiving erythropoietin on the first 3 days and on days 7, 8, and 9 had as many colonies as normal hosts or polycythemic hosts receiving erythropoietin daily, suggesting that the initial exposure to erythropoietin did not alter the ability of the transplant to supply ESC for the later development of erythroid colonies. It should be emphasized that other experiments indicate that the total CFU content of the spleens of all the experimental groups would be identical. It is only the number of observable colonies that is increased by the proliferation of the stimulated ESC.

Postulating one or more populations of cells between the CFU and the earliest recognizable hematopoietic cells appears, on the basis of the experimental evidence already presented, to be reasonable. Many problems of importance regarding the interrelationships between the CFU and the assumed intermediate populations, particularly the processes regulating the size, proliferative rate, and mechanism of accumulation of the various populations require solution. The previous experiments suggest that the ESC accumulate in the absence of erythropoietic stimulation. The results shown in Table 2 suggest that ESC in the normal mouse do not increase above a certain level in the absence of erythropoietic activity. In these three experiments groups of mice were maintained polycythemic by transfusion of irradiated isologous red

Table 2. Effect of the duration of polycythemia on the CFU of the spleen and bone marrow and on erythropoietin sensitivity.

		DURATION OF POLYCYTHEMIA			
	NONPOLYCYTHEMIC	1 WEEK	2 WEEKS	3 WEEKS	4 WEEKS
EXPERIMENT 1					
Cells/spleen	221×10^6	223×10^6	222×10^6	209×10^6	222×10^6
CFU/spleen	8300 ±355*	13,800 ±455	14,800 ±1560	20,800 ±2320	21,600 ±2040
CFU/10^6 spleen cells	37.6	61.9	66.7	99.5	97.3
Erythropoietin response (72-hr ^{59}Fe uptake)		4.2 ±0.23	5.5 ±0.26	5.2 ±0.23	4.8 ±0.19
EXPERIMENT 2					
Cells/spleen	194×10^6	172×10^6	178×10^6	227×10^6	206×10^6
CFU/spleen	6240 ±280	11,360 ±880	12,600 ±480	16,720 ±480	17,920 ±1120
CFU/10^6 spleen cells	32.2	66.0	70.8	73.7	87.0
Cells/femur	14.2×10^6	15.2×10^6	15.9×10^6	10.8×10^6	16.2×10^6
CFU/femur	2270 ±140	3720 ±330	4260 ±360	3430 ±430	3270 ±240
CFU/10^6 bone marrow cells	160	245	268	318	202
EXPERIMENT 3					
Cells/spleen	222×10^6	187×10^6	158×10^6	205×10^6	185×10^6
CFU/spleen	7360 ±440	9680 ±440	12,040 ±520	15,120 ±960	18,080 ±430
CFU/10^6 spleen cells	33.2	51.8	76.2	73.8	97.7
Cells/femur	13.8×10^6	12.1×10^6	14.3×10^6	11.4×10^6	15.6×10^6
CFU/femur	2250 ±300	2890 ±190	3640 ±310	2910 ±130	4020 ±350
CFU/10^6 bone marrow cells	163	239	255	255	258
Erythropoietin response (72-hr ^{59}Fe uptake)		3.6 ±0.16	4.2 ±0.22	3.0 ±0.20	4.2 ±0.23

* *Standard error of the mean*

blood cells. The sensitivity to one I. R. P. of intravenously administered erythropoietin and the CFU content of the spleen and femur were determined at weekly intervals for 4 weeks. It is evident that the sensitivity to erythropoietin was not increased by the prolonged suppression of erythropoiesis, but interestingly the total CFU content of the spleen was more than twice the normal value after 1 month. A slight increase in the CFU content of the femur was also observed; this increase was found, in other experiments, not to be further increased if the spleen was removed. The results suggest that in the polycythemic mouse the production of ESC from CFU is decreased, since ESC are not being stimulated to differentiate, and CFU therefore increase.

Accumulated experimental evidence indicates that the metaphase spindle poison, vinblastine, kills cells passing through mitosis (Valeriote et al., 1966; Bruchovsky et al., 1965). The short biological half-life of 3.5 hours (Valeriote and Bruce, 1965) and the fact that a threshold exists for the killing effect indicate that vinblastine kills cells for a finite period after injection into the mouse. Hodgson (1967) measured erythropoietin responsiveness in polycythemic mice receiving vinblastine injections and concluded that the ESC are in cell cycle and respond to erythropoietin in the G_1 phase of interphase. Schooley (1965) also concluded

that erythropoietin stimulated receptive cells during G_1. We have used a variation of Hodgson's experiments: 1 unit of erythropoietin was used rather than 5 units and the erythropoietin was administered intravenously rather than subcutaneously in order to limit as far as possible the availability of erythropoietin to the sensitive cells. In addition, the ^{59}Fe uptakes were determined 72 hours after the ^{59}Fe injection rather than 24 hours. Erythropoietin was first injected 6 hours after the intravenous injection of 80 μg of vinblastine. The results are shown in Fig. 1. Six hours after the vinblastine injections the CFU content of the spleen and bone marrow was only decreased by 20%, yet the responsiveness to erythropoietin was virtually abolished. These results certainly favor the view that erythropoietin does not act directly upon the CFU. In general, the temporal pattern of recovery of erythropoietin responsiveness is similar to that observed by Hodgson, except that a longer period of time was required before the values approached normal. Interestingly, complete recovery did not occur during the entire test period. Preliminary experiments which will not be presented here indicate that the rate of recovery of ESC is more rapid in normal than in polycythemic hosts, suggesting that the recovery rate is dependent upon demand.

Erythropoietin responsiveness recovers in polycythemic mice by the 10th day after mild irradiation of 150 or 200 R (Gurney, 1963; Alexanian et al., 1963). The CFU content of the spleen and bone marrow, however, does not recover in such animals until about the 15th day after irradiation (Schooley et al., 1966). These data are shown in Fig. 2. The finding that vinblastine injections kill over 40% of the CFU within 1 day after 200 R irradiation and 80 to 90% within 3 days after irradiation, rather than 20% as in the unirradiated mouse, suggests that the surviving CFU are rapidly proliferating relatively soon after the mild irradiation. The fact that the CFU content of the hematopoietic tissues does not increase in these mildly irradiated mice, although the surviving CFU are proliferating rapidly, suggests that ESC recovery has priority under the experimental conditions. Interestingly, even the early recovery of erythropoietin responsiveness in these experiments is more apparent than real, since the mice respond neither to large doses of erythropoietin nor to fractionated doses of erythropoietin in the same manner as unirradiated polycythemic mice (Schooley et al., 1968). This lack of correlation between the recovery of CFU and erythropoietin responsiveness also favors the concept of an intermediate ESC population. The data of Porteous and Lajtha (1966) and Weisman et al. (1967) agree with the above experiments, but they, in addition, report that when CFU recovery is measured by using a shielding technique that requires no transplantation, a correlation between CFU and erythropoietin responsiveness exists. They conclude that it is neither warranted nor necessary to postulate two separate cell populations. Lajtha (1966) has suggested that the difference between the results of the exogenous (transplantation) and endogenous (leg shielding) techniques for measuring CFU recovery is due to the unphysiological conditions required for making the cell suspensions in the exogenous technique. It is interesting to note, however, that when the same exogenous technique is used to measure CFU recovery after 400 or 800 R, rather than 200 R, a more rapid recovery of CFU occurs; significant increase in CFU content of the hematopoietic tissue is observed before the 8th to 10th day after irradiation (Smith et al., 1966; Till, 1963). We believe that the differences in results obtained by using the two experimental techniques are related to the feedback mechanisms involved in regulating the division and accumulation of CFU, and the mechanisms regulating the formation

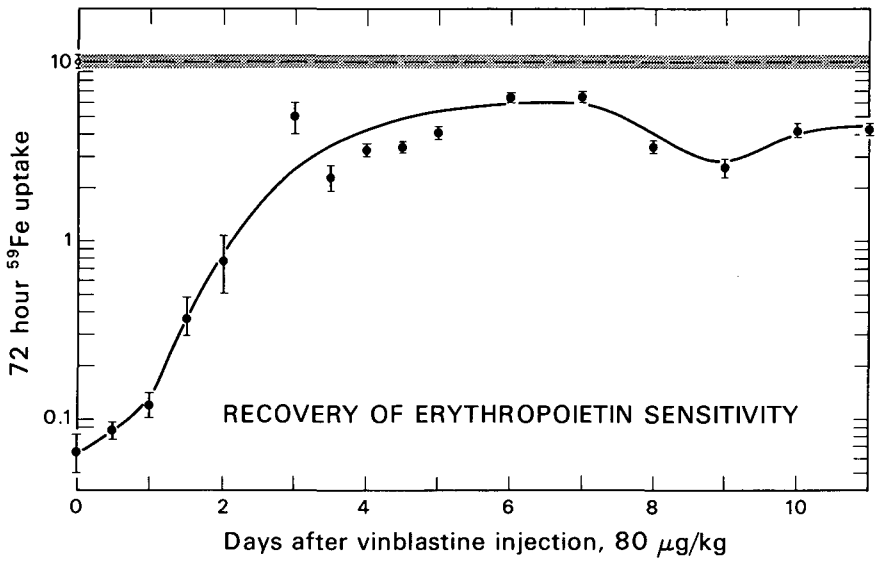

Fig. 1. Recovery of erythropoietin sensitivity after vinblastine injection.
DBL684-4722

of the intermediate populations from the CFU. It seems unlikely that the environment of a mouse initially irradiated with 200 R, and then several days later heavily reirradiated (except for a small portion of the femur) corresponds to an animal only receiving 200 R.

Bruce and McCulloch (1964), as mentioned previously, demonstrated that the CFU content of the spleen was markedly decreased after a hypoxic exposure of only 5 days. We previously concluded (Schooley et al., 1968) that this decrease was not due to the action of erythropoietin, since an even greater decrease occurred in mice exposed to hypoxia and injected with anti-erythropoietin antibody. Very little erythropoietic stimulation occurred in the antibody-injected mice regardless of the hypoxic exposure. The effect of a number of environments, hormones, and other experimental treatments on the CFU content of bone marrow and spleen is given in Fig. 3. Female C3H mice were used in all of the experiments. After the indicated treatment, single cell suspensions were made of the spleen and bone marrow. Suitable dilutions of these suspensions were injected into host mice immediately after irradiation with 1200 R ^{60}Co delivered at a dose rate of about 15 R/min. The CFU content of spleens from mice of the same age and sex measured at the same time was remarkably reproducible; the average CFU content of 10 individual spleens was 8800 ± 10, and for 10 groups of 5 spleens per group the average CFU content was 8800 ± 480. Control values were always determined at the same time with mice of the same age, since not only does the CFU content vary with age, but even in animals of the same age measured at different times may vary by 10 or 20%. The hypoxic exposure was in a chamber at a simulated altitude of 18,000 feet.

Figure 3 shows that a significant decrease in the CFU content of the spleen occurs after hypoxia and cold exposure. Hypoxic exposure combined with anti-erythropoietin injections decreased the CFU content of the spleen even more than the hypoxic exposure alone. The CFU

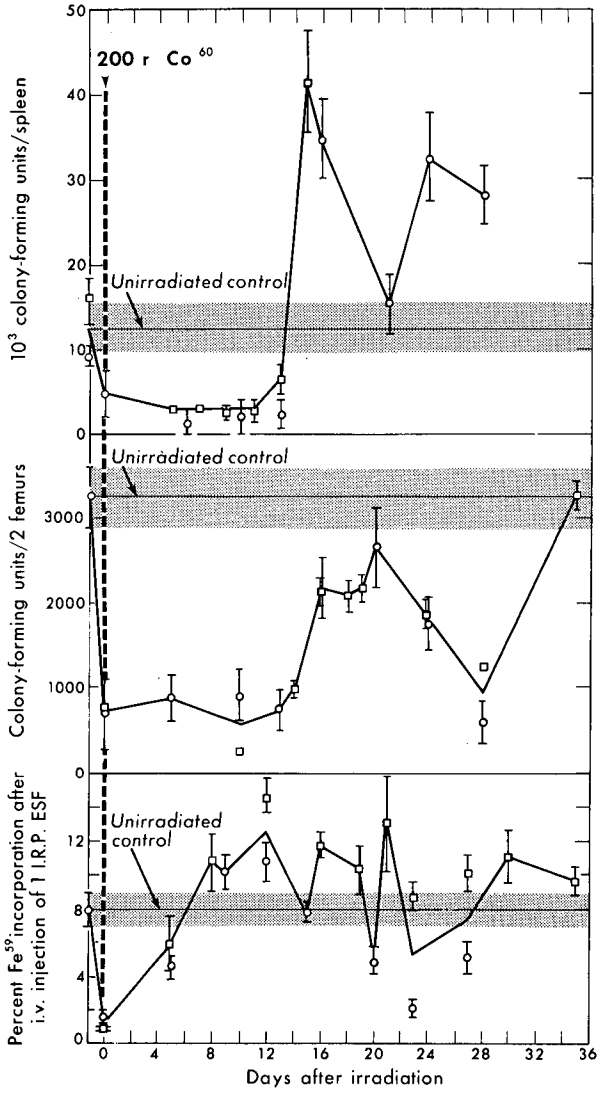

Fig. 2. Recovery of erythropoietin sensitivity and CFU following irradiation.
MUB-8542

content of the bone marrow was unaffected by either hypoxia or cold exposure; however, after splenectomy a significant decrease in the CFU content of the bone marrow was observed. Although not indicated in the figure, a significant decrease in the CFU in the circulating blood was also observed after hypoxic exposure; the CFU/10^6 nucleated cells were 2.0 compared with 5.0 in control mice.

A significant increase in the CFU content of the spleen was observed after erythropoietin injections, even when given in conjunction with the hypoxic exposure and after immunization with sheep red blood cells. Barnes and Loutit (1967) found a more than 10-fold increase in the CFU content of peripheral blood 7 days after injection of pertussis vaccine. Thyroxin caused a slight, but significant, increase in the CFU content of the spleen, probably as a result of increased erythropoietic activity. Starvation, injections of growth hormone, or hydrocortisone had no significant effect on the CFU content of either the spleen or the bone marrow.

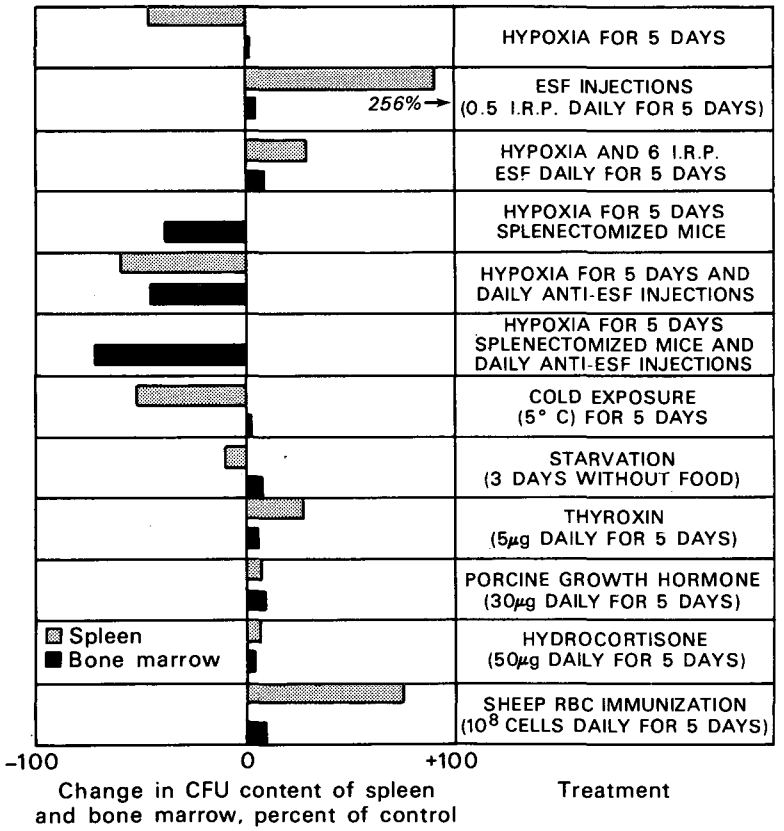

Fig. 3. Change in CFU content of spleen and bone marrow after various treatments. DBL684-4720

These experiments indicate that the decrease in the CFU content of the spleen as a result of hypoxic exposure is not due to the action of erythropoietin. The reason for the difference in the behavior of the CFU of the spleen and bone marrow is unknown at present. It is probable that this difference is related to local conditions within these tissues, but further experiments will be necessary to clarify this problem.

Reissman and Ito (1966) and Gallien-Lartigue and Goldwasser (1965) have shown in vivo and in vitro that erythropoietin does not stimulate erythropoiesis in the presence of actinomycin D, and Keighley and Lowy (1966) have shown, in addition, that actinomycin D does not prevent the formation of erythropoietin in hypoxic mice. The action of actinomycin D on developing spleen colonies was found to be analogous to the effect of polycythemia or the injection of anti-erythropoietin antibody. A transplant of 4×10^4 bone marrow cells gave 10.4 ± 0.74 colonies 10 days after transplantation. If 7.5 or 15 μg of actinomycin D were given to such mice on the 7th, 8th, and 9th days after transplantation, the colony count decreased to 5.9 ± 0.49 and 5.7 ± 0.83 colonies per spleen on the 10th day. In normal hosts 8% of the colonies were predominantly granulocytic, 10% granulocytic and megakaryocytic, 60% predominantly erythroid, 19% contained obvious erythroid, granulocytic and megakaryocytic cells, and about 3% were

primitive unidentifiable cells. The colonies of the actinomycin-D-injected mice were about 88% predominantly granulocytic, 10% granulocytic and megakaryocytic, and 2% primitive cells. These experiments indicate that the formation of erythroid colonies probably depends upon a DNA-dependent-RNA synthetic step in the process of differentiation. The finding that granulocytic development was not particularly influenced agrees with the results of Reissman and Ito (1966) in normal animals. It is possible that granulocytopoiesis is not regulated by a DNA-dependent-RNA synthetic step, but it is more likely that actinomycin D does not enter precursors of the granulocytic cells.

In conclusion: A brief presentation has been given of a considerable amount of experimental data obtained by using the spleen-colony technique and the erythropoietin-sensitivity test which appears to us consistent with the concept that intermediate populations of cells sensitive to differentiative agents exist between the colony-forming unit and the earliest recognizable cells of the hematopoietic system. Morse and Stohlman (1966), on the basis of studies of the effect of vincristine on hematopoietic tissue, have also postulated that intermediate compartments exist.

The assumption of one or more intermediate compartments of cells raises a considerable number of questions regarding the regulation of their sizes, their proliferative rates, and their various cybernetic interrelationships.

SUMMARY

Evidence is presented consistent with the view that the production of erythroid cells in spleen colonies depends on the presence of erythropoietin; however, the hormone does not act directly on the colony-forming cell. The colony-forming cell gives rise to a population of cells which is sensitive to erythropoietin. Erythropoietin regulates the differentiation of such cells by a DNA-dependent-RNA synthetic step. The erythropoietin-sensitive cells are capable of division and their proliferation as well as their formation from colony-forming cells is regulated.

ACKNOWLEDGMENTS

The technical assistance of Mrs. Virginia W. Havens, Mrs. Linda N. Cantor, Miss Judith M. Hayes and the secretarial assistance of Mrs. Grace Walpole are greatly appreciated.

REFERENCES AND NOTE

1. Alexanian, R.; Porteous, D. D.; and Lajtha, L. G.: Intern. J. Rad. Biol. 7: 87-94 (1963).
2. Barnes, D. W. H.; and Loutit, J. F.: Nature 213: 1142-1143 (1967).
3. Becker, A. J.; McCulloch, E. A.; and Till, J. E.: Nature 197: 452-454 (1963).
4. Becker, A. J.; McCulloch, E. A.; Siminovitch, L.; and Till, J. E.: Blood 26: 296-308 (1965).
5. Bruce, W. R.; and McCulloch, E. A.: Blood 23: 216-232 (1964).
6. Bruce, W. R.; and Meeker, B. E.: J. Nat. Cancer Inst. 34: 849-856 (1965).
7. Bruce, W. R.; Meeker, B. E.; and Valeriote, F. A.: J. Nat. Cancer Inst. 37: 233-245 (1966).

8. Bruchovsky, N.; Owen, A. A.; Becker, A. J.; and Till, J. E.: Cancer Res. 25: 1232-1237 (1965).
9. Chen, M. G.; and Schooley, J. C.: Transplantation 6: 121-126 (1968).
10. Curry, J. L.; and Trentin, J. J.: Developmental Biol. 15: 395-413 (1967).
11. Curry, J. L.; Trentin, J. J.; and Wolf, N.: J. Exp. Med. 125: 703-720 (1967).
12. Fowler, J. H.; Wu, A. M.; Till, J. E.; McCulloch, E. A.; and Siminovitch, L.: J. Cell. Physiol. 69: 65-72 (1967).
13. Gallien-Lartigue, O.; and Goldwasser, E.: Biochim. Biophys. Acta 103: 319-324 (1965).
14. Gurney, C. W.: Perspectives Biol. Med. 6: 233-245 (1963).
15. Gurney, C. W.; Lajtha, L. G.; and Oliver, R.: Brit. J. Haematol. 8: 461-466 (1962).
16. Hodgson, G.: Proc. Soc. Exp. Biol. Med. 125: 1206-1209 (1967).
17. Jurášková, V.; Tkadlecek, L.; and Drásil, V.: Folia Biol. 10: 381-385 (1964).
18. Keighley, G.; and Lowy, P. H.: Blood 27: 637-645 (1966).
19. Lajtha, L. G.: J. Cell. Physiol. 67 Suppl. 1: 133-148 (1966).
20. Lajtha, L. G.; Oliver, R.; and Gurney, C. W.: Brit. J. Haematol. 8: 442-460 (1962).
21. Lewis, J. P.; and Trobaugh, F. E.: Nature 204: 589-590 (1964).
22. Liron, M.; and Feldman, M.: Transplantation 3: 509-516 (1965).
23. Morse, B. S.; and Stohlman, F., Jr.: J. Clin. Invest. 45: 1241-1250 (1966).
24. Porteous, D. D.; and Lajtha, L. G.: Brit. J. Haematol. 12: 177-188 (1966).
25. Reissmann, K. R.; and Ito, K.: Blood 28: 201-212 (1966).
26. Schooley, J. C.: Blood 25: 795-808 (1965).
27. Schooley, J. C.: J. Cell. Physiol. 68: 249-262 (1966).
28. Schooley, J. C.; Cantor, L. N.; and Havens, V. W.: Exp. Hemat. 9: 55 (1966).
29. Schooley, J. C.; Garcia, J. F.; Cantor, L. N.; and Havens, V. W.: Ann. N. Y. Acad. Sci. 149: 266-280 (1968).
30. Schooley, J. C.; Hayes, J. M.; Cantor, L. N.; and Havens, V. W.: Radiation Res. 32: 875-883 (1967).
31. Siminovitch, L.; McCulloch, E. A.; and Till, J. E.: J. Cellular Comp. Physiol. 62: 327-336 (1963).
32. Smith, W. W.; Brecher, G.; Fred, S.; and Budd, R. A.: Radiation Res. 27: 710-717 (1966).
33. Till, J. E.: Am. J. Roentgenol. 90: 917-927 (1963).
34. Till, J. E.; and McCulloch, E. A.: Radiation Res. 14: 213-222 (1961).
35. Till, J. E.; McCulloch, E. A.; and Siminovitch, L.: Proc. Nat. Acad. Sci. 51: 29-36 (1964).
36. Till, J. E.; Siminovitch, L.; and McCulloch, E. A.: Blood 29: 102-113 (1967).
37. Valeriote, F. A.; and Bruce, W. R.: J. Nat. Cancer Inst. 35: 851-856 (1965).
38. Valeriote, F. A.; Bruce, W. R.; and Meeker, B. E.: Biophys. J. 6: 145-152 (1966).
39. Virolainen, M.; and Defendi, V.: Nature 217: 1069-1070 (1968).
40. Weisman, M.; Martinson, D.; Fried, W.; and Gurney, C. W.: J. Lab. Clin. Med. 69: 438-446 (1967).
41. Welshons, W. J.: in Mammalian Cytogenetics and Related Problems in Radiobiology, London, Pergamon Press, 1964, pp. 233-243.

42. Wu, A. M.; Till, J. E.; Siminovitch, L.; and McCulloch, E. A.: J. Cell. Physiol. 69: 177-184 (1967).

43. Wu, A. M.; Till, J. E.; Siminovitch, L.; and McCulloch, E. A.: J. Exp. Med. 127: 455-464 (1968).

This paper was presented at the Conference on Comparative and Species Radiosensitivity, Kyoto, Japan, May 1968.

Parallel Development of Intracellular Membranes and the Acid Secretory Mechanism of Oxyntic Cells of the Metamorphosing Bullfrog Tadpoles

Gertrude M. Forte, John G. Forte and Liangchai Limlomwongse

INTRODUCTION

Oxyntic, or acid secreting, cells in the adult bullfrog gastric mucosa contain abundant smooth-surfaced endoplasmic reticulum in the apical regions of the cells (Sedar, 1961a, 1961b; Sedar and Forte, 1964). These agranular membranes appear in the form of packed tubular components with diameters of 400-700 Å and of unspecified length. On the basis of ultrastructural studies, several investigators have presented evidence to show a possible role for the smooth-surfaced endoplasmic reticulum in the membrane transformations that accompany the process of HCl secretion (Sedar, 1961, 1965; Ito, 1961; Vial and Orrego, 1960; Forte, 1966).

The stomach of the unmetamorphosed bullfrog tadpole does not secrete HCl. In recent studies we have found that the capacity to secrete HCl develops rather late in tadpole metamorphosis (Forte, Limlomwongse and Forte, 1967). The earliest observed appearance of HCl secretion was in the stage of metamorphosis where tail reabsorption was almost complete, which corresponds to stage XXIII according to the nomenclature proposed by Taylor and Kollros (1946).

The development of such an active process as HCl secretion must be accompanied by basic structural alterations which might be useful in the interpretation of the detailed secretory mechanism. Previous studies by light microscopy on gastric glands in metamorphosing anuran forms have provided the general histological pattern of development; however, cytological detail is lacking because of obvious technical limitations (Kuntz, 1924; Janes, 1934; Kaywin, 1936). The present experiments were designed to study the general morphology and especially the fine structure of oxyntic cells of the metamorphosing tadpole gastric mucosa and to correlate observed structural development with the appearance of HCl secretion. Our findings indicate that extensive development of the smooth-surfaced endoplasmic reticulum, which is a structural characteristic of the adult oxyntic cell, begins in stages XXIII and XXIV which correlates well with the onset of HCl secretion.

METHODS

MATERIALS Bullfrog (Rana catesbeiana) tadpoles of various ages were obtained from a local supplier and were maintained in laboratory aquaria. The morphological descriptions provided by Taylor and Kollros (1946) for Rana pipiens tadpoles were used to identify the various

stages of metamorphosis. Sketches of several tadpoles used in these experiments are given in Fig. 1.

PREPARATION FOR ELECTRON MICROSCOPY Tadpoles were sacrificed by pithing, after which the abdominal cavity was opened and the stomach excised. When no further physiological experiments were carried out the pH of the stomach contents were roughly determined with indicator paper. The tubular shaped stomachs of the tadpoles were cut open longitudinally with fine scissors and dropped into cold 2.5% glutaraldehyde in 0.1 M phosphate buffer, pH 7.4. The middle portion of the stomach region was minced into small, 1 mm^2, pieces in the cold fixative and then transferred into fresh, cold glutaraldehyde fixative for 1 hour. The tissue was later post-fixed for 1 hour in 1% OsO_4 in 0.1 M phosphate buffer, pH 7.4. The tissue blocks were dehydrated through ethanol and finally embedded in Epon.

Sections were cut on the Porter-Blum ultramicrotome by using glass knives. Thick sections, 1-2μ, were cut at frequent intervals and examined with the light microscope to be certain of orientation. Such thick sections were stained for 1.5 minutes after mixing 1 drop of 1% methylene blue in 1% sodium borate with 1 drop of 1% azure blue directly on the slide with the sections. The sections were rinsed with tap water after staining. Ultrathin sections were stained with uranyl acetate and lead citrate. Thin sections were mounted on unsupported 200-mesh copper grids and were examined with either the Siemens Elmiskop I or Hitachi HU 11 microscope.

MEASUREMENT OF H^+ SECRETION When direct measurements of H^+ secretory capacity were required, the tadpole stomachs were removed and mounted as a tube onto a specially designed glass chamber depicted in Fig. 2. Bicarbonate buffered frog Ringer's solution (Forte, 1968) was placed on the serosal side of the stomach and isotonic 0.12 M NaCl was placed on the secretory or mucosal side. The air-lift mechanism shown in Fig. 2 was used both as a circulating and aerating device with the gas phase being 95%O_2-5%CO_2. Electrodes for measuring pH were placed into the mucosal bathing solution and when H^+ secretion occurred, as indicated by a lowering of the pH reading, standardized 0.02 N NaOH was added by means of a microburet. The rate of addition of the base in order to maintain the pH of the mucosal solution at the desired end point (pH 5.0) is equivalent to the rate of H^+ secretion.

OBSERVATIONS

LIGHT MICROSCOPY Sections taken from the region of the gastrointestinal tract corresponding to the position of the stomach in the unmetamorphosed stage XII tadpole show a very simplified histology (Fig. 3). The mucosal surface consists of a simple columnar epithelium; the underlying submucosa is composed of connective tissue but is devoid of any glands. At this stage of morphogenesis, the smooth muscle at the serosal side is quite undeveloped. As metamorphosis proceeds, the mucosa becomes increasingly thickened and more complex. By stage XVIII the epithelium occasionally shows deep infoldings (Fig. 4) into the underlying submucosa and a few gland-like regions are also noticeable in the connective tissue. The mucosa at this stage of development is characterized, as well, by a marked degree of cytolysis of the epithe-

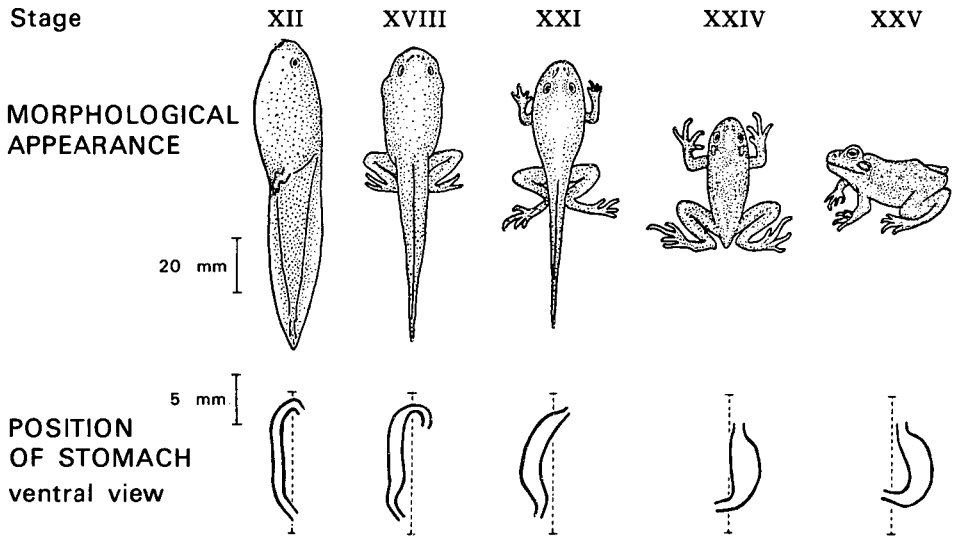

Fig. 1. A diagrammatic illustration of the gross morphological appearance of representative stages of bullfrog tadpole metamorphosis. The general position and shape of the stomach is also shown. During later stages of development the stomach rotates from the right to left side of the body cavity.
DBL688-5405

lium and by the invasion of large numbers of phagocytes. The serosal smooth muscle is considerably thickened, but there is no definitive muscularis mucosae.

The general morphological organization which is characteristic of the adult mucosa does not appear until relatively late in metamorphosis, about stage XX or XXI. A longitudinal section from the stomach of a stage XXI tadpole is shown in Fig. 5, where it appears that invaginations of the surface epithelium are continuous with gland-like structures beneath the surface. By this stage of development the gastric mucosa, and in fact the entire stomach, has noticeably thickened as a result of extensive growth of all histological components. The muscularis mucosae is well defined but the gland-like infoldings of the mucosa do not extend completely to its limits. A cross section (Fig. 6) through the gland-like structures indicates that a lumen is often lacking and that where this is the case, the glands are in fact made up of loosely aggregated cells.

More extensive development of the gastric glands has occurred by stage XXIV (Fig. 7) where the glands extend completely from the mucosal surface down to the muscularis mucosae. The general histology seen with the light microscope is similar to that observed for adult gastric preparations; cell types corresponding to the surface epithelial cells, the mucous neck cells, and the oxyntic cells are readily identified in stage XXIV.

FINE STRUCTURE OF THE DEVELOPING GASTRIC GLAND The observations reported here will be confined to the glandular regions of the tadpole gastric mucosa before and after the development of the capacity to secrete acid. Cross sections through glandular structures of stage XXII bullfrog tadpole gastric mucosa are shown in Figs. 8-10. Typical regions without and with a lumen are shown in Figs. 8 and 9, respectively. The cells contain large nuclei,

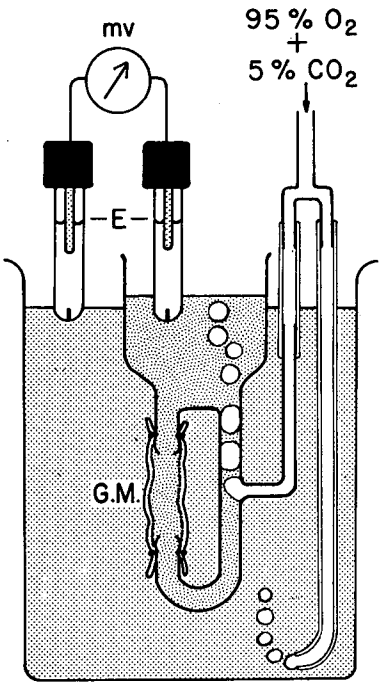

Fig. 2. Schematic diagram of apparatus used to study physiological properties of tadpole stomach. The stomach (GM) was mounted onto the glass chamber which was then inserted into a 100-mliter beaker. Solutions on both sides were stirred and aerated with 95% O_2 and 5% CO_2. The transmural potential difference (mv) was measured via calomel electrodes (E) placed on both sides of the stomach.

DBL688-5406

relatively scant cytoplasm, and have the general appearance of undifferentiated cells. Ribosomal particles are found free in the cytoplasmic matrix as well as attached to membranes in the form of rough-surfaced endoplasmic reticulum as shown in the enlarged section in Fig. 10. Mitochondria are large and quite numerous with a matrix of low density. The Golgi apparatus appears lateral to the nucleus but is not so structurally elaborate as will be seen in later metamorphic stages. The apical cytoplasm of the glandular cells is practically devoid of smooth-surfaced endoplasmic reticulum at this stage. Where glandular lumina exist the cell surfaces are relatively smooth.

In contrast to the fine structural pattern typically observed in stages XX-XXII there is a highly differentiated appearance in the glandular cells of gastric tissue from stage XXIV bullfrog tadpoles (Fig. 11). By virtue of their large and abundant mitochondria, the decrease of rough-surfaced membranes and the appearance of tubular members of the smooth-surfaced endoplasmic reticulum (ER), these glandular cells show a definite similarity to the adult oxyntic cell and thus represent what we consider a newly differentiated oxyntic cell. The most striking changes in cellular components in comparing stage XXIV with previous metamorphic stages are in the elaborate Golgi apparatus and the appearance of smooth-surfaced ER which accumulates in the apical region of the cells. The smooth-surfaced membranes at this stage consist of short straight or U-shaped tubular structures randomly distributed in the apical cytoplasm; in cross-sections their diameters range from 500 to 670 Å (Fig. 12). The space within the tubular elements of the smooth-surfaced ER in the XXIV stage of development is often electron dense (inset, Fig. 12) under the conditions of fixation and staining used in these experiments. The Golgi complex consists of several stacked cisternae which often appear to give rise to small vesicular structures by pinching off, or blebbing, of the ends of the Golgi lamellae. Many of these vesicles ranging in diameter from 400 to 670 Å can be seen at

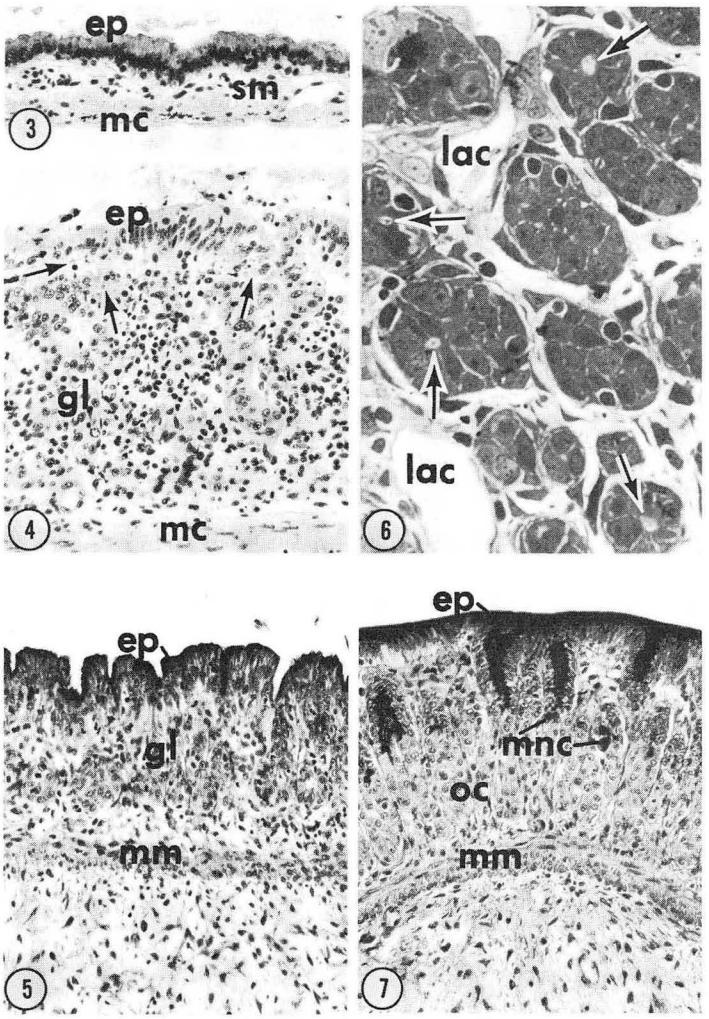

Fig. 3. Longitudinal section through the stomach of the stage XII bullfrog tadpole. The mucosal surface consists of a continuous layer of columnar epithelium (ep). The submucosal region (sm) is very simplified and the muscle coat (mc) is also undeveloped. Stained with hematoxylin and eosin. × 112

Fig. 4. Longitudinal section through stage XVIII tadpole stomach. Invaginations of the surface epithelium (ep) begin to form at this stage and appear to give rise to gland-like cell aggregations (gl). Extensive cytolysis, indicated by arrows, is also characteristic of this metamorphic stage. Further growth and development of the smooth muscle coat (mc) has occurred but a well-defined muscularis mucosae is not apparent. Stained with hematoxylin and eosin. × 112

Fig. 5. Longitudinal section through stage XXI tadpole stomach. Gland formation is extensive although the gastric glands (gl) do not extend to the well-developed muscularis mucosae (mm). The smooth muscle coats (not shown) have considerably thickened and are also well developed. The section was stained for the periodic acid Schiff reaction (PAS) which accentuates the mucous containing cells of the surface epithelium (ep). × 112

Fig. 6. A cross section through the region of the gastric glands of the stage XXII tadpole. Many glands consist of a loose aggregate of cells while others contain patent lumina indicated by arrows. Large lacunar spaces (lac) between the glands are also typically seen. Epon-imbedded section stained with methylene blue and azure blue. × 420

Fig. 7. A longitudinal section through the stage XXIV bullfrog stomach. Gastric glands are fully developed and extend completely through the mucosa to the muscularis mucosae (mm). Surface epithelial cells (ep), mucous neck cells (mnc), and oxyntic cells (oc) are readily identifiable. PAS stained. × 112

XBB688-4803

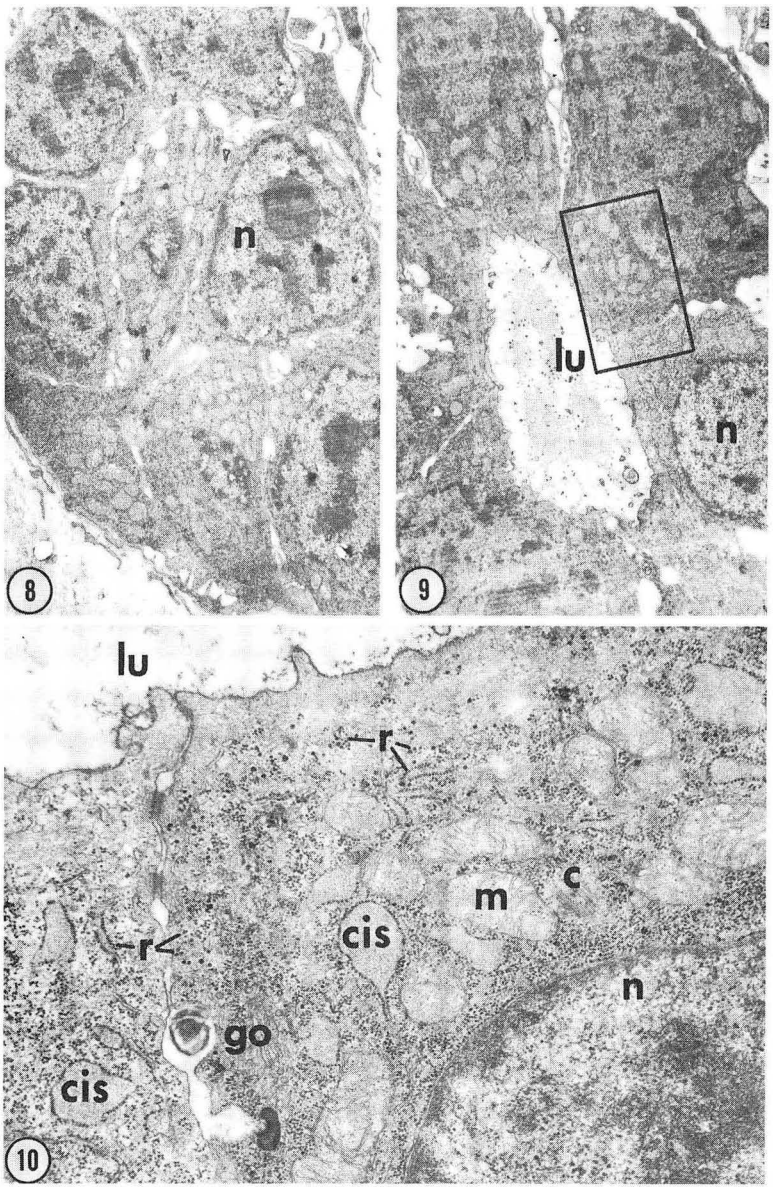

Fig. 8. Electron micrograph of cross section through a gastric gland of a stage XXII tadpole stomach. No glandular lumen is apparent in this section. Nuclei (n) are very large relative to the cell size. × 3500

Fig. 9. Cross section through stage XXII gastric gland exhibiting a patent lumen (lu). As in the previous figure the nuclei (n) are very large. The circled area is shown in greater detail in Fig. 10. × 3500

Fig. 10. An enlargement of the area indicated on the previous figure, showing greater cellular detail. Numerous ribosomal particles (r) are present throughout the cytoplasm, both free and in association with membranes. The Golgi complex (go) is present but not as extensively developed as in later metamorphic stages. Mitochondria (m), centriole (c) and a nucleus (n) are also evident in the micrograph. × 18,000

XBB688-4800

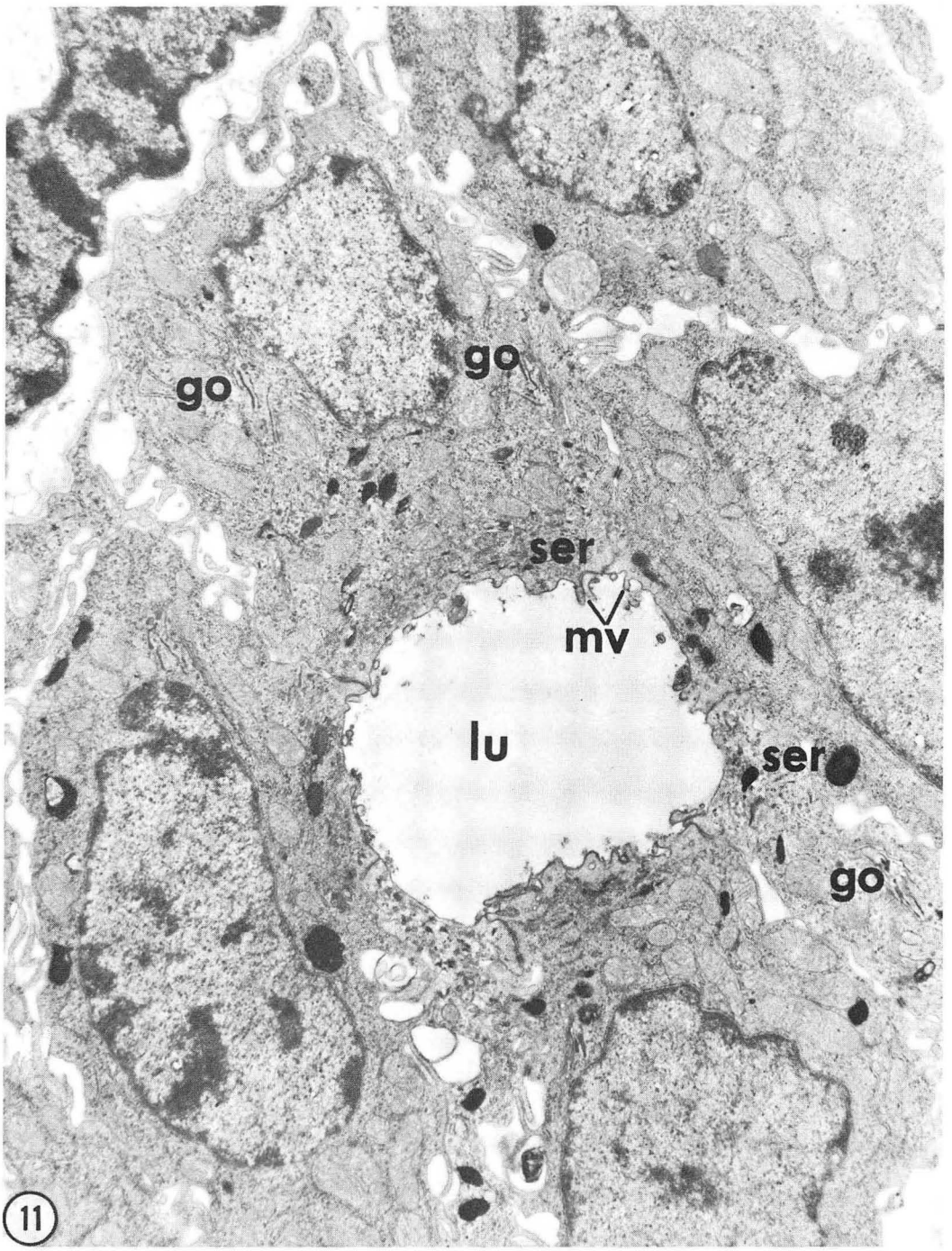

Fig. 11. Cross section through a gastric gland of the stage XXIV tadpole stomach. The stomach contents of this animal were of neutral pH as determined by indicator paper. Characteristically the gland consists of several newly differentiated oxyntic cells surrounding a patent lumen (lu). These young oxyntic cells are distinguished by the smooth-surfaced endoplasmic reticulum (ser) seen at the cell apex and by the very prominent and extensive Golgi apparatus (go). The surface membrane is relatively smooth with only occasional stubby microvilli (mv) projecting into the lumen. × 8750

XBB688-4806

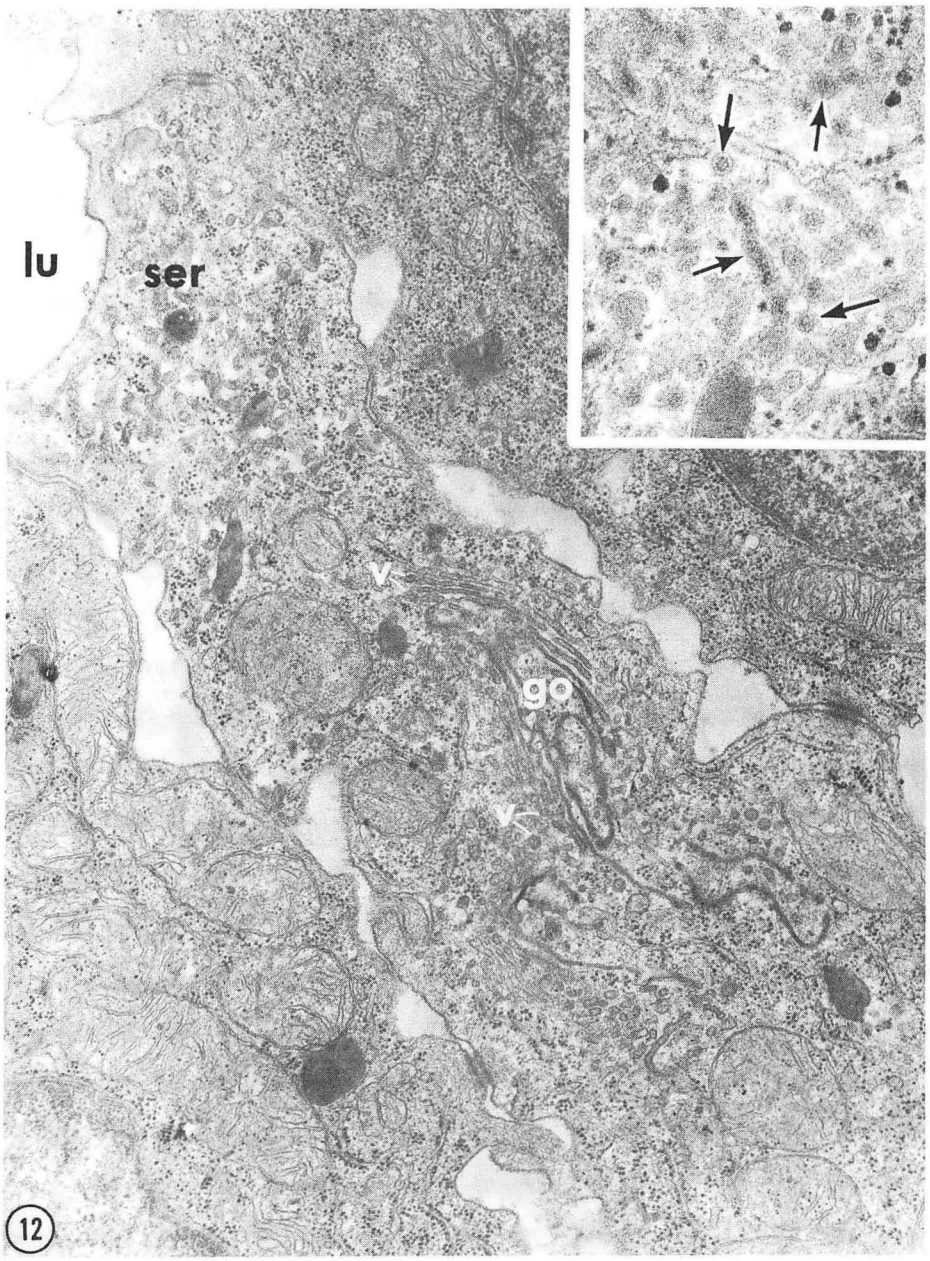

Fig. 12. Apex of a young oxyntic cell shown in greater detail. The prominent Golgi regions (go) consist of several stacked cisternae which often appear to pinch off vesicular structures (v) at their periphery. Both longitudinal and transverse profiles of the smooth-surfaced endoplasmic reticulum (ser) appear to accumulate in the apical portion of the cell. × 26,200

The inset is an enlargement of the profiles of the smooth-surfaced endoplasmic reticulum taken from a similar cell. A few of these structures (arrows) contain a very dense material of unknown origin. × 78,000

XBB688-4801

the periphery of the Golgi complex in Fig. 12. From the topographical interrelationships between the small vesicles derived from the Golgi and similar structures in the apex of the cell it appears as if the Golgi apparatus may represent the site for production and synthesis of the smooth-surfaced tubular membranes.

The surface of the glandular cells of stage XXIV tadpole stomachs with contents of neutral pH is usually smooth with only occasional stubby cytoplasmic extensions projecting into the lumen. Immediately beneath the plasma membrane are the short tubular elements of the smooth-surfaced ER. It is probably significant that these tubular structures are not seen in direct contact with the plasma membrane when the stomach has not been stimulated to secrete acid.

In stage XXV, which is the newly metamorphosed froglet, we have found that the smooth-surfaced ER has greatly increased in quantity and complexity of conformation. The Golgi complex, however, is somewhat less conspicuous than in the previous stage of metamorphosis. The complexity of the smooth ER may readily be seen in the section through oxyntic cells of a stage XXV gastric mucosa which had been stimulated to secrete acid by 10^{-4} M histamine (Fig. 13). The tubular structures can often be followed for distances of 1 μ, thus giving the appearance of greater length than those seen in the less mature oxyntic cells. The diameters of the smooth-surfaced tubules vary from 400 to 700 Å, and where they are closely packed and viewed in cross section they are often oriented in an hexagonal pattern which is a characteristic feature for the even more abundant smooth-surfaced ER present in the adult oxyntic cells. A section through the apical portion of an oxyntic cell from the stomach of an adult frog is shown in Fig. 14 for comparison. Here the numerous cross sectional and longitudinal profiles of the agranular tubules are seen to be tightly packed in the apex of the cell. As a consequence of the large quantities of smooth membranes in the adult oxyntic cell we have generally found it difficult to identify the Golgi apparatus.

COMPARISON OF RESTING AND HISTAMINE-STIMULATED TADPOLE GASTRIC MUCOSA

Experiments were performed to determine structural differences in the oxyntic cells during various physiological states of acid secretion. Tadpole stomachs were mounted onto the glass chamber where the rate of H^+ secretion was monitored prior to fixation. The apical surface of oxyntic cells in the non-secreting preparation is relatively smooth with only a few short cytoplasmic or microvillar extensions (Fig. 15). This is similar to the observed structure in stomachs fixed immediately after excision (cf. Figs. 11 and 12) and is also typical of that described for the adult resting oxyntic cell (Sedar, 1961a; Kasbekar, Forte and Forte, 1968). The tadpole gastric mucosa to which 10^{-4} M histamine had been added was secreting acid at a rate of 2.7 $\mu eq/cm^2 \cdot hr$ at the time of fixation. Table 1 summarizes the secretory data for tadpole stomachs between stage XXI and XXV. It is not until stage XXIV that the stomachs will consistently respond to secretagogues. A structural comparison of non-stimulated and histamine-stimulated stage XXIV stomachs is shown in Figs. 15 and 16 respectively. Associated with the secretory responsiveness there is a marked change in the apical surface of the oxyntic cell, which now possesses numerous long and filamentous cytoplasmic extensions projecting into the lumen (Fig. 16). At higher magnifications (Fig. 17) it appears that some of the short tubular

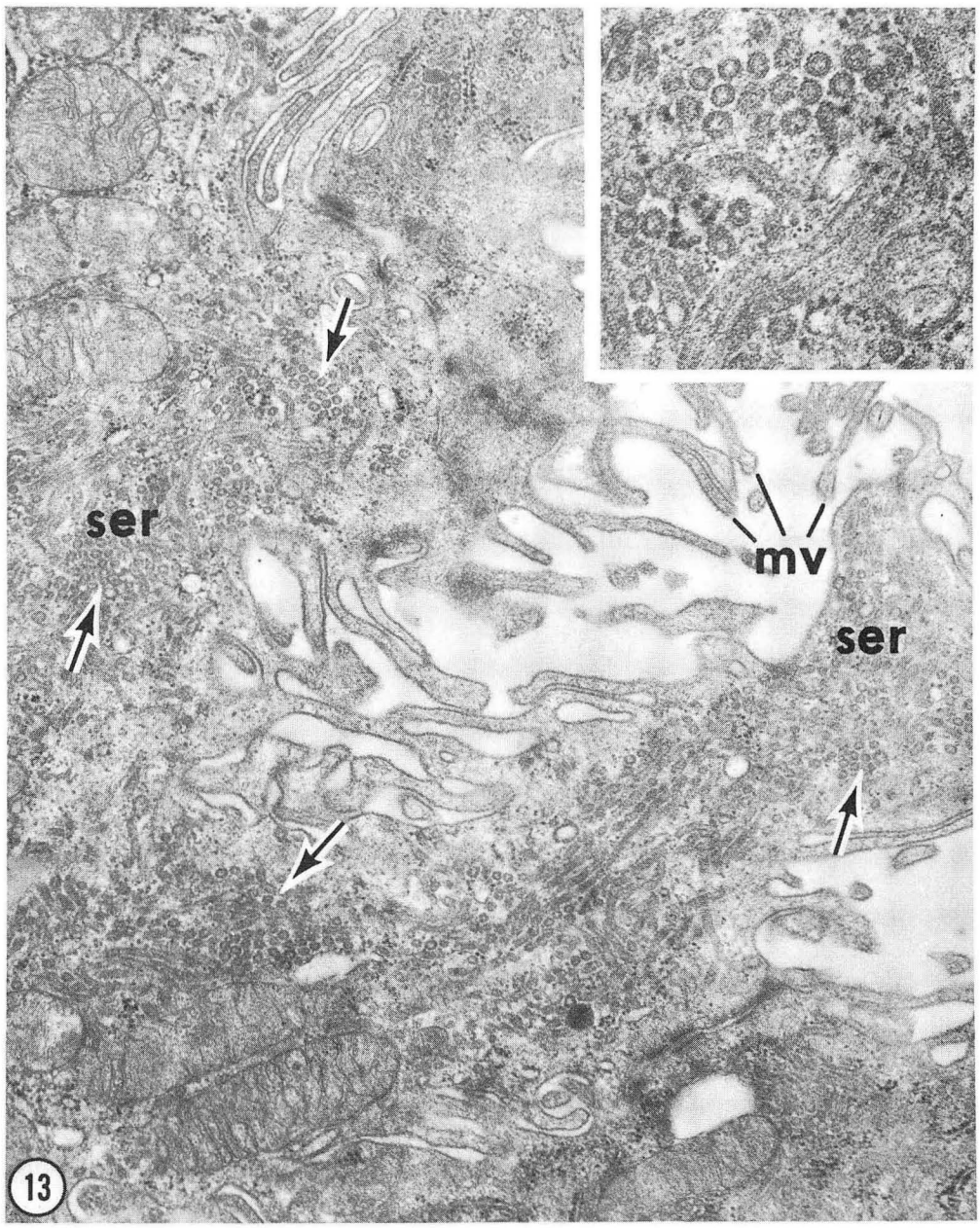

Fig. 13. Section through the anterior portion of three oxyntic cells from the stage XXV gastric mucosa. The stomach was stimulated by the addition of histamine and prior to fixation the measured rate of H^+ secretion was 2.5 $\mu eq/cm^2/hr$. The smooth-surfaced endoplasmic reticulum (ser) is more abundant than observed in the previous stage of development and occasionally cross-sectional profiles of the tubular elements appear to be arranged in a hexagonal pattern (indicated by arrows). Numerous, long microvilli (mv) extend into the lumen, a feature which is characteristic of an acid-secreting stomach. $\times$ 25,000

The inset shows in greater detail the structure of the tubular elements of the smooth-surfaced ER. $\times$ 75,000

XBB688-4802

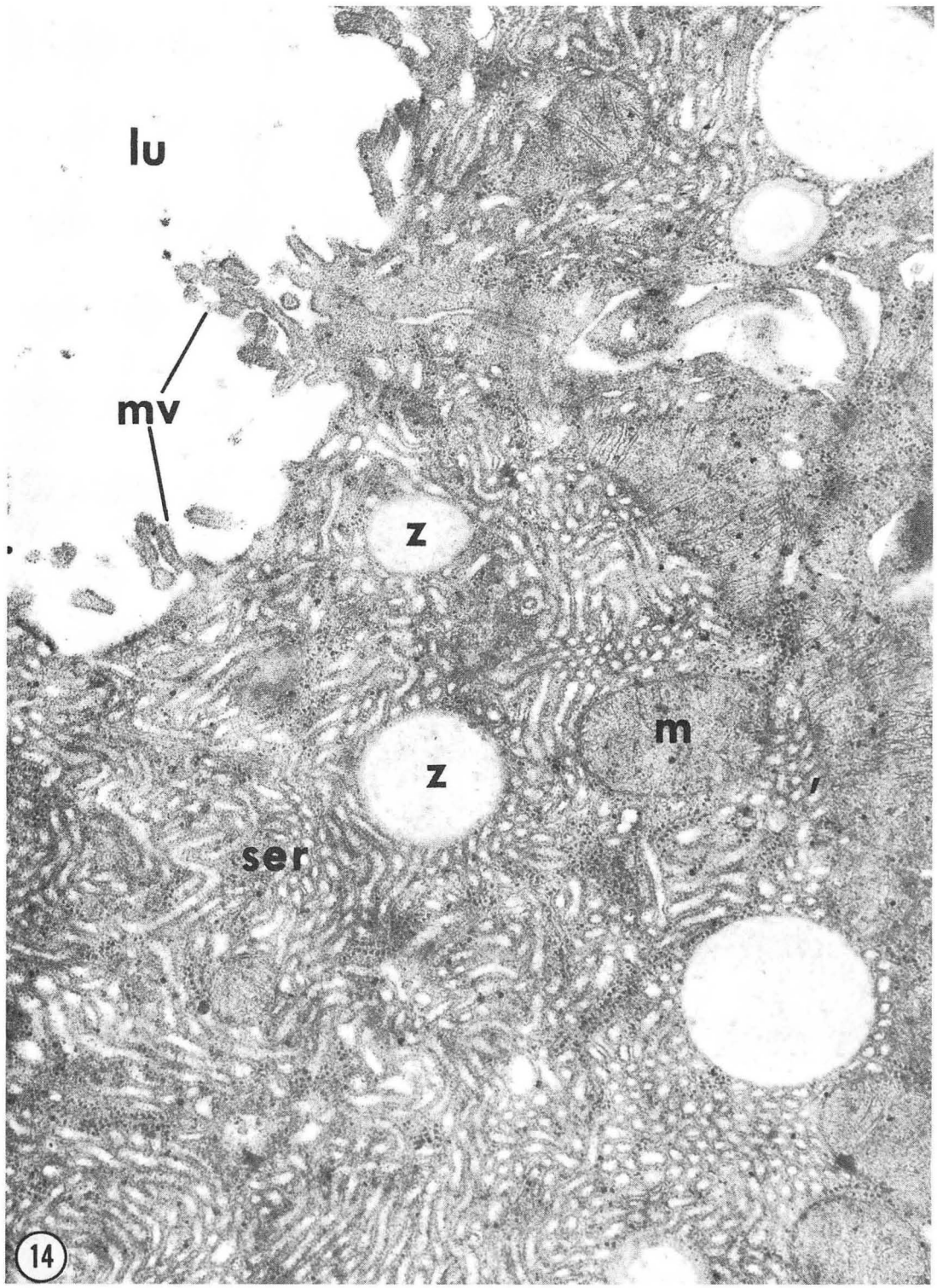

Fig. 14. An electron micrograph of the apical part of two adjacent oxyntic cells from an adult bullfrog non-secreting stomach. Note the extreme close packing of the tubular members of the smooth-surfaced ER. Several large granules presumed to be zymogen granules (z) are also present. × 32,000

XBB688-4805

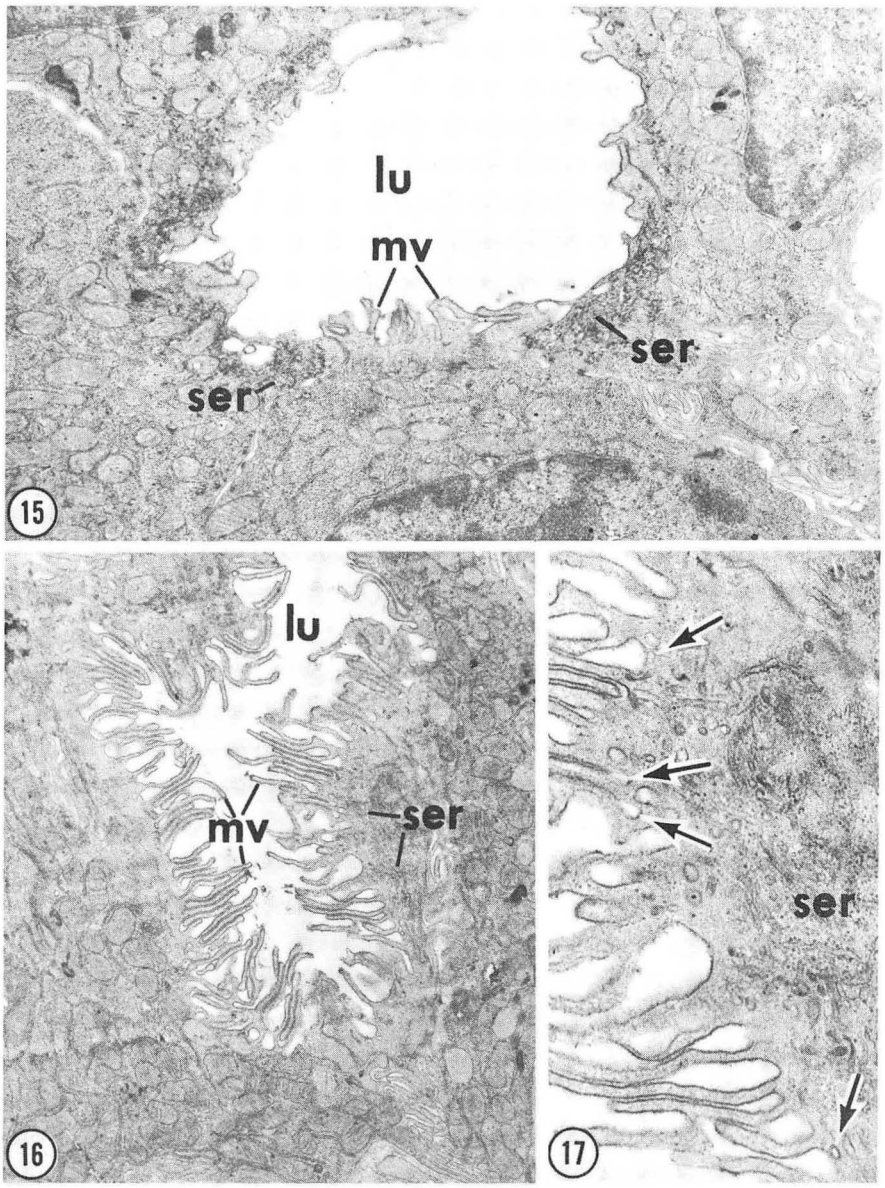

Fig. 15. A transverse section through several oxyntic cells of a non-secreting stage XXIV tadpole stomach. Prior to fixation the stomach had been mounted onto the glass chamber and no measurable H^+ secretion was detected. As was the case in Fig. 11, young oxyntic cells are recognizable by the accumulation of smooth-surfaced ER (ser) at the apex of the cell; note that two of the cells still have little or no profiles of ser. The apical cell surface contains relatively few extensions or microvilli (mv). × 8800

Fig. 16. An oblique section through a gastric gland from an actively secreting stage XXIV tadpole stomach. The stomach had been mounted on the glass chamber and was secreting acid at a rate of 2.7 $\mu eq/cm^2/hr$ after the addition of histamine. Smooth-surfaced ER (ser) can be seen in the apex of cells while numerous microvilli (mv) project into the gland lumen (lu). × 9250

Fig. 17. An enlargement of a portion of the apical surface of an oxyntic cell seen in the previous figure. This demonstrates the relationship between the profiles of the smooth-surfaced ER (ser) and the surface membrane. At points indicated by arrows it appears that tubular and vesicular members of the smooth-surfaced ER are in contact with the surface membrane. × 27,800

XBB688-4804

Table 1. Acid secretory capability of tadpole stomachs at various stages of metamorphosis.

Stage of metamorphosis	XX	XXII	XXIII	XXIV	XXV
No. of stomachs tested in chamber	3	3	5	7	4
No. of stomachs demonstrating H^+ secretion, either spontaneously or in response to secretagogues	0	0	1	7	4
Average secretory rate of responsive stomachs (μeq $H^+/cm^2 \cdot hr \pm SEM$)	--	--	0.7	1.6 ± 0.3	2.5 ± 0.4*

*Rate of acid secretion for grown adult frogs ranges from 3-6 μeq $H^+/cm^2 \cdot hr$.

structures normally subadjacent to the surface have made contact with the cell surface (arrows) and may contribute to the increased cell surface. Such characteristic changes have been observed for the adult bullfrog gastric mucosa and several investigators have proposed that the smooth-surfaced ER represents an immediate source for the membranous transformations which underlie the structural changes related to secretory activity (Sedar and Forte, 1962; Sedar, 1965; Kasbekar, Forte and Forte, 1968).

DISCUSSION

In a preliminary report from this laboratory it has been shown that HCl secretion in the metamorphosing bullfrog tadpole stomach begins rather abruptly at about stage XXIII or XXIV of development (Forte, Limlomwongse and Forte, 1967). The present investigation on the morphogenesis of the acid-secreting cell demonstrates a cell type with characteristics identifiable as an oxyntic cell at about the same stage of development. Thus for the frog stomach there is a correlation between the morphological development of a specific cell type and the functional capacity to secrete acid, similar to that shown for the fetal rabbit stomach (Menzies, 1958; Wright, 1962).

As late as stage XXI and XXII the majority of cells present in the developing gastric glands exhibit features of cytological organization that are characteristic of undifferentiated cells. These cells may well represent precursors in the morphogenesis of the oxyntic cells identified in later stages. Similar undifferentiated cells have been described by Bonneville (1963) in the developing tadpole intestinal mucosa and by Arnold (1966) in the fetal hamster stomach. These authors have proposed that such basal or stem cells represent morphogenetic precursors for the functional absorptive epithelial and mammalian parietal cell, respectively.

There are two structurally significant features which may be seen in the earliest identifiable oxyntic cells of stage XXIV tadpole gastric glands: 1) extremely elaborate and extensive Golgi complexes and 2) accumulation of short, agranular tubules in the apices of the cells. Hayward (1967), working with fetal rabbit stomachs, and Nomura (1966), with fetal human stomachs, have noted that the Golgi apparatus of the very early oxyntic cells was prominent in both species, whereas the Golgi structure in more mature oxyntic cells was poorly developed. Neither author had placed much significance on the prominent Golgi apparatus seen in the immature oxyntic cells. The elaboration of smooth-surfaced ER has also been a characteristic noted for the morphogenesis of parietal cells in the chicken (Toner, 1965), the human fetus (Nomura, 1966), and the rabbit (Hayward, 1967). Nomura (1966) and Hayward (1967) have suggested that the intracellular agranular membranes may be derived by pinocytosis from the apical plasma membrane.

For the tadpole gastric mucosa, the elaborate configuration of the Golgi complex is characteristic of the early oxyntic cell (stage XXIV) where tubular elements of the agranular ER are first beginning to appear. The Golgi complex, however, seems to lose its prominence in stage XXV. Certainly, this organelle is very inconspicuous in the adult frog oxyntic cell, and at the same time the smooth-surfaced ER is very extensive. The amount of smooth-surfaced ER appears to vary inversely with the prominence of the Golgi apparatus. We feel that the Golgi apparatus is very likely the site for synthesis of the smooth-surfaced ER which accumulates in the apical portions of the oxyntic cells. The small vesicular elements seen at the periphery of the Golgi complex in stage XXIV have dimensions similar to the cross-sectional profiles of the smooth ER. Moreover, there appears to be a continuum of vesicular profiles from the region of the Golgi apparatus to the apical secretory surface of the cells, which would be consistent with an hypothesis that the genesis of the smooth ER occurs at the Golgi. Long tubular structures may arise by fusion of the Golgi vesicles, or in fact, may be the result of a mass pinching off of the lamellar elements of the Golgi complex. Sjöstrand (1962) and Mollenhauer and Whaley (1963) have suggested that the Golgi membranes give rise to membranes associated with secretory phenomena. More recently, Jamieson and Palade (1967) have indicated that the agranular tubules of the exocrine pancreas may also be formed by coalescence of small vesicles derived from the Golgi complex.

The parallel appearance of smooth-surfaced membranes within oxyntic cells and the ability to secrete acid supports the concept that these membranes play an integral role in the HCl secretory mechanism (Sedar, 1961b, 1965; Ito, 1961; Helander, 1964; Vial and Orrego, 1960; Forte, 1966). For adult frog stomachs stimulated by histamine to secrete acid, an increase in the apical surface area of oxyntic cells is observed through what appears to be a fusion of cytoplasmic agranular tubules with the cell surface (Sedar, 1961b; Sedar and Forte, 1962). Similarly, in other preparations, such as chicken proventriculus (Toner, 1963), and bat stomach (Ito, 1961), the disappearance of apical tubules and vesicles from parietal cells occurs concomitant with the greatly increased cell surface. Oxyntic cells of resting, or non-acid-secreting, gastric mucosa of the stage XXIV tadpole have relatively smooth cell surfaces typical of non-secreting adult cells. However, when stomachs of this same metamorphic stage are stimulated to secrete acid by addition of histamine, much of the apical surface of oxyntic

cells appears to be invested with numerous cytoplasmic extensions projecting into the glandular lumen. These observations tend to confirm those of the above authors concerning integral relationships between membrane transformation and HCl secretory activity. Moreover, they show that morphogenesis of the smooth-surfaced ER is a basic prerequisite to the development of gastric secretory function.

SUMMARY

Bullfrog tadpole stomachs of various metamorphic stages were examined to determine the fine structural development of oxyntic cells and to correlate observed morphological development with the capacity to secrete HCl. It was found that in vitro tadpole stomachs can consistently be stimulated to secrete acid by stage XXIV of metamorphosis, when tail reabsorption is nearly complete. Concomitant with the appearance of HCl secretion, identifiable oxyntic cells were found in the gastric glands.

Prior to stage XXIV (stages XXI and XXII) the majority of cells present in the developing gastric glands exhibit features of cytological organization characteristic of undifferentiated cells: large nuclei, relatively scant cytoplasm, and numerous ribosomal particles within the cytoplasmic matrix. The newly differentiated oxyntic cells of stage XXIV tadpole stomachs are recognizable by the accumulation of tubular members of the smooth-surfaced endoplasmic reticulum in the apical portion of the cells. These membranous structures appear to be formed by the Golgi complex, which is extremely elaborate at this stage of development. As the animals complete metamorphosis (stage XXV) further development of the oxyntic cells occurs, especially the elaboration of the tubular components of the smooth-surfaced endoplasmic reticulum. The abundance of these membranous tubules within the apical cell regions and the pattern of their packing is similar to that observed in oxyntic cells of adult frogs.

Also consistent with studies on adult frogs, structural alterations associated with HCl secretion were seen in the later stages of metamorphosis. In stage XXIV and XXV tadpole stomachs, which had been stimulated to secrete acid by addition of histamine, the apical surfaces of oxyntic cells were invested with long filamentous microvilli which projected into the glandular lumen. These observations support the hypothesis that membrane transformations play an integral role in the mechanism of HCl secretion and they implicate the morphogenesis of the smooth-surfaced endoplasmic reticulum as a basic prerequisite in the development of gastric secretory function.

ACKNOWLEDGMENTS

We would like to thank Dr. Edward Evans for his help in the preparation of histological specimens and for his useful discussions.

This work was supported in part by grants from the U. S. Public Health Service and the American Medical Association Education and Research Foundation.

REFERENCES AND NOTES

Arnold, M. (1966): Funktionsentwicklung der magenschleimhaut des Goldhamsters. I. Drusenmagen. Z. Zellforsch. 71: 69-93.

Bonneville, M. A. (1963): Fine structural changes in the intestinal epithelium of the bullfrog during metamorphosis. J. Cell. Biol. 18: 579-597.

Forte, J. G. (1966): Current concepts on the mechanism of hydrochloric acid secretion. J. Indian Med. Profess. 12: 5637-5647.

Forte, J. G. (1968): The effect of inhibitors of HCl secretion on the unidirectional fluxes of chloride across bullfrog gastric mucosa. Biochim. Biophys. Acta 150: 136-145.

Forte, J. G.; Limlomwongse, L.; and Forte, G. M. (1967): Ion transport in the stomach of the developing bullfrog tadpole. Federation Proc. 26: 274.

Hayward, A. F. (1967): The ultrastructure of developing gastric parietal cells in the foetal rabbit. J. Anat. 101: 69-81.

Helander, H. F. (1964): Ultrastructure of secretory cells in the pyloric gland area of the mouse gastric mucosa. Ultrastruct. Res. 10: 145.

Ito, I. (1961): The endoplasmic reticulum of gastric parietal cells. J. Biophys. Biochem. Cytol. 11: 333-348.

Jamieson, J. U.; and Palade, G. E. (1967): Intracellular transport of secretory proteins in the pancreatic exocrine cell. J. Cell. Biol. 34: 577.

James, R. G. (1934): Studies on the amphibian digestive system. I. Histological changes in the alimentary tract of anuran larvae during involution. J. Exp. Zool. 66: 73-91.

Kasbekar, D. K.; Forte, G. M.; and Forte, J. G. (1968): Phospholipid turnover and ultrastructural changes in resting and secreting bullfrog gastric mucosa. Biochim. Biophys. Acta, in press.

Kaywin, L. (1936): A cytological study of the digestive system of anuran larvae during accelerated metamorphosis. Anat. Record 64: 413-441.

Kuntz, A. (1924): Anatomical and physiological changes in the digestive system during metamorphosis in Rana pipiens and Amblystome tigrinum. J. Morphol. 38: 581-598.

Menzies, G. (1958): Observations on the developmental cytology of the fundic region of the rabbits' stomach, with particular reference to the peptic cells. Quart. J. Microscop. Sci. 99: 485-496.

Mollenhauer, H. H.; and Whaley, W. G. (1963): An observation on the functioning of the Golgi apparatus. J. Cell. Biol. 17: 222-225.

Nomura, Y. (1966): On the submicroscopic morphogenesis of parietal cells in the gastric gland of the human fetus. Z. Anat. Entwicklungsgeschichte 125: 316-356.

Sedar, A. W. (1961a): Electron microscopy of the oxyntic cell in the gastric glands of the bullfrog (Rana catesbeiana). I. The non-acid-secreting gastric mucosa. J. Biophys. Biochem. Cytol. 9: 1-18.

Sedar, A. W. (1961b): Electron microscopy of the oxyntic cell in the gastric glands of the bullfrog (Rana catesbeiana). II. The acid-secreting gastric mucosa. J. Biophys. Biochem. Cytol. 10: 47-57.

Sedar, A. W. (1965): Fine structure of the stimulated oxyntic cell. Federation Proc. 24: 1360-1367.

Sedar, A. W.; and Forte, J. G. (1962): The fine structure of the histamine stimulated oxyntic cell of bullfrog in vitro gastric mucosa; in 5th Intern. Cong. Elect. Micros. Vol. 2, YY4.

Sedar, A. W.; and Forte, J. G. (1964): Effects of calcium depletion on the junctional complex between oxyntic cells of gastric glands. J. Cell. Biol. 22: 173-188.

Sjöstrand, F. S. (1962): The fine structure of the exocrine pancreas cells; in Ciba Foundation Symposium on the Exocrine Pancreas, edited by A. V. de Reuck and M. P. Cameron, Boston, Little, Brown.

Taylor, A. C.; and Kollros, J. J. (1946): Stages in the normal development of Rana pipiens larvae. Anat. Record 94: 7-23.

Toner, P. G. (1963): The fine structure of resting and active cells in the submucosal glands of the fowl proventriculus. J. Anat. 97: 575-583.

Toner, P. G. (1965): Development of the acid secretory potential in the chick embryo proventriculus. J. Anat. 99: 389-398.

Vial, J. D.; and Orrego, H. (1960): Electron microscope observations on the fine structure of parietal cells. J. Biophys. Biochem. Cytol. 7: 367.

Wright, G. H. (1962): Net transfer of water, sodium, chloride and hydrogen ions across the gastric mucosa of the rabbit foetus. J. Physiol. 163: 281-293.

G. M. Forte is the recipient of a Bay Area Heart Research Fellowship. L. Limlomwongse is the recipient of a Rockefeller Foundation Fellowship.

L. Limlomwongse and J. G. Forte are both associated with the Department of Physiology, University of California, Berkeley, California.

Flotation Rates, Molecular Weights and Hydrated Densities of the Low-Density Lipoproteins

Frank T. Lindgren, Lin C. Jensen, Robert D. Wills and Norman K. Freeman

INTRODUCTION

Several studies have indicated that the principal low-density S_f° 0-12 lipoprotein class represents a distribution in size, hydrated density, and chemical composition (1-3). The content of protein (1) appears to be the major factor determining hydrated density of this class, which ranges from approximately 1.02-1.05 g/ml. Values given for molecular weights of this class have ranged from 1.3-3 million (4-8) and depend, in part, on the techniques employed and the portion of the lipoprotein distribution studied. Because of the very nature of this distribution of values, for specific characterization it is necessary to focus on the major component as measured in the analytic ultracentrifuge. The flotation rate of this major low-density component varies from individual to individual and has a range of about S_f° 4-8 Svedberg units. Normal females have S_f° rates approximately 1 S_f° unit faster than normal males (9, 10). There also appear to be unusual flotation rates of this component associated with specific lipid and lipoprotein abnormalities (11).

Although computer techniques have been described for analysis of lipoprotein distributions (12) and for precision moving-boundary flotation rate determinations (9), neither molecular weight nor hydrated density determinations based on standard low- and high-density lipoprotein analysis have been presented. Theoretically, sufficient information is available from these runs, made simultaneously, to make such calculations. Our present method utilizes moving-boundary flotation rates, measured in 1.061 NaCl and 1.200 g/ml NaBr and corrected to zero concentration. Hydrated densities are obtained from a plot of η F° versus ρ and minimum hydrated molecular weights calculated by using Stokes' frictional factor, assuming spherical molecules. All calculations are made by use of a third, separate, computer program.

METHODS

The normal male and female subjects of this study were clinically healthy employees of Lawrence Radiation Laboratory at Livermore and Berkeley, California. Serum was prepared from nonfasting blood specimens. A complementary series of fasting male and female clinical referrals was obtained from Kaiser Hospital, Oakland, California. Unless otherwise indicated all studies were done using serum containing 1 part/10,000 Merthiolate®.

In the normal series studied, total low-density lipoprotein fractions (S_f 0-20) were isolated by preparative ultracentrifugation and total lipids were extracted as previously described (12).

Phospholipid, cholesteryl ester, and glyceride composition were determined by infrared spectrometry (13).

Ultracentrifugal lipoprotein fractionation and analytical ultracentrifugal analysis were patterned after earlier techniques (14, 15). The computer program and details are described elsewhere (12). All analytic runs were made at 25.5-26°C in modified (16) Beckman Model E ultracentrifuges. A total of 10 schlieren photographs were taken, one during acceleration and nine during the 64-min up-to-speed (UTS) run at 52,640 rpm. Figure 1 shows selected schlieren photographs of a typical low- and high-density run. The 0-, 6-, and 30-min photographs were used for low-density analysis and the 64-min for high-density analysis. In order to unambiguously determine the base-of-cell for each run, a 0.020-inch offset centerpiece was used in the flat cells. Classical moving-boundary flotation rates of the major low-density S_f° 0-12 component measured in both 1.061 g/ml NaCl and 1.200 g/ml* NaBr were calculated from a ln x versus $\omega^2 t$ plot using a second computer program (9). Normally, in 1.200 g/ml NaBr this component was measured in the 0-, 2-, 6-, 8-, 14-, and 22-min (UTS) frames; and in 1.061 g/ml NaCl it was measured in the 8-, 14-, 22-, 30-, 48-, and 64-min (UTS) frames. Boundary positions in all cases were determined by the maximum-ordinate technique (17). A third computer program, using data from the first two programs, performed the remaining calculations. Flotation rates were corrected to zero concentration by the relationship $F = F^\circ(1 - KC)$, where $K = 0.89 \times 10^{-4}$ (mg/100 ml)$^{-1}$ and C is the concentration in the cell integrated up to the low-density S_f° 0-12 peak position, averaged over the time interval used in the moving-boundary flotation-rate measurement. This average is approximated by a Moring-Claesson type of correction (18): $C = C_0(X_{BC})^2/(X_1X_2)$, where C_0 is the initial base-of-cell concentration as determined in the first analytic ultracentrifuge computer program, X_{BC} is the base-of-cell radial distance, and X_1 and X_2 are the first and last peak positions measured. In the high-density run, C is equal to the sum of both the above low-density concentration and the total high-density concentration, similarly corrected. Background densities of the lipoprotein infranatants were measured by precision refractometry at 26.0°C. This value and its corresponding calculated viscosity were extrapolated to the lipoprotein supernatant fraction (correcting for redistribution of salt during the preparative run) and corrected to the mean temperature of the analytic run. From these data a plot of ηF° versus ρ was made and a ρ intercept calculated. S_f° rates corrected to standard conditions were made according to the relationship $S_f^\circ = F^\circ(\rho_s - \sigma)(\eta)/(\rho - \sigma)\eta_s$, where standard values at 26°C for 1.745 molal NaCl were $\rho_s = 1.0630$ g/ml and $\eta_s = 1.0260$ cp.

Assuming Stokes' frictional factor for spheres, a molecular diameter was calculated from the familiar relationship $S_f^\circ = d^2(\rho_s - \sigma)/18\,\eta = d^2(1.0630 - \sigma)/184.7$, where d has been converted to Angstrom units in the final expression. Finally, a minimum hydrated molecular weight was calculated, assuming spheres, from the molecular volume, Avogadro's number, and the hydrated density (the latter closely approximated by the density of zero migration or ρ intercept): mol wt $= \pi d^3/6(10^{-8}\ \text{cm/Å})^3 N^\circ \sigma = 0.3153\ d^3\sigma$.

*Unless otherwise indicated, all densities are given at 26°C.

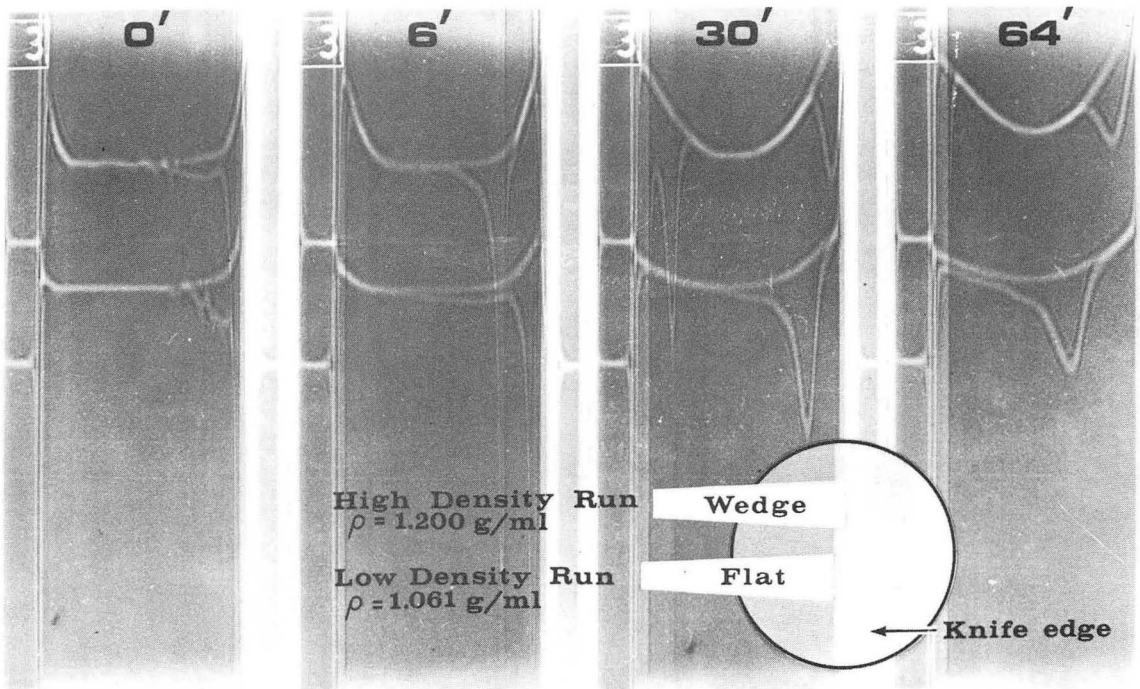

Fig. 1. Selected schlieren photographs from a typical standard low- and high-density lipoprotein analysis (Case 1710).

XBB683-1434

Narrow-band serum lipoproteins were prepared by an approach-to-equilibrium NaBr density gradient technique (2). Fractions were isolated on a density gradient (18°C, 50.3 rotor, and 50,000 rpm for 48 hours) corresponding to approximately 1.031, 1.034, and 1.037 g/ml. These isolated lipoprotein fractions were manipulated to 1.061 NaBr and 1.200 NaBr by appropriate solid NaBr addition and monitored by precision refractometry. For density calculations, the refractive increment of these lipoproteins was assumed to be 0.00154 and 0.00140 $\Delta n/g/100$ ml in the two media, respectively. Again, flotation rates were calculated and corrected to zero concentration. For this calculation the time-dependent total component concentration was used in the manner described earlier. Again, a $\eta F°$ versus ρ plot was made yielding ρ intercept values, and corrected S_f° rates were calculated. In these studies the problem of correcting for concentration dependence of the low-density component in the presence of a time-dependent high-density lipoprotein concentration (different for each individual) was avoided. Here ρ intercept values are independent of the concentration-dependence K factor, although S_f° and molecular weight values are affected. For this series, both Merthiolate® and non-Merthiolate® serum samples were studied, since we routinely use this preservative. However, no significant differences were observed between these two series.

RESULTS AND DISCUSSION

To evaluate technical reproducibility, nine aliquots of a single nonfasting sample were completely analyzed by this procedure. A measure of errors are the standard deviation of the results, which are as follows:

$$S_f^\circ\ 0\text{-}12 = 4.87 \pm 0.08 \text{ Svedbergs } (10^{-13} \text{ cm/sec/dyne/gm})$$
$$\sigma \text{ hydrated} \approx \rho \text{ intercept} = 1.0360 \pm 0.0003 \text{ g/ml } (26^\circ\text{C})$$
$$\text{molecular weight} = 1.984 \pm 0.021 \text{ (millions)}$$

Figure 2 shows schlieren photographs of both the 1.061 g/ml and 1.200 g/ml runs of one of the narrow-band lipoprotein fractions prepared from the 1.037 g/ml density gradient fraction (Merthiolate® series). All density gradient samples were analyzed at total component concentrations in the range of 261-704 mg/100 ml. Figure 3 shows the linear regression relationship between S_f° rate and ρ intercept for both the Merthiolate® and non-Merthiolate® fractions. Also plotted are the results obtained from eight standard low- and high-density analyses obtained over a period of 33 days. Nine months later nine additional analyses were performed and the mean value plotted, suggesting minimal biological variation in this person. Figure 4 shows a similar linear regression relationship of S_f° rate and molecular weight. Again, values obtained from simultaneous low- and high-density lipoprotein analyses indicate comparable results in the region of the major component compared with the same S_f° rate on the regression line obtained with isolated lipoprotein components.

The first practical application of this method involved nonfasting serum from a small, normal adult male and female population, ages 35-50 years. Figures 5 and 6 show the relationship observed between S_f° rate and the two calculated parameters, ρ intercept and molecular weight, respectively. Regression lines obtained for these plots of the population data are quite similar to those for subfractions isolated from the low-density lipoproteins of a single serum sample. For comparison with the isolated-component study, the mean male and female values are plotted on Figs. 3 and 4. At a given S_f° rate there is some variability from person to person in ρ intercept and somewhat more variability in molecular weight. Although the females have significantly higher S_f° rates than the males, there appear to be very similar regression relationships for each population. Table 1 presents the statistical results for this series of normals, including the correlations between the three variables, S_f° rate, ρ intercept, and molecular weight of the major S_f° 0-12 component. The females have faster S_f° rates (than the males), as has been observed before (9, 10); they also have approximately a 235,000 higher molecular weight and a slightly lower hydrated density.

Low-density lipoproteins of the S_f° 0-20 class were isolated from each of the above normals. Phospholipid, cholesteryl ester, and triglyceride contents of the total lipid is presented in Table 2. The females have a higher phospholipid and lower cholesteryl ester content in these molecules than the males. However, the differences are small and there is not much variability in lipid composition in these two populations. Although some relationships were observed in the females between these lipid components and the three parameters S_f° rate, σ, and molecular weight, no significant relationships were observed in the male population (see Table 3). By calculation, the mean density of the lipid moieties of each population was almost identical.

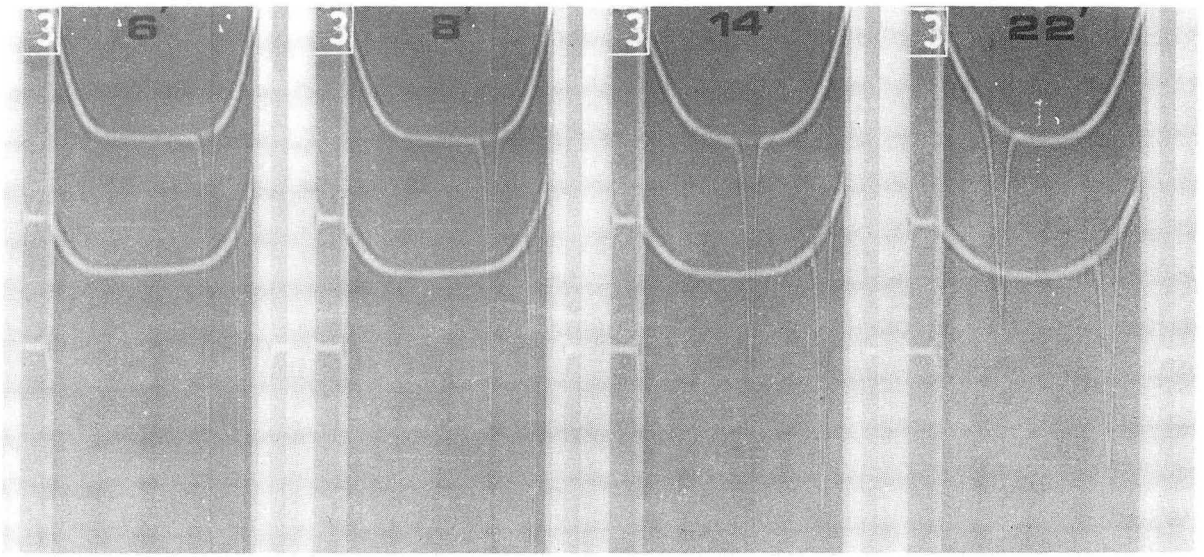

Fig. 2. Schlieren flotation photographs of isolated narrow-band S_f° 4.99 lipoproteins, Case 1710, 52,640 rpm, 26°C; upper wedge cell is ρ = 1.200 g/ml (2.755 molal NaBr, 0.194 molal NaCl), flat cell is ρ = 1.061 g/ml (0.742 molal NaBr, 0.194 molal NaCl). Lipoprotein concentration in the two media is 465 mg/100 ml.

XBB683-1435

Table 1. Results, normal, nonfasting, for subjects of ages 35 to 50 years.

	Males (16)	Females (16)	Difference
1. S_f°	6.20 ± 0.96	7.05 ± 0.83	$p < 0.01$
2. σ	1.0304 ± 0.0345	1.0284 ± 0.0311	N.S.
3. Mol wt (millions)	2.12 ± 0.20	2.36 ± 0.16	$p < 0.01$
Correlations			
1. S_f° vs σ	-0.95*	-0.95*	
2. S_f° vs mol wt	0.87*	0.76*	
3. σ vs mol wt	-0.69*	-0.52†	

*$p < 0.01$, †$p < 0.05$.

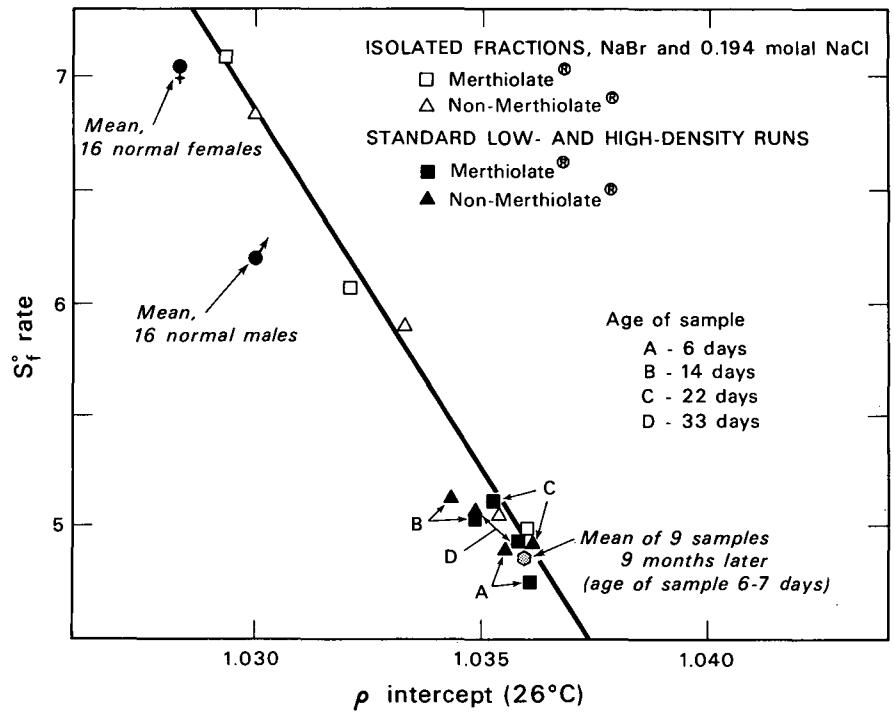

Fig. 3. Relationship between S_f° rate and ρ intercept obtained from isolated fractions and standard low- and high-density runs.

DBL683-4626

Table 2. Lipid composition and lipid σ, S_f° 0-20 lipoproteins, normal males and females.*

	Component†				
	PL	CE	TG	FC	σ(lipid)‡
Males (n = 16)	24.4 ± 2.3	55.1 ± 1.5	9.4 ± 2.4	11.0 ± 0.3	0.9803 ± 0.0016
Females (n = 16)	26.7 ± 1.8	53.4 ± 1.5	9.3 ± 2.3	10.6 ± 0.3	0.9798 ± 0.0015
Difference	$p < 0.01$	$p < 0.01$	N.S.	---	N.S.

*Mean and standard deviation, values are wt% of total lipid; free cholesterol is assumed to be 0.198 × cholesteryl ester.

†PL, CE, TG, and FC are abbreviations for phospholipid, cholesteryl ester, triglyceride, and free cholesterol, respectively.

‡Calculated by assuming additivity of densities for PL, CE, TG, and FC; individual values used are 0.97, 0.99, 0.92, and 1.067 g/ml, respectively.

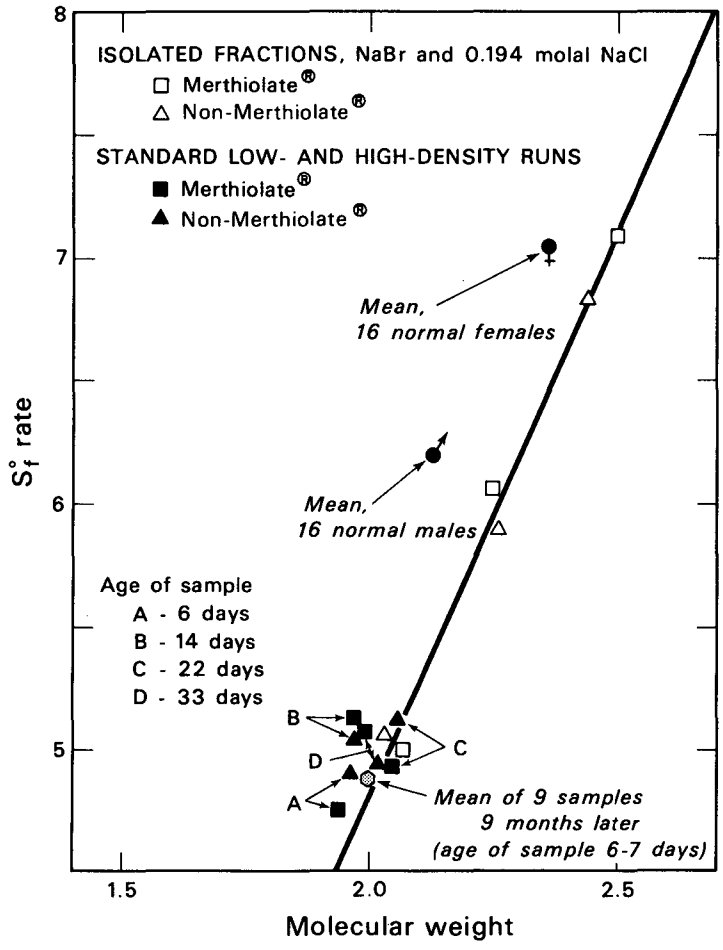

Fig. 4. Relationship between S_f° rate and molecular weight obtained from isolated fractions and standard low- and high-density runs.
DBL683-4624

Table 3. Correlations of S_f° rate, σ, and molecular weight with S_f° 0-20 lipid composition, normals.*

Parameter	PL	CE	TG	σ(lipid)
S_f° rate	0.79† (0.27)	-0.02(0.07)	-0.61‡ (-0.30)	0.47(0.26)
σ (lipoprotein)	-0.70† (-0.29)	-0.04(0.03)	0.58‡ (0.23)	-0.47(-0.17)
Mol wt	0.70† (0.23)	-0.11(0.21)	-0.46 (-0.36)	0.34(0.36)

*Normal females and males (in parentheses). †$p < 0.01$. ‡$p < 0.05$.

Also, in the females there was a moderately positive correlation of glyceride content with ρ intercept (and a low-order positive correlation in the males). These results suggest that the major factor contributing to changes in hydrated density within this class is not glyceride content but the protein content of the lipoprotein. In a much earlier density gradient study, this

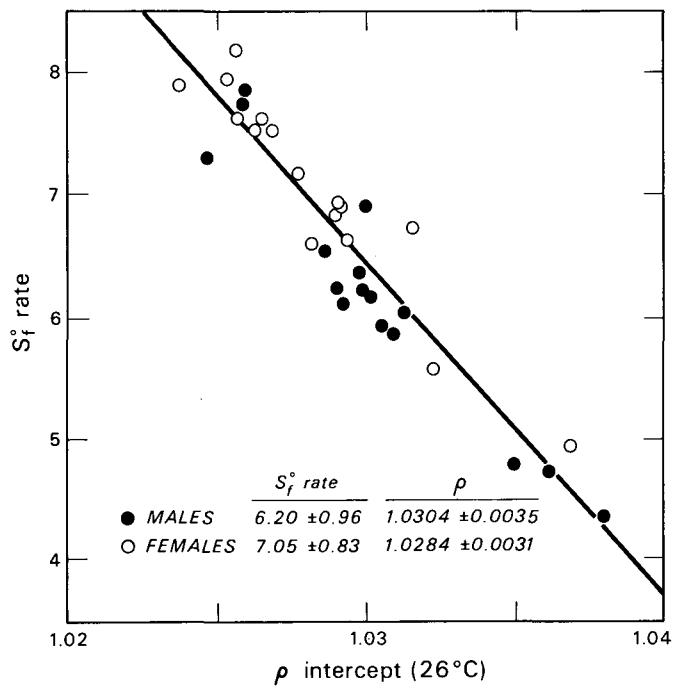

Fig. 5. Relationship between S_f° rate and ρ intercept, normal males and females. DBL684-4646

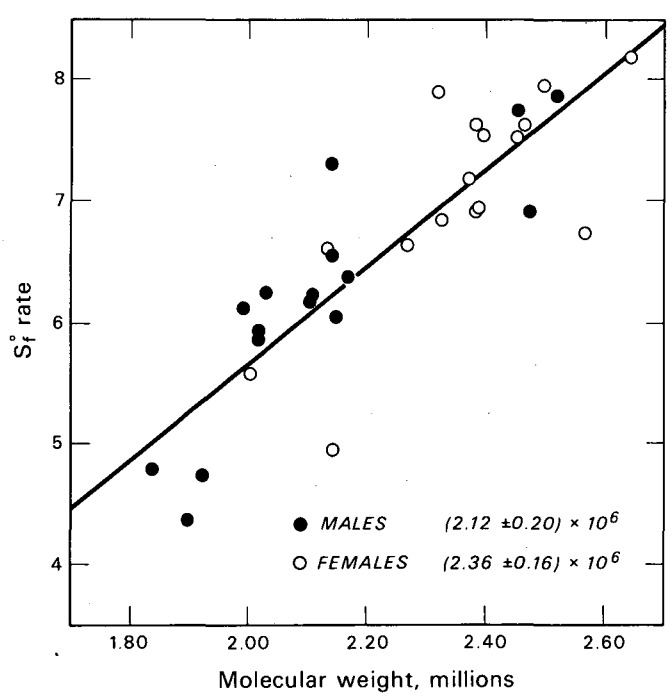

Fig. 6. Relationship between S_f° rate and molecular weight, normal males and females. DBL684-4651

relationship between protein content and lipoprotein density was observed on S_f° 3-10 subfractions from pooled human plasma (1).

This method was also applied to a series of 23 male and 23 female clinical referrals from Kaiser Hospital, Oakland, California. These patients were of a wider age range, many of them had high blood lipids, and in contrast with the normals studied, they were fasting. Table 4 presents the results for these populations, including the statistical relationships. Again, as in the normal populations, similar values, differences, and correlations were observed. The somewhat lower S_f° rates observed probably reflect a clinical population with higher levels of very-low-density lipoproteins (VLDL). Lower S_f° rates would be expected, since in both normal male and female populations there is a significant negative correlation between S_f° rate and VLDL concentration (12).

In conclusion, it is worthwhile to compare our results with a few lipoprotein values obtained earlier by others using different techniques. Bjorklund and Katz (7) compared S_f° rates, hydrated density, and molecular weights of isolated S_f° 4-8 subfractions. However, the molecular weight they obtained by light scattering was considerably higher than our present values, namely, 2.8-3.0 millions. Their data also indicated an axial ratio of 2-2.5 to 1. From somewhat similar ultracentrifugal data of the major low-density component (and assuming spheres), Oncley (6) obtained a molecular weight of 2.3 million and a hydrated density of 1.032 g/ml. The most recent hydrodynamic lipoprotein data are those of Adams (3) and Adams and Schumaker (8). They utilized equilibrium banding in the analytic ultracentrifuge, patterned after Meselson (19), to obtain lipoprotein hydrated densities. From the principal σ component resolved and a single flotation rate measurement in a very-high-density medium of NaBr (ρ = 1.481) they obtained minimum hydrated molecular weights in the range of 1.95-2.38 millions. Our data on both normals and clinical referrals are approximately of this magnitude. Recently, from equilibrium data, Scanu et al. (20) have given a range of 2.2-2.3 million molecular weight units for the major low-density component, 1.019 g/ml $< \sigma <$ 1.063 g/ml.

Although from theoretical considerations values obtained by our technique might be expected to be low by as much as 10%, the differences and the relationship observed between S_f° rate, σ, and molecular weight nonetheless are all valid. It would seem very unlikely, for example, that the shape factor for S_f° 4-8 lipoproteins would be different in males and females or would vary significantly from, say, S_f° 4 to S_f° 8. Further, in spite of difficulties in applying corrections for concentration dependence in the flotation measurements, there is no evidence that any of the observed relationships and relative differences are K-factor-dependent. Recalculating all data using K factors of 0.44 or 1.78×10^{-4} (mg/100 ml)$^{-1}$ did not significantly alter any of the relationships observed. It is estimated that a 20% error in the K factor used here, 0.89×10^{4} (mg/100 ml)$^{-1}$, would involve approximately a 5% error in molecular weight. However, in the near future, as more concentration-dependence data and shape factors become available, we may expect even more meaningful and accurate molecular weight data obtained by using this technique.

Table 4. Results, Kaiser clinical referrals, fasting. Age ranges: males, 28-66 (mean 51); females, 25-59 (mean 50).

	Males (n = 23)	Females (n = 23)	Difference
1. S_f°	5.78 ± 1.31	6.80 ± 0.91	$p < 0.01$
2. σ	1.0329 ± 0.0479	1.0291 ± 0.0339	$p < 0.01$
3. Mol wt (millions)	2.15 ± 0.27	2.31 ± 0.23	$p < 0.05$
Correlations			
1. S_f° vs σ	-0.96*	-0.89*	
2. S_f° vs mol wt	0.89*	0.74*	
3. σ vs mol wt	-0.73*	-0.35	

*Significance, $p < 0.01$.

SUMMARY

The major component of the S_f° 0-12 low-density lipoprotein class may be characterized by its S_f° rate, hydrated density, and molecular weight. All necessary information is obtained from a standard low- and high-density analytic ultracentrifugal analysis. Moving-boundary flotation rates are measured in 1.061 g/ml NaCl and 1.200 g/ml NaBr solutions and are corrected to flotation at zero concentration. Hydrated densities are calculated from ηF° versus ρ plots and minimum hydrated molecular weights calculated by using Stokes' frictional factor, assuming spherical molecules. Results indicate higher S_f° rates, higher molecular weights, and lower hydrated densities in normal females than in normal males. Molecular weights and standard deviations of the principal S_f° 0-12 component for the normal females and males were 2.36 ± 0.16 and 2.12 ± 0.20 millions, respectively.

ACKNOWLEDGMENTS

We thank Dr. Edward H. Strisower, Kaiser Hospital, Oakland, California, for kindly making available the series of clinical referral samples. This work was supported in part by Research Grant 5-RO1-HE-01882-14 from the National Hearth Institute, U. S. Public Health Service, Bethesda, Md., and by the U. S. Atomic Energy Commission.

REFERENCES

1. Oncley, J. L.; Walton, K. W.; and Cornwell, D. G.: J. Am. Chem. Soc. 30: 4666-4671 (1957).
2. Lindgren, F. T.; Nichols, A. V.; Hayes, T. L.; Freeman, N. K.; and Gofman, J. W.: Ann. N. Y. Acad. Sci. 72: 826-844 (1959).
3. Adams, G. H.: Thesis, University of Pennsylvania, 1966.
4. Oncley, J. L.; Scatchard, G.; and Brown, A.: J. Phys. Colloid Chem. 51: 184-198 (1947).
5. Lindgren, F. T.; Elliott, H. A.; and Gofman, J. W.: ibid. 55: 80-93 (1951).
6. Oncley, J. L.: Vox Sanguinis 5: 91-92 (1960).

7. Bjorklund, R.; and Katz, S.: J. Am. Chem. Soc. 78: 2122-2126 (1956).
8. Adams, G. H.; and Schumaker, V. N.: Ann. N. Y. Acad. Sci. (in press).
9. Lindgren, F. T.; Freeman, N. K.; Ewing, A. M.; and Jensen, L. C.: J. Am. Oil. Chem. Soc. 43: 281-285 (1966).
10. Mills, G. L.; Taylour, C. E.; and Wilkinson, P. A.: Clin. Chim. Acta 14: 273-275 (1966).
11. Fredrickson, D. S.; Levy, R. I.; and Lindgren, F. T.: A comparison of heritable abnormal lipoprotein patterns as defined by two different techniques, J. Clin. Invest. (to be published).
12. Ewing, A. M.; Freeman, N. K.; and Lindgren, F. T.: Advan. Lipid Res. 3: 25-61 (1965).
13. Freeman, N. K.: J. Lipid Res. 5: 236-241 (1964).
14. de Lalla, O.; and Gofman, J.: Methods Biochem. Anal. 1: 459-478 (1954).
15. del Gatto, L.; Lindgren, F. T.; and Nichols, A. V.: Anal. Chem. 31: 1397-1399 (1959).
16. Lindgren, F. T.; Freeman, N. K.; and Ewing, A. M.: in Progress in Biochemical Pharmacology, Vol. II, Basel and New York, Karger, 1967, pp. 475-499.
17. Schachman, H. K.: Ultracentrifugation in Biochemistry, New York, Academic Press, 1959, pp. 66-67.
18. Moring-Claesson, I.: Arkiv Kemi 10: 1-102 (1956).
19. Meselson, M.; Stahl, F. W.; and Vinograd, J.: Proc. Natl. Acad. Sci. U.S. 43: 581-588 (1957).
20. Scanu, A.; Pollard, H.; and Reader, W.: J. Lipid Res. 9: 342-349 (1968).

Physical-Chemical Changes in Serum Lipoproteins During Incubation of Human Serum

Alexander V. Nichols, Elaine L. Coggiola, Lin C. Jensen and Elaine H. Yokoyama

INTRODUCTION

Incubation of human serum or plasma for 24 hr at 37° results in changes in both the chemical composition of serum lipids and the distribution of serum lipids among the major classes of serum lipoproteins. The change in serum lipid composition results from an enzymatic transesterification of unesterified cholesterol by fatty acids from lecithin, and leads to a net increase in serum esterified cholesterol and lysolecithin (1). The change in lipid distribution among lipoproteins results from a net transfer of some triglycerides from the very-low-density lipoproteins (VLDL, d < 1.006 g/ml) to the low-density lipoproteins (LDL, d 1.006-1.063 g/ml) and high-density lipoproteins (HDL, d 1.063-1.20 g/ml) coupled with a reciprocal transfer of some cholesterol esters from the LDL and HDL to the VLDL during incubation (2). The lysolecithin resulting from the transesterification reaction has also been observed to accumulate in the serum protein fraction (d > 1.21 g/ml) (3). Although detailed studies have been performed on various aspects of the chemical changes in serum lipoproteins during incubation of serum, little information is available on the effects of incubation on the ultracentrifugal properties of the major classes of serum lipoproteins. The study reported here was undertaken to describe the changes in ultracentrifugal patterns following incubation and to relate them to available chemical information.

MATERIALS AND METHODS

SAMPLING Blood was drawn into sterile glass containers from nonfasting healthy males, ages 26-47. The serum was removed and after addition of penicillin and streptomycin (0.12 and 0.38 mg/ml respectively) was stored under N_2 at 4° prior to use.

INCUBATION Aliquots of serum were incubated in sealed 6-ml cellulose nitrate tubes ordinarily used for preparative ultracentrifugation. Prior to use tubes were exposed to ultraviolet light and the assembled stainless steel caps were autoclaved. The incubations were performed in a constant-temperature water bath for 24 hr at 37°. Control samples were kept in identical containers at 4° for 24 hr. In some incubation experiments, the activity of serum fatty acid transferase was inhibited by the addition (0.338 mg/ml) of p-hydroxymercuribenzoate (1) (Sigma Chemical Co., St. Louis, Mo.).

ULTRACENTRIFUGAL ANALYSES Immediately following the incubation period, aliquots of incubated and nonincubated serum were subjected to preparative and analytic ultracentrifuga-

tion procedures for determination of serum concentrations of low- and high-density lipoproteins (4). In some instances, specific lipoprotein fractions were isolated by standard preparative ultracentrifugation techniques (5). All salt solutions used in the ultracentrifugal procedures were prepared with double distilled water and contained 0.10 g/l of EDTA. Computer-derived profiles of lipoprotein distributions were obtained according to programs and procedures developed by Jensen et al. (6).

LIPID AND PROTEIN ANALYSES Serum and lipoprotein lipids were extracted, chromatographed on silicic acid, and quantified by infrared spectroscopy according to methods described earlier (7). The weight percentage of protein of HDL was calculated from N, C, and H values determined by elemental NCH analysis (8). The contribution of phospholipid N to the above values was estimated from phospholipid phosphorus values determined by the method of Bartlett (9).

RESULTS AND DISCUSSION

The effect of incubation of serum on the concentration of HDL lipoproteins is shown in Table 1. The concentrations of the $F^{\circ}_{1.20}$ 0-3.5* decreased markedly while those of the $F^{\circ}_{1.20}$ 3.5-9.0 increased. However, there was no significant change in the total HDL concentration following incubation of serum.

The effect of incubation on the average ultracentrifugal lipoprotein profile of the HDL of six subjects is shown in Fig. 1. The ultracentrifugal profile of HDL from incubated serum has a faster flotation rate for the major peak than the profile of HDL from nonincubated serum. To check if the HDL shift might possibly be due to an increase in the density of serum, occurring during incubation, we measured the background salt concentrations, following preparative ultracentrifugation of the serum, by refractometry. No increase in background salt concentrations was observed. Figure 1 also shows a computer-derived plot of the difference between the average HDL profiles for the six sera before and after incubation. Decreases in the average HDL profile occur in the range of $F^{\circ}_{1.20}$ 0-3.0, and the increases occur in the $F^{\circ}_{1.20}$ 3.0-9.0. Since the flotation ranges $F^{\circ}_{1.20}$ 0-3.5 and $F^{\circ}_{1.20}$ 3.5-9.0 have been used previously to designate the established subclasses HDL_3 and HDL_2, respectively, we have used these ranges to report the concentration changes in HDL rather than the $F^{\circ}_{1.20}$ 0-3.0 and $F^{\circ}_{1.20}$ 3.0-9.0 ranges.

Following incubation, all sera showed a substantial transesterification of unesterified cholesterol. The average increase in serum cholesterol esters was 46 ± 12 mg/100 ml. Glomset has suggested that a major source of the fatty acid for the transesterification is the lecithin of the HDL (3). Statistical evaluation of our data for the six subjects also suggests a correlation ($r = 0.9$ at a significance level of 0.05) between the increase in cholesterol ester concentration in incubated serum and the concentration of the $F^{\circ}_{1.20}$ 0-3.5 (HDL_3) in nonincubated serum.

*Flotation rates described by $F^{\circ}_{1.20}$ values are rates in Svedbergs for lipoproteins in a medium of density 1.20 g/ml (NaCl-NaBr, 26°C, 52,640 rpm), and are corrected for concentration and Johnston-Ogston effects. Flotation rate intervals designated by $F^{\circ}_{1.20}$ 0-3.5 and $F^{\circ}_{1.20}$ 3.5-9.0 correspond approximately to HDL subclasses HDL_3 and HDL_2, respectively, previously described by de Lalla et al. (10).

Table 1. Effect of 24-hr incubation of serum on concentrations of high-density lipoprotein fractions $F^{\circ}_{1.20}$ 0-3.5 and $F^{\circ}_{1.20}$ 3.5-9.0 (mg/100 ml).

Subject	$F^{\circ}_{1.20}$ 0-3.5		$F^{\circ}_{1.20}$ 3.5-9.0	
	Nonincubated	Incubated	Nonincubated	Incubated
1	243 ± 21*	159 ± 8	102 ± 4	192 ± 4
2	205 ± 26	115 ± 4	21 ± 7	98 ± 7
3	306 ± 12	190 ± 7	81 ± 2	181 ± 3
4	225 ± 4	145 ± 8	42 ± 2	94 ± 4
5	226	144	86	177
6	238	156	31	132

*Where analyses were performed in duplicate, standard deviations are given.

Our statistical correlation is based on a very small sample and certainly the series should be expanded for a definitive determination of correlation.

To evaluate the possible influence of transferase activity on the observed shift in HDL ultracentrifugal profiles, sera were incubated wherein p-hydroxymercuribenzoate was added to inhibit transferase activity. Figure 2 shows the average ultracentrifugal profiles and the differential plot for the HDL distributions from the six incubated sera now containing p-hydroxymercuribenzoate. The shift observed in HDL distribution for the inhibited sera was comparable to that for the inhibitor-free sera. With p-hydroxymercuribenzoate present, a net decrease in total HDL concentration following incubation was detected. No significant esterification of cholesterol was found in these sera during incubation (average increase in cholesterol esters was 3 ± 6 mg/100 ml).

The effect of incubation of serum on the ultracentrifugal profiles of the S°_{f} 0-400 lipoproteins was also investigated. Figure 3 shows the average computer-derived plots for the S°_{f} 0-400* lipoproteins of the six subjects following incubation of their sera with and without p-hydroxymercuribenzoate. The increases in mean concentration of the S°_{f} 0-20 lipoproteins following incubation of both series could not be proved significant from the available data. The apparent increase in mean flotation rate of the major peak in the S°_{f} 0-20 range, after incubation of inhibitor-free serum, also was not statistically significant. Although the changes in flotation rates were not significant, a significant relationship was observed between the

*Flotation rates described by S°_{f} values are rates in Svedberg units for lipoproteins in a medium of density 1.063 g/ml (NaCl, 26°C, 52,640 rpm) and are rates corrected for concentration and Johnston-Ogston effects.

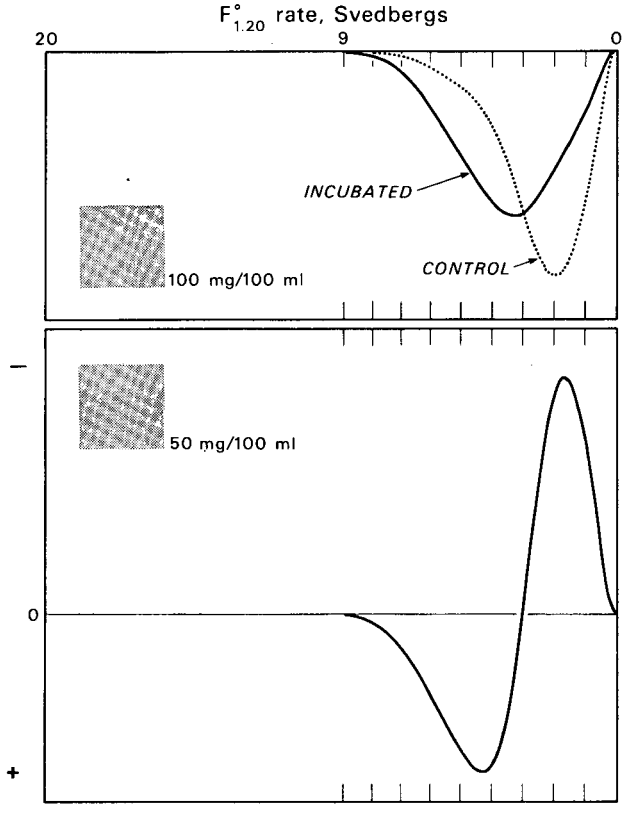

Fig. 1. Comparison of the average ultracentrifugal profiles of HDL from nonincubated and incubated sera (upper). Each of the lipoprotein profiles shown is an average profile drawn by computer from the individual profiles of six human subjects. Diagram below is a computer-derived differential plot obtained by subtracting the average lipoprotein profile of HDL, from nonincubated sera, from the average lipoprotein profile of HDL, from incubated sera.

DBL684-4692

changes in flotation rate and serum concentrations of S_f° 20-400 lipoproteins. Figure 4 shows the regression lines for the regression of the incubation-induced change in S_f° rate of the S_f° 0-20 lipoproteins, from inhibited and noninhibited sera, on the concentration of S_f° 20-400 in the sera determined prior to incubation. For sera containing elevated concentrations of S_f° 20-400 lipoproteins, the shift in S_f° rate of the S_f° 0-20 major peak is greater in noninhibited than in inhibited sera. From the above data, the changes in S_f° 0-20 flotation rates appear to have some relationship to the presence of transferase activity whereas the marked shift in HDL distribution does not. Table 2 shows the changes in lipid concentration and composition of S_f° 0-20 lipoproteins isolated from a VLDL-rich serum which was incubated with and without p-hydroxymercuribenzoate. The triglyceride concentration in this serum was 214 mg/100 ml. The very large increase in triglyceride content of the S_f° 0-20 in the presence of transferase activity suggests that transesterification is an important factor in the transfer of VLDL-triglyceride *in vitro*. In the absence of transferase activity, triglyceride transfer is also observed, but to a much lower extent than in the noninhibited serum. The apparent lack of change in the phospholipid content of the S_f° 0-20 following incubation of sera containing elevated concentrations of triglyceride has been frequently noted, and will be described in a subsequent report. No consistent changes were observed in the S_f° 20-400 distributions of the sera studied in this investigation. Since the serum S_f° 20-400 concentrations of several of our subjects were relatively low, further studies are needed to evaluate the effect of serum incubation on S_f° 20-400 lipoprotein profiles.

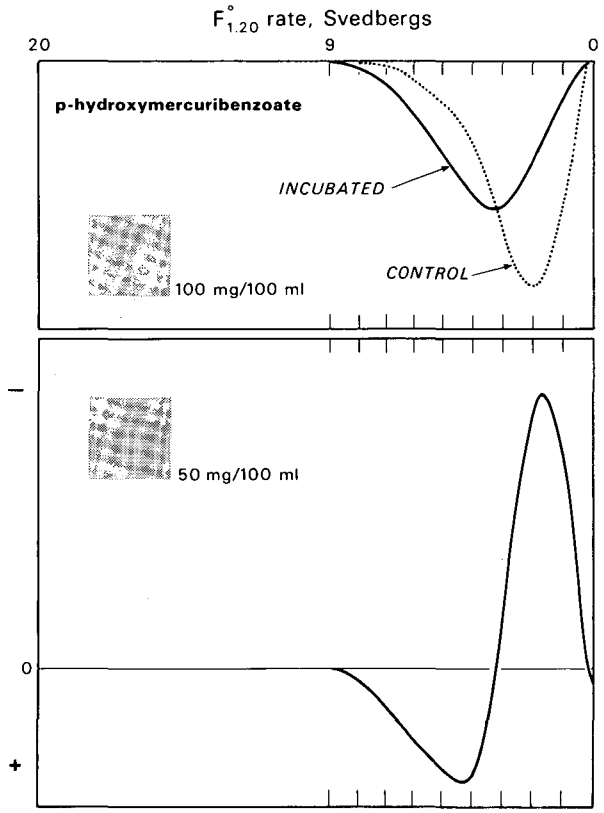

Fig. 2. Comparison of the average ultracentrifugal profiles of HDL from nonincubated and incubated sera containing p-hydroxymercuribenzoate (upper). Sera were from the same six subjects studied in Fig. 1. Diagram below is a computer-derived differential plot obtained by subtracting the average lipoprotein profile of HDL, from nonincubated sera, from the average lipoprotein profile of HDL, from incubated sera.

DBL684-4691

Table 2. Effect of 24-hr incubation on serum concentrations and composition of lipids of the S°_{f} 0-20 lipoproteins. 6-ml aliquots of serum from a nonfasting male subject were incubated for 24 hr. Controls were kept at 4°C for same period. S°_{f} 0-20 lipoproteins were isolated by preparative ultracentrifugation. Analyses were performed in duplicate and standard deviations are reported. Concentration of p-hydroxymercuribenzoate was 0.338 mg/ml. Lipid concentrations are reported as mg/100 ml in serum, and values in parentheses are percentages of total lipid.

Sample conditions	Cholesterol esters	Phospholipids	Triglycerides	Unesterified cholesterol	Unesterified fatty acids	Total lipid
Nonincubated	117 ± 2 (44)	80 ± 2 (30)	40 ± 1 (15)	30 ± 1 (11)	0.4 ± .01	267 ± 2
Incubated	136 ± 0 (45)	79 ± 1 (26)	68 ± 0 (22)	20 ± 1 (7)	0.6 ± .02	304 ± 1
			p-hydroxymercuribenzoate added			
Nonincubated	112 ± 7 (42)	80 ± 2 (30)	40 ± 0 (15)	33 ± 1 (12)	0.4 ± 0	265 ± 9
Incubated	116 ± 1 (43)	80 ± 3 (29)	45 ± 1 (17)	29 ± 1 (11)	0.5 ± .02	271 ± 6

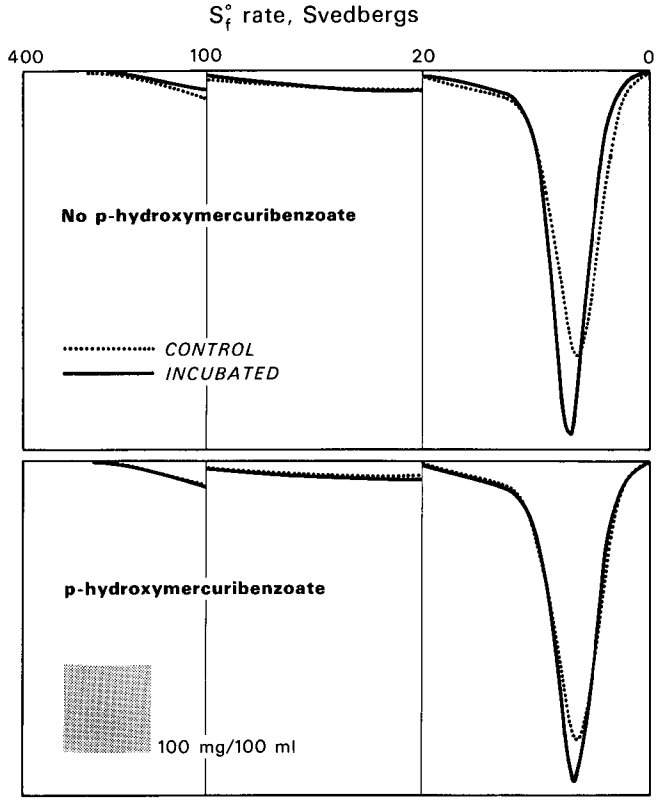

Fig. 3. Comparison of the average ultracentrifugal profiles of S_f° 0-400 lipoproteins from nonincubated and incubated sera, without (upper) and with (lower) p-hydroxymercuribenzoate. Sera were from the same six subjects in Fig. 1.
DBL684-4693

The apparent shift of the HDL profile to higher flotation rates is of interest in light of reports of changes in ultracentrifugal recovery and immunochemical properties of HDL following exposure of HDL or serum to various physical and chemical conditions. Scanu and Granda (11) subjected HDL_2 and HDL_3 to successive preparative recentrifugations and observed significant reductions in protein recovery for these fractions. They ascribed the losses to a degradation of the HDL_2 and HDL_3 with the formation of more dense lipoprotein species which appeared either in the HDL_3 or the d > 1.20 g/ml ultracentrifugal fractions. The species appearing in the d > 1.20 g/ml fraction were very low in lipid content and were designated by them as very-high-density lipoproteins (VHDL). Immunochemical studies by Scanu and Granda showed that the VHDL, derived from HDL_2 or HDL_3, and the protein moiety obtained from delipidation of HDL_2 or HDL_3 had identical immunochemical properties. He proposed the hypothesis that native HDL consists of a relatively lipid-rich lipoprotein moiety in labile association with a lipid-poor VHDL moiety. Hayashi et al. (12) were able to dissociate a lipid-poor protein from HDL by mild ether treatment; and Levy et al. (13) obtained immunochemical evidence for the release of a lipid-poor protein moiety from HDL in serum by freeze-thawing, storage, or addition of urea. Ether treatment, in addition to producing a lipid-poor protein, also shifts the distribution of the HDL in the direction of higher flotation rates. Figure 5 shows this effect of ether on the HDL distribution. This shift is highly similar to that observed following incubation of serum, and the mechanisms responsible may be comparable. Incubation of serum thus may lead to the dissociation of HDL into VHDL and relatively lipid-rich lipoprotein moieties. The latter moieties may subsequently associate to yield species with faster flotation rates.

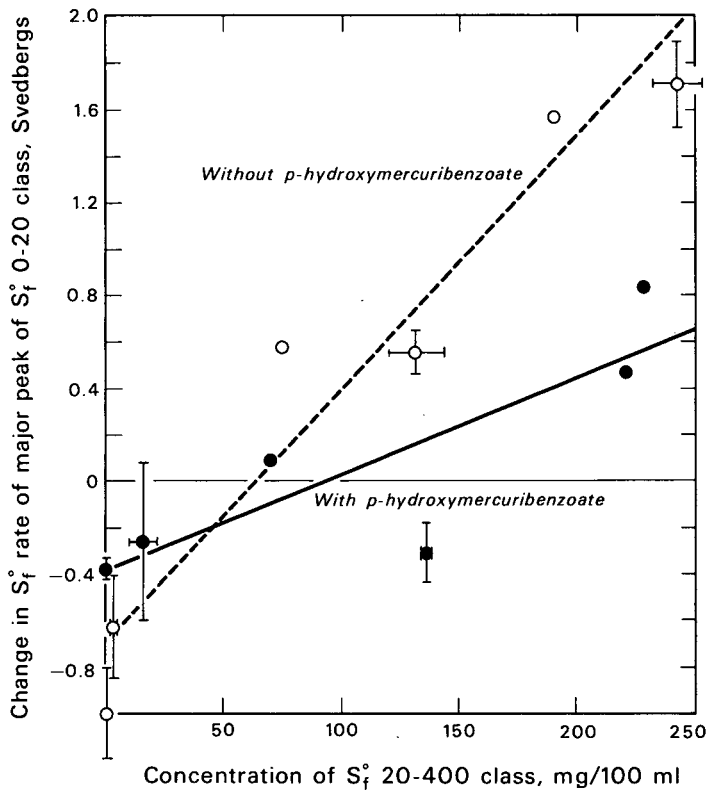

Fig. 4. Regression lines showing the regression of the change in S_f° rate of the major peak of the S_f° 0-20 class (following incubation of serum, with and without p-hydroxymercuribenzoate) on the concentration of the S_f° 20-400 class in the nonincubated serum. Where duplicate measurements were performed the mean values are plotted with lines showing ± 1 standard deviation.

DBL684-4689

Our data would suggest that during incubation the dissociating species are primarily HDL_3. Hayashi et al. also showed the formation of lipoprotein species with flotation rates in the S_f° 0-20 range after ether treatment of HDL. This observation suggests even further dissociation of protein from the HDL and subsequent association of the more lipid-rich lipoprotein residues. In our own incubation studies an increase in the concentration of the S_f° 0-20 was indicated but was not found significant. This trend towards increased values is suggestive, and may indicate the presence of all the possible processes of dissociation and association observed during exposure of HDL to ether.

To test whether protein dissociation from HDL during incubation of serum can be detected, protein analyses were performed on HDL ultracentrifugally isolated from an incubated serum sample and its control. Prior to protein analysis, the HDL fractions were subjected to dialysis against 0.202 molal NaCl to remove any low-molecular-weight nitrogenous contaminants. Triplicate analyses showed a mean percentage protein content of 52.1% (based on individual values of 52.0, 52.2, and 52.0%) and 49.1% (based on individual values of 49.2, 48.8, and 49.3%) for the HDL fractions separated from control and incubated serum aliquots, respectively. This significant reduction in protein content is in reasonable agreement with estimated reductions in protein content calculated from our ultracentrifugal analyses of the shift in HDL distribution and available information on the chemical compositions of HDL_2 and HDL_3. These data support the hypothesis that the shift in HDL distribution during incubation of serum results from an initial dissociation of lipid-poor protein from the HDL followed by an association of

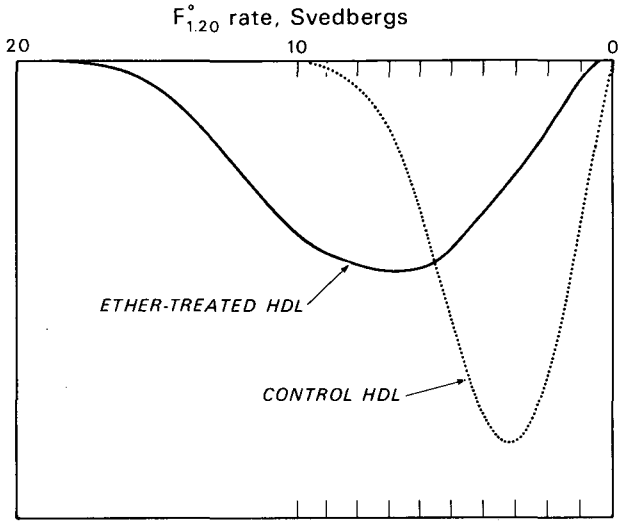

Fig. 5. Lipoprotein profiles of a total HDL fraction before and after ether treatment (12). These profiles do not represent the actual concentrations of HDL encountered in this experiment, but are presented to show the characteristics of the change in HDL distribution following ether exposure.
DBL684-4690

the relatively lipid-rich lipoprotein residues. The latter products comprise the faster floating species in the analytic ultracentrifuge. Factors influencing the above dissociations and associations during incubation of serum are under investigation. Furthermore, although comparable protein dissociation would appear to occur from the HDL in sera with and without transferase inhibitor, this does not rule out some possible relationship between such HDL protein and transferase activity in serum. In light of earlier reports (3, 14) suggesting the detection of transferase activity in ultracentrifugally isolated HDL, we are currently investigating the possible relationship of transferase activity to proteins which are in labile association with HDL.

SUMMARY

Incubation of human serum for 24 hr at 37°C resulted in a marked shift in the ultracentrifugal distribution of the high-density lipoprotein (HDL) fraction. The serum concentrations of the $F^{\circ}_{1.20}$ 0-3.5 (HDL_3) decreased whereas those of the $F^{\circ}_{1.20}$ 3.5-9.0 (HDL_2) increased. Inhibition of serum fatty acid transferase activity by p-hydroxymercuribenzoate did not inhibit the incubation-induced change in HDL distribution. A significant reduction in the protein content of the HDL, isolated from incubated serum, was detected. These data suggest that the shift in HDL distribution may result from an initial dissociation of protein from HDL_3 followed by an association of relatively lipid-rich lipoprotein residues to give HDL_2-type lipoproteins. Small order increases in S°_f rates of the major peak of the S°_f 0-20 fraction were also observed, during incubation of serum, in the presence as well as in the absence of transferase activity. The magnitude of the increase in S°_f rate was found to be directly related to the level of S°_f 20-400 lipoproteins in the serum and to be greater in the presence of transferase activity.

ACKNOWLEDGMENTS

The authors thank Dr. Frank T. Lindgren for providing the protein analyses and acknowledge the valuable technical assistance of Paul Shafer and Walter Ho. This work was supported in part by PHS Research Grant HE 10878-02 from the National Heart Institute, U. S. Public Health Service, and by the U. S. Atomic Energy Commission.

REFERENCES

1. Glomset, J. A.: Biochim. Biophys. Acta 65: 128 (1962).
2. Nichols, A. V.; and Smith, L.: J. Lipid Res. 6: 206 (1965).
3. Glomset, J. A.: Biochim. Biophys. Acta 70: 389 (1963).
4. Ewing, A. M.; Freeman, N. K.; and Lindgren, F. T.: Advan. Lipid Res. 3: 25 (1965).
5. Lindgren, F. T.; Nichols, A. V.; and Wills, R. D.: Am. J. Clin. Nutr. 9: 13 (1961).
6. Jensen, L. C.; Rich, T. H.; and Lindgren, F. T.: Donner Laboratory Semiannual Report, Biology and Medicine, Lawrence Radiation Laboratory Report UCRL-18066, Fall 1967, p. 85.
7. Freeman, N. K.; Lindgren, F. T.; and Nichols, A. V.: in R. T. Holman, W. O. Lundberg, and T. Walkin, "Progress in the Chemistry of Fats and Other Lipids," Vol. VI, New York, MacMillan (Pergamon), 1963, p. 215.
8. Hatch, F. T.; Freeman, N. K.; Jensen, L. C.; Stevens, G. R.; and Lindgren, F. T.: Lipids 2: 183 (1967).
9. Bartlett, G. R.: J. Biol. Chem. 234: 466 (1959).
10. de Lalla, O. F.; and Gofman, J. W.: in D. Glick, "Methods in Biochemical Analysis," Vol. I, New York, Wiley (Interscience), 1954, p. 459.
11. Scanu, A.; and Granda, J. L.: Biochemistry 5: 446 (1966).
12. Hayashi, S.; Lindgren, F.; and Nichols, A.: J. Am. Chem. Soc. 81: 3793 (1959).
13. Levy, R. I.; and Fredrickson, D. S.: J. Clin. Invest. 44: 426 (1965).
14. Lossow, W. J.; Shah, S. N.; and Chaikoff, I. L.: Biochim. Biophys. Acta 116: 172 (1966).

Relative Effects of Radiation on *de Novo* DNA Base Synthesis and Thymidine Incorporation into DNA

H. Saul Winchell, Serene L. Vimokesant and Rosanne B. Raley

It is generally accepted that radiation diminishes cell synthesis of DNA. Whether this effect is related to specific radiosensitive steps in the biosynthesis of DNA or whether it represents nonspecific diminution in DNA synthesis has been a subject of much speculation. The work reported here was undertaken to determine the relative radiosensitivity of the processes responsible for monocarbon fragment incorporation into DNA thymine and adenine and those responsible for incorporation of preformed thymidine into DNA.

MATERIALS AND METHODS

Within 0.5 hour after aspiration, dog bone marrow cells were given an exposure dose of X ray in the range of 50 to 3200 roentgens (R) (100 kVp, 15 mA, 0.5-cm Al filter). Within 0.5 hour following the termination of radiation the cultured cells were subjected to short-term incubation in balanced salt solution containing ^{14}C formate (Cal Biochem 16.6 mCi/mmole - final conc. 0.075 m$\underline{M}$) or serine labeled with ^{14}C in the number 3 position (Nuclear Chicago - 20.4 mCi/mmole - final conc. 0.061 m$\underline{M}$) and thymidine labeled with tritium (New England Nuclear 2.02 Ci/mole - final conc. 1.23 $\mu\underline{M}$). Following 1.5 hours of incubation at 37°C in a Dubnoff metabolic shaker, cultured tubes were immediately placed on ice and the cells washed with iced culture media. DNA was isolated by using a modification of the technique of Kay et al. (1). The washed cells were disrupted by freeze-thawing in acetone-dry ice and washed in saline, and the nucleic acids were dissolved by using sodium dodecyl sulfate (final concentration 0.4%). RNA was precipitated by adjustment of the salt concentration to 1$\underline{M}$ sodium chloride. DNA was precipitated from the supernate by the addition of alcohol, dried, and hydrolyzed in formic acid at 175°C for 35 minutes in a sealed container. The hydrolyzed DNA bases were then separated by paper chromatography [isopropyl alcohol: HCl: H_2O (2)]. Adenine and thymine were eluted from the chromatogram by use of 0.01 N HCl and the concentration of adenine and thymine within the eluate determined by UV absorption spectroscopy (263 and 264 mμ respectively), and the samples were counted for tritium and ^{14}C activity by liquid scintillation counting.

RESULTS

Figure 1 and Table 1 summarize our results of the changes in incorporation of tritiated thymidine and ^{14}C from formate into DNA bases in dog bone marrow cells following exposure to X rays. In Fig. 1 the abscissa represents radiation dose and the ordinate specific activity of label in DNA bases, expressed as % of control values. With doses of radiation below 100 R

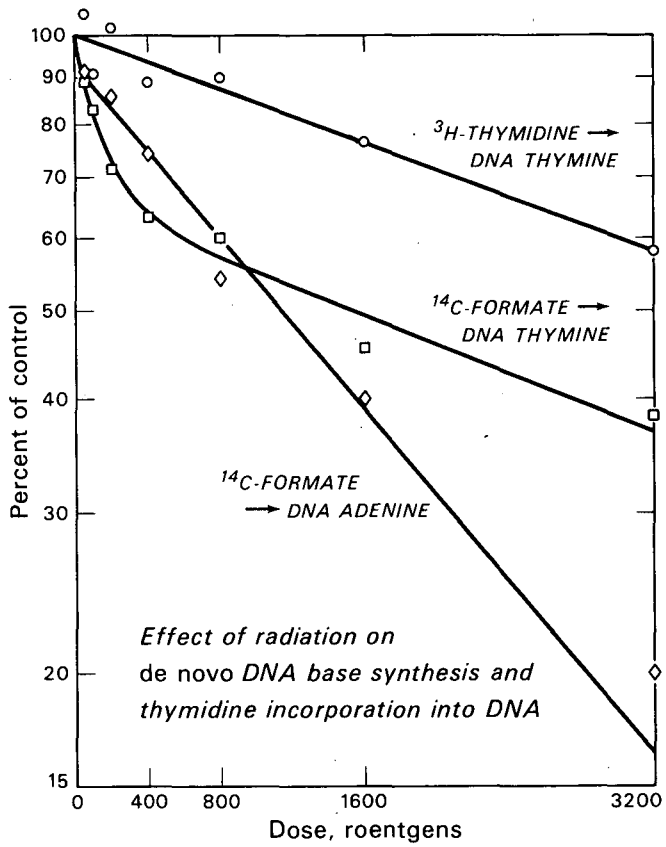

Fig. 1. The effects of radiation on de novo base synthesis and thymidine incorporation into DNA. DNA base specific activity expressed as % of control values is plotted on the ordinate, and dose in roentgens on the abscissa. The circles represent the incorporation of tritiated thymidine into DNA thymine, the squares represent the incorporation of ^{14}C from formate into DNA thymine, and the diamonds represent the incorporation of ^{14}C into DNA adenine. The data were fitted to exponential functions by using a digital computer program designed to minimize the squares of difference between the data and the fitting function. ^3H-incorporation into DNA thymine was fitted by the function $100\ e^{-1.7 \times 10^{-4} D}$. The incorporation of ^{14}C from formate into DNA thymine was fitted by the function $66\ e^{-1.8 \times 10^{-4} D} + 34\ e^{-6.9 \times 10^{-3} D}$, and the incorporation of ^{14}C from formate into adenine was fitted by the function $93\ e^{-5.4 \times 10^{-4} D} + 7\ e^{-4.9 \times 10^{-1} D}$ (where D is expressed as dose in roentgens).

DBL682-4560

there appears to be little effect on the incorporation of tritiated thymidine into DNA. Indeed, at these low doses there appears to be a modest increase in tritiated thymidine incorporation into DNA (Table 1). At higher doses of radiation, however, we note a progressive decrease in the incorporation of tritiated thymidine into DNA. In contrast to the rather minimal effect of radiation on tritiated thymidine incorporation into DNA at low radiation doses, de novo synthesis of DNA thymidine and adenine as measured by incorporation of ^{14}C from formate into these bases seems to be markedly suppressed at low radiation doses.

Table 1. Incorporation of ^{14}C from formate or serine #3-^{14}C or ^{3}H-thymidine into DNA thymine and adenine following exposure of dog bone marrow cells to X rays *in vitro*. Values presented as DNA base specific activity expressed as % of control values.

			% of control values		
Exp #	C^{14} Substrate	Dose (roentgens)	C^{14} thymine	C^{14} adenine	C^{14} thymine
2	formate	50	89.11	91.42	105.93
2	serine	50	92.06	--	103.03
2	formate	100	83.06	--	91.23
1	serine	100	74.04	72.00	96.89
2	formate	200	71.37	85.71	102.28
2	serine	200	69.05	--	104.26
2	formate	400	63.30	74.28	88.80
1	serine	400	61.07	56.00	86.20
2	formate	800	59.87	54.28	90.16
2	serine	800	59.52	--	72.89
1	serine	800	61.83	52.00	83.23
2	formate	1600	45.76	40.00	76.68
2	formate	3200	38.30	20.00	58.26

DISCUSSION

Figure 2 schematically presents the biochemical process involved in the incorporation of the tritium or ^{14}C label into DNA bases. ^{14}C from formate or from labeled serine enters the monocarbon pool attached to tetrahydrofolic acid; it is then utilized in the methylation of deoxyuridine to form thymidine and in synthesis of purines being incorporated at the #2 and #8 positions. Thus, in the present system the incorporation of ^{14}C into DNA thymine or DNA purines is a measure of *de novo* synthesis of DNA bases as well as of the incorporation of such bases into DNA. On the other hand, the incorporation of the tritium label into DNA when tritiated thymidine is used does not depend upon integrity of the monocarbon transport system. If exogenously added tritiated thymidine mixes completely with the intracellular thymidine pool, then the incorporation of tritiated thymidine into DNA is a measure of DNA synthetic rate. If, however, it does not come into mixing equilibrium with the intracellular thymidine pool, then the incorporation of tritiated thymidine into DNA may not reflect overall DNA synthesis. When one measures the incorporation of ^{32}P phosphate into DNA one presumably has an overall measure of DNA synthesis regardless of whether the bases were synthesized immediately prior to their utilization by *de novo* pathways or whether the bases arose from reutilization sites.

Previously published results (3) demonstrated significant depression of $^{32}PO_4$ incorporation into DNA following low doses of radiation (< 100 R). Such results are in contrast to the

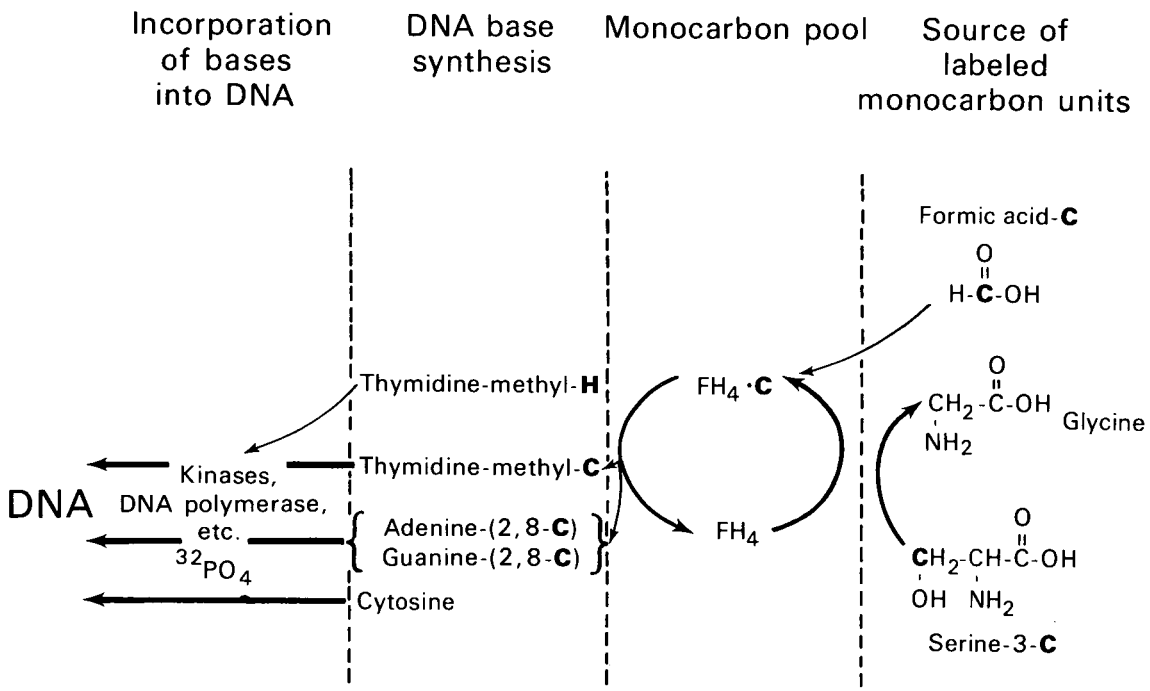

Fig. 2. Schematic representation of incorporation into DNA of ^{14}C from formic acid or serine, tritium from tritiated thymidine, and ^{32}P from $^{32}PO_4$ added to the culture medium. It is clear the $^{32}PO_4$ will be incorporated into DNA associated with all nucleic acid bases regardless of whether these bases arise from de novo synthesis or from reutilization pathways. Tritiated thymidine would be expected to mix homogeneously in the extracellular fluid with preformed thymine arising from the catabolism of DNA. It is not known whether such labeled thymidine mixes homogeneously with the entire intracellular thymidine pool. The incorporation of ^{14}C into DNA bases in the above noted scheme is a measure of both de novo synthesis of these bases and the processes required for their incorporation into DNA.
DBL682-4559

results herein presented and those discussed previously by Rasmussen and Painter (4), in which ^{3}H-thymidine incorporation into DNA was normal or increased following exposure to low doses of radiation.

If we accept the premise that the incorporation of ^{32}P phosphate into DNA is the least ambiguous method available for measuring overall DNA synthesis, then we must conclude that the incorporation of tritiated thymidine into DNA under the present circumstances is a poor measure of the overall rate of DNA synthesis. If, as claimed by Rasmussen and Painter (4), the incorporation of labeled thymidine into DNA following radiation represents in large part DNA repair processes, then such processes would have to involve replacement of DNA bases alone, leaving the pentose phosphate backbone of the nucleic acid molecule intact. If replacement of an entire segment of the DNA molecule, including the pentose phosphate backbone, occurred during DNA repair of radiation damage, one would see identical results using ^{32}P phosphate and tritiated thymidine. An alternative explanation for the above noted results is suggested by prior work from this Laboratory on the effects of methotrexate, a folic acid reductase inhibitor,

on the incorporation of ^{14}C label from #3-^{14}C-serine and the ^{3}H label from ^{3}H thymidine into DNA thymine (5). In those experiments methotrexate inhibited synthesis of ^{14}C-thymine while enhancing incorporation of the ^{3}H label into DNA thymine. These results with methotrexate are thus remarkably similar to those obtained in this experiment following exposure of bone marrow cells to X rays. Since at present there is no evidence to suggest that methotrexate causes direct damage to DNA molecules, it is difficult to ascribe the results with that agent to utilization of tritiated thymidine in DNA repair processes, as has been suggested following radiation.

Our results are consistent with the possibility that tritiated thymidine added to the cell culture media does not mix homogeneously with the intracellular thymidine pool, and its incorporation into DNA is not an accurate measure of overall DNA synthesis. However, it would be expected to mix with the thymidine released during DNA catabolism and made available for reutilization. Accordingly the incorporation of tritiated thymidine into DNA thymine may be in large part a measure of the reutilization of preformed thymine into DNA. On the other hand, the incorporation of ^{14}C-labeled monocarbon fragments from formate or serine should primarily be a measure of de novo synthesis of DNA thymine. Since in our experiments de novo synthesis of both the pyrimidine thymine and the purine adenine was markedly suppressed following radiation, we may postulate that the common metabolic pathway requiring monocarbon transport required for synthesis of both these bases may be markedly radiosensitive. Also, we may postulate that this step is much more radiosensitive than the metabolic steps required for the incorporation of DNA bases into the DNA molecule. We may further speculate that the critical radiosensitive step in this process involves radiation inactivation of tetrahydrofolic acid or the processes required for its production. Tetrahydrofolic acid is known to be quite labile, and since it is readily oxidized on exposure to room air, one would expect that it would be inactivated by the peroxides produced following radiation exposure. Indirect evidence for this postulate has been previously presented by Ngo and Winchell (6) in their studies utilizing ^{14}C-labeled histidine. We may further postulate that when de novo synthesis of DNA thymine is suppressed either by methotrexate or by radiation there is an increase in the fraction of thymine incorporated into DNA; the thymine originates from reutilization sources as opposed to de novo synthesis sources, and thus one may actually see an increase in the incorporation of tritiates thymidine into DNA, even though overall DNA synthesis may be markedly reduced.

SUMMARY

In this work the synthesis of DNA thymine and adenine utilizing monocarbon units from ^{14}C-labeled formate or #3-^{14}C-labeled serine is found to be more radiosensitive than the incorporation of tritiated thymidine into DNA thymine. Since the de novo synthesis of both the pyrimidine thymine and the purine adenine was markedly suppressed following radiation, we postulate that the common metabolic pathway requiring monocarbon transport needed in the synthesis of both these bases may be markedly radiosensitive. Furthermore we postulate that this step is more radiosensitive than metabolic steps required for the incorporation of DNA bases into the DNA molecule. Our results suggest that following radiation the incorporation of tritiated thymidine into DNA is not a good measure of overall DNA synthesis, but may rather be a measure of the incorporation of preformed thymidine, from reutilization pathways, into DNA.

REFERENCES AND NOTE

1. Kay, E. R. M.; Simmons, N. S.; and Dounce, A. L.: An improved preparation of sodium desoxyribonucleate. J. Am. Chem. Soc. 74: 1724-1726 (1952).
2. Wyatt, G. R.: The purine and pyrimidine composition of deoxypentose nucleic acids. Biochem. J. 48: 584-590 (1951).
3. Ord, M. G.; and Stocken, L. A.: The effects of X- and γ-radiation on nucleic acid metabolism in the rat *in vivo* and *in vitro*. Biochem. J. 63: 3-8 (1956).
4. Rasmussen, R. E.; and Painter, R. B.: Radiation-simulated DNA synthesis in cultured mammalian cells. J. Cell. Biol. 29: 11-19 (1966).
5. Vimokesant, S. L.; Winchell, H. S.; Pollycove, M.; and Fish, M. B.: Decreased *de novo* DNA-thymine synthesis and increased thymidine-^{3}H incorporation into DNA by human bone marrow cultured with aminopterin. Proc. Soc. Exptl. Biol. Med. 126: 621-624 (1967).
6. Ngo, T. S.; Winchell, H. S.; and Landaw, S.: Altered *in vivo* metabolism of histidine-(imidazole-2-^{14}C) in irradiated rats. Rad. Res. (in press).

Serene L. Vimokesant's present address is Faculty of Medical Science, University of Medical Sciences, Bangkok, Thailand.

Tissue Activation Studies with Alpha Particle Beams

Howard D. Maccabee, Udipi Madhvanath and Mudundi R. Raju

I. INTRODUCTION

When a fast charged particle passes through tissue, there is a certain probability that a nuclear interaction will occur with a nucleus of the medium, and that the product nucleus will be radioactive. Charged particle activation has been reviewed by Tilbury (1). Nuclear reactions initiated by positively charged particles often leave a nucleus which has too many protons for stability, and therefore tends to decay by positron emission. Examples of such reactions include (p, γ), (p, d), (p, n), (p, 2n), (d, n), (d, t), (α, n), (α, 2n), and (α, αn). Since many such activation reactions are endoergic, the incoming particle must have not only enough kinetic energy to penetrate the Coulomb barrier (2 to 5 MeV in light elements), but also enough to meet the Q-value for the reaction. For alpha particles (He^{2+} ions) of energy greater than 25 MeV, total cross sections for such reactions in carbon, nitrogen, and oxygen may be as large as 500 mb (0.5×10^{-24} cm^2). Thus when an energetic alpha particle beam passes through tissue, as in medical irradiation, it leaves behind a weak trail of radioactive nuclei, mostly short-lived positron and gamma-ray emitters.

Some of the important alpha particle activation reactions in tissue are shown in Table 1, along with the modes of decay of the radioactive product nuclei. The maximum energy of the emitted particle spectrum is given above the arrow, and the decay half-life is given below the arrow (2).

The most important characteristic of the positron decay process, for our purposes, is the fact that when the positron reaches the end of its range, it annihilates with a negative electron to form a gamma-ray pair with equal energies (0.51 MeV each) and nearly opposite momenta. Simple coincidence methods may be used to locate the point of annihilation by simultaneous detection of the gamma-ray pair. This is the basis of the activation studies to be discussed in the following sections.

II. POSITRON DECAY CURVES

Our first approach to the alpha particle activation phenomenon was to irradiate tissue and its components in the 53-MeV alpha beam of the Berkeley 88-inch sector-focused cyclotron, and measure the decay curves of the positron-emitting activated species. In a typical experiment, the sample was irradiated for 3 minutes in the cyclotron beam, with a beam current of 0.1 millimicroampere, then removed and placed in an automatic counting system. The detection system consists of a pair of NaI (Tl) scintillators aligned opposite to one another, with

Table 1. Important alpha particle activation reactions in tissue.

${}^{12}_{6}C\,(\alpha, \alpha n)$	${}^{11}_{6}C$	$\xrightarrow[20.3\ min]{\beta^+\ 0.97\ MeV}$	${}^{11}_{5}B$
${}^{12}_{6}C\,(\alpha, n)$	${}^{15}_{8}O$	$\xrightarrow[123\ sec]{\beta^+\ 1.74\ MeV}$	${}^{15}_{7}N$
${}^{12}_{6}C\,(\alpha, 2n)$	${}^{14}_{8}O$	$\xrightarrow[71\ sec]{\beta^+\ 1.81\ MeV}$	${}^{14}_{7}N$
${}^{16}_{8}O\,(\alpha, pn)$	${}^{18}_{9}F$	$\xrightarrow[110\ min]{\beta^+\ 0.635\ MeV}$	${}^{18}_{8}O$
${}^{16}_{8}O\,(\alpha, \alpha n)$	${}^{15}_{8}O$	$\xrightarrow[123\ sec]{\beta^+\ 1.74\ MeV}$	${}^{15}_{7}N$
${}^{16}_{8}O\,(\alpha, n)$	${}^{19}_{10}Ne$	$\xrightarrow[17.4\ sec]{\beta^+\ 2.22\ MeV}$	${}^{19}_{9}F$
${}^{14}_{7}N\,(\alpha, \alpha n)$	${}^{13}_{7}N$	$\xrightarrow[9.96\ min]{\beta^+\ 1.20\ MeV}$	${}^{13}_{6}C$
${}^{14}_{7}N\,(\alpha, n)$	${}^{17}_{9}F$	$\xrightarrow[66\ sec]{\beta^+\ 1.74\ MeV}$	${}^{17}_{8}O$

associated electronics. When both scintillators simultaneously detect a 0.511-MeV gamma-ray pair from positron annihilation, the resulting coincidence pulse is fed to a scaler and a pulse-height analyzer in the time-dwell mode, so that the time-dependent positron decay rate may be automatically recorded.

The simplest tissue component examined in this manner was carbon, in the form of a graphite slug; the results of this experiment are shown in Fig. 1. The decay curve has two main components. After about 20 minutes, the predominant decay mode has a half-life of 20.3 minutes, corresponding well to the isotope ${}^{11}C$, which has a known half-life of 20.3 minutes, and indicating the reaction ${}^{12}_{6}C\,(\alpha, \alpha n)\ {}^{11}_{6}C \xrightarrow{\beta^+} {}^{11}_{5}B$. The earlier decay rate, after subtraction of the extrapolated 20.3-minute activity, yields a half-life of 2 minutes. This corresponds to the isotope ${}^{15}_{8}O$, whose known half-life is 123 seconds, and indicates the reaction ${}^{12}_{6}C\,(\alpha, n)\ {}^{15}_{8}O \xrightarrow{\beta^+} {}^{15}_{7}N$.

The results of the irradiation of soft tissue (beef muscle) are shown in Fig. 2. Note that after the ${}^{11}C$ activity dies away, the primary activity is that of ${}^{18}F$, corresponding to the reaction ${}^{16}_{8}O\,(\alpha, pn)\ {}^{18}_{9}F \xrightarrow{\beta^+} {}^{18}_{8}O$. The measured half-life of 115 minutes is in fairly good agreement with the known figure of 110 minutes. This observed activity is the main result of the fact that tissue contains oxygen and other elements, in addition to carbon. Other activities were not observed because of their shorter half-lives (they decayed away before they were

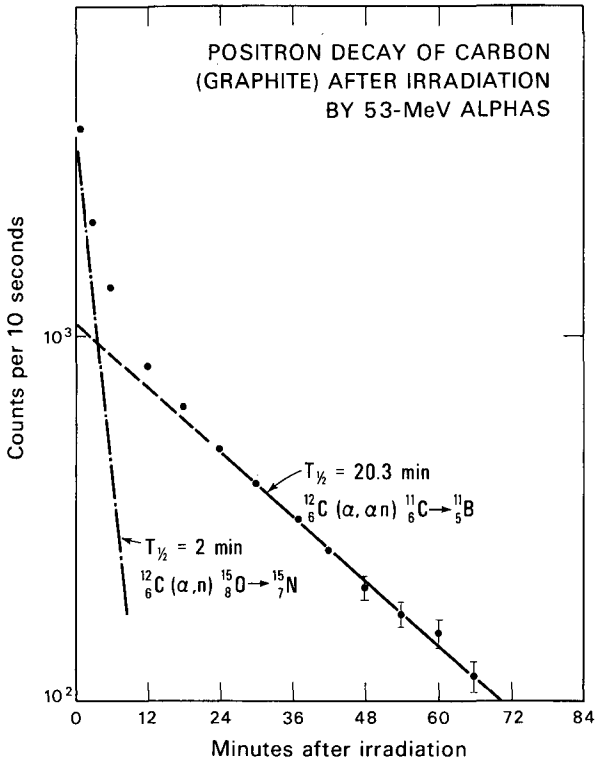

Fig. 1. Positron decay spectrum of carbon after irradiation by 53-MeV alpha particles.

DBL6711-1869

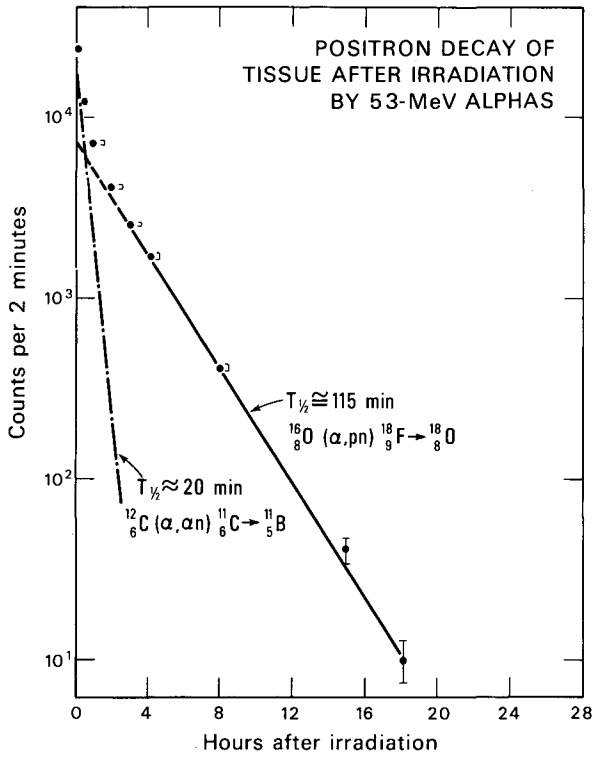

Fig. 2. Positron decay spectrum of soft tissue after irradiation by 53-MeV alpha particles.

DBL6711-1867

placed in the detector), smaller reaction cross sections, and lower abundance of the target isotope in tissue.

We have noted that the 20.3-minute activity of ^{11}C is predominant at times from 10 minutes to 1 hour after irradiation. For reasons which become evident in the next section, this time period is of primary importance, and therefore the reaction $^{12}C(\alpha, \alpha n)^{11}C$ merits closer examination. The cross section for this reaction has been measured by Lindner and Osborne (3) and Crandall et al. (4).

The energy dependence of the cross section is plotted in Fig. 3. The cross section rises steeply from the threshold at 22 MeV, and is relatively constant at around 50 mb over a wide energy range up to 380 MeV. This behavior is typical of many charged-particle activation reactions, that is, rising quickly from a threshold to a broad plateau and then gradually falling off due to competition from other reactions. Thus the activation behavior of a charged heavy particle beam in matter is likely to be a relatively uniform distribution along the track, which drops abruptly to nothing when the residual range of the particles decreases to that corresponding to the threshold energy of the reaction. In the case of fast alpha particles in tissue, all $^{12}C(\alpha, \alpha n)^{11}C$ reactions cease at 0.5 mm (0.02 in.) from the end of the track. The sharpness of this effect is tempered, however, by the initial energy spread of the beam as well as by energy straggling in the absorbing material.

III. PHANTOM STUDIES

C. A. Tobias has suggested that it might be possible to visualize and locate the Bragg ionization peak of a positively charged particle beam by observing the variation in positron activation at the end of the beam track. With this idea in mind, we irradiated several plastic phantoms with 910-MeV alpha particles from the 184-inch Berkeley synchrocyclotron, and then observed the activation pattern in the positron scintillation camera, as developed by H. O. Anger (5). The positron camera uses an image detector and a focal detector aligned on opposite sides of the subject, along with coincidence circuitry and electronic coordinate computation techniques, to produce an image of the positron annihilations within a subject. The image is in the form of dots on a cathode-ray tube, and may be photographed to yield a picture of the activation pattern.

Figure 4 is a simplified block diagram illustrating the principle of the unfocused positron camera. Figure 5 is a photograph of the positron camera in use, with the patient in position under the image detector, and an operator standing at the instrumentation console. Figure 6 is a complete block diagram of the positron camera as used in the experiments described below.

Figure 7 shows a schemiatic diagram of an experiment in which fast He^{2+} ions were stopped in a lucite phantom, and a picture of the resulting activation pattern. The 910-MeV beam was collimated through a 1/2-inch round aperture and then passed through a 1.34-inch-thick copper absorber, reducing the residual beam energy to approximately 510 MeV, and then absorbed in the plastic block. After 20,000 rads (air dose at entry) were delivered, the block was removed from the cyclotron area and transported to the positron camera. Because of

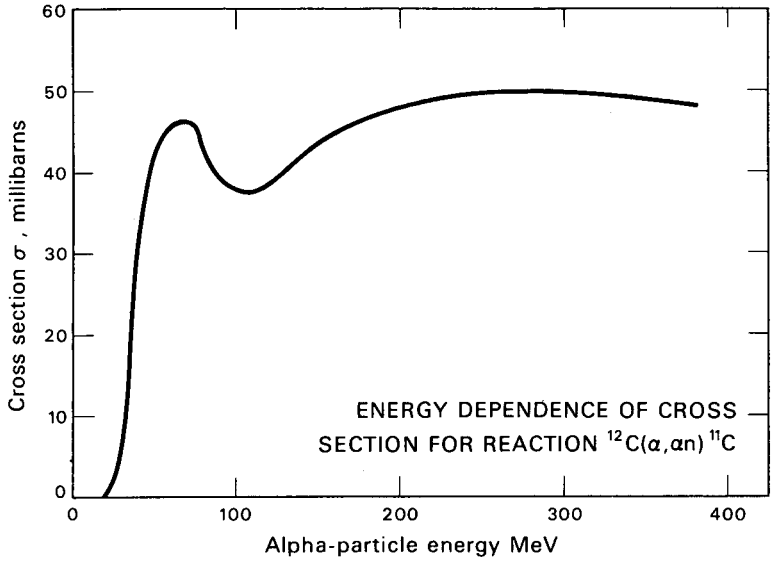

Fig. 3. Energy-dependent cross section for the reaction $^{12}C(\alpha, \alpha n)^{11}C$.
DBL6711-1868

time lost in transportation, the picture shown (1 minute exposure) was taken 20 minutes after the end of irradiation; thus, the predominant positron activity is due to the $^{12}C(\alpha, \alpha n)^{11}C \xrightarrow[20.3\ min]{\beta^+} {}^{11}B$ reaction. The initial coincidence count rate was 10,500 per minute, and the estimated activity of the block after 30 minutes was 20 μCi.

By taking scintiphotos of reference sources separated by a known distance, calibration of the length in the positron camera pictures is possible. Using this calibration, the length of the activation track due to 510 MeV alphas in lucite was measured to be 3.98 ± 0.08 inches. This compares well with the calculated length, 3.98 inches (4.00 in. range minus 0.02 in.). The transverse "fuzzing out" of the beam track is due to multiple scattering and the longitudinal variation is due to range straggling of the beam; even if these effects were not present, the picture would be blurred by the inherent resolution of the positron camera itself, which we discuss in a following section. The background dots in the portion of the lucite block not associated with the beam track are believed to be due to $^{12}C(n, 2n)^{11}C \xrightarrow{\beta^+} {}^{11}B$ reactions caused by background neutrons emanating from (α, n) reactions.

On the basis of a further experiment in which the alpha beam was completely stopped and the positron activity due to the (putatively) neutron background was observed alone, it was found that the background activity amounted to roughly 10% of the activity due to the charged particles. If one assumes that the (n, 2n) cross section is approximately equal the $(\alpha, \alpha n)$ cross section in our situation, the conclusion is that the total neutron intensity incident on the phantom is roughly 10% of the alpha particle intensity. Most of these neutrons, however, are believed to be due to nuclear reactions in the brass collimator and copper absorber, and are not believed to be associated with the cyclotron alpha beam itself.

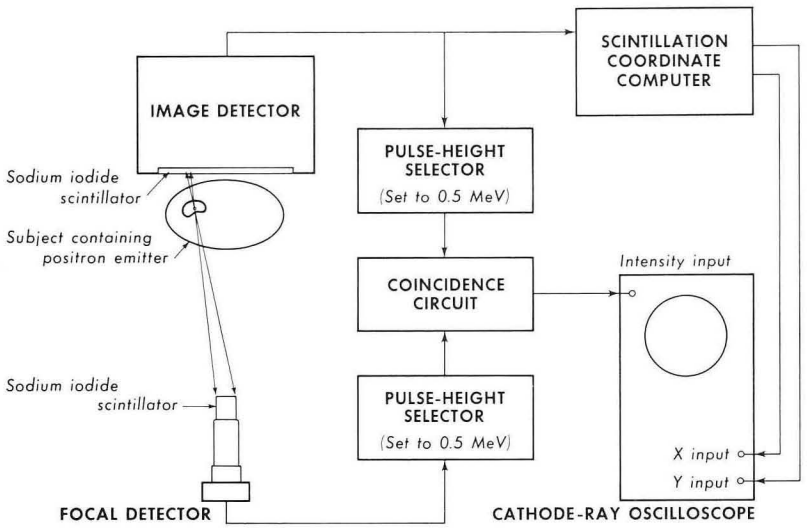

Fig. 4. Block diagram of the unfocused positron camera principle.
MUB-9034

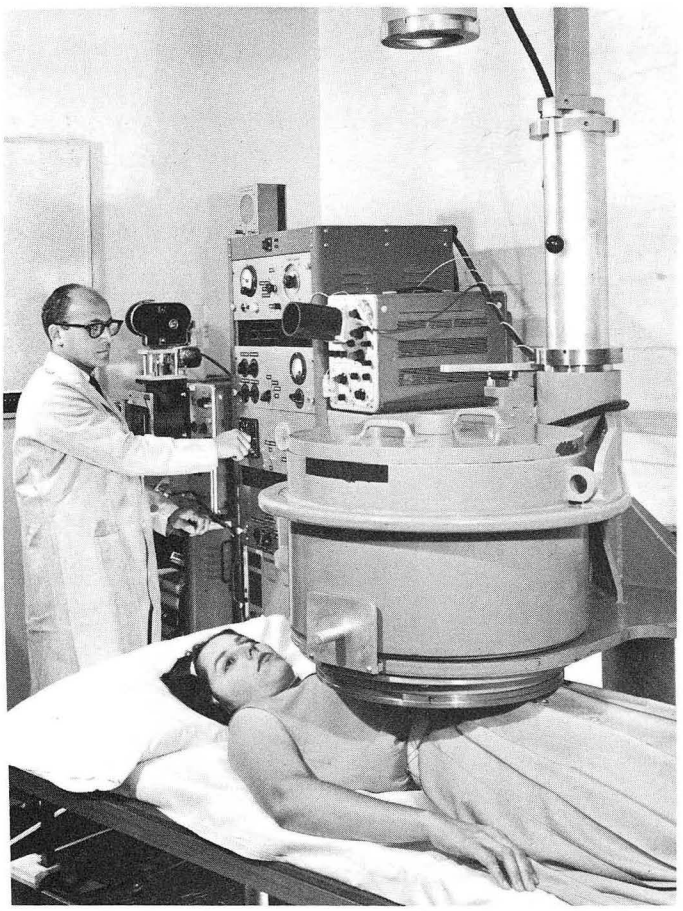

Fig. 5. Photograph of positron camera, with patient under image detector and operator at console.
JHL-5296

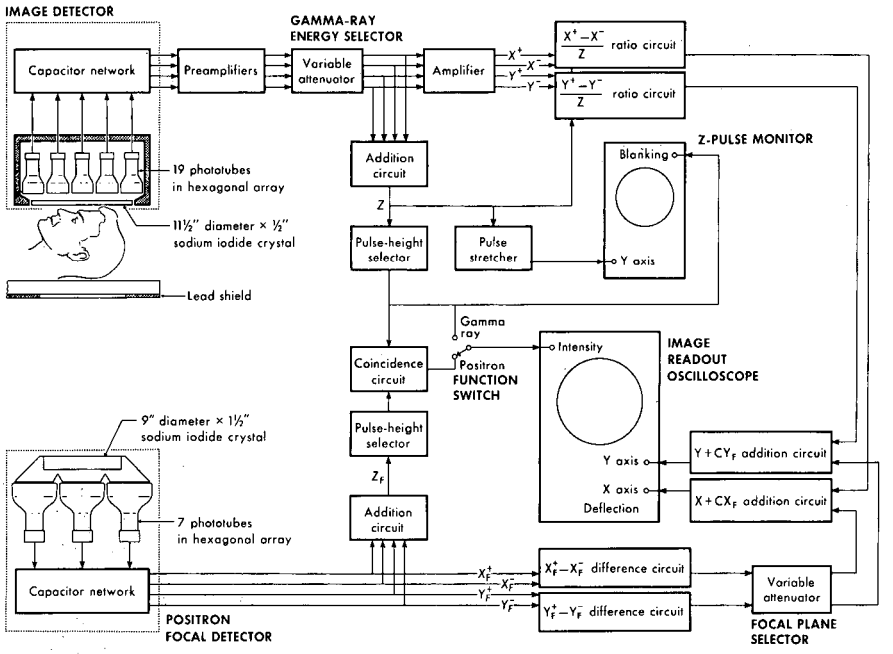

Fig. 6. Schematic diagram of positron scintillation camera, as used in this experiment series. MUB-2859A

Despite these side effects, it is clear that this technique makes it possible to visualize and locate the end of the track of a positively charged particle beam in matter. According to Raju (Ref. 6) 85 MeV is approximately the modal energy of the alpha particles at the penetration corresponding to the Bragg ionization peak of a 910-MeV alpha beam. The range-energy relation can then be used to predict that the Bragg peak is expected to occur about 4 mm "upstream" of the end of the activation track.

In the next experiment we attempted to discern the activation pattern resulting from the transmission of 910-MeV alpha beams in a situation similar to that of a patient irradiation. We used a paraffin head phantom irradiated with 2000 rads in each of three ports, separated by 1.3 inches caudally and staggered by 1 cm in the A-P direction. The collimator aperture was 1 cm by 1 cm square, and the phantom was rotated 70 deg about only one axis transverse to the beam. Figure 8 shows the irradiation scheme and the photographic results of the experiment. The nonuniformity of the activation images in intensity and lateral extent is due to the fact that the phantom was placed in the scintillation camera with the lucite holder mask and aluminum rotator adaptor still attached, and these parts added an extra activation pattern of their own (superimposed upon and collinear with that of the paraffin). It is clear, though, that the activation pattern gives good enough separation and geometric resolution to provide good information as to the course of the beam in tissue-like material. The width of the "hot spots" in the original photo was measured to be 1.1 cm, which corresponds well with the collimator opening of 1 cm.

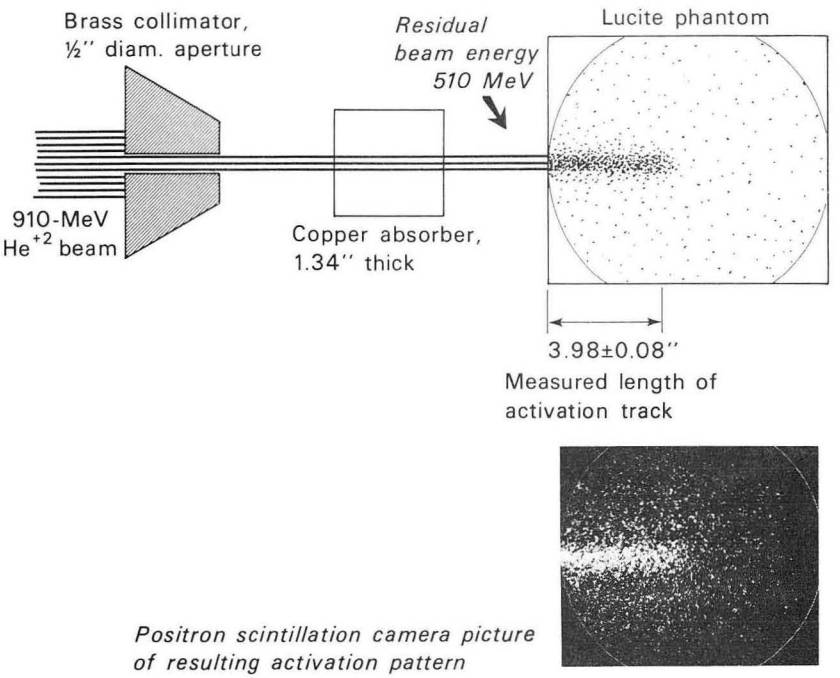

Fig. 7. Diagram of method and scintiphotograph of activation pattern resulting from 910-MeV alpha particle beam stopping in lucite phantom.
XBB6711-6558

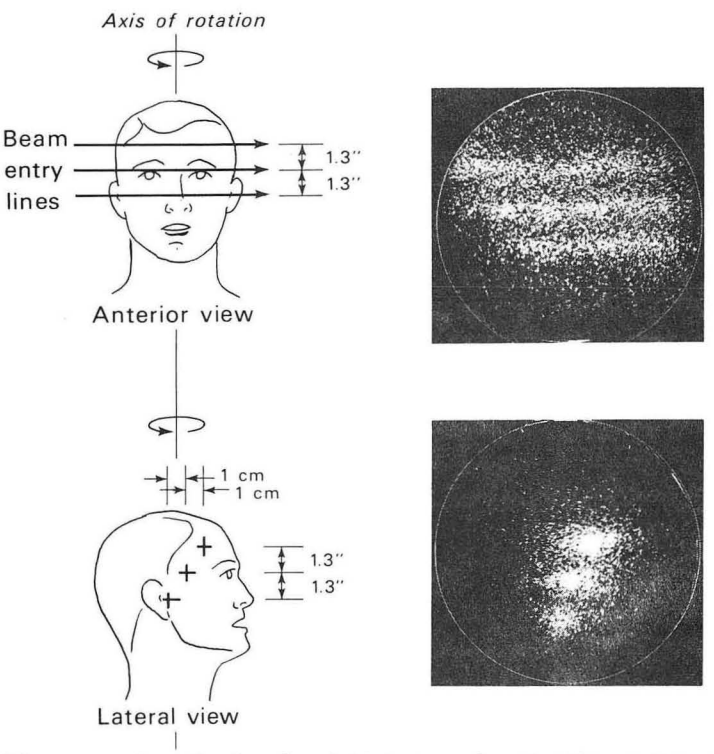

Fig. 8. Diagram of method and scintiphotos of activation pattern resulting from 910-MeV alpha beams transmitted through rotating paraffin wax head phantom.
XBB6711-6559

IV. PATIENT STUDIES

The final experiments in this series were designed to determine the activation pattern resulting from the actual irradiation regime of a patient being treated by the Donner Laboratory method of pituitary ablation by rotational superposition of transmitted 910-MeV alpha beams. Figure 9 illustrates the scheme of the rotational irradiation; the head is held in a plastic mask molded to the shape of the face and rotated by a system of automatically controlled servomechanisms, 70 deg about the x axis and 66 deg about the y axis, with the beam axis aligned roentgenographically to pass through the pituitary at all times.

In a typical single sitting of an acromegalic case (A. I.) 760 rads were administered through a 3/4-inch circular aperture. After the end of irradiation the patient was transported from the cyclotron medical cave to Donner Laboratory and positioned in the positron camera, taking 14 minutes. Figure 10 illustrates the irradiation scheme used in this case, and gives an A-P view of the positron decays recorded in 8 minutes, yielding a total of 2320 counts. The edges of the expected "butterfly" activation pattern are moderately well delineated, but the "hot spot" expected at the vertex (corresponding to the pituitary) is not clearly evident, probably due to biological "washout"; i. e., transport of ^{11}C by the circulation away from the site. It is clear, however, that this technique can be used to visualize the activation pattern (and, therefore, the dose distribution) of a positively charged particle beam in an irradiated patient. A similar picture has been obtained by Malcolm Powell (private communication, University of California Medical Center, San Francisco, 1968).

V. POSSIBLE APPLICATIONS

We envision several possible applications of the technique of tissue activation with radiation beams. Perhaps the most natural application would be the use of the positron camera as an on-line alignment tool for patient therapy with the Bragg peak of positively charged heavy-particle beams. [See, for example, Kjellberg et al. (7) or Gottschalk et al. (8).] Since alignment in the (x-y) plane transverse to the beam axis is already very good with conventional methods, the important parameter to be controlled is penetration of the beam along the beam axis (the "z" coordinate). In other words, because of variation of density and composition of tissue, bone, sinuses, etc., it is difficult to predict exactly at what depth the Bragg peak will occur. Koehler et al. (9) give a different solution to this problem. Using the activation technique, however, it might be possible to visualize the end of the beam track (and, therefore, determine the Bragg peak depth) with the administration of a few rads, and adjust the beam energy so that the peak would coincide exactly with the volume to be irradiated (e. g., tumor, pituitary, etc.). The rest of the treatment dose could then be completed. This method imposes three requirements on the activation visualization system: 1) the activation camera must be "on-line," i. e., with detectors in the treatment cave, and fast readout; 2) the spatial resolution of the activation camera must be such that it could be used to align the beam end with sufficient accuracy (e. g., ± 3 mm) in a small target; 3) the sensitivity of the activation camera must be such that it produces a usable picture with a small alignment dose (e. g., 30 rads or less).

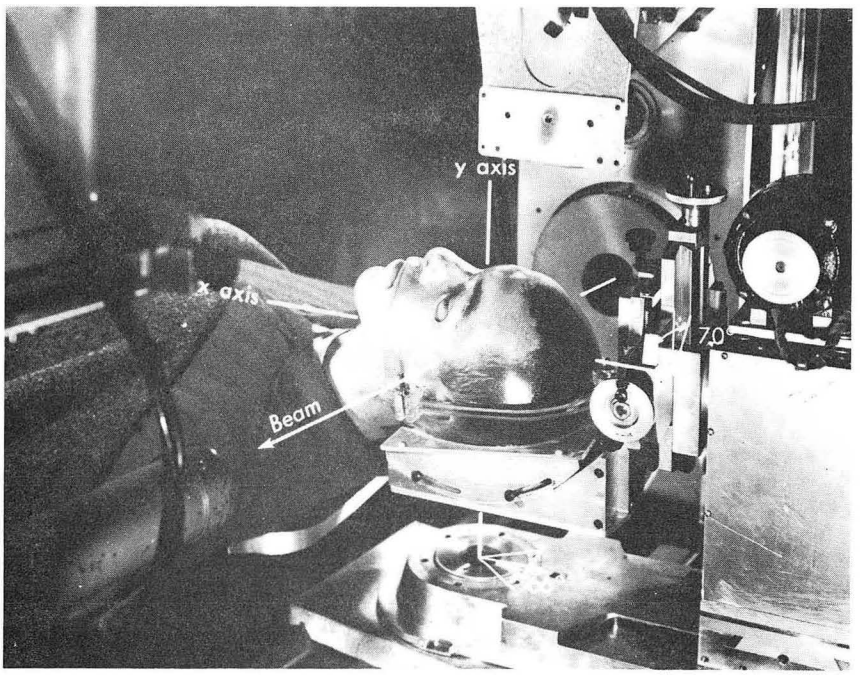

Fig. 9. Photograph of subject in head holder-rotator used in pituitary ablation technique, illustrating rotation axes and beam axis.

JHL-2897

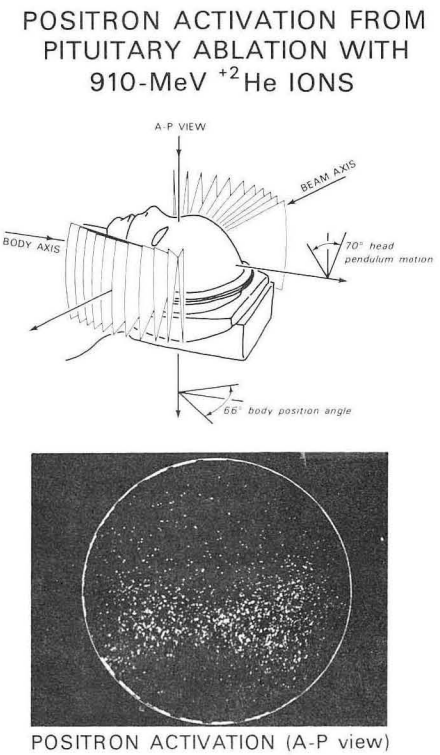

Fig. 10. Diagram of rotation technique and scintiphoto of positron activation resulting from one sitting (760 rads) of pituitary ablation therapy.

XBB6711-6560

The first requirement may be difficult: the problem envisioned is that of shielding the detectors or discriminating in some way against the background radiation present in the treatment cave. The second and third questions, resolution and sensitivity, have been examined in detail by Anger (10), and we only make a few comments on the subject. One of the inherent limitations on the positron activation camera is the fact that a 1-MeV positron has a range of about 4.3 mm in soft tissue before it is annihilated to form the gamma-ray pair which is detected. There are two factors which mitigate this effect, however. First, the positrons are emitted with a continuous "beta" energy distribution, whose maximum energy is given by the values given in Table 1; the mean energy of the distribution is about 1/3 of the maximum; and, therefore, the mean range of the positrons is less than 1/3 of the maximum. The second factor is that the positrons are emitted isotropically in the three spatial dimensions, x, y, z; if we let r equal the radial penetration of the positron, $r^2 = x^2 + y^2 + z^2$, and by isotropy, z^2 (mean) $= (1/3)\, r^2$ (mean). Since dispersion in the x and y directions is unimportant when we are considering penetration in the z direction, we are left with the conclusion that the root-mean-square penetration of the positron in the x direction before annihilation is given by z (rms) $\approx$ 0.58 r (mean). The net result is that a 1-MeV (max) positron spectrum contributes less than 1 mm to the resolution of the image in the direction of the beam axis. This contribution is thus small compared with the contribution of the NaI crystal and phototube detection array (about 5 mm), but there are several possibilities of improving the inherent detector resolution (11).

In light of the fact that 760 rads in a patient's head produced a picture with 2320 dots in 8 minutes exposure after about 18 minutes delay from beam shut-off, one might surmise that it would be impossible to get a useful picture with only 30 rads. This is not so, however; if the positron camera were "on-line" in the irradiation cave, and could be turned on immediately after beam shut-off, the much higher activity due to ^{15}O ($T_{1/2}$ = 123 sec) could be detected, and a much smaller dose would produce a useful picture. One can calculate, for example, that 30 rads of stopping alpha particles would leave an initial positron activity of about 0.15 μCi. Since the existing positron camera sensitivity is adequate to produce 2000 picture dots per minute from 1 μCi (Ref. 10), 30 rads could produce 300 dots per minute initially, and estimating that 600 dots can make a useful picture for z-direction alignment purposes, this could be accomplished with a 2-minute exposure. Thus, an "on-line" positron camera with slight improvement in sensitivity and a factor of 2 improvement in resolution could be a useful alignment and diagnostic tool for charged-particle radiation therapy.

OTHER APPLICATIONS A natural extension of the idea of visualizing the activation due to heavy charged particle beams is the possibility of visualizing other beams. Recently there has been much discussion of using other heavy-particle beams for therapy, including pi mesons, neutrons, and very heavy ions, for reasons of higher LET, lower OER, and better depth-dose distribution. It is likely that the (n, 2n) reactions occurring from neutron beams will leave a certain amount of positron activity in tissue. Unquestionably, heavy-ion beams will leave activity very similar to that of the alpha particle beams discussed above.

It might even be possible to visualize the activity from existing therapeutic electron accelerators, such as betatrons and linacs, with beam energies greater than 20 MeV. The gamma-ray bremsstrahlung can cause activation in tissue; for example, the cross section for the $^{12}C(\gamma, n)^{11}C$ reaction in carbon is 10 mb at 20 MeV (Ref. 12).

There have been several other interesting suggestions for the use of tissue activation techniques (13, 14). If a microbeam of particles were incident on a part of an organism or a cell organelle (e.g., a chloroplast), activation analysis techniques might be used to determine the location and amount of trace metals, etc. In vivo activation analysis with charged particles might prove useful for quantitative determination of tissue constituents. Also, tracer studies with short-lived radionuclides might be expedited by generating the radionuclides within an organ of the body, using a particle beam, or even by implanting radioactive ions in the body.

VI. SUMMARY

We have studied the positron-emitting activation of tissue by alpha particle beams, by using the annihilation gamma-ray coincidence detection technique, and the Anger positron camera. We have measured the decay spectrum in tissue following irradiation by 53-MeV alphas from the 88-inch cyclotron, and visualized the activation pattern resulting from a 910-MeV alpha particle beam stopping in a tissue-like plastic phantom, at the 184-inch synchrocyclotron. Also studied were the activation patterns resulting from transmission of 910-MeV alpha beams through a wax head phantom, and the activation pattern in patients' heads resulting from one sitting of the therapeutic pituitary ablation technique.

With slight improvements in resolution and sensitivity, an "on-line" positron camera technique could be useful for alignment of the end of the beam track in Bragg-peak therapy with heavy charged particles. There are other novel applications which might be possible, using tissue activation techniques.

ACKNOWLEDGMENTS

We wish to thank Edward J. Lampo and Frank T. Upham for help with detection and electronics, Hal O. Anger for the use of the positron camera and Figs. 4-6, and Cornelius A. Tobias for his encouragement and the suggestion of using the positron activation detection technique for locating the Bragg peak of heavy charged particles. Dr. Maccabee wishes to thank the U. S. Atomic Energy Commission for postdoctoral fellowship support.

REFERENCES AND NOTES

1. Tilbury, R. S.: Activation analysis with charged particles, Nat. Acad. Sci. - Nat. Res. Council Report NAS-NS-3110 (1966).
2. Data from Lederer, C. M.; Hollander, J. M.; and Perlman, I.: Table of Isotopes, New York, Wiley, 1967.
3. Lindner, M.; and Osborne, R. N.: Phys. Rev. 91: 1501 (1953).
4. Crandall, W. E.; Millburn, G. P.; Pyle, R. V.; and Birnbaum, W.: Phys. Rev. 101: 329 (1956).

5. Anger, H. O.; and Rosenthal, D. J.: in Medical Radioisotope Scanning, Vienna, IAEA, 1959, p. 59. Also: Anger, H. O.: Nucleonics 21 (10): 56 (1963).
6. Raju, M. R.: Radiation Res. Suppl. 7: 43 (1967).
7. Kjellberg, R. N.; Koehler, A. M.; Preston, W. M.; and Sweet, W. H.: in Response of the Nervous System to Ionizing Radiation, edited by T. J. Haley and R. S. Snider, Boston, Little, Brown, 1964, p. 36.
8. Gottschalk, A.; Lyman, J. T.; and McDonald, L. W.: Lawrence Radiation Laboratory Report UCRL-11184 (1963), p. 121.
9. Koehler, A. M.; Dickinson, J. G.; and Preston, W. M.: Radiation Res. 26: 334 (1965).
10. Anger, H. O.: IEEE Trans. Nucl. Sci. NS-13 (3): 380 (1966).
11. Anger, H. O.: ISA Trans. 5: 311 (1966).
12. Tilbury, R. S.; and Wahl, W. H.: Nucleonics 23 (9): 70 (1965).
13. See Biomedical Studies with Heavy Ion Beams, Lawrence Radiation Laboratory Report UCRL-17357 (1967); especially articles by Tobias, C. A., et al., p. 108; Lemmon, R. M., p. 101; Siri, W. E., et al., p. 273; Van Dyke, D. C., p. 278; Sargent, T. W., p. 281.
14. Sargent, T. W.: Whole Body Counting, Vienna, IAEA, 1962, p. 447.

Howard D. Maccabee is now at M. R. C. Radiobiological Research Unit, Harwell, Didcot, Berkshire, England.

Mudundi R. Raju is Associate Professor at the Southwest Center for Advanced Studies, Dallas, Texas.

APPENDIX: An Incomplete Bibliography on Tissue Activation and Related Areas

I. Activation Analysis (generally with neutrons)

A. Discovery

1. Hevesy, G.; and Levi, H.: Action of neutrons on rare earth elements. Kgl. Danske Videnskab. Selskab, Mat.-Fys. Medd. 14: 5 (1936).
2. Seaborg, G. T.; and Livingood, J. J.: Artificial radioactivity as a test for minute traces of an element. J. Am. Chem. Soc. 60: 1784 (1938).
3. Von Ardenne, M.; and Bernhard, F.: Z. Physik 122: 740 (1944).
4. Tobias, C. A.: AECD-2099B (1947)—the first use in biological studies. Also: Tobias, C. A.; and Dunn, R. W.: Analysis of microcomposition of biological tissue by means of induced radioactivity. Science 109: 109 (1949).
5. Brues, A. M.; and Robertson, O. H.: ANL-4108 (1947).

B. General References on Activation Analysis and its Applications in the Life Sciences

1. Albert, P.: L'Analyse par Radioactivation, Paris, Gauthier-Villars, 1964.
2. Bowen, H. J. M.; and Gibbons, D.: Radioactivation Analysis, (Clarendon) London, Oxford University Press, 1963.
3. Comar, D. (ed.): L'Analyse par Radioactivation et ses Applications aux Sciences Biologiques, Paris, Presses Universitaires de France, 1964.
4. Koch, R. C.: Activation Analysis Handbook, New York, Academic Press, 1960.
5. Lenihan, J. M. A.: Nuclear activation analysis; in Instrumentation in Nuclear Medicine, Vol. 1, edited by G. J. Hine, New York, Academic Press, 1967.

6. Lenihan, J. M. A.; and Thomson, S. J. (eds.): Activation Analysis—Proc. 1964 NATO Advanced Study Institute, New York, Academic Press, 1965.
7. Radiochemical Methods of Analysis, Proc. Symposium Salzburg, 1965, Vols. I & II, Vienna, IAEA, 1965.
8. Schulze, W.: Neutronenaktivierung als Analytisches Hilfsmittel, Stuttgart, Enke, 1962.
9. Söremark, R.: Micro element analysis by neutron activation; in Progress in Atomic Medicine, Vol. I, edited by J. T. Lawrence, New York, Grune & Stratton, 1965, p. 54.
10. Symposium on Nuclear Activation Techniques in the Life Sciences, Amsterdam, 1967, Vienna, IAEA, 1967.
11. Taylor, D.: Neutron Irradiation and Activation Analysis, London, G. Newnes, 1964.

C. In Vivo Activation Analysis

1. Activation analysis on man—a new tool for medical research?. Scientific Research, July 1967, p. 53.
2. Anderson, J., et al.: Neutron activation analysis in man in vivo. Lancet 2: 1201 (1964).
3. Peterson, P. F.; and Langham, W. H.: Neutron activation of sulfur in hair. Health Physics 12: 381 (1966).

II. Activation of Tissue by Charged Particles

1. Barbier, M.; Hutton, A.; and Pasinetti, A.: Radioactivity induced in tissues by 600 MeV protons, Geneva, CERN 66-34 (1966).
2. Birge, A. C.; Anger, H. O.; and Tobias, C. A.: Heavy charged-particle beams; in Radiation Dosimetry, edited by G. J. Hine and G. L. Brownell, New York, Academic Press, 1956—see section on activation dosimetry, p. 654.
3. Legeay, G., et al.: Dosimetrie des protons de haute-energie par mesure de beryllium-7 forme dans les tissues; in Personnel Dosimetry for Radiation Accidents, Vienna, IAEA, (1965).
4. Maccabee, H. D.; Madhvanath, U.; and Raju, M. R.: Tissue activation studies with alpha particle beams. Lawrence Radiation Laboratory Report UCRL-17929 (1968), to be published.
5. Morgan, I. L. (Texas Nuclear Corporation): Microbeam charged particle activation analysis. Personal communication (1967).
6. Odeblad, E.; and Tobias, C. A.: Autoradiography after activation of histological section with deuterons. Arch. Biochem. Biophys. 49: 452 (1954).
7. Odeblad, E.: Activation analysis with charged particles. Acta Radiol. 45: 396 (1956).
8. Sargent, T. W.: In vivo activation analysis with the Omnitron. Lawrence Radiations Laboratory Report UCRL-17357 (1967), p. 281.
9. Todd, P. W.: Proton activation in space vehicles. Lawrence Radiation Laboratory Report UCRL-10683 (1962), p. 1.

10. Van Dyke, D. C.: In vivo visualization of an accelerated particle beam using the positron scintillation camera. Lawrence Radiation Laboratory Report UCRL-17357 (1967), p. 278.

11. Watson, J. E.; Fremlin, J. H.; and Stubbins, M. I.: The distribution of carbon in human tooth enamel determined by charged particle activation analysis. Caries Res. 1: 318 (1967).

III. Related Topics in Nuclear Medicine

1. Anger, H. O.: Radioisotope cameras, in Instrumentation in Nuclear Medicine, edited by G. J. Hine, New York, Academic Press, 1967, p. 485.
Anger, H. O.: Survey of radioisotope cameras. ISA Transactions 5: 311 (1966).
Anger, H. O.: Sensitivity, resolution, and linearity of the scintillation camera. IEEE Trans. Nucl. Sci. NS-13 (3): 380 (1966).

2. Gottschalk, A., et al.: Use of the Bragg peak for brain tumor therapy. Lawrence Radiation Laboratory Report UCRL-11184 (1963), p. 121.

3. Sargent, T. W.: Metabolic studies with Fe-59, Ca-47, and C-11 in various diseases. Lawrence Radiation Laboratory Report UCRL-9718 (1961).

4. Siri, W. E.: Biomedical applications of short-lived radionuclides. Lawrence Radiation Laboratory Report UCRL-17357 (1967), p. 287.

5. Ter-Pogossian, M. M.; and Wagner, H. N.: A new look at the cyclotron for making short-lived isotopes. Nucleonics, October 1966.
Ter-Pogossian, M. M.: Short-lived radioisotopes and positron emitters in medicine, in Progress in Atomic Medicine, edited by J. T. Lawrence, New York, Grune and Stratton, 1965, p. 107.

6. Yano, Y.; and Anger, H. O.: Use of ultrashort-lived radioisotopes to visualize blood vessels and organs. Lawrence Radiation Laboratory Report UCRL-17180 (1967), submitted to J. Nucl. Med.

IV. Activation Analysis with Charged Particles, High Energy Particles, and Gamma Rays

1. Chevarier, N., et al.: Contribution a l'analyse par activation avec particules chargees. LYCEN-6714 (1967).

2. Ebert, H. G. (ed.): Proceedings of the 2nd Conference on Practical Aspects of Activation Analysis with Charged Particles, Liege (Belgium), 1967, Euratom EUR 3896 (1968).

3. Engelmann, C.: Emploi de particules autres que les neutrons en analyse par activation. Saclay, Rapport CEA-R2559 (1964).

4. Gorodetzky, S., et al.: Low energy He-3 activation analyses for carbon and oxygen. Nucl. Instr. Methods 42: 269 (1966).

5. Markowitz, S. S.; and Mahoney, J. D.: Activation analysis with He-3. Anal. Chem. 34: 329 (1962). See also Mahoney, J. D., Lawrence Radiation Laboratory Report UCRL-11780 (1965), and Ricci, E.; and Hahn, R. L.: Anal. Chem. 37: 743 (1965).

6. Modern Trends in Activation Analysis, International Conference at College Station, Texas, 1965; especially pp. 200-211, 331-336. See also Modern Trends in Activation Analysis, 1961.

7. Sklavenitis, L.: Dosimetry by activation of high energy protons. Nucl. Instr. Methods 59: 73 (1968); see also Sklavenitis, L.: Ph.D. thesis, CEA-R3376 (1967).
8. Tilbury, R. S.: Activation analysis with charged particles. NAS-NRC Nuclear Science Series Report NAS-NS-3110 (1966).
9. Tilbury, R. S.; and Wahl, W. H.: Activation analysis with high-energy particles. Nucleonics 23 (9): 70 (1965).

V. Cross Sections for Activation Reactions

1. Blatt, J. M.; and Weisskopf, V. F.: Theoretical Nuclear Physics, New York, Wiley, 1952.
2. Carpenter, R. D., et al.: $C^{12}(\alpha, n)O^{15}$. Phys. Rev. 125: 282 (1962).
3. Cochron, D. R. F.; and Knight, J. D.: $C^{12}(He^3, x)x$. Phys. Rev. 128: 1281 (1962).
4. Cook, B. C.: $C^{12}(\gamma, n)C^{11}$. Phys. Rev. 143: 724 (1966).
5. Crandall, W. E., et al.: $C^{12}(x, xn)C^{11}$. Phys. Rev. 101: 329 (1956).
6. Huizenga, J. R.; and Igo, G.: Theoretical reaction cross sections for alpha particles with an optical model. Nucl. Phys. 29: 462 (1962).
7. Kramer, K., et al.: $O^{16}(\gamma, x)$ and $C^{12}(\gamma, t)$. Z. Physik 207: 1 (1967).
8. Lindner, M.; and Osborne, R. N.: $C^{12}(\alpha, \alpha n)C^{11}$. Phys. Rev. 91: 1501 (1953).
9. McGowan, F. K.; Kim, H. J., et al.: Charged Particle Cross Section Data Center, Oak Ridge National Laboratory.
10. Photonuclear Data Index. NBS Report MP 277 (1966).
11. Shapiro, M. M.: Cross sections for the formation of the compound nucleus by charged particles. Phys. Rev. 90: 171 (1953).

Secondary Particle Contributions to the Bragg Peak of a High-Energy Heavy-Ion Beam

Stanley B. Curtis

In the analysis of the depth-dose pattern produced by a high-energy heavy-ion beam, it is important to estimate the contribution from secondary particles produced by primary nuclear interactions. In particular, it is of interest to determine the effect of these secondaries on the Bragg peak of the beam.

In this paper, we calculate a reasonable upper limit of this contribution by making a "pessimistic" assumption of the secondary emission frequency distribution. We choose for this example a 300-MeV/nucleon neon ion beam in water absorber.

The assumptions made in order to make the calculation are as follows:

(a) The high energy heavy secondary particle leaving the site of a nuclear interaction is assumed to be the residual piece of the incident ion and is assumed to continue in the forward direction with the same velocity as the incident ion. The reported rms angles for emerging heavy fragments in heavy galactic cosmic-ray interactions in emulsion (1) are 0.48 deg from incident particles with $6 \leq Z \leq 9$, and 1.14 deg from incident particles with $Z > 9$, so the straight-ahead approximation is certainly warranted in this case. The model assumed here is one in which part of the incident ion is stripped in the collision, with the fragment continuing on with negligible change in velocity.

(b) The fast α particles were also assumed to continue in the same direction and with the same velocity as the incident ion. The experimental rms angles of these α particles in emulsion ranged from 1.1 to 2.5 deg for the various incident charged components in the galactic cosmic rays (1).

(c) The residual "star" at the interaction site can be treated as if it were a pion star (2) depositing locally 30 MeV per interaction. This assumption is not critical because a very small fraction of the total dose is deposited in this way.

(d) The fast singly charged "shower" particles are neglected in this treatment because they cause a negligible effect in the region of the Bragg peak.

(e) The interaction cross section for the heavy ions is assumed constant as a function of energy. It was calculated for water from the curves in Waddington (3). The interaction mean free path, λ, was found to be 16.7 g/cm^2 for neon ions.

(f) The emission frequency was assumed to have the form indicated by the solid line in Fig. 1. This curve weights the heavier fragments (fluorine and oxygen) more than indicated by the cosmic ray data (1, 4) (shown by the dotted line in the figure), but this results in a

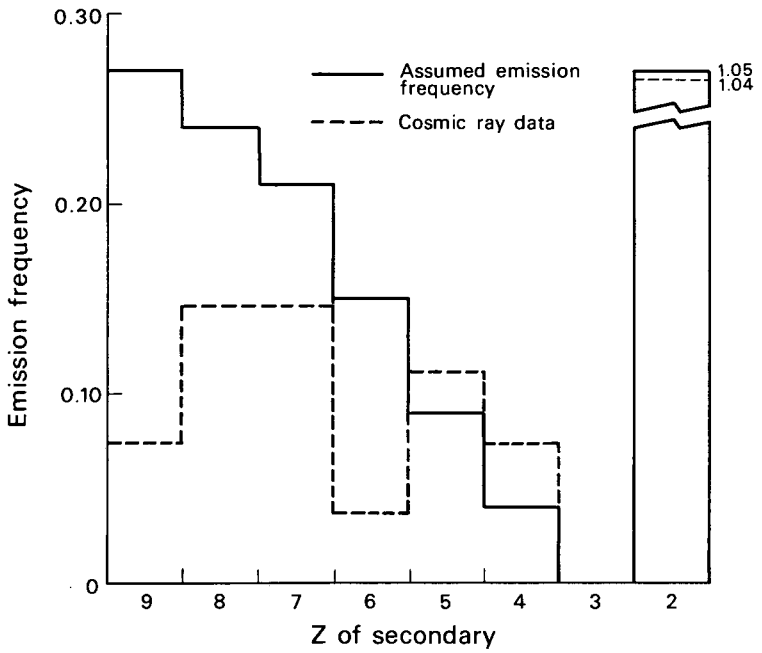

Fig. 1. Emission frequencies for secondary particles from high-energy neon ions in water. The solid line indicates a frequency highly weighted toward heavy secondaries. The dotted line gives the cosmic ray data for neon primaries from the light elements in nuclear emulsion.
DBL687-5308

"pessimistic" case for estimating the effect of secondaries on spreading the Bragg peak. Fluorine fragments deposit more dose per particle than the lighter fragments because of the Z^2 dependence of the energy loss, dE/dx. Finally, it is assumed that one heavy fragment ($Z > 2$) emerges from every interaction. From the scanty cosmic ray data (1, 4), it appeared that 67% of the neon ion interactions produced a fragment with $Z > 2$. The details of the calculation are described elsewhere (5) and are not repeated here. The expression used for the energy deposited per gram per incident ion/cm^2 at point x from secondaries of the ith type is given by

$$D_i(x) = K_i \int_0^X dn/dx' \, [dE/dx\,(x, x')_i] \, dx',$$

where K_i = the emission frequency from Fig. 1,

X = the range of the primary ion (10 g/cm^2 in this case) or x, whichever is smaller,

dn/dx' = number of interactions per unit length

$= (1/\lambda)\exp(-x'/\lambda)$, where λ is the nuclear interaction mean free path,

$dE/dx(x, x')_i$ = the ionization dE/dx at point x of a particle of type i created at x' with the same energy/nucleon as the primary at x'.

RESULTS

It is convenient to plot the secondary dose as a fraction of the primary dose at the surface. For this case, the incident primary dose is 357 MeV/g per incident ion/cm^2. The primary dose and secondary dose as a function of depth are given in Fig. 2. The primary dose is from the work of Litton (6).

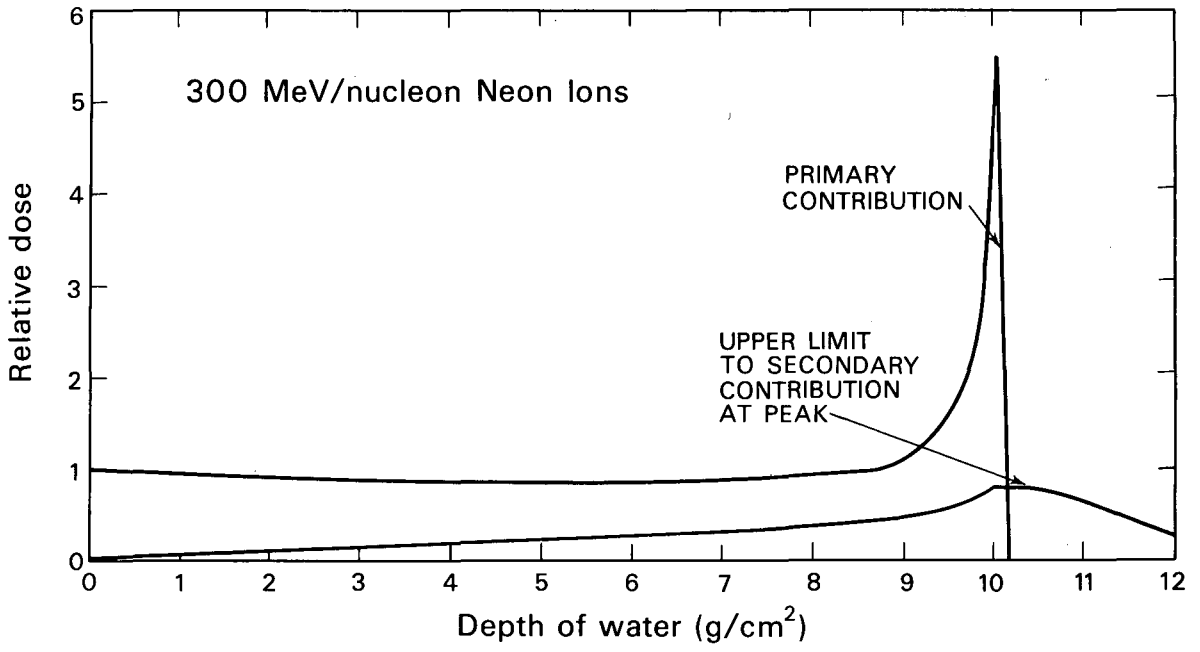

Fig. 2. Relative depth-dose curves in water for a primary neon ion beam of initial energy 300 MeV/nucleon and the estimated upper limit to the contribution from secondary particles. The emission frequency used was the solid curve in Fig. 1. DBL687-5307

To obtain an estimate of the effect of the secondary contribution on the Bragg peak, we choose a constant of 0.8, obtained from Fig. 2, as the increase from secondaries through the Bragg peak. It is easily shown that an upper limit to the fractional increase in the full width at half maximum (FWHM) due to a constant increase, Δ, through the peak region is given by

$$\text{fractional increase in FWHM} = \Delta/D_p,$$

where D_p is the original value of the dose at the peak. Thus for $\Delta = 0.8$ and $D_p = 5.5$ from Fig. 2, we find that the percentage increase in FWHM for a 300-MeV/nucleon neon ion beam in water is 15%. This is considered to be a reasonable upper limit of the effect on the FWHM from secondary particle contributions for this high-energy heavy-ion beam.

SUMMARY

An upper limit to the effect of nuclear interactions on the spreading of the Bragg peak of a 300-MeV/nucleon neon-ion beam in water has been estimated. A particular assumption is made for the emission frequency of fast secondary fragments in neon-oxygen interactions which weights the heavier fragments somewhat more than is indicated by the available cosmic ray data, so that a "pessimistic" value of the spreading is obtained. Usual assumptions, such as the straight-ahead approximation and the constancy of the interaction cross section with energy, have been made, so that a hand calculation could be carried out. The results show that an upper limit of the secondary contribution to the dose is 15% of the primary dose at the peak, and the upper limit to the percentage increase of the FWHM is also 15%. Thus, it appears that

the Bragg peak will not be spread out appreciably by the presence of secondary particles from nuclear interactions in a high-energy neon-ion beam in water.

REFERENCES

1. Fowler, P. H.; Hillier, R. R.; and Waddington, C. J.: Phil. Mag. 2: 293 (1957).
2. Fowler, P. H.: private communication, 1967.
3. Waddington, C. J.: Progr. Nucl. Phys. 8: Chap. 1, 3 (1960).
4. Rajopadhye, V. Y.; and Waddington, C. J.: Phil. Mag. 3: 19 (1958).
5. Curtis, S. B.: The Radiation Hazard to Man on Extended Missions (work done under extension of NASA Contract NASw-1362).
6. Litton, G.: Program BRAGG, A Fortran-IV Program for Calculating Bragg Curves, Flux and Current Distributions, and Energy Spectra, UCRL-17391 Rev., Feb. 1968; Penetration of High-Energy Heavy Ions, With the Inclusion of Coulomb, Nuclear, and Other Stochastic Processes (Ph. D. Thesis), UCRL-17392, Aug. 1967.

Proposed Experimental Systems for Digital Analysis and Improvement of Fourier Contrast Images in Biological Electron Microscopy

Robert M. Glaeser and Gareth Thomas

I. INTRODUCTION

The instrumental design of electron microscopes and the development of specimen preparation techniques have proceeded to the point where the analysis of molecular structure by electron microscopy might begin to compete with X-ray crystallography in terms of quantitative information and structural resolution. Recent experimental and theoretical work has suggested that the often-quoted "limitations" of electron microscopy, such as spherical, chromatic, and astigmatic aberrations in the objective lens, specimen substrate noise, and thermal damage of the specimen by electron irradiation are neither fundamental nor practical limitations. Some of these limitations can be overcome by the use of technological devices that have been developed over the past several years, and other limitations can be overcome by a more complete processing and analysis of data than has previously been common in electron microscopy. The intent of this report is to outline the theoretical basis by which it should be possible to overcome the usual limitations imposed by lens aberrations, and to discuss experimental systems that could be used for that purpose.

The theoretical considerations to be presented here follow from the assumption that the in-focus electron-optical image is the result of interference between coherently scattered plane waves. Since inelastic scattering results in electron waves that are not coherent with one another, it is necessary to remove these electrons from the image. Two methods for removing the inelastically scattered electrons from the final image are described here, and they are discussed in terms of their relative advantages and disadvantages. The practical advantages of digital analysis of image information are explored through Fourier transform theory. As a by-product, one possible method of on-line feedback-regulated focus is described. Some apparent demonstrations of Fourier contrast effects at low resolution are confirmed experimentally through the use of low-angle electron diffraction. The problem of limited resolution resulting from specimen damage in the electron beam is a serious factor with biological specimens. It is shown here that electron diffraction can be used to evaluate the preservation of labile specimens to a structural "resolution" considerably better than is possible by conventional electron microscopy.

II. THEORETICAL BASIS

A. REAL SPACE AND RECIPROCAL SPACE (FREQUENCY SPACE) The structure of an arbitrary object can be represented in two equivalent ways. The most intuitive way is by a mathematical function that describes the position in space of every atom in the object and that describes as well some property by which each atom can be identified. The electrostatic potential, due to both the nuclei and the electrons, is the atomic property most relevant to electron microscopy. A second representation of the structure can be expressed in terms of the coefficients obtained when the first representation is expanded in a series using any complete, orthogonal set of functions. The complete, orthogonal set of greatest relevance in electron microscopy is composed of the complex harmonic functions, $\left\{e^{i2\pi \vec{S}\cdot\vec{R}}\right\}$. The function V(R), which describes the electrostatic potential everywhere in the object, can be expanded in terms of coefficients $\Phi(\vec{S})$ and the orthogonal functions $e^{i2\pi \vec{S}\cdot\vec{R}}$:

$$V(\vec{R}) = \int \Phi(\vec{S})\, e^{i2\pi \vec{S}\cdot\vec{R}}\, d\tau_S .$$

The familiar operation of inversion of the Fourier transform gives the relative values of these coefficients as

$$\Phi(\vec{S}) = \int V(\vec{R})\, e^{-i2\pi \vec{S}\cdot\vec{R}}\, d\tau_R .$$

The Fourier transform $\Phi(\vec{S})$ defined in this way is usually referred to as the structure amplitude or the structure factor.

It is important to realize that the structure of the object may be specified either as the function $V(\vec{R})$ in real space or as the function $\Phi(\vec{S})$ in "reciprocal" space. The two representations are equivalent, and functions in one space can be mapped back and forth into functions in the other space through the Fourier transform. If vectors in real space are considered, in an abstract sense, to represent spatial periodicities in various directions, then vectors in reciprocal space represent spatial frequencies in the same directions, i.e., they are the reciprocals of the periodicities. If the real-space function $V(\vec{R})$ is a periodic function, then its reciprocal space transform $\Phi(\vec{S})$ has local maxima at a denumerable set of space-frequency positions, $\vec{S}_{hkl}$ (h, k, and l being the integers that index the Miller planes of the crystal). For a nonperiodic function in real space, however, the reciprocal space representation--that is, the Fourier transform--is generally a continuous function in the vector space of spatial frequencies.

B. THE FOURIER PROJECTION THEOREM A theorem of the Fourier transform that is frequently used in X-ray crystallographic studies states that the Fourier synthesis of a two-dimensional plane is reciprocal space results in a two-dimensional projection of the structure:

$$\int \Phi(S_x, S_y, 0)\, e^{i2\pi (S_x \cdot X + S_y \cdot Y)}\, dS_x\, dS_y = \int V(X, Y, Z)\, dZ \equiv V(X, Y).$$

Image formation by coherent plane waves consists of a related "conditional" projection. The useful fact remains that even for a Fourier projection the representation in one space is equivalent to the representation in the other space through the operation of Fourier transformation.

C. THE ACTUAL CASE IN ELECTRON MICROSCOPY Image formation in electron microscopy can be described through Fourier transform theory if three qualifying restrictions apply.

(1) The source of illumination should be sufficiently coherent, and the electrons should be describable as plane waves in the vicinity of the object. These conditions are easily satisfied by the appropriate use of apertures and lens excitations in the condenser system.

(2) Only elastically scattered electrons should be admitted into the image, as the inelastically scattered electrons produce image contrast of a character different from that desired here. This condition can be satisfied either through the use of an energy-filter lens or through the use of an energy-filter detector.

(3) The specimen should be thin enough that single-scattering events predominate over multiple-scattering events, so that the much simpler theory of kinematical scattering may be used rather than the full dynamical theory.

Under the conditions specified above, it can be shown that the amplitude of the scattered plane waves (the Fraunhofer diffraction pattern) is proportional to the Fourier transform of the electrostatic potential of the object. However, for a single orientation of the object it is possible to sample the Fourier transform (i.e., the amplitude of scattered radiation) only over a two-dimensional spherical surface of reciprocal space. This point can be best illustrated by the conventional Ewald sphere construction, shown in Fig. 1. The amplitude of the plane wave, scattered in the direction $\vec{k}$, can be shown to be the Fourier transform of $V(\vec{R})$ evaluated at the vector position $\vec{S}$. From Fig. 1 it is evident that the vectors $\vec{S}$ are confined to the surface of a sphere if the incident-wave vector, $\vec{k}_0$, is confined to a single direction relative to the object.

It can be shown that, if a perfect lens could be used to gather this scattered radiation, the amplitude of the waves forming the in-focus image would be equal to the Fourier synthesis of the various scattering amplitudes (Heidenreich, 1964). The scattering amplitude can itself, in fact, be observed as the Fraunhofer diffraction pattern formed in the back focal plane of the objective lens. The resulting image corresponds therefore to the Fourier synthesis from the surface of the Ewald sphere. At high resolution this conditional, or partial, projection from the Ewald sphere differs significantly from the Fourier projection from a true plane in reciprocal space. However, in the limit of very small scattering angles the Ewald sphere approaches being a plane in reciprocal space. Since small space frequencies correspond to coarse structural features, the low-resolution "Fourier contrast" image corresponds to the low-resolution "z projection" or "mass thickness" projection of the object.

A real lens differs from the perfect lens discussed above in two important ways. First of all a real lens has a limiting aperture which accepts radiation scattered out to some limiting angle. The rest of the radiation cannot participate in image formation, and hence the Fourier synthesis from the Ewald sphere is truncated at some particular value of the reciprocal space vector. As a consequence, the image detail cannot contain information about the structure to a resolution better than one over the limiting space-frequency. Table 1 shows some examples

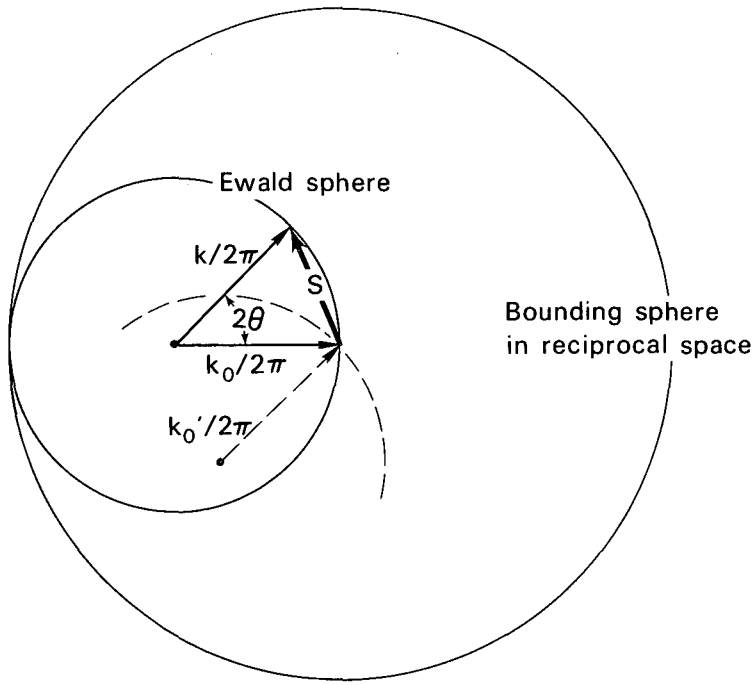

Fig. 1. The vector S lies at the center of reciprocal space, and cannot exceed the boundaries of a sphere with radius $2/\lambda$, where λ is the wavelength of the radiation. This figure shows the relationship of scattering angle, 2θ, to the position of the scattering amplitude assigned in reciprocal space by the Fourier transform of the appropriate scattering potential. The Ewald sphere is a spherical surface which describes all points of reciprocal space that can be reached through a given direction of the incident radiation. Other points in reciprocal space can be reached by changing the incident direction, say, to $k_{0'}$. DBL689-5430

of how the image resolution is affected by truncating the Fourier synthesis with an aperture placed in the back focal plane of the objective lens.

A real lens is further distinguished from the ideal lens by the fact that is possesses certain aberrations. The major aberrations encountered in axially symmetrical lenses are astigmatism, chromatic aberration, and spherical aberration.

The effect of spherical aberration upon image formation can be expressed in a particularly convenient way through the use of the Fourier transform (Hanszen, 1964). Whereas the square root of the ideal image intensity (within the constraint of truncation of the Ewald sphere) is given as

$$\left\{ I(\vec{R}) \right\}^{1/2} = \int \Phi\,(\vec{S})\, e^{i2\pi\, \vec{S}\cdot\vec{R}}\, d\tau_S,$$

it can be demonstrated that the effect of spherical aberration is to impose onto the scattering amplitude a phase shift, the magnitude of which depends upon the angle of scattering. The resulting image is given as

Table 1. Limit of useful resolution due to truncation of the Fourier synthesis.*

Objective-aperture diameter (μ)	Space-frequency cutoff (resolution) (Å)
50	5.0
30	8.5
20	12.5

*Focal length = 3.3 mm; 80-keV electrons in the equation $S = \frac{1}{d} = \frac{R}{\lambda f}$.

$$\left\{I(\vec{R})\right\}^{1/2} = \int \Phi(\vec{S})\, e^{i2\pi\, W(\vec{S})}\, e^{i2\pi\, \vec{S}\cdot\vec{R}}\, d\tau_S,$$

where $2\pi\, W(\vec{S})$ is the scattering-angle-dependent phase shift. In general, the effect of aberrations can be represented by an optical transfer function, $T(\vec{S})$, which modifies the amplitude of scattered radiation gathered by the lens so that the resulting image is imperfect:

$$\left\{I(\vec{R})\right\}^{1/2} = \int T(\vec{S})\, \Phi(\vec{S})\, e^{i2\pi\, \vec{S}\cdot\vec{R}}\, d\tau_S.$$

D. THEORETICAL BASIS FOR A SELF-FOCUSING MICROSCOPE It is a familiar fact in electron microscopy that images show minimum granularity at a given point in a through-focus series. It is now understood that the focus-dependent image granularity results from a contrast enhancement at selected space frequencies. This enhancement results in turn from the phase shift associated with the optical transfer function, $T(\vec{S})$. The point of minimum granularity might reasonably be referred to as the "in-focus" condition, since it corresponds to the resolution of the finest object details (Thon, 1967; Komoda, 1967). Thon has used optical transforms of electron micrographs to demonstrate that the magnitude of the Fourier transform at large space-frequencies is a maximum at the in-focus condition. In this way, he was able to obtain experimental confirmation of the underfocus and overfocus dependence of the optical transfer function (Thon, 1967).

It is proposed here that this same effect can be applied to regulate a microscope in a condition of "constant" focus. The first step in such a process would be to read off the image intensities in a point-by-point fashion, and then to calculate the Fourier transform of that image. It would of course be impractical to do this for the entire image raster, because of the long computational time required. In fact, it is necessary to compute the transform of only a single line in the scan, and it may be expected that it will be necessary to compute the transform at only a single space frequency. The logical choice would be the space frequency corresponding to the maximum resolution possible under the circumstances of magnification and scan-detector size. Since the condition of "true focus" for a given space frequency corresponds to the condition that the Fourier transform at that frequency be a maximum, it will be possible to deter-

mine in a sequence of subsequent scans whether the transform is decreasing, i.e., whether the instrument is drifting out of focus. If a drift in focus is detected it is necessary only to reset the objective-lens current so that the transform is again a maximum at the limiting space frequency.

E. THEORETICAL BASIS FOR CORRECTION OF IMAGE INFORMATION As stated previously, the effect of lens aberrations can be represented by an appropriate optical transfer function $T(\vec{S})$, which modifies the true scattering amplitude to produce an incorrect image,

$$\left\{I(\vec{R})\right\}^{1/2} = \int T(\vec{S})\, \Phi(\vec{S})\, e^{i2\pi\, \vec{S}\cdot\vec{R}}\, d\tau_S.$$

If the image has been recorded as a two-dimensional array of (digital) intensities it is a straightforward, if lengthy, procedure to compute the Fourier transform of the entire image:

$$\int \left\{I(\vec{R})\right\}^{1/2} e^{-i2\pi\, \vec{S}\cdot\vec{R}}\, d\tau_R = T(\vec{S})\, \Phi(\vec{S}).$$

The optical transfer function is a known function of the aberration coefficients and the degree of underfocus or overfocus (Hanszen, 1964; Thon, 1966). Thus if the entire image were recorded in a known state of focus--preferably $\Delta Z = 0$--it would be a practical matter to divide both sides of the equation by the corresponding transfer function. Subsequent transformation of the corrected scattering amplitude would produce an image corrected for the various lens aberrations:

$$\int \left[\frac{\int \left\{I(\vec{R})\right\}^{1/2} e^{-i2\pi\, \vec{S}\cdot\vec{R}}\, d\tau_R}{T(\vec{S})}\right] e^{i2\pi\, \vec{S}\cdot\vec{R}}\, d\tau_S = \int \Phi(\vec{S})\, e^{i2\pi\, \vec{S}\cdot\vec{R}}\, d\tau_S$$
$$= \left\{I(\vec{R})\right\}^{1/2}_{\text{perfect}}.$$

In addition, it is possible to remove noise from the image if either (1) the object is a crystalline or ordered structure such that its transform is readily distinguishable from that of the noise, or (2) the transform of the noise or background (substrate) has been determined in a separate experiment. The first of these techniques is certainly the more practical, and it has already been used on conventional electron micrographs, both by optical and by digital transformation (DeRosier and Klug, 1968). The principal difficulties in the use of optical transforms are (1) the original image is composed of inelastically scattered electrons as well as elastically scattered electrons; (2) the optical system itself has inevitable aberrations and sources of noise (dust on the lenses, etc.); (3) it is difficult to subtract background noise adequately with masks without introducing spurious structure into the image.

III. EXPERIMENTAL SYSTEMS

A. THE POINT-DETECTOR IMAGE-SCANNING SYSTEM The point-detector system should be located in the final image plane of the electron microscope. In practice this normally means some position immediately below the plate camera. The system would consist of a defining aperture (approximately 50 or 100 μm in diameter), an energy filter or analyzer,

and the actual detector. The energy resolution should not be less than 2 eV, but there is some disadvantage in a greater resolution than that, since the electron source has an energy spread of about 2 eV. Ideally, of course, the energy resolution should be great enough that the chromatic aberration (referred to the object),

$$\Delta r_c = C_c \, \alpha \frac{\Delta E}{E},$$

is no greater than the limiting resolution, where α is the angle of the limiting aperture. For 50-keV electrons, an aberration coefficient of 2 mm, and a desired resolution of 1 Å, $\Delta E = 0.06$ eV. In practice, the cross section for inelastic events below 5 eV is actually quite small, so that a resolution of 2 eV should be satisfactory.

Since the direct energy resolution currently possible with particle detectors is still some hundreds of electron volts, it is necessary to use some type of filter or analyzer. Basically there are two types of device possible. The electrostatic (retarding potential) filter is diagramed in Fig. 2. The center electrode is connected directly to the accelerating voltage, and provision is made to add or subtract a small bias. When operated at zero energy loss this filter has the advantage that it automatically compensates for ripple and drift in the accelerating voltage (Denbigh and Grigson, 1965). Such systems have been operated with an energy resolution of less than 2 eV. The system may also be modified to provide an energy-loss spectrum by ac differentiation of the integrated spectrum that is normally produced. In this case, the disadvantage is that the system cannot be used as a single-particle detector. The magnetic analyzer has the disadvantage that it cannot compensate for ripple in the accelerating voltage, although feedback from the output of the zero-loss detector could be used to adjust the excitation of the analyzer in compensation for drift in the accelerating potential. The advantages of velocity analysis in a magnetic field is that one can detect single particles at any desired value of energy loss, in addition to zero energy loss. A further advantage is that it is even possible to record from several channels at the same time.

Any of a number of different detectors might be used. Previous devices have used the p-n junction solid-state detector and the photomultiplier. We have successfully detected single electrons at 50 keV with a Li-drifted Si solid-state detector (with a thin gold-foil window). Perhaps the most promising detectors are the various continuous-strip electron multipliers currently offered by Bendix and by Mullard. These are virtually noise-free at room temperature, have a gain up to 10^8, and a rise time as low as 5×10^{-9} sec.

Two types of image scanning system would be suitable. The first of these would consist of x and y deflection coils or deflection plates, located in a plane between the projector lens and the filter detector. If the deflection plane is close enough to the back focal plane of the projector lens, the scanned image will enter the detector approximately along the axis of the detector. It is essential that this be the case, for those electrons which enter the detector at an angle γ to the axis will be filtered as if they had an energy $V(1-\sin^2\gamma)$. Thus an angle of 6.3×10^{-3} rad for 50-keV electrons would result in an apparent energy loss of 2 eV. If the deflection plane could not be placed close enough to the projector focal plane it would be pos-

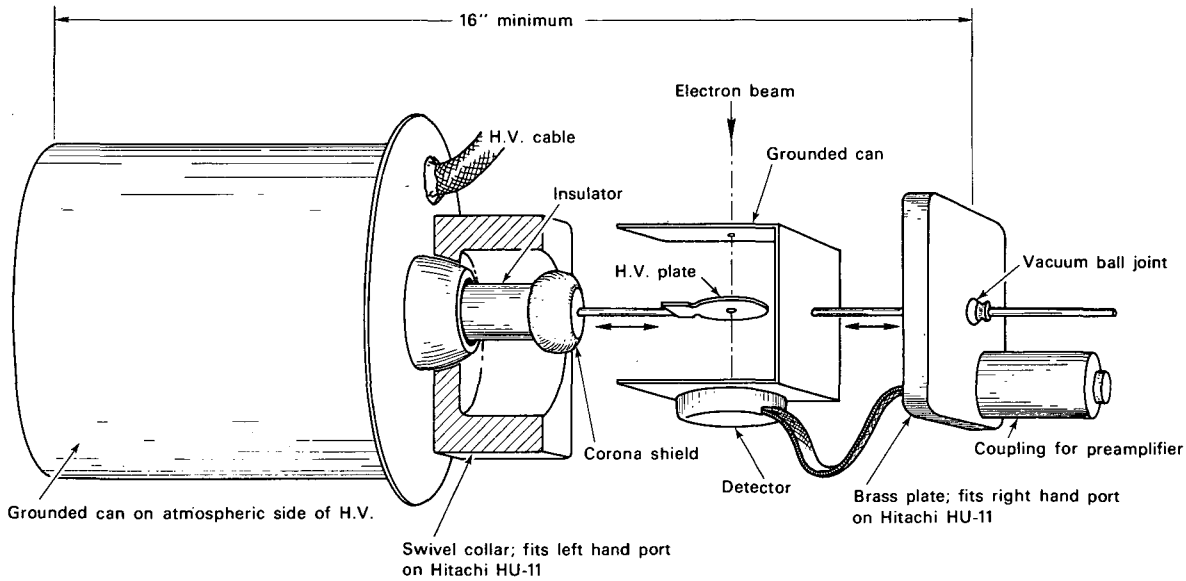

Fig. 2. Diagram of a point detector, energy filter designed to fit in the viewing chamber of the Hitachi HU 11 electron microscope. The filter is a unipotential electrostatic lens, with the center electrode adjusted to approximately the accelerating potential.

DBL689-5431

sible to add compensating x and y deflectors that would insure that the entrance angle for each scanned image point would not exceed the limiting angle for accurate energy analysis. The second alternative for the position of the deflection coils would be in a plane close to the focal plane of the intermediate (first projector) lens. In this case the proximity to the focal plane would not be so critical, and quite probably a compensating deflection would not be required.

The ideal version of the scanning electronics would permit an x-y or raster scan of a complete two-dimensional image. There is a great advantage in having a digital scan, so that each picture element can be recorded for either a constant time or a constant number of events. An analog scan would be suitable, but then the output would require a subsequent digital conversion. This would of course permit counting each picture element only for a constant time, and in addition a slit correction would have to be applied to the raw data. The scanning rate should be variable up to a frame time of 10 to 100 minutes. The magnitude of deflection should be sufficient to provide 500 to 1000 lines per image. Since the width of each line is set by the diameter of the defining aperture, this would result in a scanned image area of approximately 5×5 cm.

The computational problem associated with the feedback focus system is really quite small. Since one needs only to compute the Fourier transform of a single line, at a single point in reciprocal space, one needs only to take the sum of at most 500-1000 points:

$$\Phi(\vec{S}_x) = \sum_{\substack{\text{image}\\ \text{points}}} \left\{I(X)\right\}^{1/2} e^{i2\pi S_x \cdot X}.$$

This could be executed on a typical computer with a 4000-bit memory in much less than 0.1 sec. On the other hand the computational problem of digital transformation of as much as a 1000 × 1000 matrix into all of reciprocal space, followed by correction and resynthesis, is quite substantial. In this case it would be necessary to store the original data on disk or tape and use them as input data in a large computer program.

B. THE FILTER LENS SYSTEM Inelastically scattered electrons can also be removed from the image by an appropriately designed filter lens. It is difficult, however, to design a lens with a large (effective) chromatic aberration without introducing other large aberrations. For this reason the filter lens is normally used as the final imaging element. Even in this way, the best resolution thus far obtained with a filter-lens system has been about 100 Å (Watanabe, 1964). The filter lenses presently available are not really suitable for an experimental system which is supposed to reduce the effects of aberration. The advantage of the ideal filter lens is that it permits filtering and recording of all elements of the image in parallel. Thus for a given set of image criteria (number of picture elements, current density in the image, integrated number of events per picture element), the total field or image can be recorded in a much more reasonable time with a filter lens than with an image-scanning device. This point is discussed further in the next section, in connection with the problem of damage to the specimen by the electron beam.

C. SPECIMEN DAMAGE IN THE ELECTRON BEAM Damage to the specimen in the electron beam is necessarily a serious consideration in any proposal concerning improved resolution of the electron microscope. (Damage during preparation is considered in the next section.) The two factors of importance relative to damage in the beam are "chemical" damage due to ions and radicals produced in the specimen and in the ambient atmosphere, and heating of the specimen by excessive levels of illumination. It is indeed a serious possibility that direct radiation damage can disorder the resolvable structure of biological specimens to a degree far exceeding the instrumental resolution.

The long exposure periods necessarily associated with data acquisition through the image-scanning detector make radiation damage an especially serious hazard. Theoretical considerations are not promising on this point, yet it seems worthwhile to try some experiments that would provide more complete information on the rate at which biological specimens become disordered as a function of the dose rate, or level of electron illumination.

Some work in this direction has already been undertaken, using crystalline l-valine as a test specimen whose properties approximate those of the crystalline proteins (Glaeser et al., 1968). The disappearance of wide-angle electron diffraction patterns can be taken as a criterion of disorder in the specimen at various levels of potential resolution. The experiments have been essentially subjective to date, but there seems to be considerable evidence that the degree of damage for a given total dose is greater at a high dose rate than it is at a low dose rate. This would seem to indicate that specimen heating is at present a more serious source of structural disorder than is direct ionization or chemical damage.

It has been found that the use of a specimen cold stage does not appreciably protect crystalline valine from damage in the electron beam. Similar results have been obtained for crystalline polyethylene and other chain-folded polymers. This observation does not exclude specimen heating as a primary factor. The prospect of overcoming the problem of heat transfer from a small area on a thin film is not at all favorable, even when the heat sink is at liquid nitrogen temperature. At least at the lower magnifications it should be a practical matter to virtually eliminate specimen heating by the use of an adequate image intensifier during the period of general specimen observation and focus, and through use of correspondingly low levels of illumination during the period of image-scanning data acquisition.

Definite lower limits do apply to the levels of illumination that are practical. We may assume that 10^3 sec is a practical limit to the length of a single exposure, a minimum of 10^3 picture elements must be recorded, and the average number of events per picture element must not be less than 100 in order to provide reasonable statistics in the face of low image contrast. If we further assume that the detector has a limiting aperture with a cross-sectional area of 10^{-4} cm^2, it can be calculated that the current density in the final image must not be less than 1.6×10^{-13} A/cm^2 in order to satisfy the other criteria above. Our present subjective experience clearly indicates that a significantly greater level of illumination, perhaps as much as 1×10^{-11} A/cm^2, is possible with biological specimens if the desired magnification is less than 2×10^4. Actually a magnification of 5×10^5 would be required in order to achieve a spatial resolution of 2 Å with a detector aperture 10^{-4} cm^2 in area. At this magnification the current density in the final image would be $\approx 10^{-3}$ times that at the lower magnification, since the current density at the object must remain fixed (in the sense that it cannot exceed a maximum value, regardless of the final magnification). At the moment, a more quantitative study is required in order to determine whether biological specimens such as valine can tolerate sufficiently high levels of illumination to make the high-resolution image-scanning system a practical one.

There are, in addition, a few suggestions of some ways to raise the threshold of critical illumination: (1) Embedding media might be used to stabilize macromolecular structure against thermal disorder. (2) The design of specimen cold stages might be improved so as to help solve the problem by more adequate heat transfer. (3) The problems of rise in temperature and adequate statistics might be improved through the use of pulsed illumination, since this could provide more favorable conditions for heat transfer and cooling. It remains clear that long exposures will be required, and under these conditions it may be essential to have a system for automatic monitoring and regulation of focus.

The illumination threshold is a much less serious problem with the use of a filter lens than it is with the image-scanning filter detector. With the filter lens and photographic recording it is possible to collect data in all image channels simultaneously. Thus, in order to record an image with a virtually unlimited number of picture elements, having 10^3 events per picture element, in an exposure time not exceeding 100 sec, one requires a current density of only 1.6×10^{-14} A/cm^2. This calculation assumes that photographic emulsions (or image-converting systems) can be obtained such that an exposure of 10^3 electrons in an area of 10^{-4} cm^2 can

be quantitatively measured in terms of a resulting photographic blacking. Emulsions in common usage require a current density of approximately 10^{-10} A/cm^2 for adequate blackening over a period of 100 sec. If the period of photographic recording had to be extended to 1000 sec it would possibly be necessary to improve the stabilization of the microscope, since feedback monitoring of the focus would not be possible.

D. INITIAL PRESERVATION OF SPECIMENS The successful preservation of biological structure is a second barrier to meaningful high-resolution electron microscopy. Electron diffraction provides a sensitive means of evaluating the preservation of crystalline and other highly ordered specimens (Glaeser et al., 1968). In the future it should be used as a criterion of how well a biological sample has been preserved throughout the various procedures that are required for bringing it into the vacuum as a thin, electron-transparent specimen. Present specimen preparation techniques have been developed largely on the basis of visual morphological criteria. Even before the use of electron diffraction, considerable evidence already suggested that many of the techniques used for the preparation of small particles or of thin sections do not afford adequate preservation at high resolution. Recent electron diffraction studies have suggested that the removal of water from proteins and similar structures may be primarily responsible for the loss of crystalline order (Parsons, 1966; Murray and Ferrier, 1968).

IV. EXTENSION OF ELECTRON MICROSCOPY TO COMPLETE STRUCTURE ANALYSIS

The previous section has emphasized that if a complete digital representation were obtained of the in-focus image produced by coherently scattered electrons, then it would be theoretically possible to correct the image for noise and lens aberrations. It was also pointed out that such an image is a Fourier reconstruction from the Ewald sphere, and that at high resolution this is remarkably different from a Fourier projection from a plane in reciprocal space. The difference is perhaps negligible for small space frequencies (low resolution), but it becomes extremely important at large space-frequencies (high resolution). In fact, it is evident that a single high-resolution micrograph is essentially uninterpretable in terms of the atomic structure of the specimen.

A minimal requirement of structure analysis would be to record a series of digital images at various angles of tilt so that the corrected scattering amplitude corresponding to a true plane in reciprocal space could be selected from the small volume of reciprocal space that had been surveyed. From the Ewald sphere construction it can be seen that a tilt of at least $\pm 8 \times 10^{-2}$ rad (± 5 deg) is required to record the scattering amplitude on a single plane in reciprocal space to a resolution of 1 Å. The scattering amplitude for a single plane in reciprocal space could then be used to provide a two-dimensional projection of the structure of the object. Even such a precisely defined projection would be quite uninterpretable if there were many atoms in the unit cell. Thus it may be generally expected that it is necessary to record the scattering amplitude throughout the entire volume of reciprocal space. With an adequately designed goniometer stage one might expect to tilt a single specimen through an angle of 30 to 45 deg. Beyond that point, however, the effective specimen thickness would increase very rapidly, and other portions of reciprocal space would have to be explored with regions of the

specimen that contained crystals lying in or on the support film at different angles to begin with.

Structure analysis by electron microscopy, as outlined above, has some considerable theoretical advantages over structure analysis by direct electron diffraction (or X-ray diffraction). The advantage lies in the theoretical possibility of calculating the phases of the scattered radiation directly from the image. This avoids the great difficulty of indirect determination of phases which exist in ordinary structure analysis. In theory the image method can be applied to nonperiodic objects as well as to periodic or crystalline objects, so that in principle one could compute the structure of single particles (De Rosier and Klug, 1968). In practice, however, there would doubtless be considerable advantage in working with crystalline specimens so that it would be possible to take advantage of the redundant information in the image (Cowley and Moodie, 1957). Thus, for example, it would not matter if some of the molecules in a repeated structure became disordered through direct ionizing events, since this disorder would merely express itself as noise in a highly redundant message. In order to take advantage of such redundancy, however, it would be necessary to record all channels in parallel. This would evidently require a filter lens, and certainly could not be done with a single-channel filter-detector.

V. EXPERIMENTAL DEMONSTRATION OF FOURIER CONTRAST EFFECTS IN LOW-RESOLUTION ELECTRON MICROSCOPY

Even without the help of a filter lens it has been possible to demonstrate the importance of Fourier synthesis or "Fourier contrast" in high-resolution electron microscope images. So-called direct lattice images, which are in fact the Fourier synthesis obtained by recombination of a small number of Bragg-reflected beams (typically one or two), have been obtained with a variety of atomic and molecular solids. Such electron-optical resyntheses with a resolution exceeding 2 Å have been obtained in several laboratories, but not with biological specimens. Since the (elastic) scattering amplitude increases strongly at low angles it necessarily follows that Fourier contrast is an even more important factor in image formation at low resolution. Figure 3 shows a specimen of "880 Å" polystyrene spheres in a two-dimensional, hexagonal close-packed array. The insets show exposures of different length, revealing the low-angle electron diffraction pattern which was observed by the three-lens method (Ferrier and Murray, 1966). It should be noticed that the specimen is slightly buckled or tilted in the middle of the figure (see also the very-low-magnification inset). Figure 4 shows selected enlargements from areas within the region of tilt, compared to an enlargement of an area where the sheet was perpendicular to the incident illumination. A particularly interesting effect is shown in Fig. 4d, where the angle of tilt is evidently not great enough to destroy the hexagonal symmetry (see the domains top and bottom), but a partial dislocation of the intermediate domain results in a highly serrated Fourier synthesis. These images could be interpreted through an understanding of the way in which the Ewald sphere intersects the Fourier transform in reciprocal space. A quantitative comparison is not possible due to the presence of inelastically scattered electrons and due to a lack of precise, independent information regarding the angle of tilt.

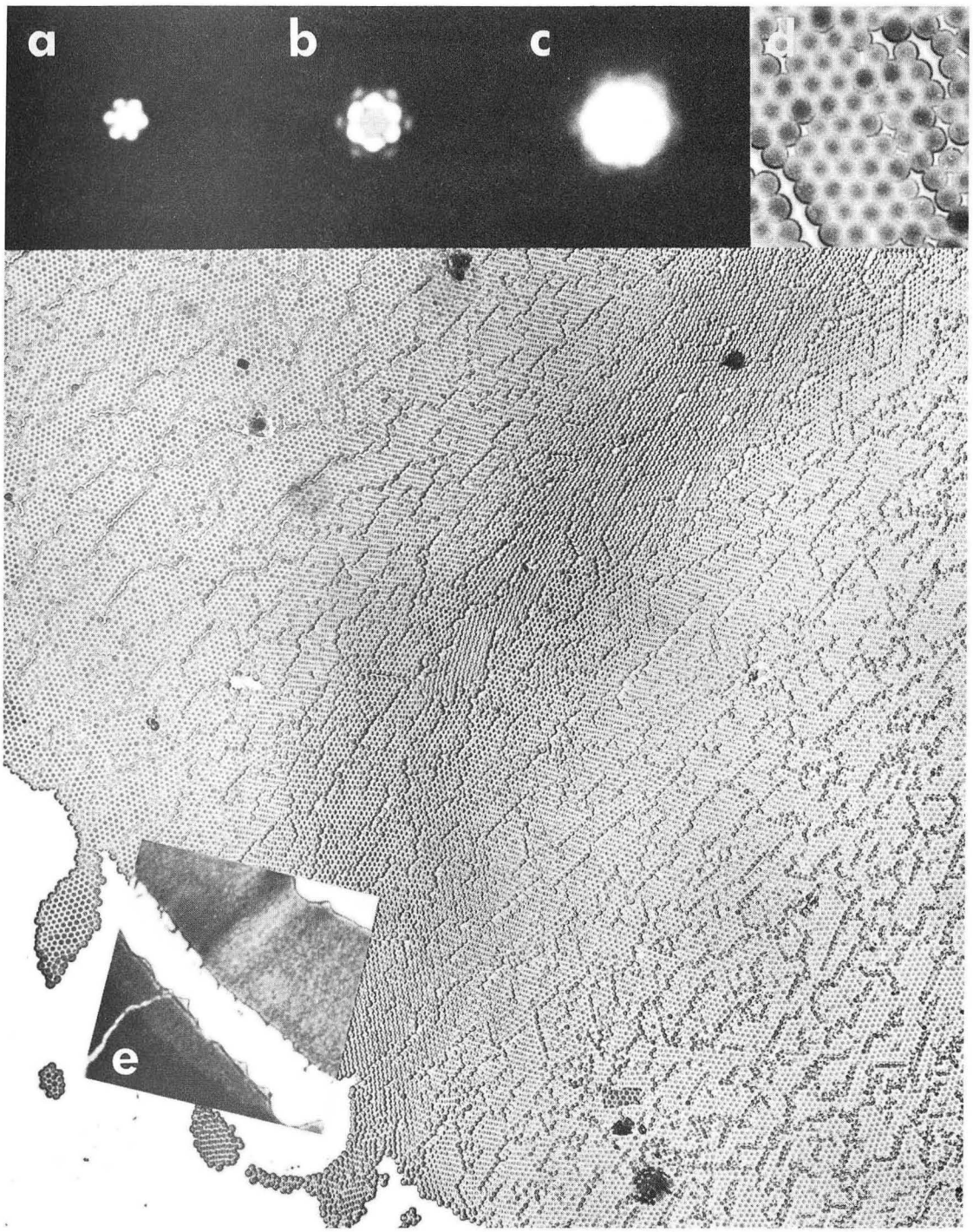

Fig. 3. General view of a two dimensional sheet of 880 Å diameter polystyrene latex spheres. Upper insets show the low angle diffraction pattern obtained with various exposure times. A magnified image shows the hexagonal packing of spheres. The sheet is somewhat warped across the center of the figure, and the nature of this warping is more clearly shown in the very low magnification inset.

XBB681-510

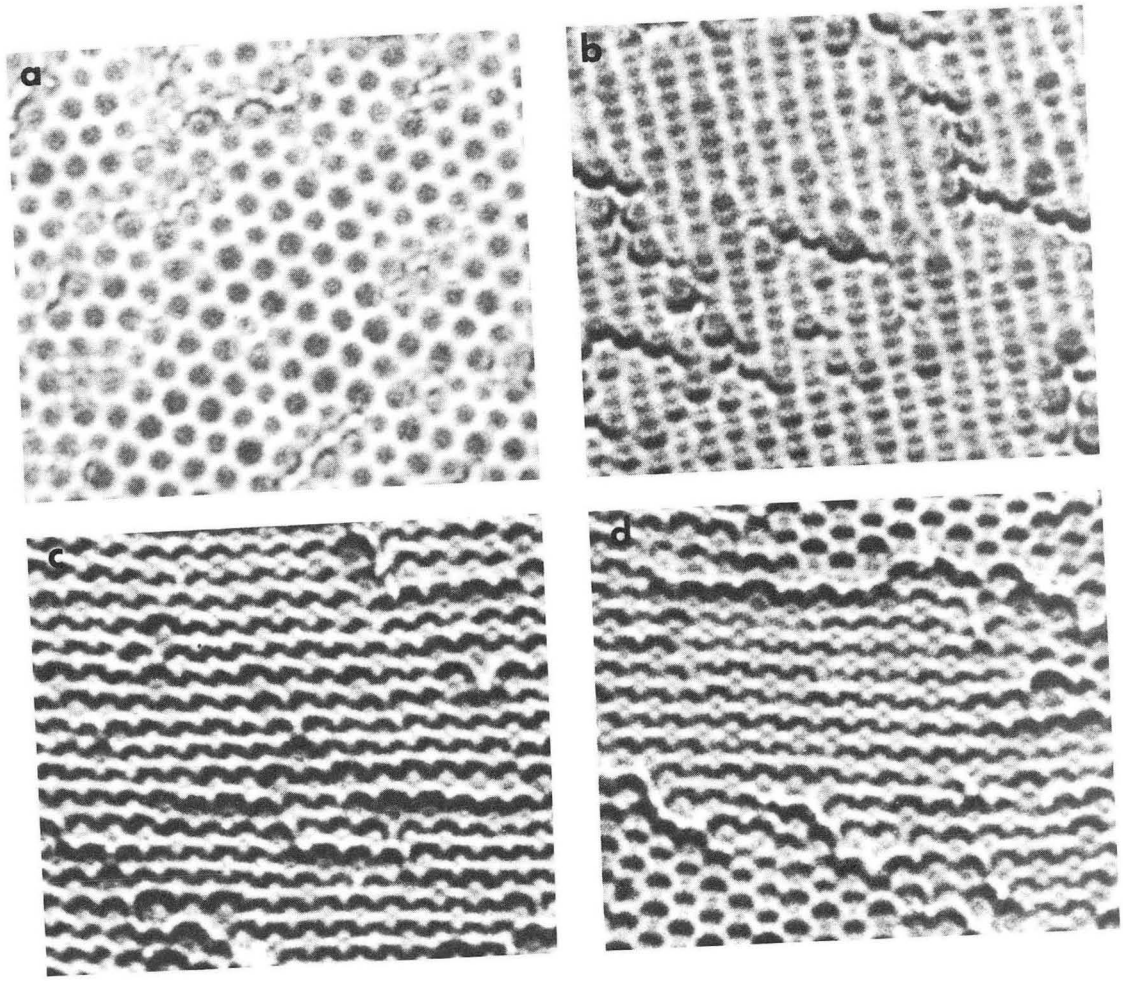

Fig. 4. Various Fourier contrast images excerpted from Fig. 3. (a) a region with hexagonal symmetry, (b) a region with linear symmetry, (c) a region with highly serrated structure, (d) another region with serrated structure, but note the emergence of hexagonal symmetry at top right and bottom left, demonstrating that the serration is not an effect of focus.
XBB684-1972

A second example of apparent low-angle Fourier contrast is shown in Fig. 5. This is a micrograph of a longitudinal thin section of striated muscle (frog skeletal muscle). The inset shows the corresponding low-angle electron diffraction pattern. The Bragg maxima can be indexed with reference to a hexagonal lattice of filaments, and these have been previously identified from electron microscopy and low-angle X-ray diffraction to be the myosin filaments.

The relative importance of coherently scattered electrons in image formation can also be evaluated by the technique of dark-field microscopy. Dark-field imaging is quite simple if the scattering angles are large (corresponding to space frequencies of 0.2 $Å^{-1}$ or more). It is quite difficult to combine dark-field microscopy with low-angle scattering, however, since the objective aperture must be positioned with great accuracy in order to pass the scattered radiation and at the same time stop the central, unscattered beam. Nevertheless, an example of low-angle, dark-field microscopy with polystyrene spheres has been reported (Yeh and Geil, 1967). In that case a long-focal-length (objective lens) technique was used rather than the three-lens technique.

VI. SOME POSSIBLE EXTENSIONS OF THE PRINCIPLE OF STRUCTURE ANALYSIS BY CORRECTION OF IMPERFECT FOURIER CONTRAST IMAGES

A. THE X-RAY MICROSCOPE The theory discussed in this paper could be applied to an X-ray microscope just as well as it has been applied to the electron microscope. While imaging lenses are not feasible, X-ray microscopes have been constructed utilizing reflection optics. In this case, aberrations of the mirror optics have prevented the development of a high-resolution X-ray microscope. It is now clear, however, that if the optical transfer function could be determined for a real X-ray microscope, then the image could be digitally corrected and high-resolution structure analysis would be possible.

The X-ray microscope would have two major advantages over the digital electron microscope discussed here. First of all, it would be possible to work with wet specimens, thereby eliminating the problems of specimen damage during preparation. The second advantage is that inelastic scattering is much less of a problem with X rays than with electrons. Thus in an X-ray microscope it would not be necessary to filter the image. This in turn would make it practical to record the (unfiltered) images photographically, that is, all channels in parallel. The resulting photographic record could be subsequently scanned and transcribed to digital intensities through an appropriate photographic blackening law. Long exposures would not be a serious problem, since the X-ray microscope would not be faced with the same difficulties of electronic stability as is the electron microscope.

B. THE FILTER-LENS ELECTRON MICROSCOPE It has already been pointed out that the filter-lens electron microscope would permit photographic recording of all image channels at one time. At present the filter lenses are of limited usefulness because of their excessive lens aberrations. Once again, however, it may be possible to take these aberrations into account in defining the total optical transfer function of the microscope. The major difficulty in such an approach would lie in determining the condition of focus. It seems possible that the condition of focus could be determined a posteriori by several trial computations, using a

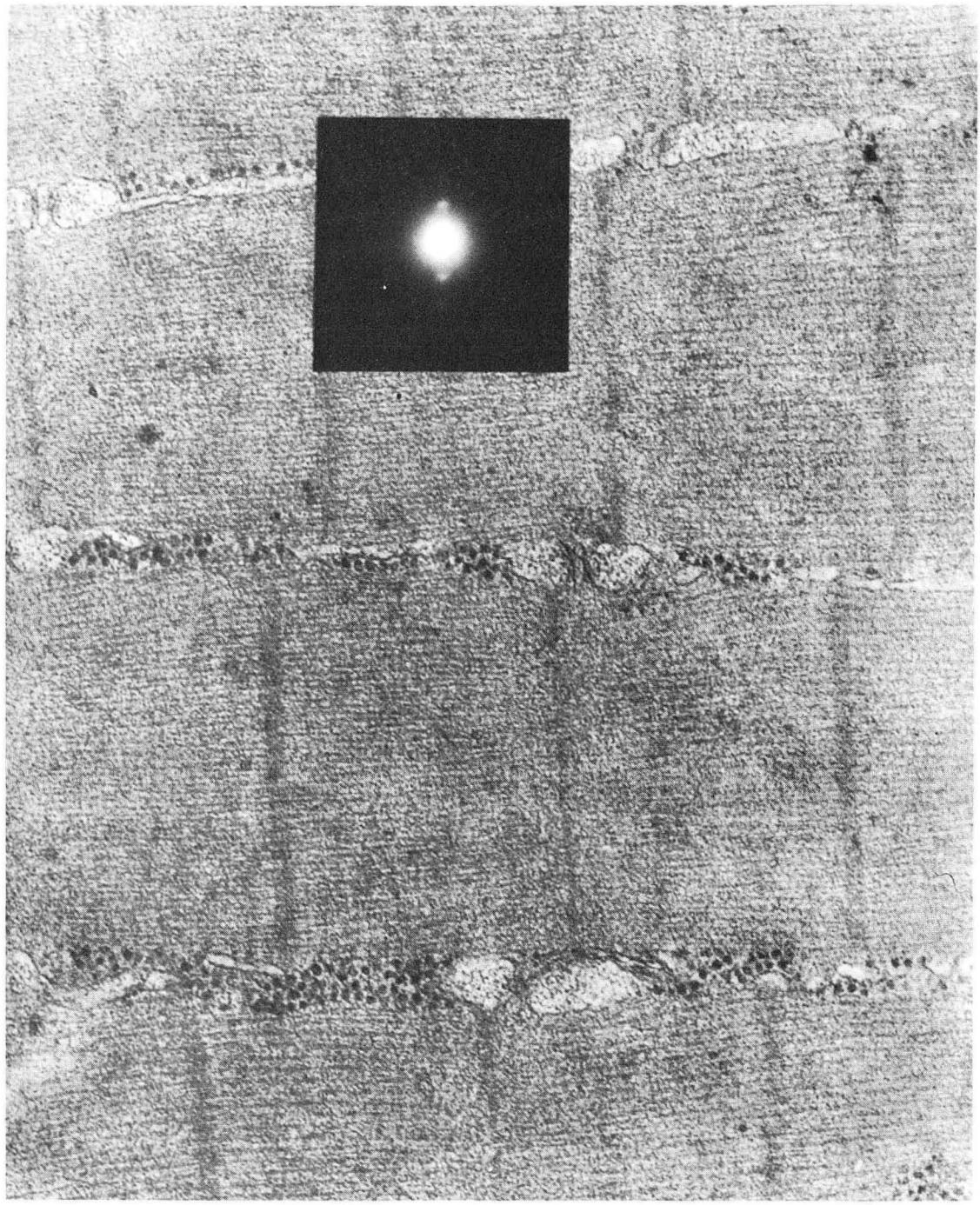

Fig. 5. Thin section of striated muscle from frog skeletal muscle. The inset shows the low angle electron diffraction pattern, confirming that Fourier contrast contributes to the image.

XBB681-511

transfer function for several values of underfocus or overfocus in order to produce a corrected image with the greatest resolution. It may nevertheless be more practical to continue development of improved filter lenses which would not, themselves, impose limiting aberrations on the image.

SUMMARY

Various experimental systems are analyzed with regard to their ability to remove inelastically scattered, noncoherent electrons from electron microscope images. The resulting images would correspond to a Fourier transform of the scattering amplitude, in accordance with the Abbé theory or diffraction theory of image formation. The object of such experimental systems is to provide image data that can be analyzed according to optical transfer function theory. It is expected that it should be possible to correct images for the effects of lens aberrations, spherical aberration in particular. Examples of Fourier contrast at low resolution are experimentally demonstrated through the technique of low-angle electron diffraction.

REFERENCES

Cowley, J. M.; and Moodie, A. F.: Proc. Phys. Soc. (London) B70: 487 (1957).

Denbigh, P. N.; and Grigson, C. W. B.: J. Sci. Instr. 42: 305 (1965).

De Rosier, D. J.; and Klug, A.: Nature 217: 130 (1968).

Ferrier, R. P.; and Murray, R. T.: J. Roy. Microscop. Soc. 85: 323 (1966).

Glaeser, R. M.; Thomas, G.; Christensen, R.; and Brammer, W. G.: in Proceedings of the 26th Annual Meeting of the Electron Microscopy Society of America, Claitor Press, 1968.

Hanszen, K.-J.; Morgenstern, B.; and Rosenbruch, K.-J.: Z. Angew. Phys. 16: 477 (1964).

Heidenreich, R. D.: Fundamentals of Transmission Electron Microscopy, New York, Interscience Publishers, 1964.

Komoda, T.: Hitachi Review 49, No. 5 (1967).

Murray, R. T.; and Ferrier, R. P.: J. Ultrastruct. Res. 21: 361 (1968).

Parsons, D. F.: in Proceedings of the Sixth International Congress for Electron Microscopy, Kyoto, 1966.

Thon, F.: Z. Naturforsch. 21a: 476 (1966).

Watanabe, H.: Japan J. Appl. Phys. 3: 480 (1964).

Yeh, G. S. Y.; and Geil, P. H.: J. Mater. Sci. 2: 457 (1967).

Staff Publications

Adams, Lawrence R.: A photographic cytophotometric method which avoids distributional error. Acta Cytol. 12: 3-8 (1968).

Amer, N.; and Tobias, C. A.: A possible explanation for the effects of magnetic fields upon biological systems. Radiation Res. Abstracts 31: 644 (1968).

Anger, H. O.; and McRae, James: Transmission scintiphotography. J. Nucl. Med. 9: 267-269 (1968).

Berry, C. A.; and Curtis, S. B.: Space radiation and other medical aspects of space travel; in Progress in Atomic Medicine, Vol. 2, edited by J. H. Lawrence, New York, Grune & Stratton, Inc., 1968, Chap. 8, pp. 217-264.

Burki, H. J.; and Okada, S.: A comparison of the killing of cultured mammalian cells induced by decay of incorporated tritiated molecules at -196°C. Biophys. J. 8: 445 (1968).

Burki, H. J.; and Okada, S.: Freezing, storage and thawing of mouse leukemic cells, L5178Y, in culture (32804). P.S.E.B.M. 127: 794 (1968).

Chen, M. G.; and Schooley, J. C.: A study on the clonal nature of spleen colonies using chromosome markers. Transplantation 6: 121-126 (1968).

Curtis, S. B.; and Raju, M. R.: A calculation of the physical characteristics of negative pion beams energy-loss distribution and Bragg curves. Radiation Res. 34: 239-255 (1968).

Engesett, Arnfinn; and Schooley, J. C.: Morphological changes following irradiation of a segment of the rat thymus. Proc. Soc. Exp. Biol. Med. 128: 26-31 (1968).

Feola, J. M.; Richman, C.; Raju, M. R.; Curtis, S. B.; and Lawrence, J. H.: Effect of negative pions on the proliferative capacity of ascites tumor cells (lymphoma) in vivo. Radiation Res. 34: 70-78 (1968).

Freifelder, Dorothy Read; and Freifelder, David: Studies on Escherichia coli sex factors. I. Specific labeling of F'Lac DNA. J. Mol. Biol. 32: 15-23 (1968).

Freifelder, Dorothy Read; and Freifelder, David: Studies in Escherichia coli sex factors. II. Some physical properties of F'Lac and F DNA. J. Mol. Biol. 32: 25-35 (1968).

Hayes, T. L.; and McDonald, L. W.: Three dimensional analysis of human blood and marrow smears using the scanning electron microscope. Clin. Res. 16: 121 (1968).

Hoff, H. F.; McDonald, L. W.; and Hayes, T. L.: An electron microscope study of the rabbit aortic intima after occlusion by brief exposure to a single ligature. Brit. J. Exp. Pathol. 49: 68-73 (1968).

Johnson, C. L.; and LaRoche, Gilles: Simulated altitude and iodine metabolism in rats. II. Effects of chronic exposure on serum and thyroid iodinated components; effects on blood fractions and some organ weights. Aerospace Med. 39: 365-375 (1968).

Jones, Hardin: A concept of lifetime tolerance to radiation; in Conference on the Pediatric Significance of Peacetime Radioactive Fallout, San Diego, March 14-16, 1966. Pediatrics 41: 271-277 (1968).

Kaskebar, D. K.; Forte, G. M.; and Forte, J. G.: Phospholipid turnover and ultrastructural changes in resting and secreting bullfrog gastric mucosa. Biochim. Biophys. Acta 163: 1-13 (1968).

King, J. L.: Dominant radiation effects in mouse populations. Genetics 58: 625-631 (1968).

Linfoot, J. A.: Heavy particle irradiation of the pituitary; in Vascular Complications of Diabetes Mellitus, edited by S. J. Kimura and W. M. Caygill, Saint Louis, C. V. Mosby Co., 1967, Chap. 17, pp. 219-226.

Loughman, W. D.; and Sargent, T. W.: Chromosome damage by LSD (answer to a letter by Herman M. Slatis). Science 159: 1493 (1968).

Loughman, W. D.; Feola, J. M.; Raju, M. R.; and Winchell, H. S.: RBE of π^- beams in the Bragg peak region determined with polyploidy induction in mammalian cells irradiated in vivo. Radiation Res. 34: 56-69 (1968).

Maccabee, H. D.; Raju, M. R.; and Tobias, C. A.: Fluctuations of energy loss by heavy charged particles in thin absorbers. Phys. Rev. 165: 469-474 (1968).

Manougian, E.: Kinetics of metabolic processes as studied with radioactive tracers; in Progress in Atomic Medicine, Vol. 2, edited by J. H. Lawrence, New York, Grune & Stratton, Inc., 1968, Chap. 7, pp. 184-216.

Ngo, T.; Winchell, H. S.; and Landaw, S.: Altered in vivo metabolism of histidine (imidazole-2-^{14}C) in irradiated rats. Radiation Res. 34: 390-395 (1968).

Nichols, A. V.; Strisower, E. H.; Lindgren, F. T.; Adamson, G. L.; and Coggiola, E. L.: Analysis of change in ultracentrifugal lipoprotein profiles following heparin and ethyl-p-chlorophenoxyisobutyrate administration. Clin. Chim. Acta 20: 277-283 (1968).

Pease, R. F. W.; and Hayes, T. L.: Biological applications of the scanning electron microscope; in Symposium on Scanning Electron Microscopy, IIT Research Institute, Chicago, April 1968, Proceedings, The scanning electron microscope—the instrument and its applications, Chicago, Jackson Press, 1968, pp. 143-154.

Raju, M. R.: Discussion; in Symposium on Microdosimetry, Ispra, Italy, Nov. 13-15, 1967, Proceedings, edited by H. G. Ebert, Brussels, European Communities, 1968, pp. 199, 410.

Roy, G.; and Tobias, C. A.: A solid state approach to the theory of the squid axon. Biophys. J., WEG, Feb. 1968, abstract.

Schooley, J. C.; Garcia, J. F.; Cantor, L. N.; and Havens, V. W.: A summary of some studies on erythropoiesis using anti-erythropoietin immune serum. Ann. N. Y. Acad. Sci. 149: Art. 1, 266-280 (1968).

Slater, J. V.; Buckhold, B.; and Tobias, C. A.: Effect on a flour beetle of irradiation during space flight, in Symposium on the Biosatellite II Experiments, Preliminary Results. BioScience 18: 595-597 (1968).

Strisower, E. H.; Kradjian, R. M.; Nichols, A. V.; Coggiola, E.; and Tsai, J.: Effect of ileal bypass on serum lipoproteins in essential hypercholesterolemia. J. Atherosclerosis Res. 8: 525-534 (1968).

Strömnaes, Ö.: Genetic changes in Saccharomyces cerevisiae grown on media containing DL-parafluorophenylalanine. Hereditas 59: 197-220 (1968).

Strömnaes, Ö.; and Mortimer, R. K.: Use of nystatin to eliminate spontaneous revertants in yeast. J. Bacteriol. 95: 197-200 (1968).

Tenforde, T.; and Macey, R.: Membrane diffusion with feedback regulation of cell volume; estimation of membrane tortuosity and diffusion coefficients. J. Theoret. Biol. 19: 232-240 (1968).

Tobias, C. A.: Cellular effects of ionizing radiation; in Biological Hazards Associated with Ionizing Radiation, New York, Pergamon Press, Ltd., 1968, in press.

Tobias, C. A., et al.: Status of research in the biophysical sciences. Biophys. J. 8: No. 6, 734-772 (1968).

Todd, P. W.: Defective mammalian cells isolated from X-irradiated cultures. Mutation Res. 5: 173-183 (1968).

Todd, P. W.; Lyman, J. J.; Armer, R. A.; Skarsgard, L. D.; and Deering, R. A.: Dosimetry and apparatus for heavy ion irradiation of mammalian cells in vitro. Radiation Res. 24: 1-23 (1968).

Todd, P. W.: Fractionated heavy ion irradiation of cultured human cells. Radiation Res. 34: 378-389 (1968).

Todd, P. W.; Winchell, H. S.; Feola, J. M.; and Jones, G. E.: Pulsed high-intensity roentgen rays. Inactivation of human cells cultured in vitro and limitations on usefulness in radiotherapy. Acta Radiol. 7: 22-26 (1968).

Van Dyke, D. C.; Nohr, M. L.; and Tennant, B.: Erythropoietin enhancing factor in serum of a calf with primary familial polycythaemia. Nature 217: 1027-1028 (1968).

Van Dyke, D. C.; Anger, H. O.; and Yano, Y.: Progress in determining bone marrow distribution in vivo; in Progress in Atomic Medicine, Vol. 2, edited by J. H. Lawrence, New York, Grune & Stratton, Inc., 1968, Chap. 3, pp. 65-84.

Winchell, H. S.: Quantitation of red cell and heme production and destruction using radioisotope kinetics; in Progress in Atomic Medicine, Vol. 2, edited by J. H. Lawrence, New York, Grune & Stratton, Inc., 1968, Chap. 4, pp. 85-112.

Yano, Y.; and Anger, H. O.: Ultrashort-lived radioisotopes for visualizing blood vessels and organs. J. Nucl. Med. 9: 2-6 (1968).

Author Index

Aceto, H., Jr. 71
Anger, H. O. 10, 23
Budinger, T. F. 64
Burki, H. J. 59
Coggiola, E. L. 140
Curtis, S. B. 171
Donald, W. G., Jr. 1
Finley, N. N. 42, 53
Forte, G. M. 112
Forte, J. G. 112
Freeman, N. K. 129
Gaffey, C. T. 82
Gee, W. 71
Glaeser, R. M. 175
Hayes, T. L. 96
Jensen, L. C. 129, 140
Lawrence, J. H. 1, 10, 42
Limlomwongse, L. 112
Lindgren, F. T. 129
Maccabee, H. D. 155
Madhvanath, U. 155
Nichols, A. V. 140
Raju, M. R. 155
Raley, R. B. 149
Ronai, P. 10, 23
Schooley, J. C. 99
Shane, L. L. 42, 53
Shipley, B. A. 42, 53
Springsteen, R. W. 71
Thomas, G. 175
Vimokesant, S. L. 149
Wiley, K. G. 36
Wills, R. D. 129
Winchell, H. S. 1, 10, 23, 36, 42, 53, 71, 149
Yokoyama, E. H. 140

Personnel

Senior Staff

John H. Lawrence, Director
Hal O. Anger
Max W. Biggs
James L. Born
Ernest L. Dobson
Norman K. Freeman
Joseph F. Garcia
Thomas L. Hayes
Hardin B. Jones
Thomas H. Jukes
Frank T. Lindgren
Howard C. Mel
Robert K. Mortimer
Alexander V. Nichols
Howard G. Parker
Donald J. Rosenthal
John C. Schooley
William E. Siri
Cornelius A. Tobias
Donald C. Van Dyke
Harry Saul Winchell

Medical Investigator Staff

Max W. Biggs
James L. Born
Thomas F. Budinger
Richard A. Carlson
Claude Y. Chong
William G. Donald, Jr.
Stephen A. Landaw
John H. Lawrence
John A. Linfoot
Edward Manougian
Howard G. Parker
James Price
Donald J. Rosenthal
Norton J. Snyder
Henry H. Stauffer
Donald C. Van Dyke
Wen C. Wei
Harry Saul Winchell

Research Staff

Henry Aceto
Nabil Amer
Gerald Connell
Stanley B. Curtis
Patricia Durbin-Heavey
Rashid A. Fawwaz
Jose M. Feola
Cornelius T. Gaffey
Robert M. Glaeser
Thomas E. Gunter
Jerry Howard
Lin C. Jensen
W. Barrie G. Jones
Lola S. Kelly
Jack L. King
William D. Loughman
David D. Love
John T. Lyman
Richard A. McGrath
James McRae
Myron Pollycove
Douglas W. Pounds
Mudundi R. Raju
Thornton W. Sargent
Richard L. Schoenbrun
Carol J. Shkurkin
Edward H. Strisower
Chiyoko Tokunaga
Graeme P. Welch
Margaret R. White
Carol M. Wildman
Yukio Yano

Postdoctoral Fellows

Brenda Buckhold
H. John Burki
Michael G. Chen
John C. Cummings
Gertrude M. Forte
John T. Leith
Tran Manh Ngo
Bruce J. Roser
Burton H. Slanger
Hannes B. Stahelin
Joel B. Swartz
Patric Tauro

Technical Staff

Gerald L. Adamson
Hilda M. Alexander
Cathryne C. Allan
Alice Beckmann
Rosemary J. Bell
Adrienne Berkowitz
Patricia J. Blanche
Mona D. Boaz
Catharine D. Boerke
Carol S. Bohlen
Jonathan Bokelman
Gerald L. Brooks
Dorothy A. Carpenter
Emanuela N. Catena
Elaine L. Coggiola
Karen R. Colyear
Mary J. Cornell
Henriette C. Cozza
Laurie M. Craise
Susan J. Daniels
Theodora M. Davis
Stuart R. Dole
Robert E. Doyle
Doris L. Dunn
Gregory C. Eggling
Ora B. Ellington
Carolee R. Finney
Myrtle L. Foster
Roscoe Frazier
Charlie M. Fuller
Patricia A. Garbutt
Queen E. Gipson
Lois R. Gumz
Dawn C. Hammond
Virginia C. Havens
Beverly D. Heinze
Jerilyn Hirshberg
Deanna Honbo
Willie M. Jackson
Karen Jarrett
Nylan M. Jeung
Natalia Kusubov
James W. Lieb
Phoebe J. Lindsay
Jennie M. London
Jean R. Luce
Josephine A. Lundberg
Justine J. Lynch
Larry E. Marbley
Patricia C. Mason
Tommie C. Mathews
Johnie A. Maxion
Lafayette McIntosh, Jr.
Tommy J. McKey
Velma B. McNeal
Victor J. Montoya
Jeanette S. Nakagawa
William D. Nance
Mary L. Nohr
Virginia I. Obie
Anne K. Poley
Rosanne B. Raley
Ralph L. Reynolds
Sarah L. Ryerson
Elizabeth E. Saghy
Willie H. Sanders
Elizabeth A. Seaholm
Barbara A. Shipley
Ellen S. Sivota
Patricia P. Smith
Virginia M. Spamer
Robert W. Springsteen
Gary R. Stevens
Sandra K. Stoddard
Velta Suna
Frances B. Taylor
Charles Thompson, Jr.
Cole Ulrichs
Rita L. Von Hungen
Susan M. Walker
Marilyn A. Williams
Robert D. Wills
Patricia C. Wood
Stephen R. Wright
Elaine H. Yokoyama
Philip E. Yost

Graduate Students

Raymond Baker
Steven A. Beckwitt
Martin L. Brown
Jeremy N. Bruenn
Ralph C. Christensen
Elizabeth J. Clark
Edward L. Elkin
Robert A. Everson
Douglas A. Ewald
Robert Foreman
David E. Garfin
Michael M. Graham
Mark N. Herman
Carl F. Hodel
Junardeen Hopkirk
William J. Horsley
Charles R. Hurlbut
Latife Ismail
Gary E. Jones
Michael W. Kaplan
Karl E. Kuning-Unte
James M. Lallas
Gustave H. Langner, Jr.
Lawrence R. Lawlor
David H. Lin
Max S. Lin
Roderick D. Macgregor, Jr.
Udipi Madhvanath
Gilbert H. Magilen
Abdel M. Mamoon
JaRue Manning
Bambino I. Martins

Graduate Students (cont.)

Peter C. Nosler
Paul H. Olague
George F. Oster
James B. Pawley
Alan S. Perelson
Esther B. Perry
David A. Pistenma
Robert G. Plantz
Donald L. Puppione
Theodore Regimbal
Michael A. Resnick
Ubaldo S. Rodarteyramon
Werner T. Schlapfer
Paul T. Shafer
Sylvia Spengler
Tom S. Tenforde
Myonggeun Yoon
David A. Zelman

Engineering and Technical Support Staff

Robert C. Aker
Elbert L. Benjamine
Delbert H. Coleman
Robert D. Creedy
Dewey D. Dean
Dorothy E. Denney
John A. Despotakis
Edward F. Dowling
James H. Edwards
John P. Flambard
John R. Gurule
Edward A. Heilstad
David A. Hoopes
Victor P. Jensen
Edward J. Lampo
Ellis H. Myers
Karen A. Peterson
Marjory H. Simpson
June L. Smith
John M. Sweeney
Frank T. Upham
Alfred A. Windsor

Administrative and Office Staff

Igor R. Blake
Baird Whaley
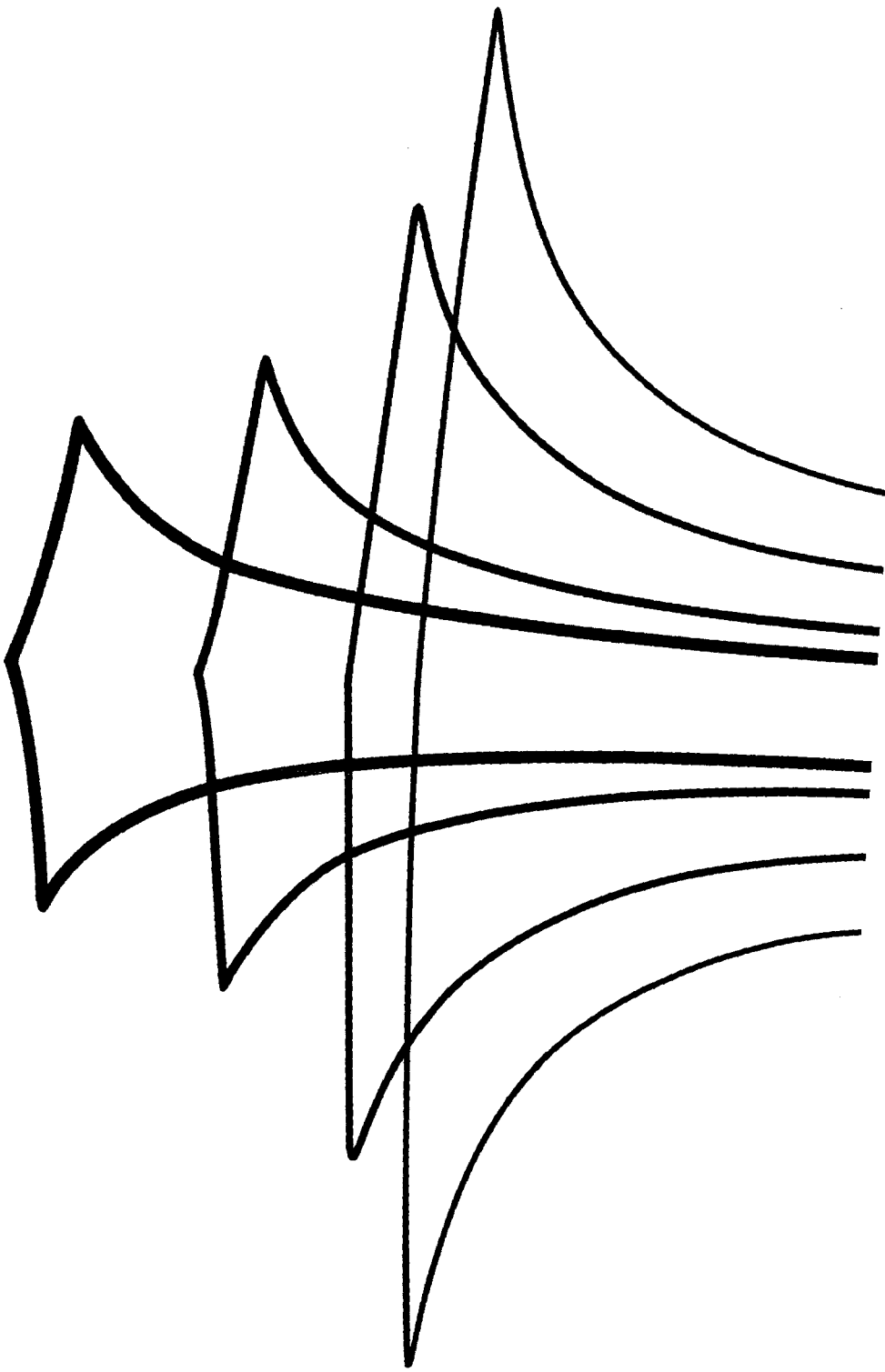
Sandra L. Bazyouros
Mary M. Bryan
Janice C. DeMoor
Marian F. Edelen
Fern V. Forsberg
Joan E. Fox
Betty M. Gale
Mary C. Harmon
Dorothy B. Hedquist
June M. Lattin
Judith S. Manning
Dorothy D. Meck
Pamela A. Mott
Shirley C. Peterson
Ruth T. Showalter
Dorothy S. Sprague
Margaret P. Swartz
Grace H. Walpole